

Multiscale Geomagnetic Field Modelling from Satellite Data

Theoretical Aspects and Numerical Applications

Thorsten Maier

Geomathematics Group
Department of Mathematics
University of Kaiserslautern, Germany

Vom Fachbereich Mathematik
der Universität Kaiserslautern
zur Erlangung des akademischen Grades
Doktor der Naturwissenschaften
(Doctor rerum naturalium, Dr. rer. nat.)
genehmigte Dissertation

1. Gutachter: Prof. Dr. Willi Freeden
2. Gutachter: Dr. Nils Olsen

Vollzug der Promotion: 4. Februar 2003
D 386

Acknowledgements

First of all, I want to express my gratitude to Prof. Dr. W. Freeden for being an inspiring mentor and for his great and continuous support concerning all the minor and major problems that have come up during my work.

I am also much obliged to Prof. Dr. N. Olsen for providing me with MAGSAT data and for reading and evaluating the thesis.

It has been a pleasure to meet the former and current members of the Geomathematics Group. I thank Dr. M. Bayer and Dr. R. Litzemberger for the great times we have had together and C. Korb for being the moving spirit of the group. I am very thankful to Dr. O. Glockner for various discussions, for proof-reading the thesis and, last but not least, for being a close friend. A special "thank you!" goes out to my 'room mate' Dipl.-Math. C. Mayer who has spent hours and hours reading about and implementing numerous gridding methods. Finally, I thank Dipl.-Math.techn. Anna Luther as well as Kai Sandfort for their support concerning the numerics.

I thank Prof. Dr. H. Lühr for inviting me (twice) to the GFZ for several days. During these stays he and his co-workers supplied me with useful information that gave me a better perspective on my own work.

Of course, I am grateful to my parents. Their friendly encouragement and support is invaluable.

I wish to thank Regina, Steffen and my brother Matthias for their friendship and patience.

Finally, the financial support of the 'Deutsche Forschungsgemeinschaft (DFG)', project 'Time-Space Dependent Multiscale Modelling of the Magnetic Field Using Satellite Data (DFG FR 761/10-1)' in the 'DFG Schwerpunktprogramm Erdmagnetische Variationen: Raum-Zeit Struktur, Ursachen und Wirkungen auf das System Erde' is also gratefully acknowledged.

Contents

Introduction	1
1 Preliminaries	8
1.1 Notations and Relations	8
1.2 Reproducing Kernel Hilbert Spaces and Splines	13
1.3 Scalar and Vector Spherical Harmonics	15
1.4 Mie Representation	23
1.5 Inverse Problems and Regularization	24
2 A General Approach to Scalar and Vectorial Multiscale Methods	28
2.1 Scalar Approach	28
2.1.1 \mathcal{H} -Fourier Expansions	28
2.1.2 \mathcal{H} -Product Kernels and \mathcal{H} -Convolutions	29
2.1.3 \mathcal{H} -Scaling Functions	31
2.1.4 \mathcal{H} -Wavelets	34
2.1.5 A Pyramid Scheme	38
2.1.6 Examples	41
2.2 Vectorial Approach	47
2.2.1 \mathfrak{h} -Fourier Expansions	47
2.2.2 \mathfrak{h} -Product Kernels and \mathfrak{h} -Convolutions	48
2.2.3 \mathfrak{h} -Scaling Functions and \mathfrak{h} -Wavelets	50
2.2.4 Example	54
2.2.5 Parenthesis: Tensorial Wavelets	58
3 Multiscale Denoising of Spherical Functions	62
3.1 Signal-to-Noise Thresholding of Scalar Fields	63
3.1.1 Spectral Signal-to-Noise Response	63

3.1.2	Multiscale Signal-to-Noise Response	68
3.1.3	Scalar Selective Multiscale Reconstruction	72
3.2	Signal-to-Noise Thresholding of Vector Fields	77
3.2.1	Vector Spectral Signal-to-Noise Response	77
3.2.2	Tensor-Based Multiscale Signal-to-Noise Response	81
3.2.3	Vector-Based Multiscale Signal-to-Noise Response	85
3.2.4	Vectorial Selective Multiscale Reconstruction	88
3.3	Example	91
4	A Wavelet Approach to Crustal Field Modelling	95
4.1	Downward Continuation in Spherical Approximation	97
4.1.1	Integral Equations for the Radial Derivative	98
4.1.2	Integral Equations for the Surface Gradient	102
4.1.3	The Inverse Problems and Spherical Regularization Wavelets	105
4.1.4	Example	111
4.2	Downward Continuation in Non-Spherical Geometries: A Combined Spline and Wavelet Approach	117
5	A Wavelet-Parametrization of the Magnetic Field in Mie Representation	122
5.1	Setup	123
5.2	Parametrization of Poloidal Fields	124
5.3	Parametrization of Toroidal Fields	130
5.4	Example	137
6	Multiscale Methods for the Analysis of Time-Dependent Spherical Vector Fields	142
6.1	Time-Space-Multiscale Approach: Variant 1	143
6.2	Time-Space-Multiscale Approach: Variant 2	154
	Summary and Outlook	163
	A Standard Geomagnetic Nomenclature	166
	Bibliography	169

Introduction

It was not until the publication of Sir William Gilbert's *De Magnete* in 1600 ([49]) that the Earth itself was seen as a great magnet. Gilbert discussed the subject of geomagnetism in a theoretical as well as an experimental framework and came to the conclusion that Earth behaved as if it were a uniformly magnetized sphere. Though at that time this was an astounding discovery, it is well known today that the subject is more complex (e.g. [66, 67, 68] as well as [8, 58]). According to its sources, the geomagnetic field comprises three major parts usually referred to as the *main* or *core field*, the *lithospheric* or *crustal field* and the *external field*. The main field is the dominant contribution and is generated by magneto-hydrodynamic dynamo action in the Earth's outer liquid core. This makes the main field a valuable tool for probing the Earth's core as well as its impact on the surrounding Earth itself. The lithospheric or crustal field is due to magnetized rocks and sediments in the Earth's crust and upper mantle. Understanding that field contribution yields insight into the structure and tectonics of the Earth and is as well widely used in the field of geoprospecting. The external field, finally, is fed by ionospheric and magnetospheric current systems and consequently contributes to the comprehension of solar-terrestrial interrelationships as well as to the understanding of the Earth's electro-magnetic environment.

Indispensable for the comprehension of the temporal and spatial structure of the geomagnetic field and its sources are precise and rather continuous measurements. After 1805 Alexander von Humboldt organized first simultaneous geomagnetic measurements at locations around the world which marks the beginning of the worldwide network of about 200 magnetic observatories today. It is this network together with ground-based or aeromagnetic surveys that helps to gain insights into the temporal behaviour of the geomagnetic field on time-scales of seconds to decades. Reasonably modelling the geomagnetic field on global or regional (e.g. continental) scales, however, requires dense and homogeneous – preferably vectorial – data sets so that ground-based observations must be regarded supplemental in this context. As regards the subject of global and dense coverage, satellites orbiting the Earth in low, near-polar orbits provide a firm basis for acquiring the necessary high resolution observations. MAGSAT (1979-1980) was the first, and for a very long time only, geomagnetic satellite mission with appropriate vector instrumentation. Despite its comparatively short duration (6 months), the MAGSAT mission built the foundation for a huge amount of scientific geomagnetic results from main to crustal as well as external field modelling and the description of the corresponding sources. The Danish satellite Ørsted, which is also equipped with highly accurate vector instrumentation, orbits the Earth since 1999 and has great impact on main field as well as external field modelling. Global sets of scalar data are provided by the Argentinean

SAC-C mission since 2001 which, however, is mainly dedicated to other geoscientific tasks. The German CHAMP mission which started in the summer of 2000 is, besides other tasks, designed for highly accurate geomagnetic field mappings. Due to its low orbit compared to Ørsted and MAGSAT and due to its advanced instrumentation, for example, it is expected to provide the scientific community with scalar as well as vector data enabling an improvement in accuracy by one order of magnitude compared to the MAGSAT results in main, crustal and external field modelling. For more information about the geomagnetic satellite missions one might contact ”<http://www.dsri.dk/multimagsatellites/>” (Ørsted, CHAMP, SAC-C) or e.g. ”<http://nsdc.gsfc.nasa.gov/database/MasterCatalog?sc=1979-094A>” (MAGSAT) as a starting point.

In geomagnetism it is not only essential to have available adequate data sets, it is also necessary to have at hand the appropriate mathematical tools allowing for reasonable analysis and physical interpretation of the field data. The standard technique of geomagnetic field modelling is the spherical Fourier expansion of a geomagnetic potential in terms of spherical harmonics (orthogonal series). The expansion coefficients (Fourier coefficients) are chosen in a way, that the gradient of the potential fits - in the sense of some suitable metric - the given data as good as possible. This method, introduced by C.F. Gauss (cf. [47]) and therefore named *Gauss Representation*, has been used for more than 150 years now, so that profound numerical methods are existent. However, in order to guarantee the existence of such a scalar potential, one assumes the corresponding magnetic field to be curl-free which, in connection with Maxwell’s equations, means that no electric current densities must be present at the satellite’s orbit. As far as Earth-bound or low-atmosphere mappings are concerned, this assumption is true since the sources of the geomagnetic field, i.e. the electric current densities, are located within the Earth’s body as well as in the iono- and magnetosphere. So, conventionally, the potential is developed by means of inner and outer harmonic representations, reflecting the external and internal contributions corresponding to the geomagnetic field sources (see e.g. [8, 66, 76, 93]). Geomagnetic satellite missions, however, collect their data within the ionosphere and therefore within a source region of the geomagnetic field. This means that satellite data do, in general, not meet the prerequisites for the application of the Gauss representation and usually need to be carefully preselected prior to the modelling process. An alternative approach to resolve this problem is given by the so-called *Mie Representation* for solenoidal vector fields, i.e. by splitting the magnetic field into so-called *poloidal* and *toroidal* parts (e.g. [7, 8, 48, 97]). As regards the magnetic field, the Mie representation can be seen as a generalization of the Gauss representation that is also valid within magnetic source regions, i.e. in regions where the electric current densities are no longer negligible. It is noteworthy that, in the quasi-static approximation of electrodynamics, the electric current densities admit a Mie representation, too, which is dependent on the Mie representation of the corresponding magnetic field. This shows that the ’direct source problem’ of calculating the magnetic effects of a given current distribution as well as the ’inverse source problem’ of calculating current systems corresponding to a given magnetic field can both be approached using the Mie representation. This is important since the (ionospheric and magnetospheric) current distributions and the resulting magnetic effects are more and more subject of recent research (see, for example, [2, 4, 5, 11, 19, 21, 65, 74, 77, 90, 91, 94]). There remains the question of how to numerically obtain – in terms of suitable

trial functions – the Mie representation of a given set of vectorial data. Both, poloidal as well as toroidal vector fields can be derived from certain scalar functions, the so-called Mie scalars. In [21, 82, 91] a spherical harmonic parametrization is suggested, i.e. the Mie scalars of the geomagnetic field and of the corresponding currents are expanded in terms of spherical harmonics such that one can fall back on the experiences made when using the Gauss representation.

Fourier techniques, whether scalar or vectorial are very attractive because of their orthogonality properties (which in the concrete examples of scalar or vector spherical harmonics leads to the interpretation in terms of multipoles). Nevertheless, the respective trial functions are of polynomial nature and consequently globally supported and do therefore not show any localization in the space domain. In the Fourier domain these functions exhibit an intrinsic ideal localization, commonly referred to as ideal frequency or momentum localization. Thus, local changes or features of a function (data) will affect the whole set of Fourier coefficients hence changing the model representation of the data function globally. *Uncertainty principles* (cf. e.g. [28, 46] for the scalar theory and [12] for a generalization to the vector case) provide adequate classifications of trial functions by determining the connection between localization in the space and Fourier domain. The essential result states that simultaneous ideal localization in space and frequency is mutually exclusive. For instance, extreme trial functions in the sense of uncertainty principles are given by scalar/vectorial spherical harmonics on the one hand and Dirac kernels/functionals on the other hand. The scalar or vector spherical harmonics show ideal localization in the Fourier domain but do not show any localization in the space domain. In contrast, the Dirac kernels are ideally localized in space but admit no frequency localization at all. An ideal system of trial functions would possess both, ideal localization in the space as well as in the Fourier domain and would hence admit models of highest resolution which were interpretable in terms of single frequencies (like multipoles, for example). In conclusion, Fourier methods are surely well suited to resolve low and medium frequency phenomena while their application to obtain high resolution global or regional models is critical. Thus, a trade-off between space and frequency localization has to be found.

Such a compromise can be obtained by special kernel functions – so-called bandlimited and non-bandlimited – which can be constructed as to decay towards high and low frequencies and consequently cover certain frequency bands which are characterized by the so-called *scale* of the kernel function. According to the uncertainty principles, this reduction of frequency localization leads to an enhancement of space localization such that these kernels show only small spatial extensions. Therefore, these kernels can be designed to show all intermediate stages of space/frequency localization (see, for example, [30]). Actually it turns out that non-bandlimited kernels show much stronger space localization properties than their bandlimited counterparts. Roughly spoken, this is due to the fact that bandlimited kernels can be represented as finite sums of polynomials and therefore – though strongly smoothed compared to polynomial functions – tend to oscillate. In contrast, non-bandlimited kernels cannot be displayed as finite sums of polynomials and hence yield a stronger space localization. This fact helps us to find a suitable characterization and categorization of the trial functions for modelling and approximation (cf. [29]): Fourier methods (in terms of scalar/vector spherical harmonics, for example) are the canonical starting point to obtain an

approximation of low frequency contributions (global modelling), while band-limited kernel functions can be used for the intermediate cases between long and short wavelengths (global to regional modelling). Due to their extreme space localization, non-bandlimited kernels can be utilized to deal with short wavelength phenomena (local modelling). Table 1 sketches this categorization of trial functions; the left hand side represents ideal frequency but no space localization and appoints polynomial functions as the appropriate trial functions. The right hand side symbolizes no frequency but ideal space localization and shows that Dirac functionals exhibit these characteristics. In between, tending from no to ideal space localization and, correspondingly, from ideal to no frequency localization, the bandlimited and non-bandlimited kernels are situated.

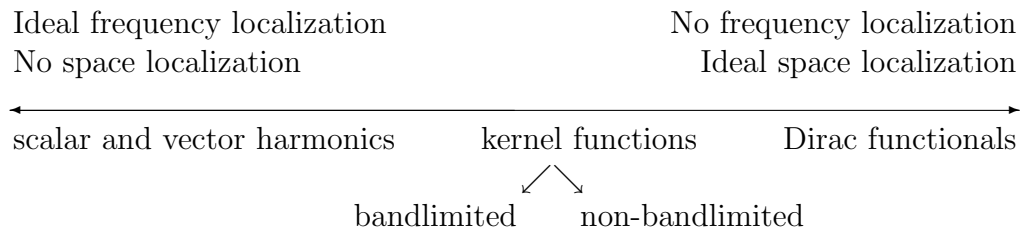


Table 1: The uncertainty principle.

Most data show correlation in space as well as in frequency, and the kernel functions with their simultaneous space and frequency localization allow for the efficient detection and approximation of essential features in the data by only using fractions of the original information (decorrelation). Using kernels at different scales (*multiscale modelling*), the corresponding approximation techniques can be constructed as to be suitable for the particular data situation. One method of multiscale modelling, i.e. based on kernel functions at different scales, are spline techniques in terms of the respective kernels. In analogy to the methods known in Earth's gravitational potential determination for example (cf. [25, 26]), harmonic spline concepts have been introduced for the geomagnetic case by [99]. Arguably, the main drawback of spline interpolation or smoothing of satellite geomagnetic data is that to each datum there corresponds a linear equation for determining the spline coefficients. Hence, due to the huge amount of data available from satellite surveys, the occurring linear systems are of high dimensions and, additionally, almost always ill-conditioned. Consequently, sophisticated solvers need to be applied. One such method is a certain variant of domain decomposition methods for such spline systems, called Multiplicative Schwartz Alternating Algorithm (see e.g. [37, 51, 56]), which significantly reduces both, runtime and memory requirements. It should also be mentioned that in [50] a special fast multipole method (FMM) is developed which is also able to accelerate an iterative solver for certain spline systems. Spline methods, however, are not the subject of this thesis.

In this thesis we are concerned with *wavelet techniques*, i.e. multiscale methods that are based on certain classes of kernel functions, the so-called *wavelets*. It is an essential characteristic of wavelet techniques that they are able to realize a *multiresolution analysis*, i.e. the function (data) space under consideration is decomposed into a nested sequence of approximating subspaces, so-called *scale spaces*. In other words, suitably constructed wavelets admit a basis property in certain function spaces the elements of which – the data functions

– admit a series representation in terms of a structured sequence of kernels at different positions and at different scales (*multiscale approximation*). It is thus possible to break up complicated functions like the geomagnetic field, electric current densities or geopotentials, into different pieces and to study these pieces separately. Consequently, the efficiency of wavelets lies in the fact that only a few wavelet coefficients are needed in areas where the data is smooth, and in regions where the data exhibits more complicated features higher resolution approximations can be derived by 'zooming-in' with more and more wavelets of higher scales and consequential stronger space-localization. To be more concrete, the procedure of multiscale approximation with wavelets is as follows. Starting from a sequence of certain kernels, so-called *scaling functions*, the multiresolution analysis of the function space under consideration is obtained in terms of the corresponding scale spaces. In each of these scale spaces an approximation of the function under consideration is constructed. For increasing scales, the approximation improves and the information contained on coarse levels is also contained in all levels of approximation above. The difference between two levels of approximation, i.e. the additional information we gain going from one scale space to the subsequent one, is called the *detail information* and is contained in what is called the *detail spaces*. The wavelets serve as basis functions in the detail spaces and consequently the function (signal) under consideration can be displayed using a combined representation in terms of scaling functions and wavelets. In spectral language, scaling functions help to build up low-pass filters while wavelets can be used to construct appropriate band-pass filters. [29, 30] extensively deal with this subject in a general context while [9, 11, 81] apply vectorial wavelet techniques to the problem of geomagnetic field modelling.

The present thesis has to be seen in the context summarized above. In the course of this thesis a comprehensive theoretical framework for the application of multiscale methods in space-borne magnetometry is established and examined from a mathematical point of view. Based on a construction principle for scalar and vectorial wavelet techniques in separable Hilbert spaces the discussed subjects include multiscale signal-to-noise thresholding, a wavelet approach to crustal field determination and downward continuation, a wavelet-parametrization of the magnetic field in Mie representation and, last but not least, simultaneous time- and space-dependent multiscale approximation. Numerical applications illustrate some of the introduced approaches and demonstrate the applicability and practicability of the proposed wavelet methods. It should be made clear that the numerical examples presented here are not intended to be detailed physical case studies but ought to be seen as the starting point for such research. A short outline of the thesis is presented next.

Chapter 1 introduces some basic notations and relations which we are going to use throughout the thesis. Additionally, a couple of well-known results useful for an easy understanding of the subsequent discussions are briefly recapitulated. Topics include reproducing kernel Hilbert spaces and splines, scalar and vector spherical harmonics, inner and outer harmonics, the Helmholtz and the Mie representation of vector fields as well as a short summary of inverse problems and their regularization.

In Chapter 2 a general approach to the theory and algorithmic aspects of wavelets in separable Hilbert spaces is presented. In Section 2.1 we start with the introduction of a scalar theory of multiscale approximation. Having the theoretical aspects at hand, we turn to some

special realizations of scalar wavelets, i.e. Legendre wavelets and scalar spherical wavelets, which will be of importance in later chapters. Section 2.2 deals with the extension of the scalar concept to the multiresolution analysis of vector fields. Spherical vectorial wavelets are presented as a certain example which turns out to be helpful for later considerations. The formulation of both, the scalar as well as the vectorial techniques, is based on the Fourier theory in the respective Hilbert spaces such that the results can easily be interpreted in terms of conventional methods.

We have to assume that, like every physical measurement, the geomagnetic satellite data are to some extent noisy. Within the context of multiresolution analysis it is therefore reasonable to think of an appropriate multiscale technique to denoise the satellite observations. The method should maintain the multiscale character of our approaches, i.e. it should be possible to deal with noise that spatially changes its frequency behaviour. This is the subject of Chapter 3. As far as (spherical) scalar fields are concerned, we recapitulate the necessary spectral theory which is then generalized to the concept of multiscale signal-to-noise thresholding in Section 3.1. Influenced by the results of the scalar case we extend the considerations to (spherical) vectorial data sets in Section 3.2. In order to do so, we first develop a spectral framework which then serves as a starting point for a generalization to a multiscale method in terms of so-called tensor radial basis functions. Though numerically difficult to handle, this tensor based approach is the canonical extension of the scalar technique. In order to obtain a multiscale method that is easily applicable, we then derive a technique in terms of vector spherical wavelets and show its equivalence to the tensor results. The chapter is completed with a numerical study illustrating the application of the vector based method to a noisy (synthetic) data set.

As far as crustal field determination is concerned, multiscale techniques are of great importance, too. Crustal field signatures are of comparatively small spatial extent and therefore it is reasonable to avoid global trial functions and choose a modelling technique that can cope with the regional features. Apart from this challenge there is the problem of *downward continuation*, i.e. calculating crustal field contributions at the Earth's surface from the vectorial data at satellite altitude. Since the magnetic signatures are exponentially smoothed out and never free of noise, this problem is known to be an *ill-posed* problem that needs proper means of regularization. In order to get a general multiscale method for the downward continuation of crustal field contributions fitting completely in the multiscale formalism of this thesis, we present in Chapter 4 a formulation of the problem in terms of integral equations which are then to be solved by so-called *regularization wavelets*. This leads to regularizations of the occurring integral equations within a multiresolution analysis where the regularization parameter plays the role of the scale in the usual wavelet approach. Consequently, a space dependent regularization is obtained mirroring the regional structure of the crustal field and enabling us to perform regional as well as global computations of spatially varying resolution. Since we derive the singular systems of the appearing integral operators explicitly, the regularization wavelets can be appropriately designed for every single integral equation under consideration. The formalism will first be introduced in spherical approximation, i.e. assuming that the radial variations of the satellite are negligible. In a second step a combined spline and wavelet approach will be presented that can incorporate the altitude variations of the satellite into the context of the integral equations. A numerical example will be given

that illustrates global as well as regional crustal field approximations at the mean Earth's surface from one month of CHAMP vector data.

The Mie representation for the geomagnetic field has the advantage that it can equally be applied in regions of vanishing as well as non-vanishing electric current densities. As we have already mentioned, it is common practise to deal with this subject in terms of a spherical harmonic parametrization, i.e. the Mie scalars of the magnetic field and of the corresponding electric current densities are expanded into a series of spherical harmonics. The global support of the spherical harmonics might limit the applicability of this approach, however, since it cannot suitably cope with current densities (and the corresponding magnetic effects) that vary rapidly with longitude or latitude, or that are confined to certain regions. In Chapter 5 we derive a *wavelet-parametrization* of the magnetic field in Mie representation which is able to reflect the various levels of space localization in form of a multiresolution analysis of the electric currents or the magnetic field, respectively. Starting point of the treatment is an expansion of the Mie scalars in terms of scalar wavelets, which then soon leads to a parametrization of the Mie representation in terms of vectorial kernel functions. The chapter is completed with a numerical application showing the global and regional determination of radial current densities from given sets of vectorial MAGSAT data.

Chapter 6, finally, deals with the subject of time-space dependent multiscale modelling of (spherical) vector fields. We assume that time-dependent vector fields can be expanded in terms of vector spherical harmonics with time-dependent Fourier coefficients. This enables us to derive two different variants of time-space dependent modelling. Variant 1, presented in Section 6.1, combines separate multiscale techniques for the temporal as well as the spatial domain. To be more concrete, Legendre wavelets and vector spherical wavelets are separately used for multiscale approximation in the temporal and the spatial domain, respectively, and the results are suitably combined to get a time-space dependent approach. The second variant, presented in Section 6.2, introduces time-space wavelets in tensor-product form. This means that Legendre wavelets and vector spherical wavelets are suitably combined to create a new set of time- and space-dependent wavelets which then can be applied to deal with time-dependent vector fields within a multiscale framework.

Chapter 1

Preliminaries

The main goal of this chapter is to provide the essential mathematical tools building the groundwork for our later considerations. We start by introducing some basic notation that will be used throughout this thesis.

1.1 Notations and Relations

The set of all integers, positive integers and non-negative integers is denoted by \mathbb{Z} , \mathbb{N} , and \mathbb{N}_0 respectively. \mathbb{R} is the set of real numbers and $\mathbb{R}^3 = \mathbb{R} \times \mathbb{R} \times \mathbb{R}$ denotes the real, three-dimensional Euclidean space with the canonical orthonormal basis ε^1 , ε^2 and ε^3 .

During the course of this thesis, we will constantly be confronted with scalar, vector and tensor fields. In order to avoid notational complications we will, unless stated otherwise, use the following scheme: Scalar Fields will be denoted by capital roman letters (F, G , etc.), vector fields are symbolized by lower-case roman letters (f, g , etc.) and tensor fields are represented by boldface roman letters (\mathbf{f}, \mathbf{g} , etc.).

Let now $x, y \in \mathbb{R}^3$, with $x = (x_1, x_2, x_3)^T$ and $y = (y_1, y_2, y_3)^T$. The inner, vector and tensor product, respectively, are defined by

$$\begin{aligned}x \cdot y &= x^T y = \sum_{i=1}^3 x_i y_i, \\x \wedge y &= (x_2 y_3 - x_3 y_2, x_3 y_1 - x_1 y_3, x_1 y_2 - x_2 y_1)^T, \\x \otimes y &= x y^T = \begin{pmatrix} x_1 y_1 & x_1 y_2 & x_1 y_3 \\ x_2 y_1 & x_2 y_2 & x_2 y_3 \\ x_3 y_1 & x_3 y_2 & x_3 y_3 \end{pmatrix}.\end{aligned}\tag{1.1}$$

As usual, a *second order tensor* $\mathbf{f} \in \mathbb{R}^{3 \times 3}$ is understood to be a linear mapping assigning to each vector $x \in \mathbb{R}^3$ a vector $y \in \mathbb{R}^3$. The tensor \mathbf{f} can be represented by its cartesian

components $F_{ij} \in \mathbb{R}$ defined by

$$F_{ij} = (\varepsilon^i)^T(\mathbf{f}\varepsilon^j) = \varepsilon^i \cdot (\mathbf{f}\varepsilon^j)$$

such that $y = \mathbf{f}x$ is equivalent to

$$y \cdot \varepsilon^i = \sum_{j=1}^3 F_{ij}(x \cdot \varepsilon^j).$$

In what follows, $tr(\mathbf{f})$ denotes the trace, and $\det(\mathbf{f})$ the determinant of \mathbf{f} . The transpose \mathbf{f}^T of \mathbf{f} is the unique tensor satisfying

$$(\mathbf{f}y) \cdot x = y \cdot (\mathbf{f}x)$$

for all $x, y \in \mathbb{R}^3$. It is also very useful to know that the tensor product $x \otimes y$, $x, y \in \mathbb{R}^3$ (see (1.1)) is the tensor that assigns to each vector $u \in \mathbb{R}^3$ the vector $(y \cdot u)x$, i.e.

$$(x \otimes y)u = (y \cdot u)x$$

for every $u \in \mathbb{R}^3$.

Moreover, we can define an inner product of two second order tensors $\mathbf{f}, \mathbf{g} \in \mathbb{R}^{3 \times 3}$ by

$$\mathbf{f} \cdot \mathbf{g} = tr(\mathbf{f}^T \mathbf{g}) = \sum_{i=1}^3 \sum_{j=1}^3 F_{ij} G_{ij} \quad (1.2)$$

and the associated norm via

$$|\mathbf{f}| = (\mathbf{f} \cdot \mathbf{f})^{1/2}.$$

Using (1.2) it can easily be seen that, for any tensor $\mathbf{f} \in \mathbb{R}^{3 \times 3}$ and any pair $x, y \in \mathbb{R}^3$, the relation

$$x \cdot (\mathbf{f}y) = \mathbf{f} \cdot (x \otimes y) \quad (1.3)$$

holds true. Moreover we have

$$(x \otimes y)\mathbf{f} = x \otimes \mathbf{f}^T y.$$

Furthermore, for vectors $x, y, w, z \in \mathbb{R}^3$ it can be seen that

$$(x \otimes y)(w \otimes z) = (y \cdot w)(x \otimes z).$$

Using the canonical orthonormal Euclidean basis $\varepsilon^1, \varepsilon^2, \varepsilon^3$ it holds true that

$$(\varepsilon^i \otimes \varepsilon^j) \cdot (\varepsilon^k \otimes \varepsilon^l) = \delta_{ik} \delta_{jl},$$

such that the nine tensors $\varepsilon^i \otimes \varepsilon^j$ are orthonormal (note that δ_{ik} denotes the Kronecker symbol). Moreover, it follows that

$$\sum_{i=1}^3 \sum_{j=1}^3 (F_{ij} \varepsilon^i \otimes \varepsilon^j)x = \sum_{i=1}^3 \sum_{j=1}^3 F_{ij}(x \cdot \varepsilon^j)\varepsilon^i = \mathbf{f}x,$$

thus $\mathbf{f} \in \mathbb{R}^{3 \times 3}$ with

$$\mathbf{f} = \sum_{i=1}^3 \sum_{j=1}^3 F_{ij} \varepsilon^i \otimes \varepsilon^j.$$

In particular, the identity tensor $\mathbf{i} \in \mathbb{R}^{3 \times 3}$ is given by

$$\mathbf{i} = \sum_{i=1}^3 \varepsilon^i \otimes \varepsilon^i.$$

Furthermore, it is easy to see that

$$\text{tr}(x \otimes y) = x \cdot y, \quad x, y \in \mathbb{R}^3,$$

and, for $\mathbf{f}, \mathbf{g}, \mathbf{h} \in \mathbb{R}^{3 \times 3}$,

$$\mathbf{f} \cdot (\mathbf{g}\mathbf{h}) = (\mathbf{g}^T \mathbf{f}) \cdot \mathbf{h} = (\mathbf{f}\mathbf{h}^T) \cdot \mathbf{g},$$

as well as

$$(\mathbf{f}x) \cdot (\mathbf{g}y) = (\mathbf{f}^T \mathbf{g}) \cdot (x \otimes y). \quad (1.4)$$

Any element $x \in \mathbb{R}^3$ with $|x| \neq 0$ may be written in the form $x = r\xi$, where $r = |x|$ is the distance from x to the origin 0 and $\xi \in \mathbb{R}^3$, $\xi = (\xi_1, \xi_2, \xi_3)^T$ is the uniquely determined directional unit vector of x . A sphere of radius R centered in the origin, i.e. the set $\{x \in \mathbb{R}^3 : |x| = R\}$ will be denoted by Ω_R . In particular, $\Omega (= \Omega_1)$ is the *unit sphere* in \mathbb{R}^3 . We set Ω^{int} for the 'inner space' of Ω , while Ω^{ext} denotes the 'outer space' of Ω .

Any point $\xi \in \Omega$ can be represented in *polar coordinates* as follows:

$$\xi = \varepsilon^3 t + \sqrt{1-t^2} (\varepsilon^1 \cos \varphi + \varepsilon^2 \sin \varphi), \quad (1.5)$$

$$-1 \leq t \leq 1, \quad 0 \leq \varphi < 2\pi, \quad t = \cos \vartheta$$

(ϑ : latitude, φ : longitude, t : polar distance) or equivalently

$$\xi = \varepsilon^1 \sin \vartheta \cos \varphi + \varepsilon^2 \sin \vartheta \sin \varphi + \varepsilon^3 \cos \vartheta.$$

Note that in the geophysical literature ϑ is sometimes also referred to as the co-latitude, depending on the parametrization of the angle. The unit vectors corresponding to the spherical polar coordinates will be denoted by ε^r , ε^φ and $\varepsilon^t = -\varepsilon^\vartheta$ and form a so-called local moving triad.

The relation of the local system to the canonical basis is given via

$$\varepsilon^r(\varphi, t) = \varepsilon^1 \sqrt{1-t^2} \cos \varphi + \varepsilon^2 \sqrt{1-t^2} \sin \varphi + \varepsilon^3 t,$$

$$\varepsilon^\varphi(\varphi, t) = -\varepsilon^1 \sin \varphi + \varepsilon^2 \cos \varphi,$$

$$\varepsilon^t(\varphi, t) = -\varepsilon^1 t \cos \varphi - \varepsilon^2 t \sin \varphi + \varepsilon^3 \sqrt{1-t^2}.$$

One can express the canonical basis vectors of \mathbb{R}^3 in terms of $\varepsilon^r, \varepsilon^\varphi, \varepsilon^t$ in the following sense:

$$\begin{aligned}\varepsilon^1 &= \varepsilon^r(\varphi, t)\sqrt{1-t^2}\cos\varphi - \varepsilon^\varphi(\varphi, t)\sin\varphi - \varepsilon^t(\varphi, t)t\cos\varphi, \\ \varepsilon^2 &= \varepsilon^r(\varphi, t)\sqrt{1-t^2}\sin\varphi + \varepsilon^\varphi(\varphi, t)\cos\varphi - \varepsilon^t(\varphi, t)t\sin\varphi, \\ \varepsilon^3 &= \varepsilon^r(\varphi, t)t + \varepsilon^t(\varphi, t)\sqrt{1-t^2}.\end{aligned}$$

See also the Appendix for some information on geophysical nomenclature concerning spherical coordinates.

In terms of polar coordinates (1.5) the gradient ∇ in \mathbb{R}^3 reads

$$\nabla_x = \xi \frac{\partial}{\partial r} + \frac{1}{r} \nabla_\xi^*,$$

where the horizontal part ∇^* is the *surface gradient* on the unit sphere Ω . Moreover, the Laplace operator $\Delta = \nabla \cdot \nabla$ in \mathbb{R}^3 has the representation

$$\Delta_x = \left(\frac{\partial}{\partial r} \right)^2 + \frac{2}{r} \frac{\partial}{\partial r} + \frac{1}{r^2} \Delta_\xi^*,$$

where Δ^* is the *Beltrami operator* on the unit sphere Ω . The *surface curl gradient* L^* on the unit sphere can be calculated from ∇^* by the relation $L_\xi^* = \xi \wedge \nabla_\xi^*$, $\xi \in \Omega$.

It is worth mentioning that the operators ∇^* , L^* and Δ^* will always be used in coordinate-free representation throughout this thesis, thereby avoiding any singularities at the poles. Nevertheless, for the convenience of the reader, we give a list of their expressions in local coordinates (see [30], for example):

$$\begin{aligned}\nabla_\xi^* &= \varepsilon^\varphi \frac{1}{\sin\vartheta} \frac{\partial}{\partial \varphi} + \varepsilon^\vartheta \frac{\partial}{\partial \vartheta}, \\ L_\xi^* &= \varepsilon^\varphi \frac{\partial}{\partial \vartheta} - \varepsilon^\vartheta \frac{1}{\sin\vartheta} \frac{\partial}{\partial \varphi}, \\ \Delta_\xi^* &= \frac{1}{\sin\vartheta} \frac{\partial}{\partial \vartheta} \sin\vartheta \frac{\partial}{\partial \vartheta} + \frac{1}{\sin^2\vartheta} \frac{\partial^2}{\partial \varphi^2}.\end{aligned}$$

A variety of function spaces will be needed in this thesis. Let $\mathcal{C}(\Sigma)$ be the set of all real and continuous functions defined on the domain $\Sigma \subset \mathbb{R}^3$ ($F : \Sigma \rightarrow \mathbb{R}$), equipped with the norm

$$\|F\|_{\mathcal{C}(\Sigma)} = \sup_{x \in D} |F(x)|.$$

A function is said to be of class $\mathcal{C}^{(k)}(\Sigma)$, $0 \leq k < \infty$, if it possesses k continuous derivatives on Σ . If $\Sigma \subset \mathbb{R}^3$ is a measurable subset, the set of scalar functions $F : \Sigma \rightarrow \mathbb{R}$ which are

measurable and for which

$$\|F\|_{\mathcal{L}^p(\Sigma)} = \left(\int_{\Sigma} |F(x)|^p d\omega(x) \right)^{\frac{1}{p}} < \infty, \quad 1 \leq p < \infty,$$

is denoted by $\mathcal{L}^p(\Sigma)$.

The space $\mathcal{L}^2(\Omega_R)$, equipped with the inner product

$$(F_1, F_2)_{\mathcal{L}^2(\Omega_R)} = \int_{\Omega_R} F_1(x) F_2(x) d\omega_R(x)$$

forms a Hilbert space. In addition, $\mathcal{L}^2(\Omega_R)$ is the completion of $\mathcal{C}^{(\infty)}(\Omega_R)$ with respect to the norm $\|\cdot\|_{\mathcal{L}^2(\Omega_R)}$, i.e. $\mathcal{L}^2(\Omega_R) = \overline{\mathcal{C}^{(\infty)}(\Omega_R)}^{\|\cdot\|_{\mathcal{L}^2(\Omega_R)}}$. Observe that for the rest of the thesis all integrals are understood in the Lebesgue sense.

Remark 1.1 *Any function of the form*

$$\begin{aligned} \tilde{G}_\xi : \Omega &\rightarrow \mathbb{R}, \quad \xi \in \Omega \text{ fixed} \\ \eta &\mapsto \tilde{G}_\xi(\eta) = G(\xi \cdot \eta), \quad \eta \in \Omega \end{aligned}$$

is called a zonal or radial basis function. The set of all zonal functions is isomorphic to the set of all functions $G : [-1, 1] \rightarrow \mathbb{R}$, hence one can regard $\mathcal{C}^{(k)}[-1, 1]$ and $\mathcal{L}^{(2)}[-1, 1]$, equipped with the corresponding norms, as subspaces of $\mathcal{C}^{(k)}(\Omega)$ and $\mathcal{L}^{(2)}(\Omega)$. The value of any zonal function $\tilde{G}_\xi(\eta)$ depends only on the spherical distance between ξ and η . This is why zonal functions are frequently called radial basis functions or, sometimes, isotropic functions.

It is very important for the main concept of this thesis that radial basis functions show an important principle for many applications on the sphere, namely rotational invariance. By taking into account the zonal functions, i.e. functions of axial symmetry, and moving their axes on the sphere, modern techniques such as spline approximation and multiscale approximation by spherical wavelets (cf. [25, 26, 43, 45, 46], for example) become possible.

Some useful relations concerning the application of the surface gradient and the surface curl gradient to radial basis functions can be given (cf. [30]), i.e. if $F \in \mathcal{C}^{(1)}[-1, 1]$, then

$$\nabla_\xi^* F(\xi \cdot \eta) = F'(\xi \cdot \eta)(\eta - (\xi \cdot \eta)\xi), \quad (1.6)$$

$$L_\xi^* F(\xi \cdot \eta) = F'(\xi \cdot \eta)\xi \wedge \eta, \quad (1.7)$$

where $\xi, \eta \in \Omega$. These relations are very important when, in later chapters, explicit representations of kernel functions are derived.

The function spaces for vector-valued spherical functions are defined in analogy to the scalar case, i.e. $\mathcal{C}^{(k)}(\Sigma)$, $0 \leq k < \infty$, denotes the space of k -times continuously differentiable vector

fields on D and $l^2(\Sigma)$ represents the space of square-integrable spherical vector fields on Σ . As in the scalar case, equipped with the inner product

$$(f, g)_{l^2(\Omega_R)} = \int_{\Omega_R} f(y) \cdot g(y) \, d\omega_R(y), \quad f, g \in l^2(\Omega_R)$$

and the corresponding norm

$$\|f\|_{l^2(\Omega_R)} = \left(\int_{\Omega_R} |f(y)|^2 \, d\omega_R(y) \right)^{1/2}, \quad f \in l^2(\Omega_R)$$

the space $l^2(\Omega_R)$ is a Hilbert space. As in the scalar case

$$l^2(\Omega_R) = \overline{c(\Omega_R)}^{\|\cdot\|_{l^2(\Omega_R)}}$$

holds true.

1.2 Reproducing Kernel Hilbert Spaces and Splines

Reproducing kernel Hilbert spaces as well as spline techniques in such spaces play an important role in many branches of constructive approximation. Though the explicit use of such methods in this thesis is of minor importance, some results and aspects will nevertheless be needed. In what follows we present a very brief summary of this subject and we recommend [6, 16, 25, 27, 29, 30] and [44] for further reading.

Definition 1.2 *Let $\Sigma \subset \mathbb{R}^n$ and let \mathcal{H} be a Hilbert space of functions $F : \Sigma \rightarrow \mathbb{R}$, equipped with the inner product $(\cdot, \cdot)_{\mathcal{H}}$. Then any function $K_{\mathcal{H}}(x, y)$ of two variables on Σ is called reproducing kernel function for the space \mathcal{H} , if*

- for each fixed $x \in \Sigma$, $K_{\mathcal{H}}(x, \cdot)$ is a member of \mathcal{H} ,
- for every function $F \in \mathcal{H}$ and for every $y \in \Sigma$, the reproducing property

$$F(x) = (F(y), K_{\mathcal{H}}(x, y))_{\mathcal{H}}$$

holds.

The following theorem summarizes the most important results from the theory of reproducing kernel Hilbert spaces (cf. [6, 16]).

Theorem 1.3 *Suppose $(\mathcal{H}, (\cdot, \cdot)_{\mathcal{H}})$ to be a Hilbert space of functions defined on $\Sigma \subset \mathbb{R}^n$, then the following statements hold true.*

- (1) \mathcal{H} possesses a reproducing kernel if and only if for each $y \in \Sigma$ the linear functional $\mathcal{L}_y(F) = F(y)$ is bounded, i.e. $|\mathcal{L}_y(F)| \leq c_y \|F\|_{\mathcal{H}}$ holds for some constant c_y and for all $F \in \mathcal{H}$.
- (2) If \mathcal{H} has a reproducing kernel then the kernel is unique.
- (3) If \mathcal{H} has a reproducing kernel and the kernel is bounded on the domain $\Sigma \subset \mathbb{R}^n$, then the Fourier expansion of a function in \mathcal{H} converges uniformly to the function.
- (4) Let \mathcal{H} have a reproducing kernel $K_{\mathcal{H}}(\cdot, \cdot)$ and, furthermore, let \mathcal{L} be a bounded linear functional defined on \mathcal{H} . Then $\mathcal{L}_x(K_{\mathcal{H}}(x, \cdot))$ is the representer of \mathcal{L} and

$$\mathcal{L}(F) = (F(y), \mathcal{L}_x(K_{\mathcal{H}}(x, y)))_{\mathcal{H}}$$

holds for all $F \in \mathcal{H}$.

- (5) If \mathcal{H} has a reproducing kernel and if $\{\mathcal{L}_x^1(K_{\mathcal{H}}(x, y)), \mathcal{L}_x^2(K_{\mathcal{H}}(x, y)), \dots\}$ is a complete sequence of functions, where \mathcal{L}_x^n , $n = 1, 2, \dots$ are bounded linear functionals defined on \mathcal{H} , then

$$\overline{\text{span}_{n=1,2,\dots}\{\mathcal{L}_x^n(K_{\mathcal{H}}(x, y))\}}^{\|\cdot\|_{\mathcal{H}}} = \mathcal{H}.$$

The last theorem enables us to formulate the solution of the interpolation problem in reproducing kernel Hilbert spaces.

In what follows, \mathcal{H} is supposed to be a reproducing kernel Hilbert space of functions defined on a subset $\Sigma \subset \mathbb{R}^n$. The interpolation problem in \mathcal{H} is given as follows: For $F \in \mathcal{H}$ and a given set of linearly independent bounded linear functionals $\mathcal{L}_1, \dots, \mathcal{L}_N$ on \mathcal{H} the smallest interpolant in the \mathcal{H} -topology, i.e.

$$\|S\|_{\mathcal{H}} = \inf_{H \in \mathcal{I}_{\mathcal{L}_1, \dots, \mathcal{L}_N}^F} \|H\|_{\mathcal{H}}, \quad (1.8)$$

is wanted. Note that $\mathcal{I}_{\mathcal{L}_1, \dots, \mathcal{L}_N}^F$ denotes the set of all possible interpolants and is given by

$$\mathcal{I}_{\mathcal{L}_1, \dots, \mathcal{L}_N}^F = \{H \in \mathcal{H} \mid \mathcal{L}_i F = \mathcal{L}_i H, i = 1, \dots, N\}.$$

The uniquely determined solution of the interpolation problem (1.8) can always be represented as a spline function in \mathcal{H} . The following definition clarifies what is meant by that.

Definition 1.4 Suppose that $\mathcal{L}_1, \dots, \mathcal{L}_N$ denote N linearly independent bounded linear functionals on a reproducing kernel Hilbert space \mathcal{H} with reproducing kernel $K_{\mathcal{H}}(\cdot, \cdot)$. Then any function of the form

$$S(x) = \sum_{i=1}^N a_i \mathcal{L}_i K_{\mathcal{H}}(\cdot, x), \quad (1.9)$$

is called an \mathcal{H} -spline relative to the system $\mathcal{L}_1, \dots, \mathcal{L}_N$. The space of all \mathcal{H} -splines relative to $\mathcal{L}_1, \dots, \mathcal{L}_N$ is an N -dimensional linear subspace of \mathcal{H} and is denoted by $\mathcal{S}_{\mathcal{H}}(\mathcal{L}_1, \dots, \mathcal{L}_N)$.

The following theorem yields the main result of spline theory.

Theorem 1.5 *Let $F \in \mathcal{H}$ be given. The interpolation problem (1.8) is uniquely solvable and its solution $S_{\mathcal{L}_1, \dots, \mathcal{L}_N}^F$ is an \mathcal{H} -spline relative to the system $\mathcal{L}_1, \dots, \mathcal{L}_N$, i.e. $S_{\mathcal{L}_1, \dots, \mathcal{L}_N}^F \in \mathcal{S}_{\mathcal{H}}(\mathcal{L}_1, \dots, \mathcal{L}_N) \cap \mathcal{I}_{\mathcal{L}_1, \dots, \mathcal{L}_N}^F$. The unique solution is given in the form (1.9), where the coefficients a_1, \dots, a_N satisfy the linear equations*

$$\sum_{i=1}^N a_i \mathcal{L}_i \mathcal{L}_j K_{\mathcal{H}}(\cdot, \cdot) = \mathcal{L}_j F, \quad j = 1, \dots, N.$$

1.3 Scalar and Vector Spherical Harmonics

Scalar as well as vector spherical harmonics are commonly used functions to cope with problems of scalar or vectorial nature and spherical geometry. While the scalar spherical harmonics form a complete orthonormal system in the Hilbert space $\mathcal{L}^2(\Omega)$ of square-integrable spherical scalar functions, the vector spherical harmonics are a complete orthonormal set in the space $l^2(\Omega)$ of square-integrable spherical vector fields. A Fourier theory in the aforementioned function spaces can thus be based on scalar and vector spherical harmonics.

The approach to scalar as well as vector spherical harmonics presented here is based on [30]. We start by introducing scalar spherical harmonics as restrictions of homogeneous harmonic polynomials in \mathbb{R}^3 to the unit sphere Ω . More explicitly, let $H_n : \mathbb{R}^3 \rightarrow \mathbb{R}$ be a homogeneous harmonic polynomial of degree n , then the restriction $Y_n = H_n|_{\Omega}$ is called a *scalar spherical harmonic of degree n* (we will drop the adjective 'scalar' as long as no confusion is likely to arise). The space of all spherical harmonics of degree n is denoted by $Harm_n(\Omega)$. This space is of dimension $2n + 1$, i.e. $d(Harm_n(\Omega)) = 2n + 1$. Spherical harmonics of different degrees are orthogonal in the sense of the $\mathcal{L}^2(\Omega)$ -inner product

$$(Y_n, Y_m)_{\mathcal{L}^2(\Omega)} = \int_{\Omega} Y_n(\xi) Y_m(\xi) d\omega(\xi) = 0, \quad n \neq m.$$

A main result of the theory of spherical harmonics is the fact that any spherical harmonic Y_n , $n \in \mathbb{N}_0$, is an infinitely often differentiable eigenfunction of the Beltrami operator corresponding to the eigenvalue $-n(n + 1)$, $n \in \mathbb{N}_0$. To be specific,

$$\Delta_{\xi}^* Y_n(\xi) = (\Delta^*)^{\wedge}(n) Y_n(\xi), \quad \xi \in \Omega, \quad Y_n \in Harm_n(\Omega),$$

where the 'spherical symbol' $\{(\Delta^*)^{\wedge}(n)\}_{n \in \mathbb{N}_0}$ of the Beltrami operator Δ^* is given by $(\Delta^*)^{\wedge}(n) = -n(n + 1)$, $n \in \mathbb{N}_0$. As we have already mentioned, the space $Harm_n(\Omega)$ is $(2n+1)$ -dimensional. Therefore, throughout the remainder of this work, we denote by $\{Y_{n,k}\}_{k=1, \dots, 2n+1}$ a (maximal) complete orthonormal system in the space $Harm_n(\Omega)$ with respect to $(\cdot, \cdot)_{\mathcal{L}^2(\Omega)}$. It is clear that $\{Y_{n,k}^{\rho_1}\}_{k=1, \dots, 2n+1}$ with $Y_{n,k}^{\rho_1} = 1/\rho_1 Y_{n,k}$ denotes an $\mathcal{L}^2(\Omega_{\rho_1})$ -orthonormal system.

A certain kind of functions which is closely related to the spherical harmonics are the so-called Legendre polynomials. Legendre polynomials can uniquely be defined by means of an eigenvalue equation with respect to the Legendre operator

$$L_t = (d/dt) (1 - t^2) (d/dt).$$

More precisely, the *Legendre polynomial* $P_n : [-1, +1] \rightarrow \mathbb{R}$ of degree n is defined as the unique infinitely often differentiable eigenfunction of the Legendre operator L_t corresponding to the eigenvalue $-n(n+1)$, i.e.

$$L_t P_n(t) = -n(n+1) P_n(t), \quad t \in [-1, +1],$$

which satisfies $P_n(1) = 1$. It is helpful to know that the Legendre operator L_t is that part of the Beltrami operator that is solely dependent on the latitude. The Legendre polynomials are orthogonal with respect to the $\mathcal{L}^2([-1, +1])$ -inner product, i.e.

$$2\pi \int_{-1}^{+1} P_n(t) P_m(t) dt = \delta_{nm} \frac{4\pi}{2n+1}.$$

The Legendre polynomial P_n has the explicit representation

$$P_n(t) = \sum_{s=0}^{\lfloor n/2 \rfloor} (-1)^s \frac{(2n-2s)!}{2^n (n-2s)! (n-s)! s!} t^{n-2s}, \quad t \in [-1, +1].$$

Another representation can be given using the Rodriguez's formula, to be more specific:

$$P_n(t) = \frac{1}{2^n n!} \left(\frac{d}{dt} \right)^n (t^2 - 1)^n, \quad t \in [-1, +1].$$

The system $\{P_n\}_{n \in \mathbb{N}_0}$ is a closed and complete set in $\mathcal{L}^2([-1, +1])$ (with respect to the norm $\|\cdot\|_{\mathcal{L}^2([-1, +1])}$). The series

$$\sum_{n=0}^{\infty} \frac{2n+1}{4\pi} G^\wedge(n) P_n$$

is called the *Legendre expansion* of G . The *Legendre coefficients* $G^\wedge(n)$, $n = 0, 1, \dots$ are given via

$$G^\wedge(n) = (G, P_n)_{\mathcal{L}^2([-1, +1])} = 2\pi \int_{-1}^{+1} G(t) P_n(t) dt.$$

For all $G \in \mathcal{L}^2([-1, +1])$ we have

$$\lim_{N \rightarrow \infty} \left\| G - \sum_{n=0}^N \frac{2n+1}{4\pi} G^\wedge(n) P_n \right\|_{\mathcal{L}^2([-1, +1])} = 0.$$

Legendre polynomials belong to the class of radial basis functions in the sense that $P_n(\xi \cdot \eta) : \eta \mapsto P_n(\xi \cdot \eta)$, $\xi \in \Omega$ fixed, $\eta \in \Omega$, is a zonal function. This is closely related to a famous theorem connecting the spherical harmonics on Ω with the univariate Legendre polynomials on the unit interval $[-1, 1]$, the so-called addition theorem of spherical harmonics:

Theorem 1.6 (*Addition Theorem*). Let $\{Y_{n,k}\}_{k=1,\dots,2n+1}$ be an orthonormal system of spherical harmonics with respect to $(\cdot, \cdot)_{\mathcal{L}^2(\Omega)}$ in $Harm_n(\Omega)$. Then

$$\sum_{k=1}^{2n+1} Y_{n,k}(\xi) Y_{n,k}(\eta) = \frac{2n+1}{4\pi} P_n(\xi \cdot \eta), \quad \xi, \eta \in \Omega.$$

The addition theorem is closely related to the fact that the Legendre polynomial (seen as zonal functions on the sphere) $P_n(\xi \cdot \cdot)$, is the only spherical harmonic of degree n that is invariant with respect to orthogonal transformations which leave $\xi \in \Omega$ fixed.

The series

$$\sum_{n=0}^{\infty} \sum_{k=1}^{2n+1} F^\wedge(n, k) Y_{n,k}$$

is called the *Fourier expansion* (or *spherical harmonic expansion*) of F with *Fourier* (or *spherical harmonic*) coefficients given by

$$F^\wedge(n, k) = \int_{\Omega} F(\xi) Y_{n,k}(\xi) d\omega(\xi),$$

$n = 0, 1, \dots; k = 1, \dots, 2n + 1$. For all $F \in \mathcal{L}^2(\Omega)$ we have

$$\lim_{N \rightarrow \infty} \left\| F - \sum_{n=0}^N \sum_{k=1}^{2n+1} F^\wedge(n, k) Y_{n,k} \right\|_{\mathcal{L}^2(\Omega)} = 0.$$

Denoting by $Harm_{p,\dots,q}(\Omega)$, $q \geq p \geq 0$ the space of all spherical harmonics of degree n with $p \leq n \leq q$. Then the orthogonality of spherical harmonics of different degrees yields

$$Harm_{p,\dots,q}(\Omega) = \bigoplus_{n=p}^q Harm_n(\Omega).$$

The dimension of $Harm_{p,\dots,q}(\Omega)$ is $\sum_{n=p}^q (2n+1)$ and, in particular, we have

$$d(Harm_{0,\dots,q}(\Omega)) = (q+1)^2.$$

If $Y_n \in Harm_n(\Omega)$, then

$$\frac{2n+1}{4\pi} \int_{\Omega} P_n(\xi \cdot \eta) Y_n(\eta) d\omega(\eta) = Y_n(\xi), \quad \xi \in \Omega.$$

In other words, $K_{Harm_n(\Omega)}(\cdot, \cdot) : \Omega \times \Omega \rightarrow \mathbb{R}$ defined by

$$K_{Harm_n(\Omega)}(\xi, \eta) = \frac{2n+1}{4\pi} P_n(\xi \cdot \eta), \quad (\xi, \eta) \in \Omega \times \Omega,$$

represents the unique reproducing kernel in $Harm_n(\Omega)$. Moreover,

$$K_{Harm_{p,\dots,q}(\Omega)}(\xi, \eta) = \sum_{n=p}^q \frac{2n+1}{4\pi} P_n(\xi \cdot \eta), \quad (\xi, \eta) \in \Omega \times \Omega$$

is the reproducing kernel in $Harm_{p,\dots,q}(\Omega)$.

The formula of Funk and Hecke,

$$\int_{\Omega} G(\xi \cdot \eta) Y_n(\eta) d\omega(\eta) = G^\wedge(n) Y_n(\xi), \quad \xi \in \Omega, \quad G \in \mathcal{L}^1[-1, +1],$$

establishes a connection between spherical harmonics and radial basis functions and – together with the reproducing kernel $K_{Harm_{p,\dots,q}(\Omega)}$ – founds the basis for the introduction of spherical singular integrals and spherical wavelets (cf. [30] and [45], for example).

As there exist infinitely many $\mathcal{L}^2(\Omega)$ -orthonormal systems in $Harm_n(\Omega)$, we present and illustrate, in Appendix A, one special example frequently used in geomagnetic applications. It is the system of Schmidt semi-normalized spherical harmonics in terms of Legendre functions (cf., e.g. [55]). A realization of a geomagnetic potential U in terms of this very system of spherical harmonics is also presented in Appendix A. A potential of this form will be used in later chapters.

For later use we now introduce the inner (outer) harmonics as the solution of the exterior (interior) Dirichlet problem in the interior Ω_R^{int} (exterior Ω_R^{ext}) of Ω_R corresponding to the \mathcal{L}^2 -boundary values $Y_{n,k}$ on Ω_R . The systems of *inner (outer) harmonics*, $\{H_{n,k}^{int}(R; \cdot)\}$ ($\{H_{n,k}^{ext}(R; \cdot)\}$), $n = 0, 1, \dots; k = 1, \dots, 2n+1$, of degree n defined by

$$H_{n,k}^{int}(R; x) = \frac{1}{R} \left(\frac{|x|}{R}\right)^n Y_{n,k}\left(\frac{x}{|x|}\right), \quad x \in \overline{\Omega_R^{int}}, \quad (1.10)$$

$$H_{n,k}^{ext}(R; x) = \frac{1}{R} \left(\frac{R}{|x|}\right)^{n+1} Y_{n,k}\left(\frac{x}{|x|}\right), \quad x \in \overline{\Omega_R^{ext}}, \quad (1.11)$$

satisfy the following properties:

- $H_{n,k}^{ext}(R; \cdot)$ is of class $C^{(\infty)}(\Omega_R^{ext})$.
- $H_{n,k}^{int}(R; \cdot)$ is of class $C^{(\infty)}(\Omega_R^{int})$.
- $H_{n,k}^{ext}(R; \cdot)$ satisfies Laplace's equation in Ω_R^{ext} , that is $\Delta_x H_{n,k}^{ext}(R; x) = 0$ for all $x \in \Omega_R^{ext}$.
- $H_{n,k}^{int}(R; \cdot)$ satisfies Laplace's equation in Ω_R^{int} , that is $\Delta_x H_{n,k}^{int}(R; x) = 0$ for all $x \in \Omega_R^{int}$.
- $H_{n,k}^{ext}(R; \cdot)|_{\Omega_R} = H_{n,k}^{int}(R; \cdot)|_{\Omega_R} = (1/R) Y_{n,k}$.
- $H_{n,k}^{ext}(R; \cdot)$ is regular at infinity, i.e. $|H_{n,k}^{ext}(R; x)| = \mathcal{O}(|x|^{-1})$ and $|\nabla_x H_{n,k}^{ext}(R; x)| = \mathcal{O}(|x|^{-2})$ as $|x| \rightarrow \infty$.

- $(H_{n,k}^i(R; \cdot), H_{p,q}^j(R; \cdot))_{\mathcal{L}^2(\Omega_R)} = \delta_{n,p} \delta_{k,q}$ for $i, j \in \{int, ext\}$.

(Note that in the case of $\Omega_R = \Omega$, we have $H_{n,k}^{int}(R; \cdot)|_{R=1} = H_{n,k}^{ext}(R; \cdot)|_{R=1} = Y_{n,k}$ for all $n = 0, 1, \dots; k = 1, \dots, 2n + 1$). Thus the system $\{Y_{n,k}^R\} = \{H_{n,k}^{ext}(R; \cdot)|_{\Omega_R}\} = \{H_{n,k}^{int}(R; \cdot)|_{\Omega_R}\}$ forms an orthonormal system in $\mathcal{L}^2(\Omega_R)$.

We proceed with the introduction of vector spherical harmonics. The approach to vector spherical harmonics as presented in this chapter allows a decomposition of square-integrable spherical vector fields into a normal and a tangential part, where the tangential field can further be split up into a curl-free and a divergence-free part. This turns out to be useful when dealing with the geomagnetic or the gravitational field, for example. In order to clarify the matters we introduce the projection operators p_{nor} and p_{tan} by

$$\begin{aligned} p_{nor}f(\xi) &= (f(\xi) \cdot \xi)\xi, \quad \xi \in \Omega, \quad f \in c(\Omega), \\ p_{tan}f(\xi) &= f(\xi) - p_{nor}f(\xi), \quad \xi \in \Omega, \quad f \in c(\Omega). \end{aligned}$$

These definitions can be extended to the case of square-integrable vector fields via

$$\begin{aligned} l_{nor}^2(\Omega) &= \{f \in l^2(\Omega) | f = p_{nor}f\}, \\ l_{tan}^2(\Omega) &= \{f \in l^2(\Omega) | f = p_{tan}f\}. \end{aligned}$$

A vector field $f \in l^2(\Omega)$ is said to be a normal (or radial) if $f = p_{nor}f$ and tangential if $f = p_{tan}f$.

The aforementioned decomposition of spherical vector fields can be established by introducing three special operators $o_\xi^{(i)}$, $i = 1, 2, 3$ mapping scalar fields to vector fields. To be specific, let $F \in \mathcal{C}^{(0_i)}(\Omega)$, then the operators $o_\xi^{(i)} : \mathcal{C}^{(0_i)}(\Omega) \rightarrow c(\Omega)$ are given by

$$\begin{aligned} o_\xi^{(1)}F(\xi) &= \xi F(\xi), \quad \xi \in \Omega, \\ o_\xi^{(2)}F(\xi) &= \nabla_\xi^* F(\xi), \quad \xi \in \Omega, \\ o_\xi^{(3)}F(\xi) &= L_\xi^* F(\xi), \quad \xi \in \Omega, \end{aligned} \tag{1.12}$$

Where 0_i is an abbreviation given by $0_1 = 0$ and $0_i = 1$ for $i \in \{2, 3\}$.

Clearly, $o_\xi^{(1)}F(\xi)$ is a radial field. From the definitions of the operators ∇_ξ^* and L_ξ^* it is easy to see that $o_\xi^{(2)}F(\xi)$ and $o_\xi^{(3)}F(\xi)$ are purely tangential. Furthermore $o_\xi^{(2)}F(\xi)$ is curl-free, whereas $o_\xi^{(3)}F(\xi)$ is divergence free, which is clear from $\nabla_\xi^* F(\xi)$ being a gradient- and $L_\xi^* F(\xi)$ being a curl-field. Additionally it is not difficult to see that

$$o_\xi^{(i)}F(\xi) \cdot o_\xi^{(j)}F(\xi) = 0, \quad \text{for all } i \neq j \quad i, j \in \{1, 2, 3\}. \tag{1.13}$$

The next step towards our definition of vector spherical harmonics is given by the well-known *Helmholtz decomposition theorem*.

Theorem 1.7 *Let $f : \Omega \rightarrow \mathbb{R}^3$ be a continuously differentiable vector field, i.e. $f \in C^1(\Omega)$. Then there exist uniquely determined scalar functions $F_1 \in C^1(\Omega)$ and $F_2, F_3 \in C^2(\Omega)$ satisfying*

$$\int_{\Omega} F_i(\xi) d\omega(\xi) = 0, \quad i = 2, 3 \quad (1.14)$$

such that

$$f = \sum_{i=1}^3 o^{(i)} F_i. \quad (1.15)$$

It should be mentioned that F_1 is just the radial projection of f while representations for the Helmholtz scalars F_2 and F_3 are available in terms of the Green's function with respect to the Beltrami operator (cf. [30]). Note that the above theorem is also valid for vector fields on Ω_R , since they are isomorphic to those on Ω .

The Helmholtz decomposition from Theorem 1.7 can also be formulated for regular surfaces but in a somewhat weaker form (cf. [8]). We just sketch the results. Let $\mathcal{U} \subset \mathbb{R}^3$ be an open set containing a regular surface S and let $F : \mathcal{U} \rightarrow \mathbb{R}$ be a continuously differentiable scalar field. Then, for every $x \in S$ the normal derivative of F is given by $\nu \cdot \nabla F$, where ν denotes the outer normal of S . The surface gradient ∇_S on S is given by $\nabla_S F = \nabla F - \nu \cdot \nabla F$. The corresponding surface curl on S is defined to be $L_S = \nu \wedge \nabla_S$ (note that these operators are generalizations of the corresponding operators on the sphere). The Helmholtz decomposition theorem for regular surfaces then reads as follows.

Theorem 1.8 *Let S be a regular surface. Let $f : S \rightarrow \mathbb{R}^3$ be a continuously differentiable vector field on S . Then there exist uniquely determined scalar functions $F_1 \in C^1(S)$ and $F_2, F_3 \in C^2(S)$ satisfying*

$$\int_S F_i(\xi) d\omega(\xi) = 0, \quad i = 2, 3$$

such that

$$f = \nu F_1 + \nabla_S F_2 + L_S F_3 = \sum_{i=1}^3 o_S^{(i)} F_i.$$

See [8] for a proof.

Motivated by the Helmholtz decomposition for the sphere we will now introduce the vector spherical harmonics. More precisely, let $Y_n \in \text{Harm}_n(\Omega)$, then any vector field

$$o^{(i)} Y_n, \quad n \geq 0, \quad i = 1, 2, 3 \quad (1.16)$$

is called a vector spherical harmonic of degree n and type i . Clearly $o^{(1)} Y_n$ is a normal field, while $o^{(2)} Y_n$ and $o^{(3)} Y_n$ are tangential fields. The next theorem defines an $l^2(\Omega)$ -orthonormal system of vector spherical harmonics, starting from an $\mathcal{L}^2(\Omega)$ -orthonormal system of scalar spherical harmonics.

Theorem 1.9 *Let the set $\{Y_{n,k}\}_{\substack{n=0,1,\dots \\ k=1,\dots,2n+1}}$ be an $\mathcal{L}^2(\Omega)$ -orthonormal system of scalar spherical harmonics. Then the system*

$$y_{n,k}^{(i)} = (\mu_n^{(i)})^{-1/2} o^{(i)} Y_{n,k}, \quad (1.17)$$

$i = 1, 2, 3, n = 0_i, 0_i + 1, \dots, k = 1, \dots, 2n + 1$ forms an $l^2(\Omega)$ -orthonormal system of vector spherical harmonics when the normalization factor is chosen to be

$$\mu_n^{(i)} = \begin{cases} 1 & \text{if } i = 1 \\ n(n+1) & \text{if } i = 2, 3. \end{cases} \quad (1.18)$$

Let $\text{harm}_n^{(i)}$ denote the set of all vector spherical harmonics of type i and degree n . Furthermore we define

$$\begin{aligned} \text{harm}_0(\Omega) &= \text{harm}_0^{(1)}(\Omega) = \text{span}\{y_{0,1}^{(1)}\}, \\ \text{harm}_n(\Omega) &= \bigoplus_{i=1}^3 \text{harm}_n^{(i)}(\Omega) = \bigoplus_{i=1}^3 \left(\text{span}\{y_{n,k}^{(i)}\}_{k=1,\dots,2n+1} \right), \quad n > 0. \end{aligned} \quad (1.19)$$

Additionally we let

$$\begin{aligned} \text{harm}_{p_i,\dots,q_i}^{(i)}(\Omega) &= \bigoplus_{n=p_i}^{q_i} \text{harm}_n^{(i)}(\Omega), \\ \text{harm}_{p,\dots,q}(\Omega) &= \bigoplus_{i=1}^3 \bigoplus_{n=p_i}^{q_i} \text{harm}_n^{(i)}(\Omega), \end{aligned} \quad (1.20)$$

where $p = (p_1, p_2, p_3)^T$, $q = (q_1, q_2, q_3)^T$ with $0_i \leq p_i \leq q_i$, $i = 1, 2, 3$. Any member of class $\text{harm}_{p,\dots,q}(\Omega)$ is called a bandlimited vector field of bandwidth $q - p$.

Using this notation, Theorem 1.9 tells us that

$$l_{(i)}^2(\Omega) = \overline{\bigoplus_{n=0_i}^{\infty} \text{harm}_n^{(i)}(\Omega)}^{\|\cdot\|_{l^2(\Omega)}} = \overline{\bigoplus_{n=0_i}^{\infty} \text{span}\{y_{n,k}^{(i)}\}_{k=1,\dots,2n+1}}^{\|\cdot\|_{l^2(\Omega)}} \quad \text{and} \quad (1.21)$$

$$l^2(\Omega) = \overline{\bigoplus_{i=1}^3 \bigoplus_{n=0_i}^{\infty} \text{harm}_n^{(i)}(\Omega)}^{\|\cdot\|_{l^2(\Omega)}}, \quad (1.22)$$

i.e. the spaces $\text{harm}_n^{(i)}(\Omega)$, $n = 0_i, \dots$ are dense in $l_{(i)}^2(\Omega)$ and the sets harm_n , $n = 0, 1, \dots$ are dense in $l^2(\Omega)$. In other words, every $l^2(\Omega)$ -vector field can be represented by means of its Fourier expansion in terms of vector spherical harmonics, i.e.

$$\lim_{N \rightarrow \infty} \left\| f - \sum_{i=1}^3 \sum_{n=0_i}^N \sum_{k=1}^{2n+1} (f^{(i)})^\wedge(n, k) y_{n,k}^{(i)} \right\|_{l^2(\Omega)} = 0, \quad \text{for all } f \in l^2(\Omega) \quad (1.23)$$

with Fourier coefficients

$$(f^{(i)})^\wedge(n, k) = \int_{\Omega} f(\xi) \cdot y_{n,k}^{(i)}(\xi) d\omega(\xi). \quad (1.24)$$

Alternatively we may of course write

$$f = \sum_{i=1}^3 f^{(i)} \quad (1.25)$$

with the vector fields $f^{(i)}$ given by

$$f^{(i)} = \sum_{n=0_i}^{\infty} \sum_{k=1}^{2n+1} (f^{(i)})^{\wedge}(n, k) y_{n,k}^{(i)}, \quad i = 1, 2, 3 \quad (1.26)$$

where the equalities are meant in the sense of the $l^2(\Omega)$ -topology. For later use we introduce the Helmholtz projectors $p_{(i)}$ corresponding to the decomposition $l^2(\Omega) = \bigoplus_{i=1}^3 l^2_{(i)}(\Omega)$ by $p_{(i)} : l^2(\Omega) \rightarrow l^2_{(i)}(\Omega)$, $f \mapsto p_{(i)}f = f^{(i)}$, $i \in \{1, 2, 3\}$.

We can extend the definitions of the $o^{(i)}$ -operators to vector fields. To be more specific, we let $f : \Omega \rightarrow \mathbb{R}^3$ be a sufficiently smooth vector field on the sphere, admitting the representation

$$f(\xi) = \sum_{\nu=1}^3 F_{\nu}(\xi) \varepsilon^{\nu}, \quad (1.27)$$

where ε^{ν} are unit coordinate vectors. Then we define $o_{\xi}^{(i)} f(\xi)$ to be

$$o_{\xi}^{(i)} f(\xi) = \sum_{\nu=1}^3 (o_{\xi}^{(i)} F_{\nu}(\xi)) \otimes \varepsilon^{\nu}, \quad i = 1, 2, 3. \quad (1.28)$$

This enables us to find the so-called Legendre tensors which, in the vector theory, play the role of the Legendre functions. That is, the (i, k) -Legendre-tensor-field of degree n $\mathbf{p}_n^{(i,k)} : \Omega \times \Omega \rightarrow \mathbb{R}^3 \otimes \mathbb{R}^3$ is defined via

$$\mathbf{p}_n^{(i,k)}(\xi, \eta) = (\mu_n^{(k)})^{-1/2} (\mu_n^{(i)})^{-1/2} o_{\xi}^{(i)} o_{\eta}^{(k)} P_n(\xi \cdot \eta), \quad \xi, \eta \in \Omega. \quad (1.29)$$

The connection between the vector spherical harmonics and the Legendre tensor can be established via the *addition theorem for vector spherical harmonics* (cf. [30]):

Theorem 1.10 *Let $\{y_{n,k}^{(i)}\}_{k=1, \dots, 2n+1}^{i=1,2,3}$ be an $l^2(\Omega)$ -orthonormal set in harm_n and let furthermore $\mathbf{p}_n^{(i,l)}$ be the (i, l) -Legendre-tensor-field of degree n . Then*

$$\sum_{k=1}^{2n+1} y_{n,k}^{(i)}(\xi) \otimes y_{n,k}^{(l)}(\eta) = \frac{2n+1}{4\pi} \mathbf{p}_n^{(i,l)}(\xi, \eta), \quad \xi, \eta \in \Omega. \quad (1.30)$$

Finally it should be stated that, as one of the most important consequences of the last theorem, the uniquely determined reproducing kernel of $\text{harm}_{p_i, \dots, q_i}^{(i)}(\Omega)$ is given by

$$\mathbf{k}_{\text{harm}_{p_i, \dots, q_i}^{(i)}(\Omega)}(\xi, \eta) = \sum_{n=p_i}^{q_i} \frac{2n+1}{4\pi} \mathbf{p}_n^{(i,i)}(\xi, \eta),$$

where the Legendre tensors $\mathbf{p}_n^{(i,i)}$, $i \in \{1, 2, 3\}$, can explicitly be presented via

$$\begin{aligned}\mathbf{p}_n^{(1,1)}(\xi, \eta) &= P_n(\xi \cdot \eta) \xi \otimes \eta, \\ \mathbf{p}_n^{(2,2)}(\xi, \eta) &= \frac{1}{n(n+1)} (P_n''(\xi \cdot \eta) (\eta - (\xi \cdot \eta) \xi) \otimes (\xi - (\xi \cdot \eta) \eta) \\ &\quad + P_n'(\xi \cdot \eta) (\mathbf{i}_{tan}(\xi) - (\eta - (\xi \cdot \eta) \xi) \otimes \eta)), \\ \mathbf{p}_n^{(2,2)}(\xi, \eta) &= \frac{1}{n(n+1)} (P_n''(\xi \cdot \eta) \xi \wedge \eta \otimes \eta \wedge \xi \\ &\quad + P_n'(\xi \cdot \eta) (\xi \cdot \eta) \mathbf{i}_{tan}(\xi) - (\eta - (\xi \cdot \eta) \xi) \otimes \xi).\end{aligned}$$

Note that \mathbf{i}_{tan} is the surface identity tensor field and is given by $\mathbf{i}_{tan} = \mathbf{i} - \xi \otimes \xi$, $\xi \in \Omega$, with the identity tensor $\mathbf{i} = \sum_{i=1}^3 \varepsilon^i \otimes \varepsilon^i$. For more details the interested reader might consult [30] and the references therein.

1.4 Mie Representation

Apart from the Helmholtz representation which has been presented in the last section, we will make use of the so-called Mie representation for solenoidal vector fields. The Mie representation is well known in the literature and we will just recapitulate some important results in a formulation that is useful for our later considerations. For a detailed and general treatment the reader might consult [7, 8, 48, 97], for example.

A vector field f on an open subset $\mathcal{U} \subset \mathbb{R}^3$ is called solenoidal if and only if the integral $\int_S f(x) \cdot \nu(x) d\omega(x)$ vanishes for every closed surface S lying entirely in U (ν denotes the outward normal of S). Every such solenoidal vector field admits a representation in terms of two uniquely defined scalar functions by means of the *Mie representation theorem* (e.g. [7, 8, 48, 97]):

Theorem 1.11 *Let $0 < R_1 < R_2$ and let $f : \Omega_{(R_1, R_2)} \rightarrow \mathbb{R}^3$ be a solenoidal vector field in the spherical shell $\Omega_{(R_1, R_2)}$. Then there exist unique scalar functions $P_f, Q_f : \Omega_{(R_1, R_2)} \rightarrow \mathbb{R}$, such that*

$$\begin{aligned}(1) \quad &\int_{\Omega_r} P_f(x) d\omega_r(x) = \int_{\Omega_r} Q_f(x) d\omega_r(x) = 0, \\ (2) \quad &f = \nabla \wedge LP_f + LQ_f,\end{aligned}$$

for all $r \in (R_1, R_2)$ with the operator L given by $Lx = x \wedge \nabla_x$.

(Note that $\Omega_{(R_1, R_2)} = \{x \in \mathbb{R}^3 : R_1 \leq |x| \leq R_2\}$). Vector fields of the form $\nabla \wedge LP_f$ are called poloidal while vector fields of the form LQ_f are denoted toroidal. For the sake of completeness we present the following theorem (cf. [8]).

Theorem 1.12 *Let $0 < R_1 < R_2$ and let $f : \Omega_{(R_1, R_2)} \rightarrow \mathbb{R}^3$ be a solenoidal vector field in the spherical shell $\Omega_{(R_1, R_2)}$. Then there exist a unique poloidal field p as well as a unique*

toroidal field t such that

$$f = p + t,$$

in $\Omega_{(R_1, R_2)}$.

For each $x = r\xi$ with $R_1 < r < R_2$ and $\xi \in \Omega$ the Mie representation $f = \nabla \wedge LP_f + LQ_f$ can be rewritten as

$$f(r\xi) = \xi \frac{\Delta_\xi^* P_f(r\xi)}{r} - \nabla_\xi^* \frac{\partial_r r P_f(r\xi)}{r} + L_\xi^* Q_f(r\xi) \quad (1.31)$$

(cf. e.g. [7, 8, 82, 91]), where we have used the abbreviation $\partial_r = \partial/\partial r$. Actually, as regards the second term, it is mathematically correct to write

$$\left(\frac{\partial}{\partial \tilde{r}} \tilde{r} P_f(\tilde{r}\xi) \right) \Big|_{\tilde{r}=r}.$$

We avoid this awkward notation, however, and stick to the easy nomenclature for the rest of the thesis. Concerning the third term, one might argue that the representation (1.31) is critical since, for the toroidal part, the operator L_x – which is an operator in \mathbb{R}^3 – is basically replaced by the L_ξ^* -operator which is a differential operator on the sphere. Consequently, in order to calculate LQ_f on Ω_r requires Q_f to be extended off the sphere. Nevertheless it can be shown that the values of LQ_f obtained on Ω_r are independent of which extension is chosen (cf. [7, 8] and the references therein) such that the above representation is mathematically sound.

Finally, we mention a last result which is concerned with the curl of a Mie representation:

Corollary 1.13 *Let $f, g : \Omega_{(R_1, R_2)} \rightarrow \mathbb{R}^3$ be two solenoidal vector fields with representations*

$$\begin{aligned} f &= \nabla \wedge LP_f + LQ_f, \\ g &= \nabla \wedge LP_g + LQ_g, \end{aligned}$$

and which are connected via $\nabla \wedge f = \lambda g$, $\lambda \in \mathbb{R} \setminus \{0\}$. Then the Mie scalars are related via

$$\begin{aligned} P_g &= \frac{1}{\lambda} Q_f, \\ Q_g &= -\frac{1}{\lambda} \Delta P_f. \end{aligned}$$

This shows us that the curl of a poloidal field is a toroidal field, and vice versa.

1.5 Inverse Problems and Regularization

In the following we recapitulate some important facts for the solution of so-called ill-posed problems which will be convenient for the reader in order to access the proposed approach

to the problem of downward continuation in Chapter 4. For detailed reviews the interested reader might consult [22, 23, 78], for example.

Let $(\mathcal{H}, (\cdot, \cdot)_{\mathcal{H}})$ and $(\mathcal{K}, (\cdot, \cdot)_{\mathcal{K}})$ be separable Hilbert spaces and let there be given a function $G \in \mathcal{K}$. We are interested in an approximation of a function $F \in \mathcal{H}$ that is related to G via the operator equation

$$A : \mathcal{H} \rightarrow \mathcal{K}, \quad AF = G,$$

where A is assumed to be a bounded linear operator. The construction of a solution is not difficult if A is bijective (i.e. a unique solution exists) and if A^{-1} is continuous (i.e. the solution depends continuously on the data). These properties are equivalent to Hadamard's definition of a *well-posed problem* (cf. [52]). If at least one of the properties is violated, then the problem is said to be *ill-posed*. This can equivalently be interpreted as follows:

- A surjective $\iff \mathcal{K} = \mathcal{R}(A)$,
- A injective $\iff \ker(A) = \{0\}$,
- A bijective $\iff A^{-1}$ exists,
- the solution depends continuously on the given data \iff continuity and boundedness of A^{-1} .

($\mathcal{R}(A)$ denotes the range, $\ker(A)$ the kernel of A). In practical applications we are generally not concerned with the ideal situation of a well-posed problem. First of all a solution of $AF = G$ exists only for those right hand sides G which are in the range of A . Errors due to unavoidable unprecise measurements, for example, result in noisy data and we may end up with $G \notin \mathcal{R}(A)$ which violates the condition of surjectivity. In order to define a solution even for non-surjective operators it is reasonable to consider an approximate solution which occupies particular properties such as the least-squares property, i.e. one seeks that very element of \mathcal{H} solving $\min_{F \in \mathcal{H}} \|AF - G\|_{\mathcal{K}}$. In the case of $G \in \mathcal{R}(A)$, the least-squares solution fulfills $\|AF - G\|_{\mathcal{K}} = 0$, of course. With A being injective, the solution F of $\min_{F \in \mathcal{H}} \|AF - G\|_{\mathcal{K}}$ is uniquely determined as the orthogonal projection of G onto $\overline{\mathcal{R}(A)}^{\|\cdot\|_{\mathcal{K}}}$, else there exist infinitely many solutions if $G \in \mathcal{R}(A)^{\perp}$. Then one usually is interested in the least-squares solution which is of minimal norm $\|F\|_{\mathcal{H}}$.

Determining the least-squares solution of minimal norm is equivalent to the determination of the (unique) generalized solution F^+ . The latter is defined via an additional mapping, the so-called *Moore-Penrose inverse* (or *generalized inverse*) $A^+ : \mathcal{R}(A) \oplus \mathcal{R}(A)^{\perp} \rightarrow \mathcal{H}$. Let A^* denote the adjoint operator of A then, for $G \in \mathcal{R}(A) \oplus \mathcal{R}(A)^{\perp}$, any $F \in \mathcal{H}$ is least-squares solution of $AF = G$ if and only if the normal equations $A^*AF = A^*G$ are fulfilled. It follows that the generalized solution is just that very least-squares solution that minimizes $\|F\|_{\mathcal{H}}$. The space of all least-squares solutions is $F^+ + \ker(A)$. It is well known that the described concept fails if $G \notin \mathcal{R}(A) \oplus \mathcal{R}(A)^{\perp}$ or the inverse operator A^{-1} is not continuous. Then, the lack of continuity needs to be replaced by a regularization of A^+ . To be specific, given the situation that only a disturbed right hand side is known instead of G , we are interested in

an approximation of the generalized solution F^+ which depends continuously on the given data.

An important tool in this context is the concept of the singular system of the operator A . More precisely, the non negative numbers $\sigma_n = \sqrt{\tau_n}$, where τ_n are the eigenvalues of the self-adjoint operator A^*A , are called the singular values of A . If A is linear and compact (cf. e.g. [57, 72]) and if $\sigma_1 \geq \sigma_2 \geq \dots \geq 0$ is the ordered sequence of the corresponding singular values, then there exist orthonormal systems $\{H_n\} \in \mathcal{H}$ and $\{K_n\} \in \mathcal{K}$ such that $AH_n = \sigma_n K_n$ and $A^*K_n = \sigma_n H_n$. The set $\{\sigma_n, H_n, K_n\}$ is called the singular system of A . The generalized inverse can be given in terms of the singular system, i.e.

$$F^+ = A^+G = \sum_{n=0}^{\infty} \sigma_n^{-1} (G, K_n)_{\mathcal{K}} H_n, \quad G \in \mathcal{R}(A) \oplus \mathcal{R}(A)^\perp.$$

If the operator A is compact then the condition that A has a finite dimensional range is fulfilled if and only if A has finitely many *singular values* σ_n , otherwise the sequence $\{\sigma_n\}$ has a unique cluster point 0, i.e. $\lim_{n \rightarrow \infty} \sigma_n = 0$. Additionally, the closure of the range of a compact operator is equivalent to the property of a finite dimensional range. It can be shown that if A is compact with non-closed range, the generalized inverse is not continuous and thus, the generalized solution F^+ does not depend continuously on the given data. A regularization can be obtained by filtering the singular value decomposition, i.e.

$$A_{\gamma_j} G = \sum_{n=0}^{\infty} F_{\gamma_j}(\sigma_n) (G, K_n)_{\mathcal{K}} H_n.$$

More precisely:

Definition 1.14 Let $\{S_{\gamma_j}\}_{\gamma_j > 0}$, with $j \in \mathbb{Z}$, $\lim_{j \rightarrow \infty} \gamma_j = 0$ as well as $\lim_{j \rightarrow -\infty} \gamma_j = \infty$, be a sequence of operators $S_{\gamma_j} : \mathcal{K} \rightarrow \mathcal{H}$ such that

$$S_{\gamma_j} K_n = F_{\gamma_j}(\sigma_n) H_n, \quad n = 0, 1, \dots$$

Furthermore, let the filter $F_{\gamma_j}(\sigma_n)$ satisfy the following properties:

- (i) $\sup_n |F_{\gamma_j}(\sigma_n)| = c(\gamma_j) < \infty$,
- (ii) $\lim_{\gamma \rightarrow 0} F_{\gamma_j}(\sigma_n) = 1$ pointwise in σ_n for all $n = 0, 1, \dots$,
- (iii) $|F_{\gamma_j}(\sigma_n)| \leq c < \infty$ for all $\gamma_j > 0$ and $n = 0, 1, \dots$

Then the family $\{S_{\gamma_j}\}_{\gamma_j > 0}$ is a regularization of A^+ .

Finally, we present three possible choices of filters F_{γ_j} , namely the truncated singular value decomposition (TSVD), the smoothed truncated singular value decomposition as well as the Tikhonov filter (TF):

(i) TSVD

$$F_{\gamma_j}(\sigma_n) = \begin{cases} \sigma_n^{-1} & : n \leq N(\gamma_j) \\ 0 & : n > N(\gamma_j). \end{cases}$$

This filter is the simplest method. The singular values are considered up to a certain threshold $N(\gamma_j)$, while all the others are discarded.

(ii) smoothed TSVD

$$F_{\gamma_j}(\sigma_n) = \begin{cases} \sigma_n^{-1} & : n \leq M(\gamma_j) \\ \sigma_n^{-1} \tau_{\gamma_j}(n) & : n = M(\gamma_j) + 1, \dots, N(\gamma_j) \\ 0 & : n > N(\gamma_j) \end{cases} ,$$

where τ_{γ_j} , is monotonically decreasing in $[M(\gamma_j), N(\gamma_j)]$.

(iii) TF

$$F_{\gamma_j}(\sigma_n) = \frac{\sigma_n}{\sigma_n^2 + \gamma_j^2}.$$

For singular values σ_n that are large compared to γ_j , we obtain $F_{\gamma_j} \simeq 1/\sigma_n$, i.e. there is almost no regularization. If the singular values are comparatively small (i.e. the errors in the data are amplified), we end up with $F_{\gamma_j} \simeq 0$ thus attenuating these effects.

Chapter 2

A General Approach to Scalar and Vectorial Multiscale Methods

This chapter briefly discusses an approach to the theory and algorithmic aspects of wavelets within a general separable functional Hilbert space framework. As far as scalar wavelets are concerned we follow our treatment in [36] (see also [29, 31]). For the case of vectorial wavelets the scalar concept is extended and the necessary modifications to the theory are presented.

The introduction of general scaling functions and wavelets will be shown to provide an adequate tool of representing each member of the Hilbert space as linear combinations of dilated and shifted copies of a corresponding 'mother kernel'. In consequence, the wavelet transform maps the elements of the Hilbert space into a two-parameter class of scale- and space-dependent elements, finally giving us the possibility to achieve accurate approximations by using only fractions of the original information about a member of the Hilbert space. For the simple and fast decomposition and reconstruction of Hilbert space elements into or, respectively, from the corresponding wavelet coefficients we present a new scalar pyramid scheme including bandlimited as well as non-bandlimited scalar kernel functions (see also our approach in [33]). For later use we define Legendre wavelets, as well as scalar and vectorial spherical wavelets as concrete examples.

2.1 Scalar Approach

2.1.1 \mathcal{H} -Fourier Expansions

We start with the Fourier theory in separable Hilbert spaces. Let $(\mathcal{H}, (\cdot, \cdot)_{\mathcal{H}})$ be a real separable Hilbert space over a certain domain $\Sigma \subset \mathbb{R}^n$, equipped with the inner product $(\cdot, \cdot)_{\mathcal{H}}$. Then there exists a countable orthonormal system $\{U_n^*\}_{n=0,1,\dots}$ which is complete in $(\mathcal{H}, (\cdot, \cdot)_{\mathcal{H}})$ and which we suppose to be known. It is a well known fact (e.g. [16]) that, in the sense of the induced norm $\|\cdot\|_{\mathcal{H}}$, each $F \in \mathcal{H}$ can be represented by its orthonormal or

Fourier expansion with respect to the system $\{U_n^*\}_{n=0,1,\dots}$, i.e. F admits the series expansion

$$F = \sum_{n=0}^{\infty} F^\wedge(n) U_n^*, \quad (2.1)$$

with Fourier coefficients

$$F^\wedge(n) = (F, U_n^*)_{\mathcal{H}}, \quad n = 0, 1, 2, \dots$$

Orthogonal expansions like (2.1) are very useful for picking out 'frequencies' n from a function $F \in \mathcal{H}$, which is due to the ideal localization of the trial functions U_n^* in the Fourier domain. Uncertainty principles, however, tell us that this is unavoidably accompanied by non-localization of the U_n^* in the space domain. As a consequence thereof, functions (signals) varying on small spatial scales cannot properly be dealt with using non-space localizing (for example polynomial) basis functions on Σ . In this context it is worth mentioning that signals frequently consist of contributions corresponding to certain frequencies which - in turn - are themselves spatially changing. This spatial distribution of frequency-content is not reflected in a Fourier series in terms of non-space localizing (e.g. polynomial) trial functions U_n^* . In what follows we are therefore going to present the necessary groundwork for introducing certain basis functions (i.e. wavelets) which enable us to automatically adapt the amount of localization in the space and Fourier domain and thus are able to cope with the aforementioned problem of space-varying frequency-content.

2.1.2 \mathcal{H} -Product Kernels and \mathcal{H} -Convolutions

Scaling functions as well as wavelets are realizations of a larger class of functions, the so-called \mathcal{H} -product kernels.

Definition 2.1 Let $\Gamma : \Sigma \times \Sigma \rightarrow \mathbb{R}$ be of the form

$$\Gamma(x, y) = \sum_{n=0}^{\infty} \Gamma^\wedge(n) U_n^*(x) U_n^*(y), \quad x, y \in \Sigma, \quad (2.2)$$

with $\Gamma^\wedge(n) \in \mathbb{R}$, $n \in \mathbb{N}_0$. Then Γ is called an \mathcal{H} -product kernel or, briefly, \mathcal{H} -kernel. The sequence $\{\Gamma^\wedge(n)\}_{n=0,1,\dots}$ is called the symbol of the \mathcal{H} -kernel (2.2).

Next we give a definition which enables us to ensure that an \mathcal{H} -kernel, for any one of the two arguments fixed, is a member of the corresponding Hilbert space.

Definition 2.2 The symbol $\{\Gamma^\wedge(n)\}_{n=0,1,\dots}$ of an \mathcal{H} -product kernel (2.2) is said to be \mathcal{H} -admissible if it satisfies the following conditions:

$$(i) \quad \sum_{n=0}^{\infty} (\Gamma^\wedge(n))^2 < \infty, \quad (ii) \quad \sum_{n=0}^{\infty} (\Gamma^\wedge(n) U_n^*(x))^2 < \infty \quad (2.3)$$

for all $x \in \Sigma$.

That is, if we have an \mathcal{H} -kernel $\Gamma : \Sigma \times \Sigma \rightarrow \mathbb{R}$ of the form (2.2) with \mathcal{H} -admissible symbol $\{\Gamma^\wedge(n)\}_{n=0,1,\dots}$, then the functions

$$\Gamma(x, \cdot) : \Sigma \rightarrow \mathbb{R}, \quad x \in \Sigma \text{ fixed},$$

respectively

$$\Gamma(\cdot, x) : \Sigma \rightarrow \mathbb{R}, \quad x \in \Sigma \text{ fixed},$$

are elements of \mathcal{H} . Definition 2.2 guarantees that the convolution (which is to be defined in Definition 2.3 below) of a Hilbert space function against an admissible \mathcal{H} -kernel is again a member of \mathcal{H} .

The basic concept for expanding functions in terms of space localizing kernels is the convolution of the functions against these kernels. The upcoming definition clarifies what is meant by that.

Definition 2.3 *Let $\Gamma : \Sigma \times \Sigma \rightarrow \mathbb{R}$ be an \mathcal{H} -kernel of the form (2.2) with \mathcal{H} -admissible symbol $\{\Gamma^\wedge(n)\}_{n=0,1,\dots}$. Furthermore let $F \in \mathcal{H}$. The \mathcal{H} -convolution of Γ against F is defined by*

$$(\Gamma *_{\mathcal{H}} F)(x) = (\Gamma(x, \cdot), F)_{\mathcal{H}} = \sum_{n=0}^{\infty} \Gamma^\wedge(n) F^\wedge(n) U_n^*(x). \quad (2.4)$$

Note that the righthand side of (2.4) immediately yields

$$(\Gamma *_{\mathcal{H}} F)^\wedge(n) = \Gamma^\wedge(n) F^\wedge(n), \quad n \in \mathbb{N}_0. \quad (2.5)$$

As we have mentioned before, an \mathcal{H} -kernel with \mathcal{H} -admissible symbol is an element of the corresponding separable Hilbert space \mathcal{H} if one argument is held fix. As a consequence of that we can expand Definition 2.3 to additionally hold for the convolution of two \mathcal{H} -kernels with \mathcal{H} -admissible symbols. By doing so we end up with

Theorem 2.4 *Let $\{\Gamma_1^\wedge(n)\}_{n=0,1,\dots}$ and $\{\Gamma_2^\wedge(n)\}_{n=0,1,\dots}$ be \mathcal{H} -admissible symbols corresponding to the \mathcal{H} -product kernels Γ_1 and Γ_2 , respectively. Then*

$$\begin{aligned} (\Gamma_1 *_{\mathcal{H}} \Gamma_2)(x, y) &= (\Gamma_1 *_{\mathcal{H}} \Gamma_2(\cdot, y))(x) \\ &= (\Gamma_1(x, \cdot), \Gamma_2(\cdot, y))_{\mathcal{H}} \\ &= \sum_{n=0}^{\infty} \Gamma_1^\wedge(n) \Gamma_2^\wedge(n) U_n^*(x) U_n^*(y) \end{aligned}$$

holds for all $x, y \in \Sigma$, and the sequence $\{(\Gamma_1 *_{\mathcal{H}} \Gamma_2)^\wedge(n)\}_{n=0,1,\dots}$ given by

$$(\Gamma_1 *_{\mathcal{H}} \Gamma_2)^\wedge(n) = \Gamma_1^\wedge(n) \Gamma_2^\wedge(n). \quad (2.6)$$

constitutes an \mathcal{H} -admissible symbol of the \mathcal{H} -kernel $\Gamma_1 *_{\mathcal{H}} \Gamma_2$.

2.1.3 \mathcal{H} -Scaling Functions

Having defined the \mathcal{H} -product kernels with \mathcal{H} -admissible symbols, the convolution of two of those kernels as well as the convolution of an \mathcal{H} -kernel against a member of the corresponding Hilbert space, we are now in a position to define the so-called \mathcal{H} -scaling functions as certain families of \mathcal{H} -product kernels. These \mathcal{H} -scaling functions will enable us to construct operators on \mathcal{H} which can be interpreted as bandpass filters for the Hilbert space functions. We start with the introduction of the so-called *dilation* and *shifting operators*.

Definition 2.5 Let $\{\Gamma_J\}$, $J \in \mathbb{Z}$, be a countable family of \mathcal{H} -product kernels with \mathcal{H} -admissible symbols. Then the dilation operator D_k , $k \in \mathbb{Z}$ is defined by

$$D_k \Gamma_J = \Gamma_{J+k}$$

and the shifting operator S_x , $x \in \Sigma$ by

$$S_x \Gamma_J = \Gamma_J(x, \cdot).$$

The kernel $\Gamma_0 \in \{\Gamma_J\}_{J \in \mathbb{Z}}$ is defined to be the mother kernel of the family, since

$$\Gamma_J(x, \cdot) = S_x D_J \Gamma_0$$

holds for all $x \in \Sigma$ and all $J \in \mathbb{Z}$.

Next, the *generating symbol* of an \mathcal{H} -scaling function, as well as the \mathcal{H} -scaling function itself will be introduced:

Definition 2.6 Let $(\Phi_0)^\wedge(n)$ be an \mathcal{H} -admissible symbol additionally satisfying

$$(i) \quad (\Phi_0)^\wedge(0) = 1,$$

$$(ii) \quad n > k \Rightarrow (\Phi_0)^\wedge(n) \leq (\Phi_0)^\wedge(k),$$

then $(\Phi_0)^\wedge(n)$ is said to be the generating symbol of the mother \mathcal{H} -scaling function given by

$$\Phi_0(x, y) = \sum_{n=0}^{\infty} (\Phi_0)^\wedge(n) U_n^*(x) U_n^*(y), \quad x, y \in \Sigma.$$

We are now interested in the dilated versions of the mother scaling function and therefore need to extend the definition of the generating symbol:

Definition 2.7 Let $\{(\Phi_J)^\wedge(n)\}_{n=0,1,\dots}$, $J \in \mathbb{Z}$, be an \mathcal{H} -admissible symbol satisfying, in addition, the following properties:

- (i) $\lim_{J \rightarrow \infty} ((\Phi_J)^\wedge(n))^2 = 1$, $n \in \mathbb{N}$,
- (ii) $((\Phi_J)^\wedge(n))^2 \geq ((\Phi_{J-1})^\wedge(n))^2$, $J \in \mathbb{Z}$, $n \in \mathbb{N}$,
- (iii) $\lim_{J \rightarrow -\infty} ((\Phi_J)^\wedge(n))^2 = 0$, $n \in \mathbb{N}$,
- (iv) $((\Phi_J)^\wedge(0))^2 = 1$, $J \in \mathbb{Z}$.

Then $\{(\Phi_J)^\wedge(n)\}_{n=0,1,\dots}$, $J \in \mathbb{Z}$ is called the generating symbol of an \mathcal{H} -scaling function. The corresponding family $\{\Phi_J\}$, $J \in \mathbb{Z}$, of \mathcal{H} -product kernels given by

$$D_J S_x \Phi_0 = \Phi_J(x, \cdot) := \sum_{n=0}^{\infty} (\Phi_J)^\wedge(n) U_n^*(x) U_n^*(\cdot), \quad x \in \Sigma,$$

is called \mathcal{H} -scaling function.

By virtue of Definition 2.7 we are thus able to represent any member of the \mathcal{H} -scaling function $\{\Phi_J\}$, $J \in \mathbb{Z}$ as a dilated and shifted version of the mother \mathcal{H} -scaling function.

From Theorem 2.4 it is obvious that, for $n = 0, 1, \dots$ and $J \in \mathbb{Z}$, the kernel $\Phi_J^{(2)} = \Phi_J *_{\mathcal{H}} \Phi_J$ is an \mathcal{H} -kernel with \mathcal{H} -admissible symbol $\{((\Phi_J)^\wedge(n))^2\}$. This helps us to prove the following theorem, which provides us with the central result in the theory of \mathcal{H} -scaling functions.

Theorem 2.8 Let $\{(\Phi_J)^\wedge(n)\}_{n=0,1,\dots}$, $J \in \mathbb{Z}$, be the generating symbol of an \mathcal{H} -scaling function $\{\Phi_J\}$. Let furthermore

$$F_J = \Phi_J^{(2)} *_{\mathcal{H}} F = (\Phi_J *_{\mathcal{H}} \Phi_J) *_{\mathcal{H}} F, \quad F \in \mathcal{H},$$

be the so-called J -level approximation of F . Then

$$\lim_{J \rightarrow \infty} F_J = F$$

holds, in the sense of the \mathcal{H} -metric, for all $F \in \mathcal{H}$.

Proof. For the sake of brevity we introduce the operator $T_J : \mathcal{H} \rightarrow \mathcal{H}$, $J \in \mathbb{Z}$, via

$$F_J = T_J F = (\Phi_J *_{\mathcal{H}} \Phi_J) *_{\mathcal{H}} F.$$

From Theorem 2.4 and by virtue of Definition 2.3 it immediately follows that

$$T_J F = \sum_{n=0}^{\infty} ((\Phi_J)^\wedge(n))^2 F^\wedge(n) U_n^*.$$

This implies that

$$\begin{aligned} \|T_J\| &= \sup_{\substack{G \in \mathcal{H} \\ \|G\|_{\mathcal{H}}=1}} \|T_J G\|_{\mathcal{H}} \\ &= \left(\sum_{n=0}^{\infty} ((\Phi_J)^\wedge(n))^4 (G^\wedge(n))^2 \right)^{\frac{1}{2}} \\ &\leq \sup_{n \in \mathbb{N}_0} ((\Phi_J)^\wedge(n))^2 \left(\sum_{n=0}^{\infty} (G^\wedge(n))^2 \right)^{\frac{1}{2}} \\ &\leq \sup_{n \in \mathbb{N}_0} ((\Phi_J)^\wedge(n))^2 < \infty \end{aligned}$$

for every $J \in \mathbb{Z}$, since $\{(\Phi_J)^\wedge(n)\}_{n=0,1,\dots}$, $J \in \mathbb{Z}$, is \mathcal{H} -admissible. Parseval's identity tells us that

$$\lim_{J \rightarrow \infty} \|T_J F - F\|_{\mathcal{H}}^2 = \lim_{J \rightarrow \infty} \sum_{n=0}^{\infty} (1 - ((\Phi_J)^\wedge(n))^2)^2 (F^\wedge(n))^2. \quad (2.7)$$

From conditions (i), (ii), and (iv) of Definition 2.7 it can be deduced that

$$0 \leq (1 - ((\Phi_J)^\wedge(n))^2)^2 \leq 1$$

is valid for all $n \in \mathbb{N}_0$. Therefore, the limit and the infinite sum in (2.7) may be interchanged. Using conditions (i) and (ii) of Definition 2.7 completes the proof. ■

From Theorem 2.8 it follows that, for any $F \in \mathcal{H}$, each double convolution

$$F_J = T_J F = (\Phi_J *_{\mathcal{H}} \Phi_J) *_{\mathcal{H}} F$$

provides us with an approximation of F at a different scale J . In terms of filtering the \mathcal{H} -product kernels $(\Phi_J *_{\mathcal{H}} \Phi_J)$ may be interpreted as low-pass filters in \mathcal{H} . T_J represents the corresponding convolution operator. Accordingly, we understand the corresponding *scale space* V_J to be the image of \mathcal{H} under the operator T_J , i.e.

$$\mathcal{V}_J = T_J(\mathcal{H}) = \{(\Phi_J *_{\mathcal{H}} \Phi_J) *_{\mathcal{H}} F \mid F \in \mathcal{H}\}.$$

The scale spaces V_J define a so-called \mathcal{H} -*multiresolution analysis (MRA)* in the following sense:

Theorem 2.9 *The scale spaces satisfy the following properties:*

- (a) $\{U_0^*\} \subset \mathcal{V}_J \subset \mathcal{V}_{J'} \subset \mathcal{H}$, $J \leq J'$,
- (b) $\bigcap_{J=-\infty}^{\infty} \mathcal{V}_J = \{U_0^*\}$,
- (c) $\bigcup_{J=-\infty}^{\infty} \mathcal{V}_J = \mathcal{H}$,
- (d) if $F_J \in \mathcal{V}_J$ then $D_{-1}F_J \in \mathcal{V}_{J-1}$, $J \in \mathbb{Z}$.

Proof. The assertion (a) follows from conditions (ii) and (iv) of Definition 2.7. The identity (b) follows from conditions (iii) and (iv) of Definition 2.7, while (c) is a direct consequence of Theorem 2.8 and condition (iii) of Definition 2.7. Assertion (d) follows immediately from Definition 2.5. ■

One might expect that there is some more structure in the MRA, e.g. that the scale spaces are of finite, predictable dimension. This, however, is in general not true. The dimension and composition of the scale spaces depend on the particular choice of the generating symbols of the \mathcal{H} -scaling functions; some more details will be given later on.

2.1.4 \mathcal{H} -Wavelets

The definition of the \mathcal{H} -scaling functions in the last section now enables us to introduce the associated \mathcal{H} -wavelets. The basic idea is to break up the functions $F \in \mathcal{H}$ into pieces of information at different locations and at different scales (i.e. different levels of resolution). Essential again is the concept of \mathcal{H} -convolutions and \mathcal{H} -product kernels.

Definition 2.10 Let $\{(\Phi_J)^\wedge(n)\}_{n=0,1,\dots}$, $J \in \mathbb{Z}$, be the generating symbol of an \mathcal{H} -scaling function as defined in Definition 2.7. Then the generating symbol

$$\{(\Psi_j)^\wedge(n)\}_{n=0,1,\dots}, \quad j \in \mathbb{Z},$$

of the associated \mathcal{H} -wavelet is defined via the refinement equation

$$(\Psi_j)^\wedge(n) = \left(((\Phi_{j+1})^\wedge(n))^2 - ((\Phi_j)^\wedge(n))^2 \right)^{\frac{1}{2}}. \quad (2.8)$$

The family $\{\Psi_j\}$, $j \in \mathbb{Z}$, of \mathcal{H} -product kernels given by

$$\Psi_j(x, y) = \sum_{n=0}^{\infty} (\Psi_j)^\wedge(n) U_n^*(x) U_n^*(y), \quad x, y \in \Sigma, \quad (2.9)$$

is called \mathcal{H} -wavelet associated to the \mathcal{H} -scaling function $\{\Phi_J\}$, $J \in \mathbb{Z}$. The corresponding mother wavelet is denoted by Ψ_0 .

As in the case of the \mathcal{H} -scaling functions, any \mathcal{H} -wavelet can be interpreted as a dilated and shifted version of the corresponding mother wavelet, i.e.

$$\Psi_j(x, \cdot) = S_x D_j \Psi_0(\cdot, \cdot),$$

where the shifting and dilation operators are given by Definition 2.5.

Similar to the definition of the operator T_j , $j \in \mathbb{Z}$, we are now led to the convolution operators $R_j : \mathcal{H} \rightarrow \mathcal{H}$ given by

$$R_j F = \Psi_j^{(2)} *_{\mathcal{H}} F = (\Psi_j *_{\mathcal{H}} \Psi_j) *_{\mathcal{H}} F, \quad F \in \mathcal{H}.$$

From the refinement equation (2.8) we can easily derive that

$$\begin{aligned} ((\Phi_{J+1})^\wedge(n))^2 &= \sum_{j=-\infty}^J ((\Psi_j)^\wedge(n))^2 \\ &= ((\Phi_0)^\wedge(n))^2 + \sum_{j=0}^J ((\Psi_j)^\wedge(n))^2. \end{aligned}$$

This is equivalent to

$$\Phi_{J+1} *_{\mathcal{H}} \Phi_{J+1} = \sum_{j=-\infty}^J (\Psi_j *_{\mathcal{H}} \Psi_j) = \Phi_0 *_{\mathcal{H}} \Phi_0 + \sum_{j=0}^J (\Psi_j *_{\mathcal{H}} \Psi_j) \quad (2.10)$$

or, in operator formulation,

$$T_{J+1} = \sum_{j=-\infty}^J R_j = T_0 + \sum_{j=0}^J R_j. \quad (2.11)$$

In terms of filtering, $\Psi_j^{(2)} = \Psi_j *_{\mathcal{H}} \Psi_j$, $j \in \mathbb{Z}$, may be interpreted as a band-pass filter. Thus, the convolution operators R_j describe the 'detail information' corresponding to a certain scale j . Therefore, in analogy to the scale spaces, we introduce the *detail spaces* via

$$\mathcal{W}_j = R_j(\mathcal{H}) = \{(\Psi_j *_{\mathcal{H}} \Psi_j) *_{\mathcal{H}} F \mid F \in \mathcal{H}\}.$$

Using the concept of the scale and detail spaces we can translate the operator equation (2.11) into a corresponding relation for the spaces:

$$\sum_{j=-\infty}^J \mathcal{W}_j = \mathcal{V}_0 + \sum_{j=0}^J \mathcal{W}_j = \mathcal{V}_{J+1}, \quad \mathcal{V}_J + \mathcal{W}_J = \mathcal{V}_{J+1}, \quad J \in \mathbb{Z}. \quad (2.12)$$

This can be interpreted as follows: The detail space \mathcal{W}_J contains all the necessary *detail information* to go from an approximation at scale J up to an approximation at scale $J + 1$. It is important to note that the sum in (2.12) is neither direct nor orthogonal. This is, as in the case of the MRA structure, dependent on the underlying generating symbols of the \mathcal{H} -scaling functions and, consequently, of the underlying \mathcal{H} -wavelets.

For later use we define, in close resemblance to the Fourier transform, the so-called wavelet transform:

Definition 2.11 *Let $F \in \mathcal{H}$ and let $\{\Psi_j\}$, $j \in \mathbb{Z}$ be an \mathcal{H} -wavelet associated to the \mathcal{H} -scaling function $\{\Phi_J\}$, $J \in \mathbb{Z}$. Then the wavelet transform WT of F at scale $j \in \mathbb{Z}$ and position $x \in \Sigma$ is given by*

$$WT(F)(j; x) = (\Psi_j(x, \cdot), F)_{\mathcal{H}} = (\Psi_j *_{\mathcal{H}} F)(x), \quad F \in \mathcal{H}. \quad (2.13)$$

The following theorem summarizes the main results of this section:

Theorem 2.12 *Let $\{(\Phi_J)^{\wedge(n)}\}_{n=0,1,\dots}$, $J \in \mathbb{Z}$, be the generating symbol of an \mathcal{H} -scaling function. Suppose that $\{(\Psi_j)^{\wedge(n)}\}_{n=0,1,\dots}$, $j \in \mathbb{Z}$, is the generating symbol of the associated \mathcal{H} -wavelet. Furthermore, let $F \in \mathcal{H}$. Then*

$$F_J = (\Phi_0 *_{\mathcal{H}} \Phi_0) *_{\mathcal{H}} F + \sum_{j=0}^{J-1} \Psi_j *_{\mathcal{H}} (WT(F)(j, \cdot)) \quad (2.14)$$

is the J -level approximation of F satisfying

$$\lim_{J \rightarrow \infty} \|F_J - F\|_{\mathcal{H}} = 0. \quad (2.15)$$

Proof. Equation (2.10) together with Theorem 2.8 and Definition 2.11 lead to the desired result. ■

Theorem 2.12 shows the essential characteristic of the \mathcal{H} -wavelets: Any $F \in \mathcal{H}$ can be approximated, starting with the coarse approximation T_0F , by successively adding the detail information R_0F, \dots, R_JF , thus ending up with the $(J + 1)$ -level approximation $T_{J+1}F$. Obviously, the 'partial reconstruction' R_jF is just the difference of two consecutive approximations, i.e. $R_jF = T_{j+1}F - T_jF$. Finally, the process of adding up detail information in order to approximate any $F \in \mathcal{H}$ guarantees the convergence in the \mathcal{H} -topology. The following scheme illustrates the results of Theorem 2.12:

$$\begin{aligned} T_0F & \quad T_1F \dots & T_jF & \quad T_{j+1}F \dots \xrightarrow{j \rightarrow \infty} F \\ \mathcal{V}_0 & \subset \mathcal{V}_1 \dots & \subset \mathcal{V}_j & \subset \mathcal{V}_{j+1} \dots = \mathcal{H} \\ \mathcal{V}_0 + \mathcal{W}_0 & + \dots + \mathcal{W}_{j-1} & + \mathcal{W}_j & + \dots = \mathcal{H} \\ T_0F + R_0F & + \dots + R_{j-1}F & + R_jF & + \dots = F. \end{aligned}$$

Bandlimited \mathcal{H} -wavelets

An important class of \mathcal{H} -scaling functions and -wavelets, yielding a more structured multiresolution analysis, are the so-called bandlimited \mathcal{H} -wavelets. They are characterized by the fact that the generating symbol $\{(\Phi_j)^\wedge(n)\}_{n=0,1,\dots}$, $j \in \mathbb{Z}$, of the associated \mathcal{H} -scaling function vanishes above a certain degree N_j . For the sake of simplicity we assume that $\{\Phi_j\}_{j \in \mathbb{Z}}$ is a family of bandlimited kernels such that

$$((\Phi_j)^\wedge(n))^2 > 0 \quad \text{for } n = 0, \dots, N_j = 2^j - 1 \quad (2.16)$$

and

$$((\Phi_j)^\wedge(n))^2 = 0 \quad \text{for } n \geq N_j + 1 = 2^j. \quad (2.17)$$

Then it is clear that, for any fixed $x \in \Sigma$,

$$\Phi_j(x, \cdot) \in \mathcal{H}_{0,\dots,2^j-1} = \text{span}\{U_0^*, \dots, U_{2^j-1}^*\} \quad (2.18)$$

and

$$\Psi_j(x, \cdot) \in \mathcal{H}_{0,\dots,2^{j+1}-1} = \text{span}\{U_0^*, \dots, U_{2^{j+1}-1}^*\} \quad (2.19)$$

hold true. Note that (2.19) follows directly from (2.16), (2.17) and the refinement equation (2.8) of Definition 2.10. As a consequence of (2.18) and (2.19) the scale and detail spaces fulfill

$$\begin{aligned} \mathcal{V}_j & = \mathcal{H}_{0,\dots,2^j-1}, \\ \mathcal{W}_j & \subset \mathcal{H}_{0,\dots,2^{j+1}-1}. \end{aligned}$$

As simple bandlimited examples we present:

(a) *Shannon scaling function*

$$(\Phi_j)^\wedge(n) = \begin{cases} 1 & \text{for } n = 0, \dots, N_j \\ 0 & \text{for } n \geq N_j + 1 \end{cases},$$

(b) *cubic polynomial (CP-) scaling function*

$$(\Phi_j)^\wedge(n) = \begin{cases} (1 - 2^{-j}n)^2(1 + 2^{-j+1}n) & \text{for } n = 0, \dots, N_j \\ 0 & \text{for } n \geq N_j + 1 \end{cases}$$

with

$$N_j = \begin{cases} 0 & \text{for } j \in \mathbb{Z}, j < 0 \\ 2^j - 1 & \text{for } j \in \mathbb{Z}, j \geq 0 \end{cases}.$$

In the case of the Shannon scaling function and the associated wavelets we are led to an orthogonal MRA and the detail and scale spaces satisfy

$$\mathcal{V}_{j+1} = \mathcal{V}_j \oplus \mathcal{W}_j \quad \text{and} \quad \mathcal{W}_j \perp \mathcal{W}_k,$$

with $k \neq j$, $j \in \mathbb{N}_0$. In the case of the cubic polynomial scaling function, the scale and detail spaces remain finite dimensional, but the detail spaces are no longer orthogonal. Other examples of bandlimited scaling functions and wavelets can be found in [30] for example. For graphical impressions see Section 2.1.6.

Non-Bandlimited \mathcal{H} -wavelets

For the sake of completeness we also present non-bandlimited \mathcal{H} -scaling functions and associated wavelets. These are generated by a generating symbol with global support (see e.g. [30] for more details). As examples we present:

(a) *Abel-Poisson scaling function*: The generating symbol $\{(\Phi_j)^\wedge(n)\}_{n=0,1,\dots}$, $j \in \mathbb{Z}$ is given by

$$(\Phi_j)^\wedge(n) = e^{nR2^{-j}}, \quad n, j \in \mathbb{N}_0, \quad R > 0.$$

The generating symbols of the associated \mathcal{H} -wavelets can be derived by the refinement equation (2.8):

$$(\Psi_j)^\wedge(n) = \sqrt{(e^{-nR2^{-j-1}})^2 - (e^{-nR2^{-j}})^2}, \quad n, j \in \mathbb{N}_0, \quad R > 0.$$

(b) *Tikhonov scaling function*: The generating symbol $\{(\Phi_j)^\wedge(n)\}_{n=0,1,\dots}$, $j \in \mathbb{Z}$ is given by

$$(\Phi_j)^\wedge(n) = \frac{\sigma_n^2}{\sigma_n^2 + \rho_j^2}, \quad n \in \mathbb{N}_0,$$

where $\{\rho_j\}_{j \in \mathbb{Z}}$ is a strictly monotonically decreasing sequence of integers satisfying

$$\lim_{j \rightarrow -\infty} \rho_j = \infty \quad \text{and} \quad \lim_{j \rightarrow \infty} \rho_j = 0,$$

and where $\{\sigma_n\}_{n \in \mathbb{N}_0}$ is a sequence satisfying

$$\sigma_n \neq 0 \quad \text{for all } n \in \mathbb{N}_0$$

as well as

$$\sum_{n=0}^{\infty} \sigma_n^2 < \infty.$$

Observe the relation to the Tikhonov filter in Section 1.5.

As a direct consequence of these constructions the scale and detail spaces are of infinite dimension and the detail spaces are not orthogonal. Nevertheless, though the MRAs obtained with non-bandlimited wavelets do not show as much structure as in the bandlimited case (orthogonality or, at least, finite dimension of the scale and detail spaces), the global support of the generating symbols is equivalent to only little localization in the Fourier domain. Thus, non-bandlimited wavelets show very strong localization properties in the space domain. For graphical impressions see Section (2.1.6).

2.1.5 A Pyramid Scheme

Up to now, we have established the theoretical basis properties for approximating Hilbert space functions in terms of scaling functions and associated wavelets. This section deals with some algorithmic aspects for the numerical application of the \mathcal{H} -wavelet concept, i.e. we present means of fast computation in terms of a so-called pyramid scheme. The approach is similar to our treatment in [33] and has been generalized to the \mathcal{H} -approach.

As can be seen from Theorems 2.8 and 2.12, it is crucial to compute double-convolutions of the form

$$V_{J_0;y} = (\Phi_{J_0}^{(2)} *_{\mathcal{H}} F)(y) = ((\Phi_{J_0} *_{\mathcal{H}} \Phi_{J_0}) *_{\mathcal{H}} F)(y) \quad (2.20)$$

and

$$W_{j;y} = (\Psi_j^{(2)} *_{\mathcal{H}} F)(y) = ((\Psi_j *_{\mathcal{H}} \Psi_j) *_{\mathcal{H}} F)(y). \quad (2.21)$$

We now assume that, to each scale $j \in \mathbb{N}_0$, there are $N_j \in \mathbb{N}_0$ known weights $w_i^{N_j} \in \mathbb{R}$ and corresponding knots $y_i^{N_j} \in \Sigma$ such that

$$\begin{aligned} V_{J_0;y} &\simeq \sum_{i=1}^{N_{J_0}} w_i^{N_{J_0}} \Phi_{J_0}^{(2)}(y, y_i^{N_{J_0}}) F(y_i^{N_{J_0}}), \\ W_{j;y} &\simeq \sum_{i=1}^{N_j} w_i^{N_j} \Psi_j^{(2)}(y, y_i^{N_j}) F(y_i^{N_j}), \quad j = J_0, \dots, J-1 \end{aligned}$$

(‘ \simeq ’ always means that the error is assumed to be negligible; more details about the so-called integration rules, i.e. the knots and corresponding weights, can be found in [30] for example).

We will now realize a pyramid scheme for the (approximate) recursive computation of the convolutions (2.20) and (2.21) for $j = J_0 \dots J-1$. We use the following ingredients: Starting from a sufficiently large J , such that

$$F(y) \simeq \Phi_J^{(2)}(\cdot, y) *_{\mathcal{H}} F \simeq \sum_{i=1}^{N_J} \Phi_J^{(2)}(y, y_i^{N_J}) \tilde{a}_i^{N_J}, \quad y \in \Sigma, \quad (2.22)$$

we want to show that the coefficient vectors

$$\tilde{a}^{N_j} = \left(\tilde{a}_1^{N_j}, \dots, \tilde{a}_{N_j}^{N_j} \right)^T \in \mathbb{R}^{N_j}, \quad j = J_0, \dots, J-1,$$

(being, of course, dependent on the function F under consideration) can be calculated such that the following statements are valid:

- (i) The vectors \tilde{a}^{N_j} , $j = J_0, \dots, J-1$, are obtainable by recursion from the values $\tilde{a}_i^{N_J}$.
- (ii) For $j = J_0, \dots, J$

$$\Phi_j^{(2)}(\cdot, y) *_{\mathcal{H}} F \simeq \sum_{i=1}^{N_j} \Phi_j^{(2)}(y, y_i^{N_j}) \tilde{a}_i^{N_j}.$$

For $j = J_0, \dots, J-1$

$$\Psi_j^{(2)}(\cdot, y) *_{\mathcal{H}} F \simeq \sum_{i=1}^{N_j} \Psi_j^{(2)}(y, y_i^{N_j}) \tilde{a}_i^{N_j}.$$

Our considerations towards this result are divided into two consecutive steps, viz. the initial step which is concerned with the highest scale J and the pyramid step which enables us to establish the recursion relation:

The Initial Step

From Theorem 2.8 it follows that, for a suitably large integer J , the kernel $\Phi_J^{(2)}$ replaces the 'Dirac-functional' δ in the sense that

$$\Phi_J^{(2)}(\cdot, y) *_{\mathcal{H}} F \simeq F(y) = (\delta *_{\mathcal{H}} F)(y) = \delta_y *_{\mathcal{H}} F, \quad (2.23)$$

where

$$\delta(x, y) = \delta_x(y) = \sum_{n=0}^{\infty} U_n^*(x) U_n^*(y).$$

Note that the series has to be understood in the distributional sense. For $i = 1, \dots, N_J$ let

$$\tilde{a}_i^{N_J} = w_i^{N_J} F(y_i^{N_J}) \quad (2.24)$$

such that

$$\begin{aligned} \Phi_J^{(2)}(y, \cdot) *_{\mathcal{H}} F &\simeq F(y) \simeq \sum_{i=1}^{N_J} w_i^{N_J} \Phi_J^{(2)}(y, y_i^{N_J}) F(y_i^{N_J}) \\ &= \sum_{i=1}^{N_J} \Phi_J^{(2)}(y, y_i^{N_J}) \tilde{a}_i^{N_J}, \quad i = 1, \dots, N_J. \end{aligned}$$

The Pyramid Step.

The central idea of the pyramid step is the existence of certain \mathcal{H} -product kernels $\Xi_j : \Sigma \times \Sigma \rightarrow \mathbb{R}$ such that

$$\Phi_j^{(2)} \simeq \Xi_j *_{\mathcal{H}} \Phi_j^{(2)} \quad (2.25)$$

and

$$\Xi_j \simeq \Xi_{j+1} *_{\mathcal{H}} \Xi_j \quad (2.26)$$

hold true. In the case of bandlimited \mathcal{H} -scaling functions the kernels Ξ_j can be chosen to be kernels of the form

$$\sum_{n=0}^{2^j-1} U_n^*(x)U_n^*(y) \in \mathcal{V}_j = \mathcal{H}_{0,\dots,2^j-1}, \quad x, y \in \Sigma,$$

(see Section 2.1.4). In the non-bandlimited case one might choose $\Xi_j = \delta \simeq \Phi_j^{(2)}$ (see (2.23); note that, if \mathcal{H} is a reproducing kernel Hilbert space, then Ξ_j can be chosen to be the reproducing kernel of that very space).

In connection with relation (2.25) we are now able to write

$$\Phi_j^{(2)} * F \simeq \Phi_j^{(2)} * \Xi_j * F \simeq \sum_{i=1}^{N_j} \Phi_j^{(2)}(\cdot, y_i^{N_j}) \tilde{a}_i^{N_j}, \quad (2.27)$$

where we have introduced the coefficients at scale j , i.e.

$$\tilde{a}_i^{N_j} = w_i^{N_j} (\Xi_j * F)(y_i^{N_j}), \quad j = J_0, \dots, J-1. \quad (2.28)$$

Hence, using Equation (2.26) it follows that

$$\begin{aligned} \tilde{a}_i^{N_j} &= w_i^{N_j} (\Xi_j * F)(y_i^{N_j}) \\ &\simeq w_i^{N_j} (\Xi_j * \Xi_{j+1} * F)(y_i^{N_j}) \\ &\simeq w_i^{N_j} \sum_{l=1}^{N_{j+1}} w_l^{N_{j+1}} \Xi_j(y_i^{N_j}, y_l^{N_{j+1}}) (\Xi_{j+1} * F)(y_l^{N_{j+1}}) \\ &= w_i^{N_j} \sum_{l=1}^{N_{j+1}} \Xi_j(y_i^{N_j}, y_l^{N_{j+1}}) \tilde{a}_l^{N_{j+1}}. \end{aligned} \quad (2.29)$$

Thus, we have managed to derive a recursion relation such that the coefficients $\tilde{a}_i^{N_{J-1}}$ can be calculated recursively starting from the data $\tilde{a}_i^{N_J}$ for the initial level J , $\tilde{a}_i^{N_{J-2}}$ can be deduced recursively from $\tilde{a}_i^{N_{J-1}}$, etc. This finally leads us to the formulae

$$\Phi_j^{(2)}(\cdot, y) * F \simeq \sum_{i=1}^{N_j} \Phi_j^{(2)}(y, y_i^{N_j}) \tilde{a}_i^{N_j}, \quad j = J_0, \dots, J,$$

and

$$\Psi_j^{(2)}(\cdot, y) * F \simeq \sum_{i=1}^{N_j} \Psi_j^{(2)}(y, y_i^{N_j}) \tilde{a}_i^{N_j}, \quad j = J_0, \dots, J-1,$$

with coefficients given by (2.24) and (2.29). This recursion procedure can be summarized in the *decomposition scheme*

$$\begin{array}{ccccccc} F & \rightarrow & \tilde{a}^{N_J} & \rightarrow & \tilde{a}^{N_{J-1}} & \rightarrow & \dots & \rightarrow & \tilde{a}^{N_{J_0}} \\ & & \downarrow & & \downarrow & & & & \downarrow \\ & & W_{J;y} & & W_{J-1;y} & & & & W_{J_0;y} \end{array} .$$

as well as the corresponding *reconstruction scheme*

$$\begin{array}{ccccc} \tilde{a}^{N_{J_0}} & & \tilde{a}^{N_{J_0+1}} & & \tilde{a}^{N_{J_0+2}} \\ \downarrow & & \downarrow & & \downarrow \\ \Psi_{\rho_{J_0}}^{(2)} * F & & \Psi_{\rho_{J_0+1}}^{(2)} * F & & \Psi_{\rho_{J_0+2}}^{(2)} * F \\ \searrow & & \searrow & & \searrow \\ \Phi_{\rho_{J_0}}^{(2)} * F & \rightarrow & + & \rightarrow & \Phi_{\rho_{J_0+1}}^{(2)} * F & \rightarrow & + & \rightarrow & \Phi_{\rho_{J_0+2}}^{(2)} * F & \rightarrow & + & \rightarrow & \dots \end{array} .$$

It should be noted that the coefficient vectors \tilde{a}^{N_j} are *independent* of the special choice of the kernel functions. This can be seen from the uniqueness of the Fourier coefficients and the fact that Equation (2.27) is equivalent to $F^\wedge(n) \simeq \sum_{i=1}^{N_j} \tilde{a}_i^{N_j} U_n^*(y_i^{N_j})$.

2.1.6 Examples

This section presents concrete examples of \mathcal{H} -scaling functions and wavelets which will be of particular importance during the further course of this work. Starting with the one dimensional Legendre wavelets (cf. [101]) defined on the unit interval, we will then present two dimensional spherical wavelets defined on spherical surfaces (see e.g. [30, 41] for further details).

Legendre Wavelets

As a first example we consider the space $\mathcal{L}^2[-1, +1]$ of square-integrable functions $F : [-1, +1] \rightarrow \mathbb{R}$, i.e. $\Sigma = [-1, +1]$ and $\mathcal{H} = \mathcal{L}^2[-1, +1]$. On the space $\mathcal{L}^2[-1, +1]$ we are able to introduce, as usual, the inner product

$$(F, G)_{\mathcal{L}^2[-1, +1]} = \int_{-1}^{+1} F(t)G(t) dt, \quad F, G \in \mathcal{L}^2[-1, +1].$$

The $\mathcal{L}^2[-1, +1]$ -orthonormal Legendre polynomials $P_n^* : [-1, +1] \rightarrow \mathbb{R}$ given by

$$P_n^* = \sqrt{\frac{2n+1}{2}} P_n, \quad n = 0, 1, \dots$$

with

$$P_n(t) = \sum_{s=0}^{[n/2]} (-1)^s \frac{(2n-2s)!}{2^n (n-2s)! (n-s)! s!} t^{n-2s}, \quad t \in [-1, +1]$$

form a Hilbert basis in $\mathcal{L}^2[-1, +1]$ (see also Section 1.3). In other words, every $F \in \mathcal{L}^2[-1, +1]$ admits a Fourier expansion $F = \sum_{n=0}^{\infty} F^\wedge(n)P_n^*$, where the Fourier coefficients read as follows:

$$F^\wedge(n) = (F, P_n^*)_{\mathcal{L}^2[-1, +1]} = \int_{-1}^{+1} F(t)P_n^*(t) dt, \quad n = 0, 1, \dots .$$

The $\mathcal{L}^2[-1, +1]$ -admissible product kernels are given by

$$\Gamma(x, t) = \sum_{n=0}^{\infty} \Gamma^\wedge(n)P_n^*(x)P_n^*(t), \quad x, t \in [-1, +1]$$

with $\Gamma^\wedge(n) \in \mathbb{R}$, $n \in \mathbb{N}_0$, where the symbol of the $\mathcal{L}^2[-1, 1]$ -kernel has to satisfy the estimates

$$(i) \quad \sum_{n=0}^{\infty} (\Gamma^\wedge(n))^2 < \infty, \quad (ii) \quad \sum_{n=0}^{\infty} (\Gamma^\wedge(n)P_n^*(t))^2 < \infty \quad (2.30)$$

for all $t \in [-1, +1]$ (see the general admissibility condition given in Definition 2.2). Note that a sufficient condition for the validity of the conditions (i) and (ii) in (2.30) is given by

$$\sum_{n=0}^{\infty} (\Gamma^\wedge(n))^2 \frac{2n+1}{2} < \infty,$$

since $|P_n(t)| \leq 1$ holds true for all $t \in [-1, +1]$ (e.g. [30]).

In correspondence to the general approach the convolution of Γ against F is defined by

$$\begin{aligned} (\Gamma *_{\mathcal{L}^2[-1, +1]} F)(x) &= (\Gamma(x, \cdot), F)_{\mathcal{L}^2[-1, +1]} \\ &= \int_{-1}^{+1} \Gamma(x, t)F(t) dt \\ &= \sum_{n=0}^{\infty} \Gamma^\wedge(n)F^\wedge(n)P_n^*(x), \quad x \in [-1, +1]. \end{aligned}$$

Let $\{(\Phi_j)^\wedge(n)\}_{n=0,1,\dots}$, $j \in \mathbb{Z}$, be the generating symbol of a scaling function $\{\Phi_j\}$. Then, as can be seen by use of Theorem 2.8,

$$\lim_{J \rightarrow \infty} \|F_J - F\|_{\mathcal{L}^2[-1, +1]} = 0$$

holds for all $F \in \mathcal{L}^2[-1, +1]$, where the J -level approximation F_J is given by

$$F_J = \int_{-1}^{+1} \Phi_J(\cdot, x) \int_{-1}^{+1} \Phi_J(x, t)F(t) dt dx = \int_{-1}^{+1} \Phi_J^{(2)}(\cdot, t)F(t) dt.$$

Accordingly, the scale spaces \mathcal{V}_j are given by

$$\mathcal{V}_j = \left\{ \int_{-1}^{+1} \Phi_j^{(2)}(\cdot, t) F(t) dt \mid F \in \mathcal{L}^2[-1, +1] \right\},$$

while the detail spaces are of the form

$$\mathcal{W}_j = \left\{ \int_{-1}^{+1} \Psi_j^{(2)}(\cdot, t) F(t) dt \mid F \in \mathcal{L}^2[-1, +1] \right\}.$$

In accordance to Definition 2.11 the wavelet transform WT at scale j and position $x \in [-1, +1]$ is defined to be:

$$(WT)(F)(j; x) = \int_{-1}^{+1} \Psi_j(x, t) F(t) dt, \quad F \in \mathcal{L}^2[-1, +1].$$

The reconstruction formula of $F \in \mathcal{L}^2[-1, +1]$ allows the (bilinear) representation

$$\begin{aligned} F &= \int_{-1}^{+1} \Phi_0(\cdot, x) \int_{-1}^{+1} \Phi_0(x, t) F(t) dt dx \\ &+ \sum_{j=0}^{\infty} \int_{-1}^{+1} \Psi_j(\cdot, x) (WT)(F)(j; x) dx \end{aligned}$$

which is just a special realization of Theorem 2.12.

Spherical Wavelets

As reference space we now use the space $\mathcal{L}^2(\Omega)$ of square-integrable functions $F : \Omega \rightarrow \mathbb{R}$ on the unit sphere Ω in three-dimensional Euclidean space \mathbb{R}^3 (i.e.: $\Sigma = \Omega \subset \mathbb{R}^3$ and $\mathcal{H} = \mathcal{L}^2(\Omega)$, see also Chapter 1). We consider $\mathcal{L}^2(\Omega)$ to be equipped with the inner product

$$(F, G)_{\mathcal{L}^2(\Omega)} = \int_{\Omega} F(\xi) G(\xi) d\omega(\xi), \quad F, G \in \mathcal{L}^2(\Omega).$$

As $\mathcal{L}^2(\Omega)$ -orthonormal system we choose the system $\{Y_{n,k}\}_{\substack{n=0,1,\dots \\ k=1,\dots,2n+1}}$ of spherical harmonics $Y_{n,k}$ of degree n and order k . Clearly, every function $F \in \mathcal{L}^2(\Omega)$ can be represented in the form

$$F = \sum_{n=0}^{\infty} \sum_{k=1}^{2n+1} F^\wedge(n, k) Y_{n,k},$$

where the Fourier coefficients are given by

$$F^\wedge(n, k) = (F, Y_{n,k})_{\mathcal{L}^2(\Omega)} = \int_{\Omega} F(\eta) Y_{n,k}(\eta) d\omega(\eta).$$

In accordance to our general results, the $\mathcal{L}^2(\Omega)$ -product kernels are of the form

$$\Gamma(\xi, \eta) = \sum_{n=0}^{\infty} \sum_{k=1}^{2n+1} \Gamma^\wedge(n) Y_{n,k}(\xi) Y_{n,k}(\eta)$$

with $\Gamma^\wedge(n) \in \mathbb{R}$ for $n = 0, 1, \dots; k = 1, \dots, 2n + 1$, where

$$\sum_{n=0}^{\infty} (\Gamma^\wedge(n))^2 \frac{2n+1}{4\pi} < \infty$$

is a sufficient condition for the $\mathcal{L}^2(\Omega)$ -admissibility (see Definition 2.2 and note that $|Y_{n,k}(\xi)| \leq \sqrt{(2n+1)/4\pi}$ for all $\xi \in \Omega$). For the sake of completeness we mention that non-isotropic spherical kernels can also be constructed. It is clear that the generating symbol is then given to be dependent on $n \in \mathbb{N}_0$ as well as $k = 1, \dots, 2n + 1$. The $\mathcal{L}^2(\Omega)$ -admissibility can then be guaranteed by assuming

$$\sum_{n=0}^{\infty} \sum_{k=1}^{2n+1} (\Gamma^\wedge(n, k))^2 \frac{2n+1}{4\pi} < \infty.$$

The convolution of Γ against F is canonically understood to be

$$\begin{aligned} (\Gamma *_{\mathcal{L}^2(\Omega)} F)(\xi) &= (\Gamma(\xi, \cdot), F)_{\mathcal{L}^2(\Omega)} \\ &= \int_{\Omega} \Gamma(\xi, \eta) F(\eta) d\omega(\eta) \\ &= \sum_{n=0}^{\infty} \sum_{k=1}^{2n+1} \Gamma^\wedge(n) F^\wedge(n, k) Y_{n,k}(\xi), \quad \xi \in \Omega. \end{aligned}$$

Let $\{(\Phi_J)^\wedge(n)\}_{n=0,1,\dots}$, $J \in \mathbb{Z}$, be the generating symbol of a scaling function $\{\Phi_J\}$. Then, by use of Theorem 2.8, we have

$$\lim_{J \rightarrow \infty} \|F_J - F\| = 0$$

for all $F \in \mathcal{L}^2(\Omega)$, where F_J is accordingly given by

$$F_J = \int_{\Omega} \Phi_J^{(2)}(\cdot, \eta) F(\eta) d\omega(\eta).$$

The scale and detail spaces as well as the wavelet transform are given in canonical way i.e.

$$\mathcal{V}_j = \left\{ \int_{\Omega} \Phi_j^{(2)}(\cdot, \eta) F(\eta) d\omega(\eta) \mid F \in \mathcal{L}^2(\Omega) \right\},$$

for the scale spaces,

$$\mathcal{W}_j = \left\{ \int_{\Omega} \Psi_j^{(2)}(\cdot, \eta) F(\eta) d\omega(\eta) \mid F \in \mathcal{L}^2(\Omega) \right\},$$

for the detail spaces and finally

$$(WT)(F)(j; \xi) = \int_{\Omega} \Psi_j(\xi, \eta) F(\eta) d\omega(\eta), \quad F \in \mathcal{L}^2(\Omega)$$

for the wavelet transform.

The reconstruction formula of Theorem 2.12 for recovering a function $F \in \mathcal{L}^2(\Omega)$ now reads

$$F = \int_{\Omega} \Phi_0^{(2)}(\cdot, \eta) F(\eta) d\omega(\eta) + \sum_{j=0}^{\infty} \int_{\Omega} \Psi_j^{(2)}(\cdot, \eta) F(\eta) d\omega(\eta) .$$

Figures 2.1 to 2.3 present some illustrations of generators for scaling functions and wavelets as well as the corresponding kernel functions. Note that the plots show continuous versions of the generating symbols for better visibility. The abscissa of the kernel plots shows the angle between the two argument vectors $\xi, \eta \in \Omega$ of the corresponding kernel function $\Phi(\xi, \eta)$ or $\Psi(\xi, \eta)$, respectively. Looking at the Shannon generators in Figure 2.1 (top), one can realize what orthogonality of a multiresolution analysis means, i.e. the generating functions of the Shannon wavelets show no overlap thus creating a comparatively good localization in the Fourier domain. Consequently, in the space domain, the Shannon kernels show strong oscillations. As one can see from Figure 2.2, the generating functions of the CP kernels are less localized in the Fourier domain and overlap significantly. This, however, results in kernel functions which are much less oscillating in the space domain or, in other words, show a much better localization there. Last but not least we present some graphical illustrations of the non-bandlimited Abel-Poisson kernels in Figure 2.3. Since their generating symbols basically cover the whole Fourier domain the space localization is much higher than in the bandlimited examples. Observe that every example presented so far shows a basic feature of the wavelet approach: Increasing the scale parameter reduces the localization in the Fourier domain and consequently increases the space localization. It should be remarked that the balance of localization in the Fourier as well as the space domain is quantitatively given by uncertainty principles (as well known in theoretical physics). For a formulation of such uncertainty principles for wavelets the reader is directed to [28].

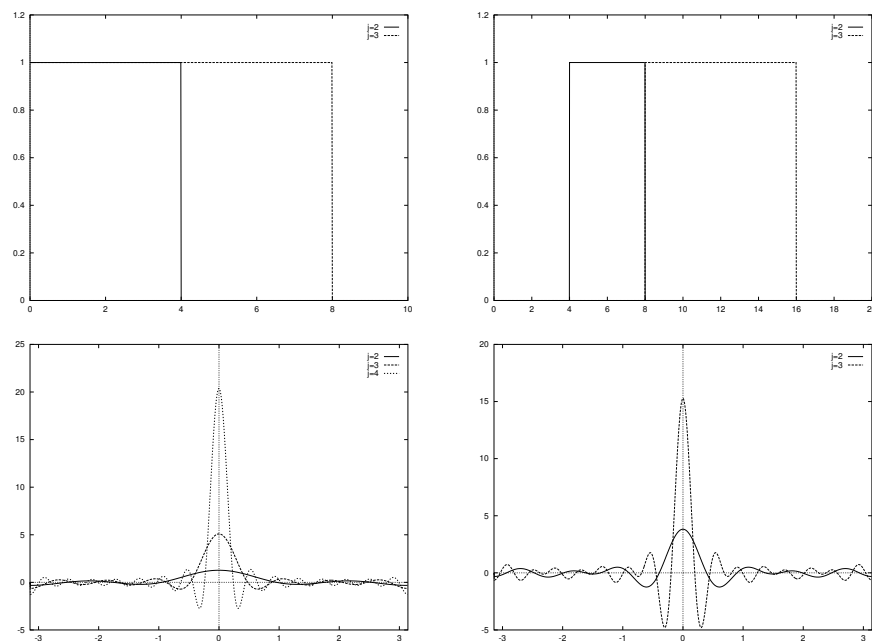


Figure 2.1: Top: Continuous versions of generating symbols of Shannon scaling functions (left) and wavelets (right) at different scales j . Bottom: Shannon scaling functions (left) and wavelets (right) at different scales j ; the abscissa shows the angle between the two argument vectors in radian.

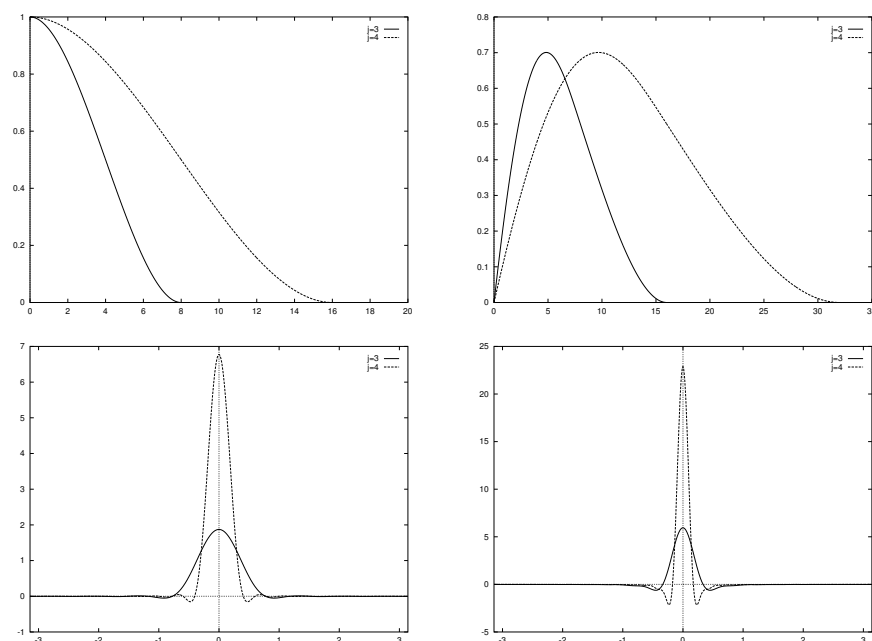


Figure 2.2: Top: Continuous versions of generating symbols of CP scaling functions (left) and wavelets (right) at different scales j . Bottom: CP scaling functions (left) and wavelets (right) at different scales j ; the abscissa shows the angle between the two argument vectors in radian.

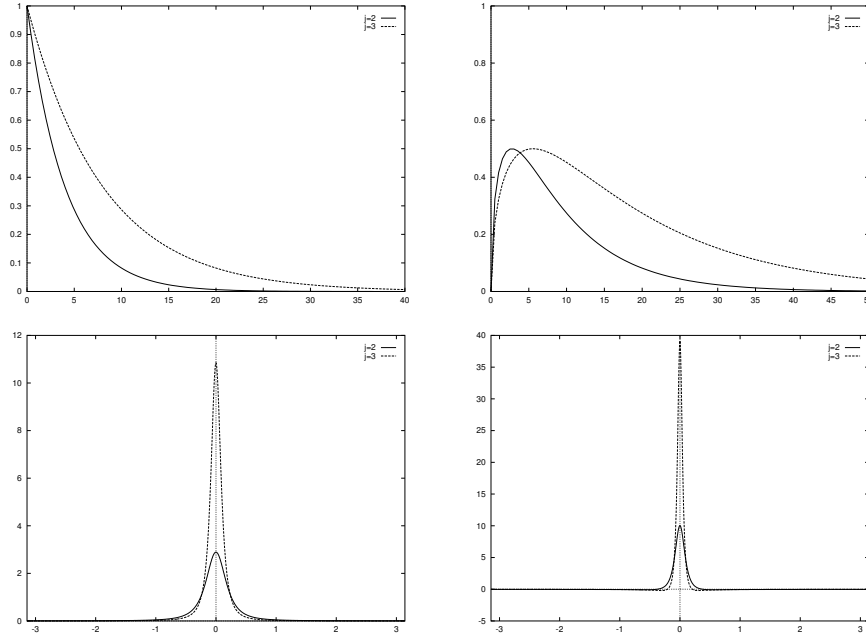


Figure 2.3: Top: Continuous versions of generating symbols of Abel-Poisson scaling functions (left) and wavelets (right) at different scales j . Bottom: Abel-Poisson scaling functions (left) and wavelets (right) at different scales j ; the abscissa shows the angle between the two argument vectors in radian.

2.2 Vectorial Approach

While, up to now, we have dealt with scalar \mathcal{H} -wavelets on domains $\Sigma \subset \mathbb{R}^n$, i.e. $\Gamma : \Sigma \times \Sigma \rightarrow \mathbb{R}$, we will now extend the theory to the case of vectorial \mathfrak{h} -wavelets on regular surfaces, i.e. we will deal with vectorial kernel functions $\gamma : \Sigma' \times \Sigma' \rightarrow \mathbb{R}^3$, where $\Sigma' \subset \mathbb{R}^3$ is a regular surface. Since the formalism is closely related to the previously introduced scalar approach, the treatise will be brief.

2.2.1 \mathfrak{h} -Fourier Expansions

Let now $(\mathfrak{h}, (\cdot, \cdot)_{\mathfrak{h}})$ be a real separable Hilbert space over a regular surface $\Sigma' \subset \mathbb{R}^3$. We suppose that we know a complete countable orthonormal system $\{u_n^{*(i)}\}_{n=0_i, 0_i+1, \dots}^{i=1,2,3}$ in \mathfrak{h} , where the index i is in accordance to the Helmholtz decomposition on regular surfaces (see Section 1.3). It is clear that, in the sense of the induced norm $\|\cdot\|_{\mathfrak{h}}$, each element $f \in \mathfrak{h}$ can be represented by its vectorial Fourier series, that is

$$f = \sum_{i=1}^3 \sum_{n=0_i}^{\infty} (f_n^{(i)})^{\wedge}(n) u_n^{*(i)}, \quad (2.31)$$

where the Fourier coefficients are given by

$$(f_n^{(i)})^\wedge(n) = (f, u_n^{*(i)})_{\mathfrak{h}}, \quad i = 1, 2, 3, \quad n = 0_i, 0_i + 1, \dots$$

2.2.2 \mathfrak{h} -Product Kernels and \mathfrak{h} -Convolutions

In order to replace the vectorial Fourier expansion with an expansion in terms of vectorial \mathfrak{h} -product kernels, it is crucial to define the kernel functions and convolutions in an appropriate manner. As in the scalar case, we start with the definitions of the \mathfrak{h} -product kernels, the admissibility conditions and finally end up with the corresponding convolutions.

Definition 2.13 *Let $(\mathfrak{h}, (\cdot, \cdot)_{\mathfrak{h}})$ and $(\mathcal{H}, (\cdot, \cdot)_{\mathcal{H}})$ be real separable Hilbert spaces of vectorial and scalar functions on the regular surface Σ' , respectively. Let furthermore $\{u_n^{*(i)}\}_{n=0_i, 0_i+1, \dots}^{i=1, 2, 3}$ and $\{U_n^*\}_{n=0, 1, \dots}$ be corresponding countable, orthonormal and complete systems. Any kernel function $\gamma^{(i)} : \Sigma' \times \Sigma' \rightarrow \mathbb{R}^3$ of the form*

$$\gamma^{(i)}(x, y) = \sum_{n=0_i}^{\infty} (\gamma^{(i)})^\wedge(n) U_n^*(x) u_n^{*(i)}(y), \quad x, y \in \Sigma', \quad (2.32)$$

with $(\gamma^{(i)})^\wedge(n) \in \mathbb{R}$, $i \in \{1, 2, 3\}$, $n = 0_i, 0_i + 1, \dots$ is called an \mathfrak{h} -product kernel of type i or, briefly, \mathfrak{h} -kernel of type i . For $i \in \{1, 2, 3\}$ the sequences $\{(\gamma^{(i)})^\wedge(n)\}_{n=0_i, 0_i+1, \dots}$ are called the symbol of the \mathfrak{h} -kernel of type i . The kernel obtained by summing up the type i kernels, i.e.

$$\gamma(x, y) = \sum_{i=1}^3 \sum_{n=0_i}^{\infty} (\gamma^{(i)})^\wedge(n) U_n^*(x) u_n^{*(i)}(y), \quad x, y \in \Sigma', \quad (2.33)$$

is called an \mathfrak{h} -product kernel or, briefly, \mathfrak{h} -kernel.

The definition of admissibility is similar to the scalar case:

Definition 2.14 *For $i \in \{1, 2, 3\}$ the symbols $\{(\gamma^{(i)})^\wedge(n)\}_{n=0_i, 0_i+1, \dots}$ of type i \mathfrak{h} -product kernels are said to be \mathfrak{h} -admissible if they satisfy the following conditions:*

$$(i) \quad \sum_{n=0}^{\infty} ((\gamma^{(i)})^\wedge(n))^2 < \infty, \quad (ii) \quad \sum_{n=0}^{\infty} ((\gamma^{(i)})^\wedge(n) U_n^*(x))^2 < \infty$$

for all $x \in \Sigma'$.

In contrast to the scalar approach, we now have to introduce two different convolutions, i.e. a decomposition convolution (the \mathfrak{h} -convolution) which yields a scalar valued function and a reconstruction convolution (the \star -convolution) which maps scalar functions to vectorial functions:

Definition 2.15 Let, for $i \in \{1, 2, 3\}$, $\gamma^{(i)} : \Sigma' \times \Sigma' \rightarrow \mathbb{R}^3$ be \mathfrak{h} -kernels of type i as given in (2.32) with \mathfrak{h} -admissible symbols. The \mathfrak{h} -convolution of $\gamma^{(i)}$ against a vector-valued function $f \in \mathfrak{h}$ is defined by

$$(\gamma^{(i)} *_{\mathfrak{h}} f)(x) = (\gamma^{(i)}(x, \cdot), f)_{\mathfrak{h}} = \sum_{n=0_i}^{\infty} (\gamma^{(i)})^{\wedge}(n) (f^{(i)})^{\wedge}(n) U_n^*. \quad (2.34)$$

The \star -convolution of $\gamma^{(i)}$ against a scalar-valued function $F \in \mathcal{H}$ is defined to be

$$(\gamma^{(i)} \star F)(x) = \sum_{n=0_i}^{\infty} (\gamma^{(i)})^{\wedge}(n) F^{\wedge}(n) u_n^{*(i)}. \quad (2.35)$$

Furthermore, by definition, we let

$$\gamma *_{\mathfrak{h}} f = \sum_{i=1}^3 \gamma^{(i)} *_{\mathfrak{h}} f$$

and

$$\gamma \star F = \sum_{i=1}^3 \gamma^{(i)} \star F,$$

where the \mathfrak{h} -kernel γ is obtained from the kernels $\gamma^{(i)}$ by summation (see (2.33)).

Remark 2.16 As a first consequence of Definition 2.15 it is clear that the \mathfrak{h} -convolution (2.34) yields a scalar-valued function whereas the \star -convolution (2.35) yields a vector-valued function. In addition, utilizing Definition 2.14, we can state that

$$\begin{aligned} \gamma^{(i)} *_{\mathfrak{h}} \cdot &: \mathfrak{h} \rightarrow \mathcal{H}, \\ \gamma^{(i)} \star \cdot &: \mathcal{H} \rightarrow \mathfrak{h}. \end{aligned}$$

From the types of functions involved in the aforementioned convolutions it becomes obvious that the \mathfrak{h} -convolution can be interpreted as a scalar product in the Hilbert space \mathfrak{h} . The \star -convolution, however, represents a scalar vector multiplication. It is also noteworthy that, due to condition (ii) in Definition 2.14, the \mathfrak{h} -kernels $\gamma^{(i)}(x, \cdot)$ as well as $\gamma(x, \cdot)$, $x \in \Sigma'$ fixed, are elements of \mathfrak{h} .

The next theorem, which can be seen in close relation to Theorem 2.4, leads us to the construction of \mathfrak{h} -scaling functions and \mathfrak{h} -wavelets in the subsequent sections.

Theorem 2.17 Let, for $i \in \{1, 2, 3\}$, $\gamma_1^{(i)}$ and $\gamma_2^{(i)}$ be \mathfrak{h} -kernels of type i with corresponding \mathfrak{h} -admissible symbols. Let, furthermore, γ_1 and γ_2 be the corresponding \mathfrak{h} -kernels. For each $f \in \mathfrak{h}$ it holds that

$$\gamma_2^{(i)} \star \gamma_1^{(i)} *_{\mathfrak{h}} f = \sum_{n=0_i}^{\infty} (\gamma_1^{(i)})^{\wedge}(n) (\gamma_2^{(i)})^{\wedge}(n) (f^{(i)})^{\wedge}(n) u_n^{*(i)}$$

as well as

$$\gamma_2 \star \gamma_1 \star_{\mathfrak{h}} f = \sum_{i=1}^3 \sum_{n=0_i}^{\infty} (\gamma_1^{(i)})^{\wedge}(n) (\gamma_2^{(i)})^{\wedge}(n) (f^{(i)})^{\wedge}(n) u_n^{*(i)}.$$

Proof. Using Definition 2.15 where the right hand side of Equation (2.34) serves as the function F in Equation (2.35) proves the assertion. ■

2.2.3 \mathfrak{h} -Scaling Functions and \mathfrak{h} -Wavelets

With the definitions of the \mathfrak{h} -product kernels, admissibility conditions and convolutions at hand, we can now proceed with the introduction of the corresponding \mathfrak{h} -scaling functions and \mathfrak{h} -wavelets. This, however, will enable us to come up with a multiresolution analysis similar to the scalar case. As far as the dilation and shifting operators are concerned, we can apply Definition 2.5 and just have to note that the dilation operator, when applied to a vectorial kernel, acts on each symbol corresponding to type i simultaneously.

Definition 2.18 Let, for $i \in \{1, 2, 3\}$, $(\varphi_0^{(i)})^{\wedge}(n)$ be \mathfrak{h} -admissible symbols which additionally satisfy

$$(i) \quad (\varphi_0^{(i)})^{\wedge}(0) = 1,$$

$$(ii) \quad n > k \Rightarrow (\varphi_0^{(i)})^{\wedge}(n) \leq (\varphi_0^{(i)})^{\wedge}(k),$$

then $(\varphi_0^{(i)})^{\wedge}(n)$ is said to be the generating symbol of the mother \mathfrak{h} -scaling function of type i , viz

$$\varphi_0^{(i)}(x, y) = \sum_{n=0_i}^{\infty} (\varphi_0^{(i)})^{\wedge}(n) U_n^*(x) u_n^{*(i)}(y), \quad x, y \in \Sigma'.$$

The vector $(\varphi_0)^{\wedge}(n) = \left((\varphi_0^{(1)})^{\wedge}(n), (\varphi_0^{(2)})^{\wedge}(n), (\varphi_0^{(3)})^{\wedge}(n) \right)^T$ is called the generating symbol of the \mathfrak{h} -scaling function given by

$$\varphi_0(x, y) = \sum_{i=1}^3 \sum_{n=0_i}^{\infty} (\varphi_0^{(i)})^{\wedge}(n) U_n^*(x) u_n^{*(i)}(y), \quad x, y \in \Sigma'.$$

Being interested in the dilated versions of the mother scaling functions we extend the definition of the generating symbols:

Definition 2.19 Let, for $i \in \{1, 2, 3\}$, $\left\{ (\varphi_J^{(i)})^{\wedge}(n) \right\}_{n=0_i, 0_i+1, \dots}$, $J \in \mathbb{Z}$, be an \mathfrak{h} -admissible

symbol satisfying, in addition, the following properties:

- (i) $\lim_{J \rightarrow \infty} \left(\left(\varphi_J^{(i)} \right)^\wedge (n) \right)^2 = 1$,
- (ii) $\left(\left(\varphi_J^{(i)} \right)^\wedge (n) \right)^2 \geq \left(\left(\varphi_{J-1}^{(i)} \right)^\wedge (n) \right)^2$,
- (iii) $\lim_{J \rightarrow -\infty} \left(\left(\varphi_J^{(i)} \right)^\wedge (n) \right)^2 = 0$,
- (iv) $\left(\left(\varphi_J^{(i)} \right)^\wedge (0) \right)^2 = 1$.

Then $\left\{ \left(\varphi_J^{(i)} \right)^\wedge (n) \right\}_{n=0_i, 0_i+1, \dots}$, $J \in \mathbb{Z}$, $i \in \{1, 2, 3\}$, is called the generating symbol of an \mathfrak{h} -scaling function of type i . The corresponding family $\left\{ \varphi_J^{(i)} \right\}$, $J \in \mathbb{Z}$, $i \in \{1, 2, 3\}$, of \mathfrak{h} -product kernels given by

$$\varphi_J^{(i)}(x, y) := \sum_{n=0_i}^{\infty} \left(\varphi_J^{(i)} \right)^\wedge (n) U_n^*(x) u_n^{*(i)}(y), \quad x, y \in \Sigma'$$

is called \mathfrak{h} -scaling function of type i . The \mathfrak{h} -scaling function $\{\varphi_J\}$, $J \in \mathbb{Z}$ is defined by

$$\varphi_J(x, y) := \sum_{i=1}^3 \sum_{n=0_i}^{\infty} \left(\varphi_J^{(i)} \right)^\wedge (n) U_n^*(x) u_n^{*(i)}(y), \quad x, y \in \Sigma'$$

and the vectors $\left\{ \left(\varphi_J \right)^\wedge (n) \right\}_{n=0_i, 0_i+1, \dots}$, $J \in \mathbb{Z}$, given by

$$\left(\varphi_J \right)^\wedge (n) = \left(\left(\varphi_J^{(1)} \right)^\wedge (n), \left(\varphi_J^{(2)} \right)^\wedge (n), \left(\varphi_J^{(3)} \right)^\wedge (n) \right)^T$$

denote the corresponding generating symbol.

Combining Theorem 2.17 with Definitions 2.18 and 2.19 we can come up with the following result:

Theorem 2.20 Let, for $i \in \{1, 2, 3\}$ and $J \in \mathbb{Z}$, $\left\{ \left(\varphi_J^{(i)} \right)^\wedge (n) \right\}_{n=0_i, 0_i+1, \dots}$ be the generating symbols of \mathfrak{h} -scaling functions of type i , i.e. $\left\{ \varphi_J^{(i)} \right\}$. Let $\{\varphi_J\}$ be the corresponding \mathfrak{h} -scaling function. For $f \in \mathfrak{h}$ let

$$f_J^{(i)} = \varphi_J^{(i)} \star \varphi_J^{(i)} *_{\mathfrak{h}} f$$

and

$$f_J = \varphi_J \star \varphi_J *_{\mathfrak{h}} f$$

be the type i J -level approximations and the J -level approximation of f , respectively. Then

$$\lim_{J \rightarrow \infty} \|f_J^{(i)} - f^{(i)}\|_{\mathfrak{h}} = 0, \quad i \in \{1, 2, 3\}$$

and

$$\lim_{J \rightarrow \infty} \|f_J - f\|_{\mathfrak{h}} = 0.$$

Proof. By virtue of Equation (2.31) and Theorem 2.17 we have

$$\begin{aligned} \lim_{J \rightarrow \infty} \left\| \sum_{i=1}^3 f_J^{(i)} - f \right\|_{\mathfrak{h}}^2 &= \\ \lim_{J \rightarrow \infty} \sum_{i=1}^3 \sum_{n=0_i}^{\infty} \left(\left(\varphi_J^{(i)} \right)^{\wedge(n)} - 1 \right)^2 \left(f^{(i)} \right)^{\wedge(n)} &. \end{aligned} \quad (2.36)$$

Using Definitions 2.18 and 2.19 it is easy to see that $\left(\left(\varphi_J^{(i)} \right)^{\wedge(n)} - 1 \right)$ is smaller than one, hence we can interchange sum and limit in (2.36). Using conditions (i) and (ii) of Definition 2.19 completes the proof. ■

We immediately proceed with the introduction of \mathfrak{h} -wavelets, that is:

Definition 2.21 Let, for $i \in \{1, 2, 3\}$ and $J \in \mathbb{Z}$, $\left\{ \left(\varphi_J^{(i)} \right)^{\wedge(n)} \right\}_{n=0_i, 0_i+1, \dots}$ be the generating symbols of \mathfrak{h} -scaling functions of type i . Then, for $i \in \{1, 2, 3\}$ and $j \in \mathbb{Z}$, the generating symbols

$$\left\{ \left(\psi_j^{(i)} \right)^{\wedge(n)} \right\}_{n=0_i, 0_i+1, \dots}$$

of the associated \mathfrak{h} -wavelets of type i are defined via the refinement equation

$$\left(\psi_j^{(i)} \right)^{\wedge(n)} = \left(\left(\varphi_{j+1}^{(i)} \right)^{\wedge(n)} - \left(\varphi_j^{(i)} \right)^{\wedge(n)} \right)^{\frac{1}{2}}. \quad (2.37)$$

The families $\left\{ \psi_j^{(i)} \right\}$, $j \in \mathbb{Z}$, $i \in \{1, 2, 3\}$, of \mathfrak{h} -product kernels given by

$$\psi_j^{(i)}(x, y) = \sum_{n=0_i}^{\infty} \left(\psi_j^{(i)} \right)^{\wedge(n)} U_n^*(x) u_n^{*(i)}(y), \quad x, y \in \Sigma',$$

are called \mathfrak{h} -wavelets of type i associated to the \mathfrak{h} -scaling functions $\left\{ \varphi_J^{(i)} \right\}$ of type i , $J \in \mathbb{Z}$. The family $\left\{ \psi_j \right\}$, $j \in \mathbb{Z}$, defined by

$$\psi_j = \sum_{i=1}^3 \psi_j^{(i)} \quad (2.38)$$

is called the \mathfrak{h} -wavelet associated to the \mathfrak{h} -scaling function $\left\{ \varphi_J \right\}$, $J \in \mathbb{Z}$.

Closely resembling the scalar case, we are now in a position to define the wavelet transform for vector fields $f \in \mathfrak{h}$:

Definition 2.22 Let $f \in \mathfrak{h}$ and let $\left\{ \psi_j^{(i)} \right\}$, $j \in \mathbb{Z}$, $i \in \{1, 2, 3\}$, be the \mathfrak{h} -wavelets of type i associated to $\left\{ \varphi_J^{(i)} \right\}$, $J \in \mathbb{Z}$, i.e. the \mathfrak{h} -scaling function of type i . Then the type i wavelet transform $WT^{(i)}$ of f at scale $j \in \mathbb{Z}$ and position $x \in \Sigma'$ is given by

$$WT^{(i)}(f)(j, x) = \left(\psi_j^{(i)}(x, \cdot), f \right)_{\mathfrak{h}} = \left(\psi_j^{(i)} *_{\mathfrak{h}} f \right)(x), \quad f \in \mathfrak{h}.$$

The wavelet transform of f at scale $j \in \mathbb{Z}$ and position $x \in \Sigma'$ is defined via

$$WT(f)(j, x) = (\psi_j(x, \cdot), f)_{\mathfrak{h}} = (\psi_j *_{\mathfrak{h}} f)(x), \quad f \in \mathfrak{h},$$

where ψ_j is given as in (2.38).

With the formalism constructed so far, we can state the main result of the vectorial wavelet approach, i.e. we can establish a multiscale reconstruction principle for vector-valued functions.

Theorem 2.23 *Let $\{\psi_j^{(i)}\}$, $j \in \mathbb{Z}$, $i \in \{1, 2, 3\}$, be the \mathfrak{h} -wavelets of type i associated to $\{\varphi_J^{(i)}\}$, $J \in \mathbb{Z}$, i.e. the \mathfrak{h} -scaling function of type i . Furthermore, for $f \in \mathfrak{h}$ and $i \in \{1, 2, 3\}$, let*

$$f_J^{(i)} = \varphi_0^{(i)} \star (\varphi_0^{(i)} *_{\mathfrak{h}} f) + \sum_{j=0}^{J-1} \psi_j^{(i)} \star (WT^{(i)}(f)(j, \cdot))$$

as well as

$$f_J = \varphi_0 \star (\varphi_0 *_{\mathfrak{h}} f) + \sum_{j=0}^{J-1} \psi_j \star (WT(f)(j, \cdot)).$$

Then

$$\lim_{J \rightarrow \infty} \|f_J^{(i)} - f^{(i)}\|_{\mathfrak{h}} = 0, \quad i \in \{1, 2, 3\}$$

and

$$\lim_{J \rightarrow \infty} \|f_J - f\|_{\mathfrak{h}} = 0.$$

Proof. Via summation we obtain from the refinement equation (2.37) that

$$((\varphi_{J+1}^{(i)})^{\wedge}(n))^2 = ((\varphi_0^{(i)})^{\wedge}(n))^2 + \sum_{j=0}^J ((\psi_j^{(i)})^{\wedge}(n))^2, \quad i \in \{1, 2, 3\}.$$

This, however, is equivalent to

$$\varphi_{J+1}^{(i)} \star (\varphi_{J+1}^{(i)} *_{\mathfrak{h}} f) = \varphi_0^{(i)} \star (\varphi_0^{(i)} *_{\mathfrak{h}} f) + \sum_{j=0}^J \psi_j^{(i)} \star (\psi_j^{(i)} *_{\mathfrak{h}} f), \quad i \in \{1, 2, 3\},$$

which, in combination with Theorem 2.20, leads to the required result. ■

In terms of filtering the application of $\varphi_J \star \varphi_J *_{\mathfrak{h}}$, respectively $\varphi_J^{(i)} \star \varphi_J^{(i)} *_{\mathfrak{h}}$, to a vector-valued function $f \in \mathfrak{h}$ can be interpreted as low-pass filtering of this function, while the application of $\psi_j \star \psi_j *_{\mathfrak{h}}$, respectively $\psi_j^{(i)} \star \psi_j^{(i)} *_{\mathfrak{h}}$, is equivalent to the application of a band-pass filter. Therefore, in analogy to the scale and detail spaces of the scalar approach, we can define vectorial scale and detail spaces via

$$\begin{aligned} v_j^{(i)} &= \{\varphi_j^{(i)} \star \varphi_j^{(i)} *_{\mathfrak{h}} f \mid f \in \mathfrak{h}\}, \quad i \in \{1, 2, 3\}, \\ v_j &= \{\varphi_j \star \varphi_j *_{\mathfrak{h}} f \mid f \in \mathfrak{h}\}, \\ w_j^{(i)} &= \{\psi_j^{(i)} \star \psi_j^{(i)} *_{\mathfrak{h}} f \mid f \in \mathfrak{h}\}, \quad i \in \{1, 2, 3\}, \quad \text{and} \\ w_j &= \{\psi_j \star \psi_j *_{\mathfrak{h}} f \mid f \in \mathfrak{h}\}. \end{aligned}$$

The spaces $v_j^{(i)}$ are the scale spaces of type i and scale j , v_j the scale spaces of scale j . The spaces $w_j^{(i)}$, respectively w_j , are the detail spaces of type i and scale j , respectively the detail spaces of scale j . The detail spaces contain all the necessary detail information to go from approximations at lower scales to approximations at subsequently higher scales, i.e.

$$v_0^{(i)} + \sum_{j=0}^J w_j^{(i)} = v_{J+1}^{(i)}, \quad v_J^{(i)} + w_J^{(i)} = v_{J+1}^{(i)}, \quad J \in \mathbb{Z}, \quad i \in \{1, 2, 3\},$$

and

$$v_0 + \sum_{j=0}^J w_j = v_{J+1}, \quad v_J + w_J = v_{J+1}, \quad J \in \mathbb{Z}.$$

The concept of a multiresolution analysis for vector fields can, of course, be carried over from the scalar case and will, for the sake of brevity, be omitted (compare Definitions 2.7 and 2.19). In the vectorial case it is also possible to construct bandlimited and non-bandlimited \mathfrak{h} -scaling functions and wavelets. The construction principles are those given in the scalar case, but need to be applied to each generating symbol of type i , simultaneously. Last but not least we present a realization of \mathfrak{h} -wavelets, namely spherical vectorial wavelets, which will be of tremendous importance for our further considerations.

2.2.4 Example

Spherical Vectorial Wavelets

Now we consider the space $l^2(\Omega)$ of square-integrable vector-valued functions $f : \Omega \rightarrow \mathbb{R}^3$ on the unit sphere (i.e. $\Sigma' = \Omega \subset \mathbb{R}^3$, $\mathfrak{h} = l^2(\Omega)$, see also Chapter 1). Equipped with the inner product

$$(f, g)_{l^2(\Omega)} = \int_{\Omega} f(\eta) \cdot g(\eta) \, d\omega(\eta), \quad f, g \in l^2(\Omega),$$

$l^2(\Omega)$ is a Hilbert space. Using the $\mathcal{L}^2(\Omega)$ -orthonormal system $\{Y_{n,k}\}_{\substack{n=0,1,\dots, \\ k=1,\dots,2n+1}}$ of spherical harmonics we are able to introduce an $l^2(\Omega)$ -orthonormal system

$$\left\{ y_{n,k}^{(i)} \right\}_{\substack{i=1,2,3 \\ n=0_i, 0_i+1, \dots, \\ k=1, \dots, 2n+1}} \quad (2.39)$$

via

$$\begin{aligned} y_{n,k}^{(1)}(\xi) &= \xi Y_{n,k}(\xi), \\ y_{n,k}^{(2)}(\xi) &= \frac{1}{\sqrt{(n(n+1))}} \nabla_{\xi}^* Y_{n,k}(\xi), \\ y_{n,k}^{(3)}(\xi) &= \frac{1}{\sqrt{(n(n+1))}} L_{\xi}^* Y_{n,k}(\xi), \end{aligned}$$

where $\xi \in \Omega$. Using the system (2.39), every function $f \in l^2(\Omega)$ can then be represented by its Fourier series, i.e.

$$f = \sum_{i=1}^3 \sum_{n=0_i}^{\infty} \sum_{k=1}^{2n+1} (f^{(i)})^{\wedge}(n, k) y_{n,k}^{(i)}$$

with coefficients

$$(f^{(i)})^{\wedge}(n, k) = \int_{\Omega} f(\eta) \cdot y_{n,k}^{(i)}(\eta) \, d\omega(\eta).$$

Using $\mathcal{H} = \mathcal{L}^2(\Omega)$, the vectorial $l^2(\Omega)$ -kernel functions of type i are of the form (see Definition 2.13)

$$\gamma^{(i)}(\xi, \eta) = \sum_{n=0_i}^{\infty} \sum_{k=1}^{2n+1} (\gamma^{(i)})^{\wedge}(n) Y_{n,k}(\xi) y_{n,k}^{(i)}(\eta), \quad (2.40)$$

and the vectorial $l^2(\Omega)$ -kernel functions are then derived by

$$\gamma(\xi, \eta) = \sum_{i=1}^3 \gamma^{(i)}(\xi, \eta),$$

with $(\gamma^{(i)})^{\wedge}(n) \in \mathbb{R}$ for $i \in \{1, 2, 3\}$, $n = 0, 1, \dots$. Admissibility is guaranteed provided that

$$\sum_{n=0_i}^{\infty} ((\gamma^{(i)})^{\wedge}(n))^2 \frac{2n+1}{4\pi} < \infty$$

is assumed (see [9, 10]). It should be observed that, if P_n denotes the Legendre polynomial of degree n , we obtain (see Equations (1.6) and (1.7))

$$\nabla_{\xi}^* P_n(\xi \cdot \eta) = (\eta - (\xi \cdot \eta)\xi) P_n'(\xi \cdot \eta),$$

$$L_{\xi}^* P_n(\xi \cdot \eta) = \xi \wedge \eta P_n'(\xi \cdot \eta),$$

such that singularities at the poles are completely avoided by use of the kernel representations (2.40). In connection with the addition theorem (see Theorem 1.6) of scalar spherical harmonics this leads to the following, numerically very useful, representations of the vectorial kernel functions of type i :

$$\gamma^{(1)}(\xi, \eta) = \xi \sum_{n=0_i}^{\infty} \sum_{k=1}^{2n+1} \frac{2n+1}{4\pi} (\gamma^{(1)})^{\wedge}(n) P_n(\xi \cdot \eta),$$

$$\gamma^{(2)}(\xi, \eta) = (\eta - (\xi \cdot \eta)\xi) \sum_{n=0_i}^{\infty} \sum_{k=1}^{2n+1} \frac{2n+1}{4\pi} \frac{1}{\sqrt{n(n+1)}} (\gamma^{(2)})^{\wedge}(n) P_n'(\xi \cdot \eta),$$

$$\gamma^{(3)}(\xi, \eta) = (\xi \wedge \eta) \sum_{n=0_i}^{\infty} \sum_{k=1}^{2n+1} \frac{2n+1}{4\pi} \frac{1}{\sqrt{n(n+1)}} (\gamma^{(3)})^{\wedge}(n) P_n'(\xi \cdot \eta)$$

(that is the kernels separate into a vectorial and a scalar part; the vectorial part is easily available and the scalar sum can be calculated via fast and stable algorithms. See [81] for

details on the numerical realization). Using those kernels, two kinds of convolutions need to be introduced (cf. [10] and Definition 2.15), i.e. a convolution of vectorial kernels against vectorial functions - resulting in scalar coefficients - and a convolution of vectorial kernels against scalar valued functions - enabling us to reconstruct a vectorial function from scalar coefficients. The corresponding convolutions are given by

$$(\gamma * f)(\xi) = \int_{\Omega} \gamma(\xi, \eta) \cdot f(\eta) \, d\omega(\eta) \quad (2.41)$$

$$= \sum_{i=1}^3 \sum_{n=0_i}^{\infty} \sum_{k=1}^{2n+1} (\gamma^{(i)})^{\wedge}(n) (f^{(i)})^{\wedge}(n, k) Y_{n,k}(\xi), \quad \xi \in \Omega, \quad (2.42)$$

mapping vector fields onto scalar fields and

$$(\gamma \star F)(\xi) = \int_{\Omega} \gamma(\eta, \xi) F(\eta) \, d\omega(\eta) \quad (2.43)$$

$$= \sum_{i=1}^3 \sum_{n=0_i}^{\infty} \sum_{k=1}^{2n+1} (\gamma^{(i)})^{\wedge}(n) F^{\wedge}(n, k) y_{n,k}^{(i)}(\xi), \quad \xi \in \Omega, \quad (2.44)$$

mapping scalar functions onto vectorial functions. Applying both convolutions consecutively to a function $f \in l^2(\Omega)$ results in

$$\gamma \star \gamma * f = \sum_{i=1}^3 \sum_{n=0_i}^{\infty} \sum_{k=1}^{2n+1} ((\gamma^{(i)})^{\wedge}(n))^2 (f^{(i)})^{\wedge}(n, k) y_{n,k}^{(i)}. \quad (2.45)$$

Hence, the reconstruction formula recovering a function $f \in l^2(\Omega)$ now reads

$$f = \Phi_0 \star \Phi_0 * f + \sum_{j=0}^{\infty} \Psi_j \star \Psi_j * f$$

with $\varphi_0 = \sum_{i=1}^3 \varphi_0^{(i)}$ and $\psi_j = \sum_{i=1}^3 \psi_j^{(i)}$.

Figures 2.4 and 2.5 compare a vector spherical harmonic of type 3 with a CP spherical vectorial wavelet of type 3. Both functions are plotted on a globe in order to illustrate the support of these functions when used in geoapplications.

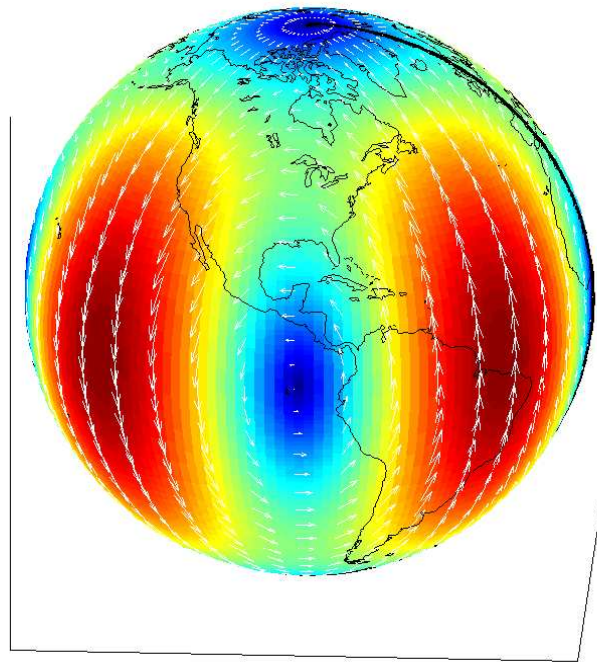


Figure 2.4: Vector spherical harmonic of type 3, degree 2 and order 1. Colors indicate absolute value and arrows the direction.

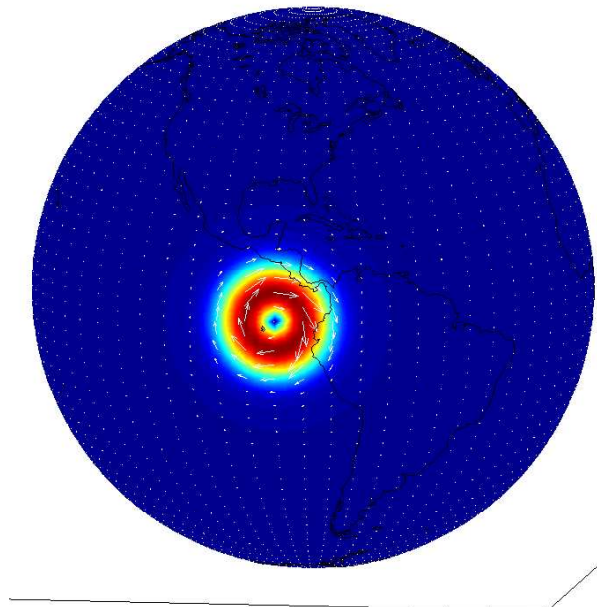


Figure 2.5: CP spherical vectorial wavelet of type 3 and scale 4. Colors indicate absolute value and arrows the direction.

2.2.5 Parenthesis: Tensorial Wavelets

The last section on spherical vectorial wavelets provides us with a technique that is easily put into numerical practise. From a theoretical point of view, however, the canonical way of dealing with spherical vector fields in a multiscale framework is given by tensor radial basis functions and tensor convolutions (e.g. [30]). Though tensor radial basis functions cannot be derived in our general treatise of \mathcal{H} - and \mathfrak{h} -product kernels, we will extensively use them in Section 3.2.2. This is why we will present a brief introduction here, based on [30] and our treatise in [34]. It should be noted that in [87] a more general approach to wavelets in Hilbert spaces is formulated which allows the derivation of tensor radial basis functions as well as scalar radial basis functions; however, this approach does not allow the use of \mathfrak{h} -product kernels – especially spherical vectorial wavelets – which are one of the most important tools of this thesis. Nevertheless, the concept of tensor radial basis functions is closely related to that of spherical vectorial scaling functions and wavelets. The connection can be established by means of appropriate definitions of the corresponding convolution operators (see Theorem 2.28 and [10, 12]).

The reason for tensor radial basis functions being the canonical tool for a multiscale treatment of spherical vector fields is based on a main result in vector spherical harmonic theory (see [12, 30]: The reproducing kernels of the spaces $harm_{l\dots m}^{(i)}(\Omega)$ are given by linear combinations of Legendre tensors of type i , i.e.:

$$\sum_{n=l}^m \frac{2n+1}{4\pi} \mathbf{p}_n^{(i,i)}.$$

Consequently, any $f \in l^2(\Omega)$ can be expressed as follows:

$$f = \sum_{i=1}^3 \sum_{n=0_i}^{\infty} \frac{2n+1}{4\pi} \int_{\Omega} \mathbf{p}_n^{(i,i)}(\cdot, \eta) f(\eta) d\omega(\eta) . \quad (2.46)$$

Definition 2.24 Any function $\mathbf{h}^{(i)} : \Omega \times \Omega \rightarrow \mathbb{R}^{3 \times 3}$, $i \in \{1, 2, 3\}$, of the form

$$\mathbf{h}^{(i)}(\xi, \eta) = \sum_{n=0_i}^{\infty} \frac{2n+1}{4\pi} (\mathbf{h}^{(i)})^{\wedge}(n) \mathbf{p}_n^{(i,i)}(\xi, \eta), \quad (\xi, \eta) \in \Omega \times \Omega,$$

is called (square-summable) tensor radial basis function of type i if its symbol $\{(\mathbf{h}^{(i)})^{\wedge}(n)\}_{n=0_i, 0_i+1, \dots} \subset \mathbb{R}$ satisfies the condition:

$$\sum_{n=0_i}^{\infty} \frac{2n+1}{4\pi} ((\mathbf{h}^{(i)})^{\wedge}(n))^2 < \infty .$$

$\mathbf{h} = \sum_{i=1}^3 \mathbf{h}^{(i)}$ with $\mathbf{h}^{(i)}$ (square-summable) tensor radial basis functions of type i is called (square-summable) tensor radial basis function.

A key property of a tensor radial basis function \mathbf{h} is its invariance under orthogonal transformations \mathbf{t} , i.e.,

$$\mathbf{h}(\mathbf{t}\xi, \mathbf{t}\eta) = \mathbf{t}\mathbf{h}(\xi, \eta)\mathbf{t}^T, \quad (\xi, \eta) \in \Omega \times \Omega .$$

This property falls back upon the Legendre tensors

$$\mathbf{p}_n^{(i,i)}(\mathbf{t}\xi, \mathbf{t}\eta) = \mathbf{t}\mathbf{p}_n^{(i,i)}(\xi, \eta)\mathbf{t}^T, \quad (\xi, \eta) \in \Omega \times \Omega .$$

Looking at Equation (2.46) the following definition is sound:

Definition 2.25 Let $\mathbf{h}_1^{(i)}, \mathbf{h}_2^{(i)}$ be (square-summable) tensor radial basis functions of type i . Suppose that f is of class $l^2(\Omega)$. Then $\mathbf{h}_1^{(i)} * f$ defined by

$$\left(\mathbf{h}_1^{(i)} * f\right)(\xi) = \int_{\Omega} \mathbf{h}_1^{(i)}(\xi, \eta) f(\eta) d\omega(\eta), \quad \xi \in \Omega,$$

is called the convolution of $\mathbf{h}_1^{(i)}$ against f . Furthermore, $\mathbf{h}_2^{(i)} * \mathbf{h}_1^{(i)}$ defined by

$$\left(\mathbf{h}_2^{(i)} * \mathbf{h}_1^{(i)}\right)(\xi, \eta) = \int_{\Omega} \mathbf{h}_2^{(i)}(\xi, \zeta) \mathbf{h}_1^{(i)}(\zeta, \eta) d\omega(\zeta), \quad (\xi, \eta) \in \Omega \times \Omega,$$

is said to be the ‘ $*$ ’ convolution of $\mathbf{h}_2^{(i)}$ against $\mathbf{h}_1^{(i)}$. Additionally, we let

$$\mathbf{h}_2 * \mathbf{h}_1 = \sum_{i=1}^3 \mathbf{h}_2^{(i)} * \mathbf{h}_1^{(i)}.$$

It can be shown that

$$\mathbf{h}_2 * \mathbf{h}_1 * f = \sum_{i=1}^3 \sum_{n=0_i}^{\infty} \sum_{k=1}^{2n+1} (\mathbf{h}_1^{(i)})^{\wedge}(n) (\mathbf{h}_2^{(i)})^{\wedge}(n) (f^{(i)})^{\wedge}(n, k) y_{n,k}^{(i)}. \quad (2.47)$$

Utilizing Definitions 2.19 and 2.21 as well as Definition 2.25 we are now in a position to define tensor scaling functions and wavelets:

Definition 2.26 Let $\left\{ \left(\Phi_j^{(i)} \right)^{\wedge}(n) \right\}_{n=0_i, 0_i+1 \dots}$ and $\left\{ \left(\Psi_j^{(i)} \right)^{\wedge}(n) \right\}_{n=0_i, 0_i+1 \dots}$ be generating symbols of $l^2(\Omega)$ -scaling functions and corresponding wavelets of type i , $i \in \{1, 2, 3\}$. The corresponding families $\left\{ \Phi_j^{(i)} \right\}$ and $\left\{ \Psi_j^{(i)} \right\}$ of tensor kernels defined by

$$\Phi_j^{(i)}(\xi, \eta) = \sum_{n=0_i}^{\infty} \sum_{k=1}^{2n+1} (\Phi_j^{(i)})^{\wedge}(n) y_{n,k}^{(i)}(\xi) \otimes y_{n,k}^{(i)}(\eta), \quad (\xi, \eta) \in \Omega^2, \quad j \in \mathbb{Z}$$

and

$$\Psi_j^{(i)}(\xi, \eta) = \sum_{n=0_i}^{\infty} \sum_{k=1}^{2n+1} (\Psi_j^{(i)})^{\wedge}(n) y_{n,k}^{(i)}(\xi) \otimes y_{n,k}^{(i)}(\eta), \quad (\xi, \eta) \in \Omega^2, \quad j \in \mathbb{Z}$$

are called *tensorial scaling functions*, respectively *wavelets*, of type i . Furthermore we set

$$\Phi_j = \sum_{i=1}^3 \Phi_j^{(i)}$$

and

$$\Psi_j = \sum_{i=1}^3 \Psi_j^{(i)}$$

to be the *tensorial scaling functions* and *wavelets*.

This, together with Equation (2.47), suffices to proof the following:

Theorem 2.27 *Let $f \in l^2(\Omega)$. Suppose $\{\Phi_j^{(i)}\}$ and $\{\Psi_j^{(i)}\}$ to be tensorial scaling functions and wavelets of type i and let $\Phi_J = \sum_{i=1}^3 \Phi_J^{(i)}$ as well as $\Psi_j = \sum_{i=1}^3 \Psi_j^{(i)}$, $j, J \in \mathbb{Z}$. Then*

$$\lim_{J \rightarrow \infty} \left\| \Phi_J^{(i)} * \Phi_J^{(i)} * f - f^{(i)} \right\|_{l^2(\Omega)} = 0, \quad i = 1, 2, 3,$$

and

$$\lim_{J \rightarrow \infty} \left\| \Phi_J * \Phi_J * f - f \right\|_{l^2(\Omega)} = 0$$

as well as

$$\lim_{J \rightarrow \infty} \left\| \left(\Phi_0^{(i)} * \Phi_0^{(i)} * f + \sum_{j=0}^J \Psi_j^{(i)} * \Psi_j^{(i)} * f \right) - f^{(i)} \right\|_{l^2(\Omega)} = 0, \quad i = 1, 2, 3,$$

and

$$\lim_{J \rightarrow \infty} \left\| \left(\Phi_0 * \Phi_0 * f + \sum_{l=0}^{\infty} \Psi_l * \Psi_l * f \right) - f \right\|_{l^2(\Omega)} = 0.$$

It is this theorem that serves as the starting point for our considerations in Section 3.2.2.

It will be essential for our examinations in Section 3.2.3 that the link between the tensor and the vector formalism can be established via the convolutions in the tensor case (see Definition 2.25) and the two convolutions defined for the vector case (cf. Definition 2.15 for the general vectorial case and equations (2.41) and (2.43) for the case of spherical vectorial wavelets):

Theorem 2.28 *Let f be of class $l^2(\Omega)$. Assume that h, k are (square-summable) vector radial basis functions. Moreover, suppose that \mathbf{h}, \mathbf{k} are (square-summable) tensor radial basis functions with*

$$(\mathbf{h}^{(i)})^\wedge(n) = (h^{(i)})^\wedge(n),$$

$$(\mathbf{k}^{(i)})^\wedge(n) = (k^{(i)})^\wedge(n),$$

for all $n = 0_i, 0_i + 1, \dots$ and $i \in \{1, 2, 3\}$. Then

$$\mathbf{h} * \mathbf{k} * f = h \star k * f .$$

A proof can be found in [10] and is, for the convenience of the reader, recapitulated here.

Proof. From (2.47) we know that

$$\mathbf{h} * \mathbf{k} * f = \sum_{i=1}^3 \sum_{n=0_i}^{\infty} \sum_{k=1}^{2n+1} (\mathbf{h}^{(i)})^{\wedge}(n) (\mathbf{k}^{(i)})^{\wedge}(n) (f^{(i)})^{\wedge}(n, k) y_{n,k}^{(i)}.$$

Using the assumption that

$$(\mathbf{h}^{(i)})^{\wedge}(n) = (h^{(i)})^{\wedge}(n),$$

$$(\mathbf{k}^{(i)})^{\wedge}(n) = (k^{(i)})^{\wedge}(n),$$

for all $n = 0_i, 0_i + 1, \dots$ and $i \in \{1, 2, 3\}$ this leads to

$$\mathbf{h} * \mathbf{k} * f = \sum_{i=1}^3 \sum_{n=0_i}^{\infty} \sum_{k=1}^{2n+1} (h^{(i)})^{\wedge}(n) (k^{(i)})^{\wedge}(n) (f^{(i)})^{\wedge}(n, k) y_{n,k}^{(i)}.$$

The completeness of vector spherical harmonics together with (2.45) yields

$$\mathbf{h} * \mathbf{k} * f = h \star k * f .$$

■

This theorem, however, shows us that the different types of bilinear convolutions lead to equivalent results. This is of tremendous importance for our consideration concerning multiscale denoising of spherical vector fields in Chapter 3.

Chapter 3

Multiscale Denoising of Spherical Functions

When dealing with real geophysically relevant data it should be kept in mind that each measurement does not really give the value of the observable under consideration but that – at least to some extent – the data are contaminated with noise. That is, in order to successfully improve geomathematical field modelling, one main aspect is to extract the true portion of the observable from the actual signal. In consequence, a particular emphasis lies on the subject of denoising. This endeavor is precisely the goal in statistical function estimation. Here, the interest is to ‘smooth’ the noisy data in order to obtain an estimate of the underlying function. In Euclidean theory of wavelets signal processors now have new, fast tools that are well-suited for denoising signals (for a survey the reader is e.g. referred to [89] and the references therein).

The objective of this Chapter is to introduce multiscale signal-to-noise thresholding thus providing the wavelet oriented basis of denoising spherical scalar or vectorial data sets. Our approach is essentially influenced by the concept of sparse wavelet representations in Euclidean geometries (e.g. [102, 17, 18]) as well as the stochastic model – based on spectral properties of signals and noise – used in satellite geodesy (see [95, 55] and the references therein). As far as vectorial, especially geomagnetic satellite data sets are concerned another, in some sense geometric, approach should be mentioned. This method, introduced and extended in [61, 62, 63] and [60] is mainly concerned with the reduction of noise produced by (anisotropic) attitude uncertainties of the satellite and is especially well suited for satellite missions where the attitude error (due to star cameras etc.) can be well estimated.

We start with the treatment of scalar data. First we will recapitulate the necessary spectral theory in terms of spherical harmonics which is then generalized to the concept of multiscale signal-to-noise thresholding (see also [40, 33]). Influenced by the results of the scalar case we will extend the treatment to vectorial data sets (cf. also our treatment in [34]). Here the first step will be the development of a spectral framework in terms of vector spherical harmonics. This will then serve as a starting point for a generalization to a multiscale method in terms of tensor spherical wavelets. Though numerically difficult to handle, this approach is the

canonical extension of the scalar approach. In order to get a multiscale technique that is easily applicable we then develop a multiscale framework in terms of vector spherical wavelets and show its equivalence to the tensor based approach.

3.1 Signal-to-Noise Thresholding of Scalar Fields

3.1.1 Spectral Signal-to-Noise Response

In the geosciences it is often reasonable to consider a measurement (after possible linearization) as a linear operator Λ acting on an 'input signal' F producing an 'output signal' G , i.e.

$$\Lambda F = G.$$

Λ is supposed to be an operator mapping the space $\mathcal{L}^2(\Omega)$ onto itself such that

$$\Lambda Y_{n,k} = \Lambda^\wedge(n, k) Y_{n,k}, \quad (n, k) \in \mathcal{N}, \quad (3.1)$$

where the so-called *symbol* $\{\Lambda^\wedge(n, k)\}_{(n,k) \in \mathcal{N}}$ is the sequence of the real numbers $\Lambda^\wedge(n, k)$ and where we have used the abbreviation

$$\mathcal{N} = \{(n, k) | n = 0, 1, \dots; k = 1, \dots, 2n + 1\}.$$

It is clear that different linear operators Λ are characterized by means of different symbols $\{\Lambda^\wedge(n, k)\}_{(n,k) \in \mathcal{N}}$. From Equation (3.1) and the Fourier representation of F we obviously can conclude that the spectrum $\{G^\wedge(n, k)\}_{(n,k) \in \mathcal{N}}$ of the output signal can, in terms of the spectrum $\{F^\wedge(n, k)\}_{(n,k) \in \mathcal{N}}$ of the input signal, be described by a simple multiplication by the 'transfer' $\Lambda^\wedge(n, k)$.

Thus far only a (deterministic) function model has been discussed. If a comparison of the 'output function' with the actual value were done, discrepancies would be observed. A mathematical description of these discrepancies has to follow the laws of probability theory in a stochastic model (see e.g. [89]). Usually the observations are not looked upon as a time series, but rather a function \tilde{G} on the sphere Ω (' \sim ' for stochastic). According to this approach we assume that we have

$$\tilde{G} = G + \tilde{\varepsilon},$$

where $\tilde{\varepsilon}$ is the *observation noise*. Moreover, in our approach motivated by information in satellite technology (see [95] and the references therein), we suppose the *covariance* to be known, i.e.

$$\text{Cov} [\tilde{G}(\xi), \tilde{G}(\eta)] = E [\tilde{\varepsilon}(\xi), \tilde{\varepsilon}(\eta)] = K(\xi, \eta), \quad (\xi, \eta) \in \Omega \times \Omega,$$

where the covariance kernel K is given as follows:

Definition 3.1 Let $K : \Omega \times \Omega \rightarrow \mathbb{R}$ be a kernel of the form

$$K(\xi, \eta) = \sum_{(n,k) \in \mathcal{N}} K^\wedge(n, k) Y_{n,k}(\xi) Y_{n,k}(\eta)$$

where the symbol $\{K^\wedge(n, k)\}_{(n, k) \in \mathcal{N}}$ satisfies the conditions

(C1) $K^\wedge(n, k) \geq 0$ for all $(n, k) \in \mathcal{N}$,

(C2) $\sum_{n=0}^{\infty} \frac{2n+1}{4\pi} \sup_{k=1, \dots, 2n+1} (K^\wedge(n, k))^2 < \infty$.

Then K is called a covariance kernel.

It is noteworthy that this approach assumes that the first two statistical moments suffice for a complete description, that the error spectrum can be considered invariant over the measurement's period and that one realization in space (or mission time) is enough to deduce the stochastic characteristics. We do not discuss the details of this subject but direct the reader to the treatment in [104] and the references therein.

Degree Variances

Using the fact that any 'output function' (more clearly the output signal, i.e. the observable) can be expanded into an orthogonal series in terms of spherical harmonics

$$\begin{aligned} \tilde{G} = \widetilde{\Lambda F} &= \sum_{(n, k) \in \mathcal{N}} \Lambda^\wedge(n, k) \tilde{F}^\wedge(n, k) Y_{n, k} \\ &= \sum_{(n, k) \in \mathcal{N}} \tilde{G}^\wedge(n, k) Y_{n, k} \end{aligned}$$

in the sense of $\|\cdot\|_{\mathcal{L}^2(\Omega)}$, we get a spectral representation of the form

$$\tilde{G}^\wedge(n, k) = (\widetilde{\Lambda F})^\wedge(n, k) = \Lambda^\wedge(n, k) \tilde{F}^\wedge(n, k), \quad (n, k) \in \mathcal{N}. \quad (3.2)$$

Since this representation clearly distinguishes between the different degrees and orders one is led to observe the root-mean-square power per spherical harmonic degree and order, respectively per degree, to characterize the signal:

Definition 3.2 Let $G \in \mathcal{L}^2(\Omega)$. Let, for $(n, k) \in \mathcal{N}$, $G^\wedge(n, k)$ be the corresponding orthogonal coefficients. Then, for $(n, k) \in \mathcal{N}$, the signal degree and order variances of G are defined by

$$\begin{aligned} \text{Var}_{n, k}(G) &= \int_{\Omega} \int_{\Omega} G(\xi) G(\eta) Y_{n, k}(\xi) Y_{n, k}(\eta) d\omega(\xi) d\omega(\eta) \\ &= (G^\wedge(n, k))^2. \end{aligned} \quad (3.3)$$

Correspondingly, for $n \in \mathbb{N}_0$, the signal degree variances of G are defined by

$$\begin{aligned} \text{Var}_n(G) &= \frac{2n+1}{4\pi} \int_{\Omega} \int_{\Omega} G(\xi)G(\eta)P_n(\xi \cdot \eta)d\omega(\xi)d\omega(\eta) \\ &= \sum_{k=1}^{2n+1} (G^\wedge(n, k))^2 \\ &= \sum_{k=1}^{2n+1} \text{Var}_{n,k}(G). \end{aligned}$$

From Parseval's identity we get that

$$\|G\|_{\mathcal{L}^2(\Omega)}^2 = \sum_{n=0}^{\infty} \text{Var}_n(G) = \sum_{(n,k) \in \mathcal{N}} \text{Var}_{n,k}(G), \quad (3.4)$$

connecting the signal degree and order variances as well as the signal degree variances with the ' $\mathcal{L}^2(\Omega)$ -energy' of the corresponding function.

In order to determine the variances in the case of the 'output function' $\tilde{G} = \widetilde{\Lambda F}$ we can use representation (3.2) and end up with

$$\text{Var}_{n,k}(\widetilde{\Lambda F}) = \left(\left(\widetilde{\Lambda F} \right)^\wedge(n, k) \right)^2$$

and

$$\text{Var}_n(\widetilde{\Lambda F}) = \sum_{k=1}^{2n+1} \left(\left(\widetilde{\Lambda F} \right)^\wedge(n, k) \right)^2.$$

It should be noted that physical devices do not transmit signals of arbitrarily high frequency without severe attenuation. Therefore, the 'transfer' $\Lambda^\wedge(n, k)$ usually tends to zero with increasing degree n . Consequently, the amplitude spectra of the responses (observations) to functions (signals) of finite $\mathcal{L}^2(\Omega)$ -energy are negligibly small beyond some finite frequency. Thus, because of the frequency limiting nature of the used devices and because of the resulting nature of the 'transmitted signals', one is soon led to consider bandlimited functions. These are functions $\tilde{G} \in \mathcal{L}^2(\Omega)$, whose amplitude spectra vanish for all $n > N \in \mathbb{N}_0$, N fixed. In other words $\text{Var}_n(\tilde{G}) = 0$ for all $n > N$.

Degree Error Covariances

The spectral approach to signal-to-noise thresholding is, in addition to the previously defined degree variances, based on similar measures calculated from the a priorily known covariance kernel of the noise:

Definition 3.3 Let, in accordance with Definition 3.1, $\{K^\wedge(n, k)\}_{(n, k) \in \mathcal{N}}$ be the symbol of a covariance kernel $K : \Omega \times \Omega \rightarrow \mathbb{R}$. Then the degree and order error covariance of K is defined by

$$\begin{aligned} \text{Cov}_{n, k}(K) &= \int_{\Omega} \int_{\Omega} K(\xi, \eta) Y_{n, k}(\xi) Y_{n, k}(\eta) d\omega(\xi) d\omega(\eta) \\ &= K^\wedge(n, k), \quad n \in \mathcal{N}. \end{aligned} \quad (3.5)$$

For $n \in \mathbb{N}_0$, the spectral degree error covariance of K is defined by

$$\begin{aligned} \text{Cov}_n(K) &= \sum_{k=1}^{2n+1} \int_{\Omega} \int_{\Omega} K(\xi, \eta) Y_{n, k}(\xi) Y_{n, k}(\eta) d\omega(\xi) d\omega(\eta) \\ &= \sum_{k=1}^{2n+1} K^\wedge(n, k) \\ &= \sum_{k=1}^{2n+1} \text{Cov}_{n, k}(K). \end{aligned}$$

Definition 3.3 shows that the degree and order error covariance is just given by the orthogonal coefficient of the corresponding covariance kernel K .

In order to make the preceding considerations more concrete we present two examples of spectral error covariances:

Example 3.4 Bandlimited white noise. Suppose that for some $n_K \in \mathbb{N}_0$

$$K^\wedge(n, k) = K^\wedge(n) = \begin{cases} \frac{\sigma^2}{(n_K + 1)^2} & , \quad n \leq n_K, k = 1, \dots, 2n + 1 \\ 0 & , \quad n > n_K, k = 1, \dots, 2n + 1, \end{cases}$$

where $\tilde{\varepsilon}$ is assumed to be $N(0, \sigma^2)$ -distributed. The associated covariance kernel is isotropic and reads

$$K(\xi, \eta) = \frac{\sigma^2}{(n_K + 1)^2} \sum_{n=0}^{n_K} \frac{2n + 1}{4\pi} P_n(\xi \cdot \eta) .$$

Apart from a multiplicative constant this kernel can be understood as a truncated Dirac δ -functional.

Example 3.5 Non-bandlimited colored noise. Assume that $K : \Omega \times \Omega \rightarrow \mathbb{R}$ is given in such a way that

(i) $K^\wedge(n, k) = K^\wedge(n) > 0$ for an infinite number of pairs $(n, k) \in \mathcal{N}$,

(ii) for $\varepsilon > 0$ and for some $\delta \in (1 - \varepsilon, 1)$ the integral $\int_{-1}^{\delta} K(t) dt$ is sufficiently small and

(iii) $K(\xi, \xi)$ coincides with σ^2 for all $\xi \in \Omega$.

A concrete realization is given by

$$K(\xi, \eta) = \frac{\sigma^2}{\exp(-c)} \exp(-c(\xi \cdot \eta)),$$

where c is to be understood as the inverse spherical correlation length (first degree Gauß–Markov model). Another realization, i.e. the model of small correlation length, is based on locally supported singular integrals and can be found in [33].

Spectral Estimation

With Definitions 3.2 and 3.3 at hand we are now in a position to compare the signal spectrum with that of the noise and thus can decide whether signal or noise are dominant. The next definition clarifies the situation (cf. [40, 33]):

Definition 3.6 *Signal and noise spectrum intersect at the degree and order resolution set $\mathcal{N}_{\text{res}} \subset \mathcal{N}$ defined by the following relations:*

(i) *signal dominates noise*

$$\text{Var}_{n,k}(\widetilde{\Lambda F}) \geq \text{Cov}_{n,k}(K), \quad (n, k) \in \mathcal{N}_{\text{res}},$$

(ii) *noise dominates signal*

$$\text{Var}_{n,k}(\widetilde{\Lambda F}) < \text{Cov}_{n,k}(K), \quad (n, k) \notin \mathcal{N}_{\text{res}} .$$

In order to obtain an estimated denoised version $\widehat{\Lambda F}$ of the signal $\widetilde{\Lambda F}$, the signal must somehow be filtered. Filtering is achieved by convolving a square-summable product kernel $L : \Omega \times \Omega \rightarrow \mathbb{R}$ with symbol $\{L^\wedge(n, k)\}_{(n,k) \in \mathcal{N}}$ against ΛF , i.e.

$$\widehat{\Lambda F} = \int_{\Omega} L(\cdot, \eta) \widetilde{\Lambda F}(\eta) \, d\omega(\eta).$$

In spectral language this reads

$$\widehat{\Lambda F}(n, k) = L^\wedge(n, k) \widetilde{\Lambda F}(n, k), \quad (n, k) \in \mathcal{N}.$$

Two important types of filters are well known:

(i) *Spectral thresholding.* This filtering technique is best represented by the filter equation

$$\widehat{\Lambda F} = \sum_{(n,k) \in \mathcal{N}} I_{\mathcal{N}_{\text{res}}}(n, k) L^\wedge(n, k) \left(\widetilde{\Lambda F} \right)^\wedge(n, k) Y_{n,k},$$

where $I_{\mathcal{N}_{res}}$ denotes the *indicator function of the set* \mathcal{N}_{res} . This approach represents a ‘keep or kill’ filtering, where the signal dominated coefficients are filtered by a square-summable product kernel, while the noise dominated coefficients are set to zero. This thresholding can be thought of as a non-linear operator on the set of coefficients, resulting in a set of estimated coefficients. As a special realization of this filter we mention the *ideal low-pass (Shannon) filter*, the kernel of which can best be characterized by its spectral properties:

$$L^\wedge(n, k) = L^\wedge(n) = \begin{cases} 1 & , (n, k) \in \mathcal{N}_{res} \\ 0 & , (n, k) \notin \mathcal{N}_{res}. \end{cases}$$

In that case all contributions corresponding to pairs $(n, k) \in \mathcal{N}_{res}$ are allowed to pass, whereas all other portions of the signal are completely eliminated.

(ii) *Wiener-Kolmogorov filtering*. In the spectral domain this filter is given by

$$L^\wedge(n) = \frac{Var_n(\widetilde{\Lambda F})}{Var_n(\widetilde{\Lambda F}) + Cov_n(K)}, \quad n \in \mathbb{N}_0 .$$

Assuming complete independence of signal and noise this filter produces an optimal weighting between signal and noise. Note that the Wiener-Kolmogorov filter bears a close resemblance to the Tikhonov kernel used for the regularization of ill-posed inverse problems.

3.1.2 Multiscale Signal-to-Noise Response

In the preceding section we have recapitulated the theory of spectral signal-to-noise thresholding. The definitions of variances and error covariances in this approach are mainly influenced by the fact that the signal under consideration can be represented in terms of a spherical harmonic expansion. The main subject of this section is to extend this theory to the multiscale case, i.e. we present a method that makes use of the wavelet representation of a signal. It is clear that the main task is to find suitable definitions of variances and error covariances which, due to the space localizing character of the wavelets, will not be functions of degree and order, but of scale and position. In Chapter 2 (see Equation (2.10) in connection with Theorem 2.12 as well as pages 43 ff.) we have verified that any output signal $\tilde{G} \in \mathcal{L}^2(\Omega)$ can be represented in multiscale approximation by means of spherical wavelets:

$$\tilde{G} = \sum_{j=-\infty}^{+\infty} \int_{\Omega} \Psi_j^{(2)}(\cdot, \eta) \tilde{G}(\eta) d\omega(\eta),$$

where the equality is understood in $\|\cdot\|_{\mathcal{L}^2(\Omega)}$ -sense. For our further considerations it is useful to introduce the Hilbert space $\mathcal{L}^2(\mathbb{Z} \times \Omega)$ of functions $H : \mathbb{Z} \times \Omega \rightarrow \mathbb{R}$ satisfying

$$\sum_{j=-\infty}^{\infty} \int_{\Omega} (H(j; \eta))^2 d\omega(\eta) < \infty .$$

For $H, H_1, H_2 \in \mathcal{L}^2(\mathbb{Z} \times \Omega)$, the inner product as well as the norm in $\mathcal{L}^2(\mathbb{Z} \times \Omega)$ are given by

$$(H_1, H_2)_{\mathcal{L}^2(\mathbb{Z} \times \Omega)} = \sum_{j=-\infty}^{+\infty} \int_{\Omega} H_1(j; \eta) H_2(j; \eta) d\omega(\eta),$$

respectively

$$\|H\|_{\mathcal{L}^2(\mathbb{Z} \times \Omega)} = \left(\sum_{j=-\infty}^{+\infty} \int_{\Omega} (H(j; \eta))^2 d\omega(\eta) \right)^{1/2}. \quad (3.6)$$

Scale and Space Variances

The form of the definition of the spectral degree and order variances (see Definition 3.2) leads us to a similar definition for the so-called scale and space variances of functions, more explicitly, in Equation (3.3) we formally replace the spherical harmonics of certain degrees and orders by wavelets of certain scales at certain positions:

Definition 3.7 *Let $G \in \mathcal{L}^2(\Omega)$ and let the family $\{\Psi_j\}$, $j \in \mathbb{Z}$, of $\mathcal{L}^2(\Omega)$ -product kernels be an $\mathcal{L}^2(\Omega)$ -wavelet. Then the scale and space variance of G at position $\eta \in \Omega$ and scale $j \in \mathbb{Z}$ is defined by*

$$Var_{j;\eta}(G) = \int_{\Omega} \int_{\Omega} G(\xi) G(\zeta) \Psi_j(\xi, \eta) \Psi_j(\zeta, \eta) d\omega(\xi) d\omega(\zeta) .$$

The corresponding integrated quantity is defined to be the scale variance of G at scale $j \in \mathbb{Z}$ given by

$$Var_j(G) = \int_{\Omega} Var_{j;\eta}(G) d\omega(\eta) .$$

If these quantities satisfy a relation similar to Equation (3.4), i.e. if they can reasonably be connected to the \mathcal{L}^2 -norm of the function under consideration, then we can assume Definition 3.7 to be sound. The necessary connection is established by the following theorem:

Theorem 3.8 *Let $G \in \mathcal{L}^2(\Omega)$. Let $Var_{j;\cdot}$ and Var_j , $j \in \mathbb{Z}$, be defined as in Definition 3.7. Then it holds that*

$$\begin{aligned} \|G\|_{\mathcal{L}^2(\Omega)}^2 &= \sum_{j=-\infty}^{+\infty} Var_j(G) \\ &= \sum_{j=-\infty}^{+\infty} \int_{\Omega} Var_{j;\eta}(G) d\omega(\eta) \\ &= \|Var_{\cdot;\cdot}(G)\|_{\mathcal{L}^2(\mathbb{Z} \times \Omega)}^2 . \end{aligned}$$

Proof. Starting with (3.6) we get

$$\begin{aligned}
& \|Var_{\cdot, \cdot}(G)\|_{\mathcal{L}^2(\mathbb{Z} \times \Omega)}^2 \\
&= \sum_{j=-\infty}^{\infty} \int_{\Omega} \left(\int_{\Omega} \int_{\Omega} (G)(\xi) (G)(\zeta) \Psi_j(\xi, \eta) \Psi_j(\zeta, \eta) d\omega(\xi) d\omega(\zeta) \right) d\omega(\eta) \\
&= \sum_{j=-\infty}^{\infty} \int_{\Omega} \int_{\Omega} (G)(\xi) (G)(\zeta) \Psi_j^{(2)}(\xi, \zeta) d\omega(\xi) d\omega(\zeta) \\
&= \sum_{(n,k) \in \mathcal{N}} ((G)^\wedge(n, k))^2 \sum_{j=-\infty}^{\infty} ((\Psi_j)^\wedge(n))^2 \\
&= (G, G)_{\mathcal{L}^2(\Omega)}.
\end{aligned}$$

As all integrations are understood in the sense of the Lebesgue integral, the Beppo-Levi Theorem justifies to interchange integration and summation. ■

Using (3.2) we add, by way of explanation, the following spectral representation:

$$Var_j(\widetilde{\Lambda F}) = \int_{\Omega} Var_{j; \eta}(\widetilde{\Lambda F}) d\omega(\eta) \quad (3.7)$$

$$= \sum_{(n,k) \in \mathcal{N}} (\Psi_j^\wedge(n))^2 \left((\widetilde{\Lambda F})^\wedge(n, k) \right)^2 \quad (3.8)$$

$$= \sum_{(n,k) \in \mathcal{N}} (\Psi_j^\wedge(n))^2 \left(\Lambda^\wedge(n, k) \tilde{F}^\wedge(n, k) \right)^2. \quad (3.9)$$

Scale and Space Error Covariances

Having defined the scale and space variances for signals, the missing link is a corresponding definition for the scale and space error covariances which will replace the degree error covariances of the spectral approach. In accordance with our approach in Definition 3.7, we replace the spherical harmonics in Equation (3.5) with wavelets corresponding to the multiscale representation of functions.

Definition 3.9 *Let, in accordance with Definition 3.1, $K : \Omega \times \Omega \rightarrow \mathbb{R}$ be a covariance kernel. Let the family $\{\Psi_j\}$, $j \in \mathbb{Z}$, of $\mathcal{L}^2(\Omega)$ -product kernels be an $\mathcal{L}^2(\Omega)$ -wavelet. Then the scale and space error covariance at scale $j \in \mathbb{Z}$ and position $\eta \in \Omega$ is defined by*

$$Cov_{j; \eta}(K) = \int_{\Omega} \int_{\Omega} K(\xi, \zeta) \Psi_j(\xi, \eta) \Psi_j(\zeta, \eta) d\omega(\xi) d\omega(\zeta), \quad \eta \in \Omega.$$

The integrated quantity

$$Cov_j(K) = \int_{\Omega} Cov_{j; \eta}(K) d\omega(\eta)$$

is said to be the scale error covariance at scale $j \in \mathbb{Z}$.

In spectral representation the scale and space error covariance can be expressed as

$$Cov_{j;\eta}(K) = \sum_{(n,k) \in \mathcal{N}} K^\wedge(n,k) (\Psi_j^\wedge(n))^2 (Y_{n,k}(\eta))^2 ,$$

while

$$Cov_j(K) = \frac{1}{4\pi} \sum_{(n,k) \in \mathcal{N}} Cov_n(K) (\Psi_j^\wedge(n))^2 . \quad (3.10)$$

This is of course reasonable compared to (3.7), (3.8) and (3.9). Note that from our stochastic model, i.e. the special representation of the covariance as a product kernel, the scale error covariance cannot be dependent on the position $\eta \in \Omega$; a fact that is also indicated by Equation (3.10).

Scale and Space Estimation

As in the spectral approach of the previous section, we now need a criterion to decide whether noise or signal are predominant. Since with the scale and space variances as well as the scale and space error covariances we have defined local measures dependent on the location $\eta \in \Omega$ under consideration, the criterion is also of local nature:

Definition 3.10 *Signal and noise scale intersect at the so-called scale and space resolution set \mathcal{Z}_{res} with $\mathcal{Z}_{res} \subset \mathcal{Z} = \mathbb{Z} \times \Omega$ defined by*

(i) *signal dominates noise*

$$Var_{j;\eta}(\widetilde{\Lambda F}) \geq Cov_{j;\eta}(K), \quad (j;\eta) \in \mathcal{Z}_{res} ,$$

(ii) *noise dominates signal*

$$Var_{j;\eta}(\widetilde{\Lambda F}) < Cov_{j;\eta}(K), \quad (j;\eta) \notin \mathcal{Z}_{res} .$$

Similar to what is done in the spectral approach, we are able to replace the (unknown) error-free function ΛF of the representation

$$\begin{aligned} (\Lambda F)_J &= \int_{\Omega} \Phi_{\rho_{J_0}}^{(2)}(\cdot, \zeta) (\Lambda F)(\zeta) d\omega(\zeta) \\ &+ \sum_{j=J_0}^{J-1} \int_{\Omega} \Psi_{\rho_j}^{(2)}(\cdot, \zeta) (\Lambda F)(\zeta) d\omega(\zeta) \end{aligned}$$

by (an estimate from) the error-affected function $\widetilde{\Lambda F}$ such as

$$\begin{aligned} (\widetilde{\Lambda F})_J &= \int_{\Omega} \Phi_{\rho_{J_0}}^{(2)}(\cdot, \zeta) (\widetilde{\Lambda F})(\zeta) d\omega(\zeta) \\ &+ \sum_{j=J_0}^{J-1} \int_{\Omega} \Psi_{\rho_j}^{(2)}(\cdot, \zeta) (\widetilde{\Lambda F})(\zeta) d\omega(\zeta), \end{aligned}$$

$J > J_0$. It is clear that, in order to get a good approximation of the true signal, the signal and the noise content as given in Definition 3.10 needs to be incorporated in the approximation process. This is the subject of the next section.

3.1.3 Scalar Selective Multiscale Reconstruction

Starting point is the multiscale approximation

$$(\widetilde{\Lambda F})_J = \Phi_{J_0} * \Phi_{J_0} * \widetilde{\Lambda F} + \sum_{j=J_0}^{J-1} \Psi_j * \Psi_j * \widetilde{\Lambda F}$$

with $J > J_0$. The double convolutions

$$\begin{aligned} \tilde{V}_{J_0; \eta}(\widetilde{\Lambda F}) &= (\Phi_{J_0} * \Phi_{J_0} * \widetilde{\Lambda F})(\eta) \\ &= \int_{\Omega} \Phi_{J_0}(\eta, \zeta) \int_{\Omega} \Phi_{J_0}(\xi, \zeta) \widetilde{\Lambda F}(\xi) d\omega(\xi) d\omega(\zeta) \end{aligned}$$

and

$$\begin{aligned} \tilde{W}_{j; \eta}(\widetilde{\Lambda F}) &= (\Psi_j * \Psi_j * \widetilde{\Lambda F})(\eta) \\ &= \int_{\Omega} \Psi_{J_0}(\eta, \zeta) \int_{\Omega} \Psi_{J_0}(\xi, \zeta) \widetilde{\Lambda F}(\xi) d\omega(\xi) d\omega(\zeta) \end{aligned}$$

need to be calculated by approximate integration in combination with the criteria presented in Definition 3.10. We base our considerations on approximate integration formulae (see also our comments in Section 2.1.5 and, for a detailed discussion of approximate integration, [30] and the references therein) with weights $v_s^{N_j}, w_l^{L_j} \in \mathbb{R}$ and associated knots $\zeta_s^{N_j}, \xi_l^{L_j} \in \Omega$, $s = 1, \dots, N_j$, $l = 1, \dots, L_j$, of the form:

$$\begin{aligned} \tilde{V}_{J_0; \eta}(\widetilde{\Lambda F}) &\simeq \sum_{s=1}^{N_{J_0}} v_s^{N_{J_0}} \Phi_{J_0}(\eta, \zeta_s^{N_{J_0}}) \tilde{a}_s^{N_{J_0}}, \\ \tilde{W}_{j; \eta}(\widetilde{\Lambda F}) &\simeq \sum_{s=1}^{N_j} v_s^{N_j} \Psi_j(\eta, \zeta_s^{N_j}) \tilde{b}_s^{N_j}, \quad j = J_0, \dots, J-1, \end{aligned}$$

where

$$\tilde{a}_s^{N_{J_0}} \simeq \sum_{l=1}^{L_{J_0}} w_l^{L_{J_0}} \Phi_{J_0}(\xi_l^{L_{J_0}}, \zeta_s^{N_{J_0}}) \widetilde{\Lambda F}(\xi_l^{L_{J_0}}), \quad (3.11)$$

$$\tilde{b}_s^{N_j} \simeq \sum_{l=1}^{L_j} w_l^{L_j} \Psi_j(\xi_l^{L_j}, \zeta_s^{N_j}) \widetilde{\Lambda F}(\xi_l^{L_j}). \quad (3.12)$$

The sign ' \simeq ' always means that the error is assumed to be negligible. The large 'true' coefficients are the ones that ought to be included in a selective reconstruction for estimating an unknown field. It is sensible to include only coefficients $\tilde{a}_s^{N_{J_0}}$ and $\tilde{b}_s^{N_j}$ larger than some specified threshold value. In accordance with Definition 3.10 'larger' coefficients are taken to be those that satisfy the estimates (cf. Definitions 3.7 and 3.9)

$$\begin{aligned} & \left(\tilde{a}_s^{N_{J_0}} \right)^2 \\ &= \int_{\Omega} \int_{\Omega} \widetilde{\Lambda F}(\alpha) \widetilde{\Lambda F}(\beta) \Phi_j(\alpha, \zeta_s^{N_{J_0}}) \Phi_j(\beta, \zeta_s^{N_{J_0}}) d\omega(\alpha) d\omega(\beta) \\ &\simeq \sum_{p=1}^{L_{J_0}} \sum_{q=1}^{L_{J_0}} w_p^{L_{J_0}} w_q^{L_{J_0}} \Phi_{J_0}(\xi_p^{L_{J_0}}, \zeta_s^{N_{J_0}}) \Phi_{J_0}(\xi_q^{L_{J_0}}, \zeta_s^{N_{J_0}}) \widetilde{\Lambda F}(\xi_p^{L_{J_0}}) \widetilde{\Lambda F}(\xi_q^{L_{J_0}}) \\ &\geq \sum_{p=1}^{L_{J_0}} \sum_{q=1}^{L_{J_0}} w_p^{L_{J_0}} w_q^{L_{J_0}} \Phi_{J_0}(\xi_p^{L_{J_0}}, \zeta_s^{N_{J_0}}) \Phi_{J_0}(\xi_q^{L_{J_0}}, \zeta_s^{N_{J_0}}) K(\xi_p^{L_{J_0}}, \xi_q^{L_{J_0}}) \\ &\simeq \int_{\Omega} \int_{\Omega} \Phi_{J_0}(\alpha, \zeta_s^{N_{J_0}}) \Phi_{J_0}(\beta, \zeta_s^{N_{J_0}}) K(\alpha, \beta) d\omega(\alpha) d\omega(\beta) \\ &= k_{\Phi_{J_0}}(\zeta_s^{N_{J_0}}) \end{aligned} \quad (3.13)$$

and

$$\begin{aligned} & \left(\tilde{b}_s^{N_j} \right)^2 \\ &= \int_{\Omega} \int_{\Omega} \Psi_j(\alpha, \zeta_s^{N_j}) \Psi_j(\beta, \zeta_s^{N_j}) \widetilde{\Lambda F}(\alpha) \widetilde{\Lambda F}(\beta) d\omega(\alpha) d\omega(\beta) \\ &\simeq \sum_{p=1}^{L_j} \sum_{q=1}^{L_j} w_p^{L_j} w_q^{L_j} \Psi_j(\xi_p^{L_j}, \zeta_s^{N_j}) \Psi_j(\xi_q^{L_j}, \zeta_s^{N_j}) \widetilde{\Lambda F}(\xi_p^{L_j}) \widetilde{\Lambda F}(\xi_q^{L_j}) \\ &\geq \sum_{p=1}^{L_j} \sum_{q=1}^{L_j} w_p^{L_j} w_q^{L_j} \Psi_j(\xi_p^{L_j}, \zeta_s^{N_j}) \Psi_j(\xi_q^{L_j}, \zeta_s^{N_j}) K(\xi_p^{L_j}, \xi_q^{L_j}) \\ &\simeq \int_{\Omega} \int_{\Omega} \Psi_j(\alpha, \zeta_s^{N_j}) \Psi_j(\beta, \zeta_s^{N_j}) K(\alpha, \beta) d\omega(\alpha) d\omega(\beta) \\ &= k_{\Psi_j}(\zeta_s^{N_j}) \end{aligned} \quad (3.14)$$

(the values $k_{\Phi_{J_0}}(\zeta_s^{N_{J_0}})$ and $k_{\Psi_j}(\zeta_s^{N_j})$ are introduced as abbreviations of the appearing double integrals).

With the threshold values $k_{\Phi_{J_0}}(\zeta_s^{N_{J_0}})$, $s = 1, \dots, N_{J_0}$, and $k_{\Psi_j}(\zeta_s^{N_j})$, $s = 1, \dots, N_j$, which are to be calculated from the a priori known covariance kernel K , an estimator for the sought-after approximation can be written in the form

$$\begin{aligned} (\widehat{\Lambda F})_J(\eta) &= \sum_{s=1}^{N_{J_0}} I_{\{(\tilde{a}_s^{N_{J_0}})^2 \geq k_{\Phi_{J_0}}(\zeta_s^{N_{J_0}})\}} v_s^{N_{J_0}} \Phi_{J_0}(\eta, \zeta_s^{N_{J_0}}) \tilde{a}_s^{N_{J_0}} \\ &+ \sum_{j=J_0}^{J-1} \sum_{s=1}^{N_j} I_{\{(\tilde{b}_s^{N_j})^2 \geq k_{\Psi_j}(\zeta_s^{N_j})\}} v_s^{N_j} \Psi_j(\eta, \zeta_s^{N_j}) \tilde{b}_s^{N_j}. \end{aligned}$$

I_A denotes the indicator function of the set A . This means, in other words, that the 'large' coefficients relative to the threshold are used in the approximation while the small coefficients are set to zero. Up to now, the thresholding estimators for the true coefficients $V_{J_0;\eta}(\widehat{\Lambda F})$ and $W_{j;\eta}(\widehat{\Lambda F})$ can be written in the form

$$\begin{aligned} V_{J_0;\eta}(\widehat{\Lambda F}) &= \sum_{s=1}^{N_{J_0}} \delta_{k_{\Phi_{J_0}}(\zeta_s^{N_{J_0}})}^{\text{hard}} \left(\left(\tilde{a}_s^{N_{J_0}} \right)^2 \right) v_s^{N_{J_0}} \Phi_{J_0}(\eta, \zeta_s^{N_{J_0}}) \tilde{a}_s^{N_{J_0}}, \\ W_{j;\eta}(\widehat{\Lambda F}) &= \sum_{s=1}^{N_j} \delta_{k_{\Psi_j}(\zeta_s^{N_j})}^{\text{hard}} \left(\left(\tilde{b}_s^{N_j} \right)^2 \right) v_s^{N_j} \Psi_j(\eta, \zeta_s^{N_j}) \tilde{b}_s^{N_j}, \end{aligned}$$

where the function $\delta_\lambda^{\text{hard}}$ is the *hard thresholding function*

$$\delta_\lambda^{\text{hard}}(x) = \begin{cases} 1 & , \quad |x| \geq \lambda \\ 0 & , \quad |x| < \lambda \end{cases}.$$

As in the spectral approach, the hard or 'keep or kill' thresholding operation is not the only reasonable way of estimating the coefficients. Considering the fact that the coefficients $\tilde{V}_{J_0;\eta}(\widehat{\Lambda F})$ and $\tilde{W}_{j;\eta}(\widehat{\Lambda F})$ consist of both, a signal and a noise contribution, it might be desirable to attempt to isolate the signal part by removing the noisy part (see also Subsection 3.1.1 pages 67 ff.). This idea leads to the *soft thresholding function* (cf. the considerations by [17, 18])

$$\delta_\lambda^{\text{soft}}(x) = \begin{cases} \max\{0, 1 - \frac{\lambda}{|x|}\} & , \quad x \neq 0 \\ 0 & , \quad x = 0, \end{cases}$$

which can also be used in the above identities. When soft thresholding is applied to a set of empirical coefficients, only coefficients greater than the threshold (in absolute value) are included, but their values are 'shrunk' toward zero by an amount equal to the threshold λ .

The following theorem summarizes our results and presents the general thresholding multi-scale estimator.

Theorem 3.11 *Let $\{\Phi_j\}$ and $\{\Psi_j\}$, $j \in \mathbb{Z}$, be an $\mathcal{L}^2(\Omega)$ -scaling function and an $\mathcal{L}^2(\Omega)$ -wavelet, respectively. Let, furthermore, $v_s^{N_j}, w_l^{L_j} \in \mathbb{R}$ be integration weights and $\zeta_s^{N_j}, \xi_l^{L_j} \in$*

Ω , $s = 1, \dots, N_j$, $l = 1, \dots, L_j$, the associated knots of approximate integration formulae. Assume δ_λ to be either the hard or the soft thresholding function.

If the coefficients $\tilde{a}_s^{N_{J_0}}$ and $\tilde{b}_s^{N_j}$ are given as in equations (3.11) and (3.12), respectively, while the threshold values $k_{\Phi_{J_0}}(\zeta_s^{N_{J_0}})$ and $k_{\Psi_j}(\zeta_s^{N_j})$ are calculated from the covariance kernel K as shown in (3.13) and (3.14), then the thresholding multiscale estimator of a signal $\widetilde{\Lambda F}$ reads

$$\begin{aligned} \widehat{\Lambda F}_J(\eta) &= \sum_{s=1}^{N_{J_0}} \delta_{k_{\Phi_{J_0}}(\zeta_s^{N_{J_0}})} \left(\left(\tilde{a}_s^{N_{J_0}} \right)^2 \right) v_s^{N_{J_0}} \Phi_{J_0}(\eta, \zeta_s^{N_{J_0}}) \tilde{a}_s^{N_{J_0}} \\ &+ \sum_{j=J_0}^{J-1} \sum_{s=1}^{N_j} \delta_{k_{\Psi_j}(\zeta_s^{N_j})} \left(\left(\tilde{b}_s^{N_j} \right)^2 \right) v_s^{N_j} \Psi_j(\eta, \zeta_s^{N_j}) \tilde{b}_s^{N_j} . \end{aligned}$$

Using this approach, $(\widehat{\Lambda F})_J$ is first approximated by a thresholded $(\widetilde{\Lambda F})_{J_0}$ which represents the denoised smooth components of the data. Then the coefficients at a higher resolution are thresholded such that the noise is suppressed but the fine details are included in the calculation. The whole approximation is, due to the characteristics of the scaling functions and wavelets, space adapting.

It should be remarked that the whole process of selective multiscale thresholding can of course be combined with the pyramid scheme as presented in Section 2.1.5. For an extensive derivation we direct the reader to our treatise in [33]. Here we just mention the main result, i.e. the representation of the thresholding multiscale estimator in terms of coefficients obtainable by means of the pyramid scheme. Again, the starting point are approximate integration formulae with given weights $w_i^{N_j} \in \mathbb{R}$ and associated knots $\eta_i^{N_j} \in \Omega$. In the nomenclature of Section 2.1.5 we start from a sufficiently large scale J such that

$$\widetilde{\Lambda F}(\eta) \simeq \Phi_J^{(2)}(\cdot, \eta) * \widetilde{\Lambda F} \simeq \sum_{i=1}^{N_J} \Phi_J^{(2)}(\eta, \eta_i^{N_J}) \tilde{a}_i^{N_J}, \quad \eta \in \Omega,$$

where the coefficients for the initial step are given by

$$\tilde{a}_i^{N_J} = w_i^{N_J} \left(\widetilde{\Lambda F} \right) (\eta_i^{N_J}), \quad i = 1, \dots, N_J.$$

The coefficients $\tilde{a}_i^{N_{J-1}}$ can be calculated recursively starting from the data $\tilde{a}_i^{N_J}$ for the initial level J , $\tilde{a}_i^{N_{J-2}}$ can be deduced recursively from $\tilde{a}_i^{N_{J-1}}$, etc. where the recursion relation reads

$$\tilde{a}_i^{N_j} = w_i^{N_j} \sum_{l=1}^{N_{j+1}} \Xi_j(\eta_i^{N_j}, \eta_l^{N_{j+1}}) \tilde{a}_i^{N_{j+1}}, \quad j = 0 \dots J$$

(the different choices of the kernel Ξ_j have been explained in Section 2.1.5).

Having achieved the recursion relation, the thresholding criteria have to be incorporated.

This is done via the estimate

$$\begin{aligned}
\left(\tilde{a}_i^{N_j}\right)^2 &= \left(w_i^{N_j} \left(\Xi_j * \widetilde{\Lambda F}\right) (\eta_i^{N_j})\right)^2 \\
&= (w_i^{N_j})^2 \int_{\Omega} \int_{\Omega} \widetilde{\Lambda F}(\xi) \widetilde{\Lambda F}(\zeta) \Xi_j(\xi, \eta_i^{N_j}) \Xi_j(\zeta, \eta_i^{N_j}) d\omega(\xi) d\omega(\zeta) \\
&\geq (w_i^{N_j})^2 \int_{\Omega} \int_{\Omega} K(\xi, \zeta) \Xi_j(\xi, \eta_i^{N_j}) \Xi_j(\zeta, \eta_i^{N_j}) d\omega(\xi) d\omega(\zeta) \\
&= (k_i^j)^2
\end{aligned}$$

which basically corresponds to Definition 3.10. Summarizing our results the following representation of the thresholding multiscale estimator can be obtained in combination with the pyramid scheme:

$$\begin{aligned}
\left(\widehat{\Lambda F}\right)_J &= \sum_{i=1}^{N_{J_0}} \delta_{(k_i^{J_0})^2} \left((\tilde{a}_i^{N_{J_0}})^2\right) \Phi_J^{(2)}(\cdot, \eta_i^{N_{J_0}}) \tilde{a}_i^{N_{J_0}} \\
&\quad + \sum_{j=J_0}^{J-1} \sum_{i=1}^{N_j} \delta_{(k_i^j)^2} \left((\tilde{a}_i^{N_j})^2\right) \Psi_j^{(2)}(\cdot, \eta_i^{N_j}) \tilde{a}_i^{N_j},
\end{aligned}$$

where δ_λ is the previously defined hard or soft thresholding function.

3.2 Signal-to-Noise Thresholding of Vector Fields

While up to now we have dealt with a multiscale denoising procedure for spherical scalar fields, we are now concerned with the extension of this approach to spherical vector fields. Analogously to the scalar case we start in Section 3.2.1 with the definition of the respective covariance kernels and present the spectral theory in terms of vector spherical harmonics. Section 3.2.2 deals with multiscale signal-to-noise thresholding of vector fields based on tensorial radial basis functions. This approach is the canonical extension of the scalar theory but holds some disadvantages for numerical implementations, though. Therefore, in Section 3.2.3, we use the tensorial technique to develop a method based on vector radial basis functions, an approach being well suited for numerical realizations (see also our treatment in [34]).

3.2.1 Vector Spectral Signal-to-Noise Response

In analogy to the scalar case (cf. Section 3.1.1) let us think of an 'output signal' g as produced by a linear operator $\mathbf{\Lambda}$ applied to an 'input signal' f

$$\mathbf{\Lambda}f = g,$$

where $\mathbf{\Lambda}$ is an operator mapping $l^2(\Omega)$ onto itself such that

$$\mathbf{\Lambda}y_{n,k}^{(i)} = (\mathbf{\Lambda}^{(i)})^\wedge(n, k) y_{n,k}^{(i)}$$

for $i = 1, 2, 3$, $(n, k) \in \mathcal{N}^{(i)}$. The symbol $\left\{ (\mathbf{\Lambda}^{(i)})^\wedge(n, k) \right\}_{(n,k) \in \mathcal{N}^{(i)}}$ is supposed to be sequences of real numbers for $i = 1, 2, 3$. Note that we have used the abbreviation

$$\mathcal{N}^{(i)} = \{(n, k) | n = 0_i, 0_i + 1, \dots; k = 1, \dots, 2n + 1\}$$

($0_1 = 0$, $0_i = 1$, for $i = 2, 3$).

In practise, an error-affected 'output signal'

$$\tilde{g} = g + \tilde{\varepsilon},$$

is observed, where $\tilde{\varepsilon}$ is the *observation noise*. Analogously to the scalar case and in accordance with the approach used by [95] we assume that

$$\text{Cov}[\tilde{g}(\xi), \tilde{g}(\eta)] = E[\tilde{\varepsilon}(\xi), \tilde{\varepsilon}(\eta)] = \mathbf{k}(\xi, \eta), \quad (\xi, \eta) \in \Omega \times \Omega,$$

is known, where the tensorial covariance kernel $\mathbf{k}(\cdot, \cdot) : \Omega \times \Omega \rightarrow \mathbb{R}^{3 \times 3}$ is explicitly given by:

Definition 3.12 Let $\mathbf{k}^{(i)} : \Omega \times \Omega \rightarrow \mathbb{R}^{3 \times 3}$, $i \in \{1, 2, 3\}$, be a tensor kernel of the form

$$\begin{aligned} \mathbf{k}^{(i)}(\xi, \eta) &= \sum_{(n,k) \in \mathcal{N}^{(i)}} (\mathbf{k}^{(i)})^\wedge(n, k) (\mu_n^{(i)})^{-1} o_\xi^{(i)} o_\eta^{(i)} Y_{n,k}(\xi) Y_{n,k}(\eta) \\ &= \sum_{(n,k) \in \mathcal{N}^{(i)}} (\mathbf{k}^{(i)})^\wedge(n, k) y_{n,k}^{(i)}(\xi) \otimes y_{n,k}^{(i)}(\eta), \quad (\xi, \eta) \in \Omega^2, \end{aligned}$$

with the symbol $\{(\mathbf{k}^{(i)})^\wedge(n, k)\}_{(n, k) \in \mathcal{N}^{(i)}}$, $i \in \{1, 2, 3\}$, satisfying the conditions:

$$(C1) \quad (\mathbf{k}^{(i)})^\wedge(n, k) \geq 0 \text{ for } (n, k) \in \mathcal{N}^{(i)},$$

$$(C2) \quad \sum_{(n, k) \in \mathcal{N}^{(i)}} (\mathbf{k}^{(i)})^\wedge(n, k) \sup_{\eta \in \Omega} \left(y_{n, k}^{(i)}(\eta)\right)^2 < \infty .$$

Then $\mathbf{k}^{(i)}$, $i \in \{1, 2, 3\}$ is called a tensorial covariance kernel of type i , while

$$\mathbf{k} = \sum_{i=1}^3 \mathbf{k}^{(i)}$$

is called a tensorial covariance kernel.

Degree Variances

Any 'output function' (output signal) can be expanded into an orthogonal series in terms of vector spherical harmonics:

$$\begin{aligned} \tilde{g} = \widetilde{\Lambda}f &= \sum_{i=1}^3 \sum_{(n, k) \in \mathcal{N}^{(i)}} (\Lambda^{(i)})^\wedge(n, k) (\tilde{f}^{(i)})^\wedge(n, k) y_{n, k}^{(i)} \\ &= \sum_{i=1}^3 \sum_{(n, k) \in \mathcal{N}^{(i)}} (\tilde{g}^{(i)})^\wedge(n, k) y_{n, k}^{(i)}, \end{aligned}$$

where the equality has to be understood in the sense of $\|\cdot\|_{l^2(\Omega)}$. Using this series expansion we get, for $i \in \{1, 2, 3\}$, the spectral representation

$$(\tilde{g}^{(i)})^\wedge(n, k) = (\widetilde{\Lambda}f)^\wedge(n, k) = (\Lambda^{(i)})^\wedge(n, k) (\tilde{f}^{(i)})^\wedge(n, k), \quad (n, k) \in \mathcal{N}^{(i)}.$$

This is the vectorial analogue for Equation (3.2) and also hints at using the root-mean-square power per degree and order, respectively per degree, to characterize the vectorial signal. Motivated by the corresponding definitions for the scalar case and by Parseval's identity we define:

Definition 3.13 Let $g \in l^2(\Omega)$. Let, for $i \in \{1, 2, 3\}$ and $(n, k) \in \mathcal{N}^{(i)}$, $(g^{(i)})^\wedge(n, k)$ be the corresponding orthogonal coefficients. Then, for $i \in \{1, 2, 3\}$ and $(n, k) \in \mathcal{N}^{(i)}$, the signal degree and order variances of type i of g are defined by

$$\begin{aligned} \text{Var}_{n, k}^{(i)}(g) &= \int_{\Omega} \int_{\Omega} \left(y_{n, k}^{(i)}(\xi) \otimes y_{n, k}^{(i)}(\eta)\right) \cdot (g(\xi) \otimes g(\eta)) \, d\omega(\xi) \, d\omega(\eta) \\ &= \int_{\Omega} \int_{\Omega} g(\xi) \cdot \left(y_{n, k}^{(i)}(\xi) \otimes y_{n, k}^{(i)}(\eta)\right) g(\eta) \, d\omega(\xi) \, d\omega(\eta) \\ &= \left((g^{(i)})^\wedge(n, k)\right)^2. \end{aligned}$$

Accordingly the signal degree variances of type i of g are given by

$$\begin{aligned} \text{Var}_n^{(i)}(g) &= \frac{2n+1}{4\pi} \int_{\Omega} \int_{\Omega} g(\xi) \cdot \mathbf{p}_n^{(i,i)}(\xi, \eta) g(\eta) d\omega(\eta) d\omega(\xi) \\ &= \sum_{k=1}^{2n+1} \left((g^{(i)})^{\wedge}(n, k) \right)^2 \\ &= \sum_{k=1}^{2n+1} \text{Var}_{n,k}^{(i)}(g), \end{aligned}$$

while the signal degree variances of g read as follows:

$$\text{Var}_n(\widetilde{\Lambda}f) = \sum_{i=1}^3 \text{Var}_n^{(i)}(\widetilde{\Lambda}f).$$

Obviously, by virtue of Parseval's identity, we obtain

$$\left\| \widetilde{\Lambda}f \right\|_{l^2(\Omega)} = \sum_{i=1}^3 \sum_{(n,k) \in \mathcal{N}^{(i)}} \text{Var}_{n,k}^{(i)}(\widetilde{\Lambda}f),$$

again connecting the signal degree and order variances as well as the signal degree variances with the ' $l^2(\Omega)$ -energy' of the corresponding vectorial signal.

It is clear that the remarks concerning the frequency limiting characteristics of physical devices and the resulting bandlimited nature of the 'transmitted signals' are valid in the vectorial case as well. That is, one is usually able to consider bandlimited vector fields $\tilde{g} \in l^2(\Omega)$, the signal degree variances of which satisfy $\text{Var}_n(\tilde{g}) = 0$ for all $n > N \in \mathbb{N}$.

Degree Error Covariances

In addition to the previously defined signal variances the tensorial covariance kernel \mathbf{k} is used to calculate suitable measures to characterize the noise:

Definition 3.14 *In accordance with Definition 3.12, let*

$$\left\{ (\mathbf{k}^{(i)})^{\wedge}(n, k) \right\}_{(n,k) \in \mathcal{N}^{(i)}}, \quad i \in \{1, 2, 3\}$$

be the symbol of a tensorial covariance kernel $\mathbf{k} : \Omega \times \Omega \rightarrow \mathbb{R}^{3 \times 3}$. Then the degree and order

error covariance of type i is given by

$$\begin{aligned}
& Cov_{n,k}^{(i)}(\mathbf{k}) \\
&= \int_{\Omega} \int_{\Omega} \left(y_{n,k}^{(i)}(\xi) \otimes y_{n,k}^{(i)}(\eta) \right) \cdot \mathbf{k}(\xi, \eta) \, d\omega(\xi) \, d\omega(\eta) \\
&= \sum_{l=1}^3 \sum_{(p,q) \in \mathcal{N}^{(i)}} (\mathbf{k}^{(l)})^{\wedge}(p, q) \int_{\Omega} \int_{\Omega} \left(y_{n,k}^{(i)}(\eta) \cdot y_{p,q}^{(l)}(\eta) \right) \left(y_{n,k}^{(i)}(\xi) \cdot y_{p,q}^{(l)}(\xi) \right) \, d\omega(\xi) \, d\omega(\eta) \\
&= (\mathbf{k}^{(i)})^{\wedge}(n, k).
\end{aligned}$$

Moreover the error covariance of type i as well as the error covariance are defined by

$$Cov_n^{(i)}(\mathbf{k}) = \sum_{k=1}^{2n+1} Cov_{n,k}^{(i)}(\mathbf{k}) = \sum_{k=1}^{2n+1} (\mathbf{k}^{(i)})^{\wedge}(n, k)$$

and

$$Cov_n(\mathbf{k}) = \sum_{i=1}^3 \sum_{k=1}^{2n+1} (\mathbf{k}^{(i)})^{\wedge}(n, k).$$

Examples 3.4 and 3.5 can be applied to the case of tensorial error covariance kernels in a canonical way.

Spectral Estimation

The signal-to-noise relation is determined by the degree and order resolution set $\mathcal{N}_{res}^{(i)}$ of type i :

Definition 3.15 *Signal and noise spectrum intersect at the degree and order resolution set of type i , $\mathcal{N}_{res}^{(i)} \subset \mathcal{N}^{(i)}$, defined by the following relations:*

(i) *signal dominates noise*

$$Var_{n,k}^{(i)}(\widetilde{\Lambda}f) \geq Cov_{n,k}^{(i)}(\mathbf{k}), \quad (n, k) \in \mathcal{N}_{res}^{(i)},$$

(ii) *noise dominates signal*

$$Var_{n,k}^{(i)}(\widetilde{\Lambda}f) < Cov_{n,k}^{(i)}(\mathbf{k}), \quad (n, k) \notin \mathcal{N}_{res}^{(i)}.$$

The technique of filtering the signal $\widetilde{\Lambda}f$ in order to get an estimated denoised version $\widehat{\Lambda}f$ can be canonically carried over from the scalar case (cf. Section 3.1.1 pages 67 ff.)

3.2.2 Tensor-Based Multiscale Signal-to-Noise Response

We now want to extend the theory of scalar multiscale signal-to-noise response to the case of noisy vector fields, keeping in mind the spectral approach in terms of vector spherical harmonics. Theorem 2.27 forms the basis necessary to continue with our multiscale approach since it is equivalent to the fact that the output signal \tilde{g} can be presented in multiscale approximation as follows:

$$\tilde{g} = \tilde{\Lambda}f = \sum_{j=-\infty}^{\infty} \Psi_j * \Psi_j * (\tilde{\Lambda}f),$$

where $\{\Psi_j\}$ are tensorial wavelets and the equality is understood in the $\|\cdot\|_{l^2(\Omega)}$ -sense. Therefore, it is useful for our further considerations to introduce the space $l^{(2)}(\mathbb{Z} \times \Omega)$ of fields $h : \mathbb{Z} \times \Omega \rightarrow \mathbb{R}^3$ satisfying the inequality

$$\sum_{j=-\infty}^{\infty} \int_{\Omega} (h(j; \eta) \cdot h(j; \eta)) d\omega(\eta) < \infty.$$

The space $l^{(2)}(\mathbb{Z} \times \Omega)$ is a Hilbert space equipped with the inner product

$$(h_1, h_2)_{l^{(2)}(\mathbb{Z} \times \Omega)} = \sum_{j=-\infty}^{\infty} \int_{\Omega} (h_1(j; \eta) \cdot h_2(j; \eta)) d\omega(\eta)$$

corresponding to the norm

$$\|h\|_{l^{(2)}(\mathbb{Z} \times \Omega)} = \left(\sum_{j=-\infty}^{\infty} \int_{\Omega} |h(j; \eta)|^2 d\omega(\eta) \right)^{1/2}. \quad (3.15)$$

Tensor Based Scale and Space Variances

Having introduced tensor scaling functions and wavelets in Section 2.2.5 we can use these kernel functions to introduce the tensor based scale and space variances for vector fields. The next definition clarifies what is meant by that:

Definition 3.16 *Let $g \in l^2(\Omega)$ and let the family $\{\Psi_j^{(i)}\}$, $j \in \mathbb{Z}$, $i \in \{1, 2, 3\}$, be a tensor wavelet in the sense of Definition 2.26. Then the tensor based scale and space variance at position $\eta \in \Omega$, scale $j \in \mathbb{Z}$ and type $i \in \{1, 2, 3\}$ of g is defined by*

$$TVar_{j;\eta}^{(i)}(g) = \int_{\Omega} \int_{\Omega} \left(\Psi_j^{(i)}(\xi, \eta) \Psi_j^{(i)}(\eta, \zeta) \right) \cdot (g(\xi) \otimes g(\zeta)) d\omega(\xi) d\omega(\zeta),$$

while the tensor based scale and space variance at $\eta \in \Omega$ and scale $j \in \mathbb{Z}$ is given by

$$TVar_{j,\eta}(g) = \sum_{i=1}^3 TVar_{j;\eta}^{(i)}(g).$$

The corresponding integrated quantities are defined to be the tensor based scale variance of type $i \in \{1, 2, 3\}$ of g , i.e.

$$TVar_j^{(i)}(g) = \int_{\Omega} TVar_{j;\eta}^{(i)}(g) d\omega(\eta),$$

and the tensor based scale variance of g ,

$$TVar_j(g) = \sum_{i=1}^3 TVar_j^{(i)}(g).$$

If, with this definitions, we can find a relation similar to Theorem 3.8 we can reasonably connect the l^2 -norm of the vector field under consideration with the tensor based scale and space variances. The following theorem states this result and justifies Definition 3.16.

Theorem 3.17 *Suppose $g \in l^2(\Omega)$. Let $TVar_j$ and $TVar_{j,\cdot}$, $j \in \mathbb{Z}$ be given as in Definition 3.16. Then*

$$\begin{aligned} \|g\|_{l^2(\Omega)}^2 &= \sum_{j=-\infty}^{\infty} TVar_j(g) \\ &= \sum_{j=-\infty}^{\infty} \int_{\Omega} TVar_{j;\eta}(g) d\omega(\eta) \\ &= \|TVar_{\cdot,\cdot}(g)\|_{l^2(\mathbb{Z} \times \Omega)}^2 \end{aligned}$$

holds true.

Proof. On the one hand we have

$$\begin{aligned} &\sum_{i=1}^3 \sum_{j=-\infty}^{\infty} \int_{\Omega} \int_{\Omega} \int_{\Omega} \left(\Psi_j^{(i)}(\xi, \eta) \Psi_j^{(i)}(\eta, \zeta) \right) \cdot \\ &\quad \cdot (g(\xi) \otimes g(\zeta)) d\omega(\xi) d\omega(\zeta) d\omega(\eta) \\ &= \sum_{i=1}^3 \sum_{j=-\infty}^{\infty} \int_{\Omega} \int_{\Omega} \int_{\Omega} \Psi_j^{(i)}(\eta, \xi) g(\xi) \cdot \Psi_j^{(i)}(\eta, \zeta) g(\zeta) d\omega(\xi) d\omega(\zeta) d\omega(\eta) \\ &= \|TVar_{\cdot,\cdot}(g)\|_{l^2(\mathbb{Z} \times \Omega)}^2 \end{aligned}$$

where we have used the Equation (1.4) and the fact that for the tensorial kernels we have $\Psi(\xi, \eta) = (\Psi(\eta, \xi))^T$.

On the other hand it holds that

$$\begin{aligned}
& \sum_{i=1}^3 \sum_{j=-\infty}^{\infty} \int_{\Omega} \int_{\Omega} \int_{\Omega} \left(\Psi_j^{(i)}(\xi, \eta) \Psi_j^{(i)}(\eta, \zeta) \right) \cdot \\
& \quad \cdot (g(\xi) \otimes g(\zeta)) \, d\omega(\xi) \, d\omega(\zeta) d\omega(\eta) \\
&= \sum_{i=1}^3 \sum_{j=-\infty}^{\infty} \int_{\Omega} \int_{\Omega} \left(\Psi_j^{(i)} * \Psi_j^{(i)} \right) (\xi, \zeta) \cdot (g(\xi) \otimes g(\zeta)) \, d\omega(\xi) \, d\omega(\zeta) \\
&= \sum_{i=1}^3 \sum_{j=-\infty}^{\infty} \int_{\Omega} \int_{\Omega} g(\xi) \cdot \left(\left(\Psi_j^{(i)} * \Psi_j^{(i)} \right) (\xi, \zeta) g(\zeta) \right) \, d\omega(\xi) \, d\omega(\zeta) \\
&= \sum_{i=1}^3 \sum_{j=-\infty}^{\infty} \int_{\Omega} g(\xi) \cdot \left(\Psi_j^{(i)} * \Psi_j^{(i)} * g \right) (\xi) \, d\omega(\xi) \\
&= \sum_{i=1}^3 \sum_{(n,k) \in \mathcal{N}^{(i)}} \left((g^{(i)})^{\wedge}(n, k) \right)^2 \sum_{j=-\infty}^{\infty} \left(\left(\Psi_j^{(i)} \right)^{\wedge}(n) \right)^2 \\
&= \|g\|_{l^2(\Omega)}^2,
\end{aligned}$$

where we have used Definition 2.25 and relation (1.3). This completes the proof (note that again all integrations are understood in the Lebesgue-sense and that the interchange of summation and integration is justified by the Beppo-Levi Theorem). ■

For the 'output signal' $\tilde{g} = \widetilde{\Lambda}f$ we get, in spectral representation,

$$TVar_{j,\eta}^{(i)}(\widetilde{\Lambda}f) = \sum_{(n,k) \in \mathcal{N}^{(i)}} \left(\left(\Psi_j^{(i)} \right)^{\wedge}(n) \right)^2 \left(\left((\widetilde{\Lambda}f)^{(i)} \right)^{\wedge}(n, k) \right)^2 \left(y_{n,k}^{(i)}(\eta) \right)^2$$

and

$$TVar_j^{(i)}(\widetilde{\Lambda}f) = \sum_{(n,k) \in \mathcal{N}^{(i)}} \left(\left(\Psi_j^{(i)} \right)^{\wedge}(n, k) \right)^2 \left(\left((\widetilde{\Lambda}f)^{(i)} \right)^{\wedge}(n, k) \right)^2,$$

which completely resembles equations (3.8) and (3.9) of the scalar multiscale approach.

Tensor Based Scale and Space Error Covariances

What we need now to complete the tensor based theory are the corresponding definitions for the scale and space error covariances. With our results up to now, these definitions are straightforward.

Definition 3.18 *Let, in accordance with Definition 3.12, $\mathbf{k} : \Omega \times \Omega \rightarrow \mathbb{R}^{3 \times 3}$ be a tensorial covariance kernel. Suppose the family $\left\{ \Psi_j^{(i)} \right\}$, $j \in \mathbb{Z}$, $i \in \{1, 2, 3\}$, to be a tensor wavelet in*

the sense of Definition 2.26. The tensor based scale and space error covariance at position $\eta \in \Omega$, scale $j \in \mathbb{Z}$, and type $i \in \{1, 2, 3\}$ is given by

$$TCov_{j;\eta}^{(i)}(\mathbf{k}) = \int_{\Omega} \int_{\Omega} \left(\Psi_j^{(i)}(\xi, \eta) \Psi_j^{(i)}(\eta, \zeta) \right) \cdot \mathbf{k}(\xi, \zeta) d\omega(\xi) d\omega(\zeta).$$

Furthermore,

$$TCov_{j;\eta}(\mathbf{k}) = \sum_{i=1}^3 TCov_{j;\eta}^{(i)}(\mathbf{k})$$

denotes the tensor based scale and space error covariance at position $\eta \in \Omega$ and scale $j \in \mathbb{Z}$. The tensor based scale error covariance of type i is defined by

$$TCov_j^{(i)}(\mathbf{k}) = \int_{\Omega} TCov_{j;\eta}^{(i)}(\mathbf{k}) d\omega(\eta),$$

whereas

$$TCov_j(\mathbf{k}) = \sum_{i=1}^3 TCov_j^{(i)}(\mathbf{k})$$

is the tensor based scale error covariance.

By way of explanation we add the corresponding spectral representations:

$$TCov_{j;\eta}^{(i)}(\mathbf{k}) = \sum_{(n,k) \in \mathcal{N}^{(i)}} (\mathbf{k}^{(i)})^{\wedge}(n, k) \left((\Psi_j^{(i)})^{\wedge}(n) \right)^2 \left(y_{n,k}^{(i)}(\eta) \right)^2,$$

$$TCov_j^{(i)}(\mathbf{k}) = \sum_{(n,k) \in \mathcal{N}^{(i)}} (\mathbf{k}^{(i)})^{\wedge}(n, k) \left((\Psi_j^{(i)})^{\wedge}(n) \right)^2$$

and

$$TCov_j(\mathbf{k}) = \sum_{i=1}^3 \sum_{(n,k) \in \mathcal{N}^{(i)}} (\mathbf{k}^{(i)})^{\wedge}(n, k) \left((\Psi_j^{(i)})^{\wedge}(n) \right)^2.$$

The correspondence to the scalar case is obvious. Note that the multiscale noise model is able to specify pointwise dependent error covariances which is not possible in spectral theory by means of vector spherical harmonics.

Tensor Scale and Space Estimation

A criterion to decide whether noise or signal are predominant is given by the tensor based scale and space resolution sets of type i . To be more specific:

Definition 3.19 *Signal and noise scale 'intersect' at the so-called tensor based scale and space resolution set $\mathcal{TZ}_{res}^{(i)}(\eta) \subset \mathcal{Z} = \mathbb{Z} \times \Omega$ of type i at position η defined by:*

(i) *signal dominates noise*

$$TVar_{j;\eta}^{(i)}(\widetilde{\Lambda}f) \geq TCov_{j;\eta}^{(i)}(\mathbf{k}), \quad (j; \eta) \in \mathcal{TZ}_{res}^{(i)}(\eta).$$

(ii) *noise dominates signal*

$$TVar_{j;\eta}^{(i)}(\widetilde{\Lambda}f) < TCov_{j;\eta}^{(i)}(\mathbf{k}), \quad (j; \eta) \notin \mathcal{TZ}_{res}^{(i)}(\eta).$$

Finally we have managed to complete the tensor based theory. It is clear that the next step would be to combine this approach with a tensorial multiscale approximation in order to develop a tensorial selective multiscale reconstruction principle. Though tensor kernels obviously present a suitable tool to construct an elegant theoretical approach they are, from the view of numerical realization, a very complicated matter. This is why we do not develop a selective reconstruction algorithm using tensor kernels but try to find a vectorial analogue based on the tensorial results. This is the main subject of the next section.

3.2.3 Vector-Based Multiscale Signal-to-Noise Response

In Chapter 2, i.e. in Section 2.2.4, we have shown spherical vectorial scaling functions and wavelets to be appropriate kernels to approximate spherical vector fields within a multiscale framework. In Section 3.2.2, however, we have introduced the use of spherical tensorial scaling functions and wavelets as a canonical extension to the scalar approach. It is clear that somehow both techniques need to be connected. The link between both, the tensor and the vector formalism, has already been established by Theorem 2.28. This theorem, however, shows us that the different types of bilinear convolutions lead to equivalent results. Therefore, our attempts to replace the formal tensor approach to signal-to-noise thresholding of vector fields by a vectorial technique in order to obtain easier computability is justified.

Vector Based Scale and Space Variances

In what follows we define vector based scale and space variances in correspondence to the tensor based quantities. Then we show that the vector based measures are equivalent to the tensor based ones.

Definition 3.20 *Let $g \in l^2(\Omega)$ and let the family $\{\psi_j^{(i)}\}$, $j \in \mathbb{Z}$, $i \in \{1, 2, 3\}$, be a spherical vector wavelet. The vector based scale and space variance at position $\eta \in \Omega$, scale $j \in \mathbb{Z}$ and type $i \in \{1, 2, 3\}$ is defined by*

$$VVar_{j;\eta}^{(i)}(g) = \int_{\Omega} \int_{\Omega} \left(\psi_j^{(i)}(\xi, \eta) \otimes \psi_j^{(i)}(\zeta, \eta) \right) \cdot (g(\xi) \otimes g(\zeta)) \, d\omega(\xi) \, d\omega(\zeta) .$$

The vector based scale variance at scale $j \in \mathbb{Z}$ of type i is given by

$$VVar_j^{(i)}(g) = \int_{\Omega} VVar_{j;\eta}^{(i)}(g) \, d\omega(\eta),$$

while the vector based scale variance at scale $j \in \mathbb{Z}$ reads as follows

$$VVar_j(g) = \sum_{i=1}^3 VVar_j^{(i)}(g) .$$

For the 'output signal' $\tilde{g} = \widetilde{\Lambda}f$ we calculate $VVar_{j;\eta}^{(i)}(\widetilde{\Lambda}f)$ in spectral language and obtain

$$VVar_{j;\eta}^{(i)}(\widetilde{\Lambda}f) = \sum_{(n,k) \in \mathcal{N}^{(i)}} \left(\left(\psi_j^{(i)} \right)^\wedge (n) \right)^2 \left(\left(\left(\widetilde{\Lambda}f \right)^{(i)} \right)^\wedge (n,k) \right)^2 \left(Y_{n,k}(\eta) \right)^2 .$$

Hence it follows that

$$TVar_j^{(i)}(\widetilde{\Lambda}f) = VVar_j^{(i)}(\widetilde{\Lambda}f), \quad i \in \{1, 2, 3\}$$

and

$$TVar_j(\widetilde{\Lambda}f) = VVar_j(\widetilde{\Lambda}f) .$$

But this is just what we tried to establish, vector based quantities that lead to results equivalent to the tensor based approach. In conclusion we can find the connection between the vector based scale and space variances and the $l^2(\Omega)$ -energy of the signal under consideration:

$$\|\widetilde{\Lambda}f^{(i)}\|_{l^2(\Omega)} = \|TVar^{(i)}.;.(\widetilde{\Lambda}f)\|_{l^2(\mathbb{Z} \times \Omega)} = \|VVar^{(i)}.;.(\widetilde{\Lambda}f)\|_{l^2(\mathbb{Z} \times \Omega)} .$$

What remains is the definition of the corresponding error covariances.

Vector Based Scale and Space Error Covariances

The vector based multiscale error theory is based on the vector analog to the tensor based error covariances:

Definition 3.21 *Let the family $\{\psi_j^{(i)}\}$, $j \in \mathbb{Z}$, $i \in \{1, 2, 3\}$, be a spherical vector wavelet and suppose $\mathbf{k} : \Omega \times \Omega \rightarrow \mathbb{R}^{3 \times 3}$ to be a tensorial covariance kernel. Then the vector based scale and space error covariance at position $\eta \in \Omega$, scale $j \in \mathbb{Z}$, and type $i \in \{1, 2, 3\}$ is given by*

$$VCov_{j;\eta}^{(i)}(\mathbf{k}) = \int_{\Omega} \int_{\Omega} \left(\psi_j^{(i)}(\xi, \eta) \otimes \psi_j^{(i)}(\zeta, \eta) \right) \cdot \mathbf{k}(\xi, \zeta) \, d\omega(\xi) \, d\omega(\zeta) .$$

Furthermore we define

$$VCov_{j;\eta}(\mathbf{k}) = \sum_{i=1}^3 VCov_{j;\eta}^{(i)}(\mathbf{k}) .$$

The vector based scale error covariance of type i is defined by

$$VCov_j^{(i)}(\mathbf{k}) = \int_{\Omega} VCov_{j;\eta}^{(i)}(\mathbf{k}) \, d\omega(\eta) .$$

Expressing $VCov_{j;\eta}^{(i)}(\mathbf{k})$ in terms of spherical harmonics we end up with

$$TCov_j^{(i)}(\mathbf{k}) = VCov_j^{(i)}(\mathbf{k}), \quad i \in \{1, 2, 3\}$$

as well as

$$TCov_j(\mathbf{k}) = VCov_j(\mathbf{k}) .$$

This, however, is just the sought for equivalence of tensor based and vector based error covariances and justifies, together with the corresponding result for the signal scale and space variances, the use of the vector based approach.

Vector Scale and Space Estimation

The decision whether noise or signal are predominant can be made using

Definition 3.22 *Signal and noise scale intersect at the so-called vector based scale and space resolution set $\mathcal{VZ}_{\text{res}}^{(i)}(\eta) \subset \mathbb{Z} = \Omega \times \mathbb{R}$ of type $i \in \{1, 2, 3\}$ at position $\eta \in \Omega$ given by*

(i) *signal dominates noise*

$$VVar_{j;\eta}^{(i)}(\widetilde{\Lambda}f) \geq VCov_{j;\eta}^{(i)}(\mathbf{k}), \quad (j; \eta) \in \mathcal{VZ}_{\text{res}}^{(i)} .$$

(ii) *noise dominates signal*

$$VVar_{j;\eta}^{(i)}(\widetilde{\Lambda}f) < VCov_{j;\eta}^{(i)}(\mathbf{k}), \quad (j; \eta) \in \mathcal{VZ}_{\text{res}}^{(i)} .$$

Similar to what we have done in the case of the scalar multiscale method, the vector variant of multiscale approximation of a signal function can be formulated by replacing the unknown error-free field $(\Lambda f)^{(i)}$, $i \in \{1, 2, 3\}$, being approximated by

$$(\Lambda f)_J^{(i)} = \varphi_{J_0}^{(i)} \star \varphi_{J_0}^{(i)} * (\Lambda f) + \sum_{j=J_0}^{J-1} \psi_j^{(i)} \star \psi_j^{(i)} * (\Lambda f),$$

by the error-affected field $(\widetilde{\Lambda}f)^{(i)}$, $i \in \{1, 2, 3\}$ such that

$$(\widetilde{\Lambda}f)_J^{(i)} = \varphi_{J_0}^{(i)} \star \varphi_{J_0}^{(i)} * (\widetilde{\Lambda}f) + \sum_{j=J_0}^{J-1} \psi_j^{(i)} \star \psi_j^{(i)} * (\widetilde{\Lambda}f),$$

$J > J_0$. It is obvious that, in order to obtain a suitable approximation of the true signal, the different signal and noise content, i.e. the criteria given by the vector based scale and position resolution set, have to be incorporated in the approximation process. The next section deals with this subject.

3.2.4 Vectorial Selective Multiscale Reconstruction

Initial point is the multiscale approximation

$$(\widetilde{\mathbf{A}f})_J^{(i)} = \varphi_{J_0}^{(i)} \star \varphi_{J_0}^{(i)} * (\widetilde{\mathbf{A}f}) + \sum_{j=J_0}^{J-1} \psi_j^{(i)} \star \psi_j^{(i)} * (\widetilde{\mathbf{A}f}).$$

As in the previously developed scalar framework there are coefficients

$$\begin{aligned} \tilde{p}_{J_0}^{(i)}(\widetilde{\mathbf{A}f})(\eta) &= \int_{\Omega} \varphi_{J_0}^{(i)}(\eta, \zeta) \int_{\Omega} \varphi_{J_0}^{(i)}(\xi, \zeta) \cdot (\widetilde{\mathbf{A}f})(\xi) \, d\omega(\xi) \, d\omega(\zeta), \\ \tilde{r}_j^{(i)}(\widetilde{\mathbf{A}f})(\eta) &= \int_{\Omega} \psi_j^{(i)}(\eta, \zeta) \int_{\Omega} \psi_j^{(i)}(\xi, \zeta) \cdot (\widetilde{\mathbf{A}f})(\xi) \, d\omega(\xi) \, d\omega(\zeta), \end{aligned}$$

which have to be calculated by approximate integration combined with the criteria given in Definition 3.22. Again we chose integration formulae with weights $(v^{(i)})_s^{N_j}$, $(w^{(i)})_l^{L_j} \in \mathbb{R}$ and knots $\zeta_s^{N_j}$, $\xi_l^{L_j} \in \Omega$, $s = 1, \dots, N_j$; $l = 1, \dots, L_j$, of the form:

$$\begin{aligned} \tilde{p}_{J_0}^{(i)}(f)(\eta) &\simeq \sum_{s=1}^{N_{J_0}} (v^{(i)})_s^{N_{J_0}} \varphi_{J_0}^{(i)}(\eta, \zeta_s^{N_{J_0}}) (\tilde{a}^{(i)})_s^{N_{J_0}}, \\ \tilde{r}_j^{(i)}(f)(\eta) &\simeq \sum_{s=1}^{N_j} (v^{(i)})_s^{N_j} \psi_j^{(i)}(\eta, \zeta_s^{N_j}) (\tilde{b}^{(i)})_s^{N_j}, \quad j = J_0, \dots, J-1, \end{aligned}$$

where

$$(\tilde{a}^{(i)})_s^{N_{J_0}} \simeq \sum_{l=1}^{L_{J_0}} (w^{(i)})_l^{L_{J_0}} \varphi_{J_0}^{(i)}(\xi_l^{L_{J_0}}, \zeta_s^{N_{J_0}}) \cdot (\widetilde{\mathbf{A}f})(\xi_l^{L_{J_0}}), \quad (3.16)$$

$$(\tilde{b}^{(i)})_s^{N_j} \simeq \sum_{l=1}^{L_j} (w^{(i)})_l^{L_j} \psi_j^{(i)}(\xi_l^{L_j}, \zeta_s^{N_j}) \cdot (\widetilde{\mathbf{A}f})(\xi_l^{L_j}). \quad (3.17)$$

Note that the sign ' \simeq ' means that we assume the error to be negligible. Reasonably only those coefficients are included that are in accordance with the thresholds given by the corresponding scale and space resolution sets $\mathcal{VZ}_{res}^{(i)}$. That is, only those coefficients containing a predominant amount of the signal are considered in the reconstruction process.

More explicitly we get

$$\begin{aligned}
& \left((\tilde{a}^{(i)})_s^{N_{J_0}} \right)^2 \\
&= \int_{\Omega} \int_{\Omega} \left(\varphi_{J_0}^{(i)}(\alpha, \zeta_s^{N_{J_0}}) \otimes \varphi_{J_0}^{(i)}(\beta, \zeta_s^{N_{J_0}}) \right) \cdot \left((\tilde{\Lambda}f)(\alpha) \otimes (\tilde{\Lambda}f)(\beta) \right) d\omega(\alpha) d\omega(\beta) \\
&\simeq \sum_{p=1}^{L_{J_0}} \sum_{q=1}^{L_{J_0}} (w^{(i)})_p^{L_{J_0}} (w^{(i)})_q^{L_{J_0}} \left(\varphi_{J_0}^{(i)}(\xi_p^{L_{J_0}}, \zeta_s^{N_{J_0}}) \otimes \varphi_{J_0}^{(i)}(\xi_q^{L_{J_0}}, \zeta_s^{N_{J_0}}) \right) \\
&\quad \cdot \left((\tilde{\Lambda}f)(\xi_p^{L_{J_0}}) \otimes (\tilde{\Lambda}f)(\xi_q^{L_{J_0}}) \right) \\
&\geq \sum_{p=1}^{L_{J_0}} \sum_{q=1}^{L_{J_0}} (w^{(i)})_p^{L_{J_0}} (w^{(i)})_q^{L_{J_0}} \left(\varphi_{J_0}^{(i)}(\xi_p^{L_{J_0}}, \zeta_s^{N_{J_0}}) \otimes \varphi_{J_0}^{(i)}(\xi_q^{L_{J_0}}, \zeta_s^{N_{J_0}}) \right) \cdot \mathbf{k}(\xi_p^{L_{J_0}}, \xi_q^{L_{J_0}}) \\
&\simeq \int_{\Omega} \int_{\Omega} \varphi_{J_0}^{(i)}(\alpha, \zeta_s^{N_{J_0}}) \otimes \varphi_{J_0}^{(i)}(\beta, \zeta_s^{N_{J_0}}) \cdot \mathbf{k}(\alpha, \beta) d\omega(\alpha) d\omega(\beta) \\
&= \kappa_{\varphi_{J_0}^{(i)}}(\zeta_s^{N_{J_0}})
\end{aligned}$$

and

$$\begin{aligned}
& \left((\tilde{b}^{(i)})_s^{N_j} \right)^2 \\
&= \int_{\Omega} \int_{\Omega} \left(\psi_j^{(i)}(\alpha, \zeta_s^{N_j}) \otimes \psi_j^{(i)}(\beta, \zeta_s^{N_j}) \right) \cdot \left((\tilde{\Lambda}f)(\alpha) \otimes (\tilde{\Lambda}f)(\beta) \right) d\omega(\alpha) d\omega(\beta) \\
&\simeq \sum_{p=1}^{L_j} \sum_{q=1}^{L_j} (w^{(i)})_p^{L_j} (w^{(i)})_q^{L_j} \left(\psi_j^{(i)}(\xi_p^{L_j}, \zeta_s^{N_j}) \otimes \psi_j^{(i)}(\xi_q^{L_j}, \zeta_s^{N_j}) \right) \cdot \left((\tilde{\Lambda}f)(\xi_p^{L_j}) \otimes (\tilde{\Lambda}f)(\xi_q^{L_j}) \right) \\
&\geq \sum_{p=1}^{L_j} \sum_{q=1}^{L_j} (w^{(i)})_p^{L_j} (w^{(i)})_q^{L_j} \left(\psi_j^{(i)}(\xi_p^{L_j}, \zeta_s^{N_j}) \otimes \psi_j^{(i)}(\xi_q^{L_j}, \zeta_s^{N_j}) \right) \cdot \mathbf{k}(\xi_p^{L_j}, \xi_q^{L_j}) \\
&\simeq \int_{\Omega} \int_{\Omega} \psi_j^{(i)}(\alpha, \zeta_s^{N_j}) \otimes \psi_j^{(i)}(\beta, \zeta_s^{N_j}) \cdot \mathbf{k}(\alpha, \beta) d\omega(\alpha) d\omega(\beta) \\
&= \kappa_{\psi_j^{(i)}}(\zeta_s^{N_j}) .
\end{aligned}$$

In combination with the hard and soft thresholding functions (cf. Section 3.1.3) we can summarize our results for a multiscale thresholding estimator of the signal:

Theorem 3.23 *Let $\{\varphi_j\}$ and $\{\psi_j\}$, $j \in \mathbb{Z}$, be an $l^2(\Omega)$ -scaling function and an $l^2(\Omega)$ -wavelet, respectively. Let, furthermore, $(v^{(i)})_s^{N_j}, (w^{(i)})_l^{L_j} \in \mathbb{R}$ be integration weights and $\zeta_s^{N_j}, \xi_l^{L_j} \in \Omega$, $s = 1, \dots, N_j$, $l = 1, \dots, L_j$, the associated knots of approximate integration formulae. Assume δ_λ to be either the hard or the soft thresholding function.*

If the coefficients $(\tilde{a}^{(i)})_s^{N_{J_0}}$ and $(\tilde{b}^{(i)})_s^{N_j}$ are given as in equations (3.16) and (3.17), respectively, and if $\kappa_{\varphi_{J_0}^{(i)}}(\zeta_s^{N_{J_0}})$ as well as $\kappa_{\psi_j^{(i)}}(\zeta_s^{N_j})$ are the corresponding threshold values, then the vector based thresholding multiscale estimator of a signal $\tilde{\Lambda}f$ reads

$$\begin{aligned} (\widehat{\Lambda}f)_J^{(i)}(\eta) &= \sum_{s=1}^{N_{J_0}} \delta_{\kappa_{\varphi_{J_0}^{(i)}}(\zeta_s^{N_{J_0}})} \left(\left((\tilde{a}^{(i)})_s^{N_{J_0}} \right)^2 \right) (v^{(i)})_s^{N_{J_0}} \varphi_{J_0}^{(i)}(\eta, \zeta_s^{N_{J_0}}) (\tilde{a}^{(i)})_s^{N_{J_0}} \\ &+ \sum_{j=J_0}^{J-1} \sum_{s=1}^{N_j} \delta_{\kappa_{\psi_j^{(i)}}(\zeta_s^{N_j})} \left(\left((\tilde{b}^{(i)})_s^{N_j} \right)^2 \right) (v^{(i)})_s^{N_j} \psi_j^{(i)}(\eta, \zeta_s^{N_j}) (\tilde{b}^{(i)})_s^{N_j} . \end{aligned}$$

Therefore, as in the scalar multiscale approach, the estimated signal consists of a thresholded smooth part representing the overall features and, additionally, contributions due to coefficients at higher resolution which are thresholded such that the noise is suppressed but the fine details are included in the reconstruction.

3.3 Example

In order to test and illustrate the functionality of multiscale signal-to-noise thresholding we will present an example using synthetic geomagnetic vector data. The data are synthesized on a grid of nodal points due to [20]. More explicitly, the grid used is such that on each spherical latitude, as well as on each spherical longitude, there will be an equal number of equiangular distributed nodal points. Consequently, the data density in polar regions is higher than in the vicinity of the equator thus mimicking the situation known from satellites with almost polar orbits. During the process of decomposition and reconstruction this effect is taken into account by weighting each data point by integration weights which attenuate the contributions of the polar regions in the appropriate way (see [20] for more details on this subject). As a reference field b_{clear} we use a vectorial data set generated from a bandlimited (up to degree and order 12) geomagnetic potential due to [13]. The noisy data set b_{noisy} is calculated from b_{clear} by adding bandlimited white noise of variance σ and bandlimit n_K of approximately 2.9 and 60 (see Sections 3.1.1 and 3.2.1), respectively, to each of the three field components in spherical polar coordinates. This procedure resulted in noise of the order of magnitude of 10^0 Nanoteslas (nT) in field components of the order of magnitude of 10^4 nT. In what follows we restrict ourselves to the radial component ($-\varepsilon^r$ component) and one of the tangential components (ε^φ component). The results for the ε^θ component are similar and will therefore be omitted. Figure 3.1 shows $-(b_{noisy} \cdot \varepsilon^r)$ and $(b_{noisy} \cdot \varepsilon^\varphi)$ (i.e. the geomagnetic downward and east components of b_{noisy}), respectively, while Figure 3.2 shows the absolute value of the noise contained in these components. In

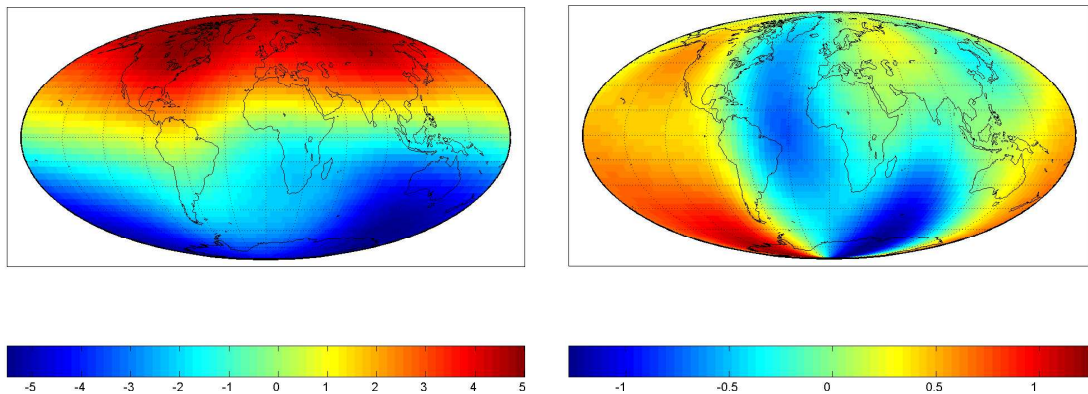


Figure 3.1: $-\varepsilon^r$ component (left) and ε^φ component (right) of the noisy geomagnetic input data b_{noisy} (in 10000 nT).

order to denoise the noisy data set b_{noisy} , it is decomposed and reconstructed using spherical vectorial Shannon wavelets of type $i \in \{1, 2\}$ up to a maximum scale $J_{max} = 3$. Note that, since the input data is a gradient field, we need not use type $i = 3$ vector wavelets. Applying the method of hard thresholding, only those wavelet coefficients containing a predominant amount of the clear signal are used during the reconstruction process in accordance with our considerations in Sections 3.2.3 and 3.2.4. Using this approach, the root-mean-square error of the noisy $-\varepsilon^r$ component w.r.t. the reference field b_{clear} , $(\Delta\varepsilon_{noisy}^r)_{rms} = 4.9$ [nT],

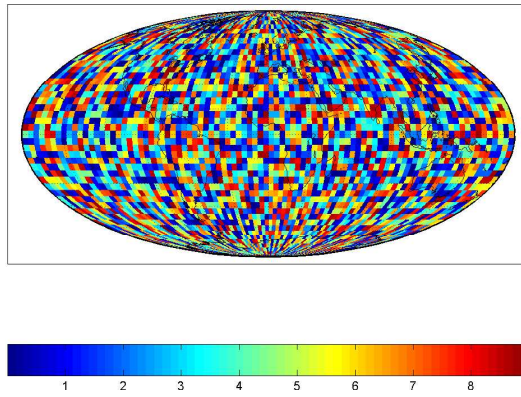
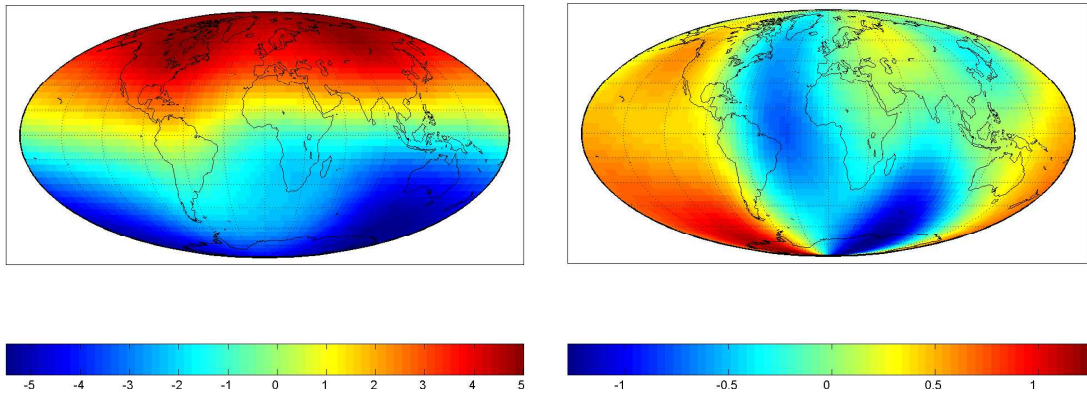
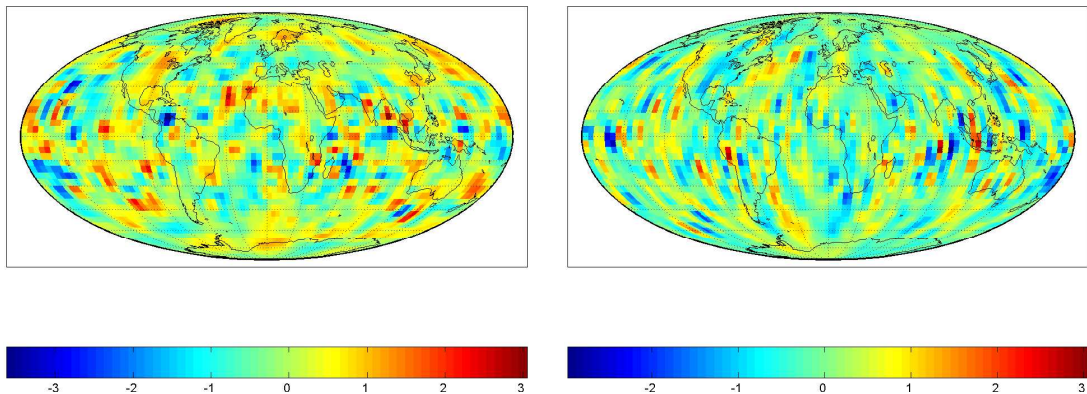


Figure 3.2: Absolute value of noise [nT].

has been reduced to $(\Delta\varepsilon_{denoised}^r)_{rms} = 0.6$ [nT], which is an improvement of about 87 per cent. In the ε^φ component we have $(\Delta\varepsilon_{noisy}^\varphi)_{rms} = 4.9$ [nT] and $(\Delta\varepsilon_{denoised}^r)_{rms} = 0.5$ [nT] which is an improvement of about 89 per cent. The denoised reconstructions of the $-\varepsilon^r$ and ε^φ components can be seen in Figure 3.3. Figure 3.4 shows the corresponding errors w.r.t. the reference field b_{clear} .

Figure 3.3: Denoised reconstructions of the $-\varepsilon^r$ component (left) and the ε^φ component (right) in 10000 nT.Figure 3.4: Error of the denoised reconstructions of the $-\varepsilon^r$ component (left) and the ε^φ component (right) w.r.t. the reference data set b_{clear} [nT].

As can be expected, comparing Figures 3.2 and 3.4 we see how the comparatively rough structure of the noise has been smoothed out and attenuated by the denoising procedure.

For illustrational purposes we present Figures 3.5, 3.6 and 3.7 showing a multiscale analysis of the radial component including scales $J = 1, 2$ and 3, respectively, giving an impression of what happens on the different scales of the denoising process. The plots on the left hand side show the difference between the denoised partial wavelet reconstruction of the noisy data and the corresponding partial reconstruction without applying the denoising procedure. Consequently, these plots give an illustration of how strong the noise influences this very scale and of how active the denoising procedure is on this scale. The right hand sides present the difference between the denoised partial reconstruction of the noisy data and a corresponding partial reconstruction of the reference data set, thus showing how the noise (or what is left of it) influences the final approximation. On the left of Figure 3.5 one can hardly see any structure and the order of magnitude of the plotted difference is 10^{-6} nT. This is understandable if one takes into account that the noise is very small compared to the vector field at scale $J = 1$. Nevertheless, we can see an error in the reconstruction (right hand side of Figure 3.5) which, though small in magnitude, has a large spatial structure. This large spatial extend reflects the typical size of spatial features at this scale. The difference between the denoised and the undenoised partial reconstruction at scale $J = 2$ is of the order 10^{-3} nT and can be seen on the left of Figure 3.6. This increasing difference shows that the noise plays a more important role at scale $J = 2$ than at scale $J = 1$ since the noise at this scale becomes comparable with the vector field. Of course, this results in an increased - but still small - error of the denoised reconstruction with respect to the corresponding clear data (Figure 3.6, right). Again the spatial extend of the visible features is correspondent to the typical lengthscales at scale $J = 2$. Going up to scale $J = 3$ we obtain similar effects, i.e. an increasing difference between the denoised and the undenoised partial reconstruction (order of magnitude 10^0 , Figure 3.7, left) and a larger error with respect to the reference data (Figure 3.7, right). Again the reason is the noise which, at this scale, is of the same order of magnitude as the vector field.

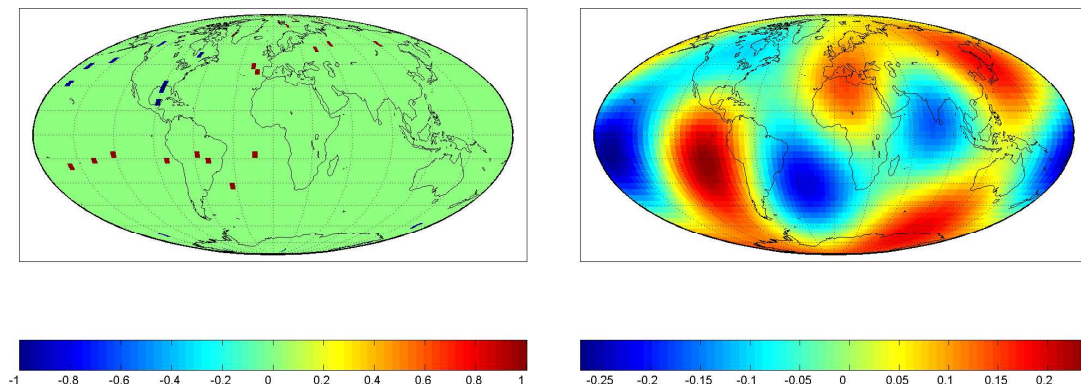


Figure 3.5: Difference between partial reconstruction with and without denoising (left, 10^{-6} [nT]); difference between partial reconstruction with denoising and partial reconstruction of reference data (right, [nT]); scale $J = 1$.

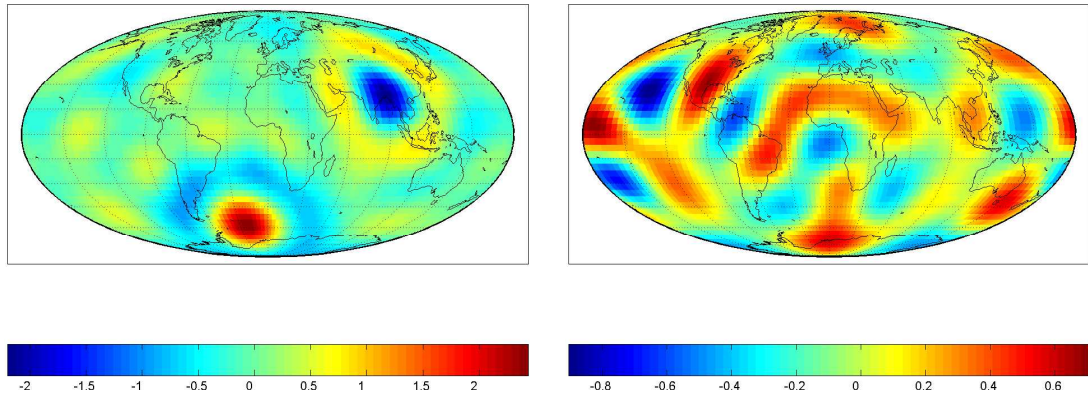


Figure 3.6: Difference between partial reconstruction with and without denoising (left, 10^{-3} [nT]); difference between partial reconstruction with denoising and partial reconstruction of reference data (right, [nT]); scale $J = 2$.

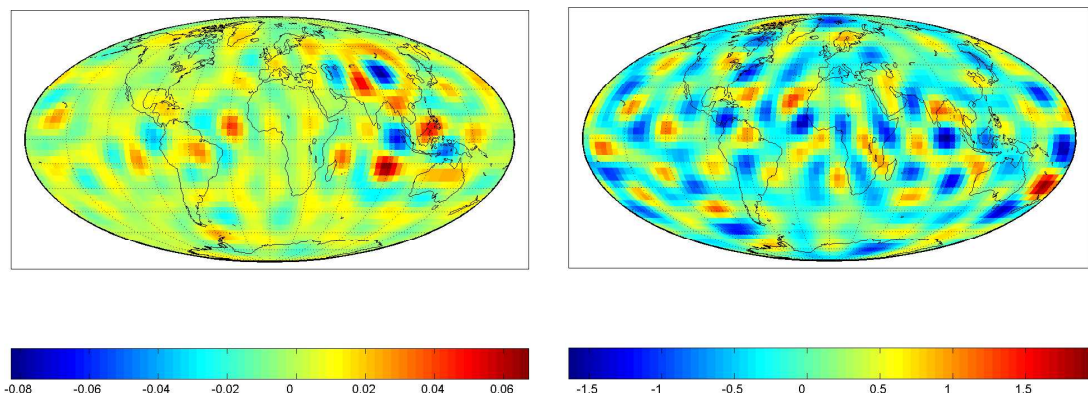


Figure 3.7: Difference between partial reconstruction with and without denoising (left, 10^0 [nT]); difference between partial reconstruction with denoising and partial reconstruction of reference data (right, [nT]); scale $J = 3$.

This example clearly demonstrates the functionality and effectiveness of the multiscale approach. As far as the noise is concerned, the use of 'white noise' or 'bandlimited white noise' is a reasonable and widespread tool for testing such numerical procedures. Nevertheless, it is clear that in the future more realistic noise models (i.e. covariance kernels in a form appropriate for our technique) need to be developed for recent satellite missions and then need to be tested under realistic conditions as soon as they are available. Then a combined application of this technique and the methods derived in Chapter 4, for example, to actual satellite data become reasonable. First investigations in this direction can be found in [105].

Last but not least we need to mention that for physical reasons we cannot assume the input data to be a pure gradient field in the case of real satellite data. This means that type 3 vector wavelets need to be used in the denoising process, too. However, this is not a difficulty since various examples of vector wavelet modelling of all types ($i = 1, 2, 3$) have been already successfully applied to geomagnetic satellite data (e.g. [81, 9] and [11]).

Chapter 4

A Wavelet Approach to Crustal Field Modelling

Lithospheric magnetization gives rise to a geomagnetic field contribution that can be mapped by appropriately low-flying satellites. The German geoscientific satellite CHAMP, for example, is designed, among other tasks, for such lithospheric studies. CHAMP provides us with highly accurate scalar (Overhauser magnetometer) as well as vectorial (Fluxgate magnetometer, FGM) data on an almost circular orbit with almost global coverage. While the scalar data are commonly used to derive magnetic anomaly maps at satellite height, the vectorial data are usually used to derive crustal field maps at Earth's level, a process commonly referred to as downward continuation.

The standard technique for crustal field modelling and downward continuation is to assume the existence of a scalar harmonic geomagnetic potential. The potential is expanded in terms of scalar spherical harmonics with a predefined bandlimit (i.e. maximum degree) and the corresponding expansion coefficients are determined such that the resulting geomagnetic field is in accordance with the given data. Obviously, assuming the existence of a harmonic potential is a critical point when satellite data are used. It is this assumption that makes the selection and preprocessing of proper data sets a crucial point (see also [58, 83, 93] and Section 4.1.4). A very detailed and recent review on several theoretical and practical aspects of crustal field determination from satellite data is presented in [58]. [13, 14, 15, 103], for example, apply variants of the standard technique to satellite data (mostly MAGSAT data) in order to obtain crustal field contributions. Nevertheless, though being the standard approach, spherical harmonic analysis does not reflect the special characteristics of the crustal field particularly well. Crustal field contributions are of regional or local spatial structure and the modelling technique should take this into account. This becomes more and more important in view of the many modern satellite missions supplying us with continuous, highly accurate scalar as well as vectorial geomagnetic data of almost dense global coverage. Consequently, the mathematical tools to calculate the crustal field contributions should take into consideration the regional and local characteristics. [54, 53], for example, consider spherical cap harmonic analysis (SCHA) as an alternative approach to regional modelling, involving associated Legendre functions of integral order but non-integral degree

resulting in the possibility to consider regional data sets. Though this method is well suited for regional modelling, there are some known drawbacks (cf. [58] for a review), e.g. the geomagnetic potential determined by SCHA has infinite discontinuities at the opposite pole and its radial dependence must include non-integer powers of the spherical harmonic degree n in order to approximate the real radial dependence of the field. Furthermore, the SCHA regional solutions cannot be incorporated into a global modelling concept since the potentials obtained from SCHA are only valid approximations over the spherical cap that is used for their derivation and significantly differ from the real potential anywhere else. Downward continuation of SCHA potentials (or their derivatives) is also critical if the altitude range of the data is exceeded (see [58] and the references therein). The authors of [1] apply an ansatz based on the space localizing Abel-Poisson kernel function and therefore make allowance for the regional structures of geomagnetic crustal field signatures. This approach is, from a potential-theoretical point of view, somewhat related to what we will present here, the theoretical procedure as well as the numerical realizations are completely different, though. Promising up to date results obtained from analyzing CHAMP data sets in terms of spherical harmonics can be found in [83].

Based on the existence of a harmonic scalar geomagnetic potential, the basic idea of our treatment is to formulate the problem of downward continuation in terms of integral equations relating the radial or the tangential projections of the geomagnetic field at satellite height with the magnetic field at the Earth's surface (see also [1]). From a mathematical point of view, these integral equations are exponentially ill-posed and their numerical solution requires regularization. As an appropriate solution method a multiscale technique in terms of scalar and vectorial regularization kernels is proposed. As regards the construction of those kernel functions we take advantage of the fact that we can determine the singular systems of the aforementioned integral operators analytically. Section 4.1 approaches the subject in spherical approximation, i.e. we assume the Earth's surface and the satellite's orbit to be spheres of fixed radii centered around the origin. This approximation can be utilized if the satellite's track is almost circular or the effects of height variations of the satellite can be neglected. Applying this approach turns out to be advantageous from a numerical point of view since the solution of linear systems of equations can be avoided completely. A numerical example illustrating how to apply the spherical technique to a CHAMP vectorial data set in order to calculate the geomagnetic crustal field at the mean Earth surface is given in Section 4.1.4. In Section 4.2 we will extend the spherical approach by means of (harmonic) splines leading to an ansatz which is also suitable for non-spherical geometries but is of higher complexity as far as numerical realizations are concerned. Our overall treatment is significantly influenced by the general approach to spaceborne geodata in [29], the introduction of regularization wavelets in [42] and the multiscale treatment of the satellite-to-satellite tracking problem (SST) in [32] which, from a mathematical point of view, is closely related to the subject of this chapter. For additional reading the interested reader might also consult [38, 39] and [98]. [22, 23, 78] deal with integral equations and inverse problems in a general functional-analytic framework.

4.1 Downward Continuation in Spherical Approximation

In the course of this section we suppose the spherical approximation to be valid, more explicitly we assume the Earth's surface Ω_{ρ_1} as well as the satellite's orbit Ω_{ρ_2} to be spheres of fixed radii $\rho_1, \rho_2 \in \mathbb{R}^+$, $\rho_1 < \rho_2$, centered around the origin. If the data used are suitably chosen and preprocessed (i.e. data of quiet days and night local times, correction for external field contributions as well as corresponding induced internal parts etc., (see e.g. [58, 83, 93] and Section 4.1.4), we can assume that there exists a geomagnetic potential $U_{mag} : \overline{\Omega_{\rho_1}^{ext}} \rightarrow \mathbb{R}$ harmonic in $\Omega_{\rho_1}^{ext}$. The geomagnetic field is then just given by $b = \nabla U_{mag}$. We render the class of potentials under consideration more precisely:

Definition 4.1 *Let $\{Y_{n,k}\}_{(n,k) \in \mathcal{N}}$ and $\{Y_{n,k}^{\rho_1}\}_{(n,k) \in \mathcal{N}}$ be $\mathcal{L}^2(\Omega)$ - and $\mathcal{L}^2(\Omega_{\rho_1})$ -orthonormal systems of spherical harmonics, respectively. Then the space $Pot(\Omega_{\rho_1}^{ext})$ is defined to be the space of all potentials $U : \overline{\Omega_{\rho_1}^{ext}} \rightarrow \mathbb{R}$ of the form*

$$U(x) = \sum_{n=0}^{\infty} \sum_{k=1}^{2n+1} U_{\rho_1}^{\wedge}(n, k) \left(\frac{\rho_1}{|x|} \right)^n \frac{1}{|x|} Y_{n,k} \left(\frac{x}{|x|} \right), \quad x \in \overline{\Omega_{\rho_1}^{ext}}, \quad (4.1)$$

with Fourier coefficients

$$U_{\rho_1}^{\wedge}(n, k) = \int_{\Omega_{\rho_1}} U(x) Y_{n,k}^{\rho_1}(x) d\omega_{\rho_1}(x)$$

that satisfy

$$\sum_{n=0}^{\infty} \sum_{k=1}^{2n+1} |U_{\rho_1}^{\wedge}(n, k)|^2 < \infty.$$

More explicitly, the space $Pot(\Omega_{\rho_1}^{ext})$ consists of all harmonic functions in $\Omega_{\rho_1}^{ext}$ corresponding to square-integrable Dirichlet boundary conditions on Ω_{ρ_1} , i.e. $U|_{\Omega_{\rho_1}} \in \mathcal{L}^2(\Omega_{\rho_1})$. From a physical point of view this guarantees finite energy of the corresponding gradient field (e.g. the geomagnetic field) on Ω_{ρ_1} and all other spheres Ω_r with $\rho_1 \leq r < \infty$.

The gradient fields corresponding to the potentials of class $Pot(\Omega_{\rho_1}^{ext})$ can easily be derived using the decomposition of the ∇ -operator in terms of the $o^{(i)}$ -operators (see Section 1.3). For $U \in Pot(\Omega_{\rho_1}^{ext})$ we obtain

$$\begin{aligned} f_U(x) &= (\nabla U)(x) \\ &= \sum_{n=0}^{\infty} \sum_{k=1}^{2n+1} U_{\rho_1}^{\wedge}(n, k) \left(\frac{\rho_1}{|x|} \right)^n \left(-\frac{n+1}{|x|^2} o^{(1)} Y_{n,k} \left(\frac{x}{|x|} \right) + \frac{1}{|x|^2} o^{(2)} Y_{n,k} \left(\frac{x}{|x|} \right) \right), \end{aligned}$$

for all $x \in \overline{\Omega_{\rho_1}^{ext}}$. Applying the Helmholtz-projectors $p_{(i)}$ (see Section 1.3) to the last result we end up with the following lemma (cf. [32]):

Lemma 4.2 *Let $U \in Pot(\Omega_{\rho_1}^{ext})$. Then, for $\rho_1 \leq r < \infty$ and $x \in \overline{\Omega_{\rho_1}^{ext}}$ it holds that:*

- (i) $p_{(1)}(\nabla U)(x)|_{\Omega_r} = 0$ if and only if $U = 0$,
- (ii) $p_{(2)}(\nabla U)(x)|_{\Omega_r} = 0$ if and only if $U(x) = c/|x|$ for a constant $c \in \mathbb{R}$,
- (iii) $p_{(3)}(\nabla U)(x)|_{\Omega_r} = 0$.

Consequently, any potential $U \in Pot(\Omega_{\rho_1}^{ext})$ is uniquely determined by its first order radial derivative or, up to an additive zero-order term, by its surface gradient field on Ω_r . In case of U being the geomagnetic potential, the constant c in Lemma 4.2 can be set to zero because there exist no magnetic monopoles, i.e. the zero-order term vanishes and it also suffices to know the surface gradient field on Ω_r in order to determine the potential uniquely. This is the starting point for our further treatment.

4.1.1 Integral Equations for the Radial Derivative

We now investigate the background for the case of given negative first order radial derivative at some height r and therefore establish its connection to the potential as well as the corresponding gradient field which is the physically interesting quantity, actually. Note that the negative radial derivative is chosen in order to obtain positive singular values later on. If we let $U \in Pot(\Omega_{\rho_1}^{ext})$ and $x \in \overline{\Omega_{\rho_1}^{ext}}$ with $x = r\xi$, $\rho_1 \leq r < \infty$, $\xi \in \Omega$, then it can easily be deduced that

$$-\frac{\partial}{\partial r}U(r\xi) = \sum_{n=0}^{\infty} \sum_{k=1}^{2n+1} \left(\frac{\rho_1}{r}\right)^n \frac{n+1}{r} U_{\rho_1}^{\wedge}(n, k) Y_{n,k}^r(\xi), \quad (4.2)$$

with $\{Y_{n,k}^r\}_{(n,k) \in \mathcal{N}}$ being an $\mathcal{L}^2(\Omega_r)$ -orthonormal systems of spherical harmonics. Comparing equations (4.1) and (4.2) we immediately get (see also [32]):

Lemma 4.3 *Let the operator $\Lambda_{Pot} : \mathcal{L}^2(\Omega_{\rho_1}) \rightarrow \mathcal{L}^2(\Omega_r)$ be defined via*

$$(\Lambda_{Pot}F)(x) = \int_{\Omega_{\rho_1}} K_{\Lambda_{Pot}}(x, y) F(y) d\omega_{\rho_1}(y), \quad F \in \mathcal{L}^2(\Omega_{\rho_1}), \quad x \in \Omega_r,$$

where the integral kernel is defined by

$$K_{\Lambda_{Pot}}(x, y) = \sum_{n=0}^{\infty} \sum_{k=1}^{2n+1} (\Lambda_{Pot})^{\wedge}(n) Y_{n,k}^r(x) Y_{n,k}^{\rho_1}(y), \quad y \in \Omega_{\rho_1}$$

with symbol $\{(\Lambda_{Pot})^{\wedge}(n)\}_{n=0,1,\dots}$ given by

$$(\Lambda_{Pot})^{\wedge}(n) = \left(\frac{\rho_1}{r}\right)^n \frac{n+1}{r}.$$

Let $U \in Pot(\Omega_{\rho_1}^{ext})$, and let G be the corresponding negative radial derivative. Then it holds that

$$G(x) = (\Lambda_{Pot}U)(x) = \int_{\Omega_{\rho_1}} K_{\Lambda_{Pot}}(x, y)U(y) d\omega_{\rho_1}(y), \quad x \in \Omega_r. \quad (4.3)$$

We have thus managed to establish a connection between the potential and its given negative first order radial derivatives in terms of the integral equation (4.3).

Evaluating Equation (4.2) on Ω_{ρ_1} , a straightforward calculation leads to the following result:

Lemma 4.4 *Let the operator $\Lambda_{AP} : \mathcal{L}^2(\Omega_{\rho_1}) \rightarrow \mathcal{L}^2(\Omega_r)$ be defined via*

$$(\Lambda_{AP}F)(x) = \int_{\Omega_{\rho_1}} K_{\Lambda_{AP}}(x, y)F(y) d\omega_{\rho_1}(y), \quad F \in \mathcal{L}^2(\Omega_{\rho_1}), \quad x \in \Omega_r,$$

where the kernel function is defined to be

$$K_{\Lambda_{AP}}(x, y) = \sum_{n=0}^{\infty} \sum_{k=1}^{2n+1} (\Lambda_{AP})^{\wedge}(n) Y_{n,k}^r(x) Y_{n,k}^{\rho_1}(y), \quad y \in \Omega_{\rho_1}$$

with symbol $\{(\Lambda_{AP})^{\wedge}(n)\}_{n=0,1,\dots}$ given by

$$(\Lambda_{AP})^{\wedge}(n) = \left(\frac{\rho_1}{r}\right)^n.$$

Let G_{ρ_1} , G_r denote the negative radial derivative of $U \in Pot(\Omega_{\rho_1}^{ext})$ on Ω_{ρ_1} and Ω_r , respectively. Then it holds that

$$rG_r(x) = (\Lambda_{AP}\rho_1 G_{\rho_1})(x) = \int_{\Omega_{\rho_1}} K_{\Lambda_{AP}}(x, y)\rho_1 G_{\rho_1}(y) d\omega_{\rho_1}, \quad x \in \Omega_r. \quad (4.4)$$

$K_{\Lambda_{AP}}$ is the so-called Abel-Poisson kernel function which is well known from potential theory. By means of Lemma 4.4 we have established the link between the negative radial derivative of a potential $U \in Pot(\Omega_{\rho_1}^{ext})$ on Ω_{ρ_1} and the corresponding values on Ω_r via the integral equation (4.4). Note that we actually connect rG_r and $\rho_1 G_{\rho_1}$, i.e. the negative first order radial derivative times the radius of the sphere where it is taken, since these are harmonic functions.

Now, we direct our attention to the surface gradient field. Applying ∇^* to Equation (4.1) it follows that

$$\begin{aligned} \nabla_{\xi}^* U(x) = \nabla_{\xi}^* U(r\xi) &= \sum_{n=0}^{\infty} \sum_{k=1}^{2n+1} U_{\rho_1}^{\wedge}(n, k) \left(\frac{\rho_1}{r}\right)^n \frac{1}{r} \nabla_{\xi}^* Y_{n,k}(\xi) \\ &= \sum_{n=0}^{\infty} \sum_{k=1}^{2n+1} U_{\rho_1}^{\wedge}(n, k) \left(\frac{\rho_1}{r}\right)^n \frac{1}{r} \sqrt{n(n+1)} y_{n,k}^{(2)}(\xi), \end{aligned} \quad (4.5)$$

where we have utilized the definition of the vector spherical harmonics in Section 1.3. Evaluating this on the surface Ω_{ρ_1} we end up with

$$\begin{aligned} (\nabla^*U)(\rho_1\xi) &= \sum_{n=0}^{\infty} \sum_{k=1}^{2n+1} U_{\rho_1}^{\wedge}(n, k) \frac{1}{\rho_1} \sqrt{n(n+1)} y_{n,k}^{(2)}(\xi) \\ &= \sum_{n=0}^{\infty} \sum_{k=1}^{2n+1} U_{\rho_1}^{\wedge}(n, k) \sqrt{n(n+1)} y_{n,k}^{(2),\rho_1}(\xi). \end{aligned}$$

Remembering the orthogonality relations of the vector spherical harmonics, the last result helps us to find the integral operator wanted.

Lemma 4.5 *Let the operator $\lambda_{\nabla^*} : l_{(2)}^2(\Omega_{\rho_1}) \rightarrow \mathcal{L}^2(\Omega_r)$ be defined via*

$$(\lambda_{\nabla^*}f)(x) = \int_{\Omega_{\rho_1}} k_{\lambda_{\nabla^*}}(x, y) \cdot f(y) \, d\omega_{\rho_1}(y), \quad f \in l_{(2)}^2(\Omega_{\rho_1}), \quad x \in \Omega_r,$$

where the vectorial kernel function is given by

$$k_{\lambda_{\nabla^*}}(x, y) = \sum_{n=0_2}^{\infty} \sum_{k=1}^{2n+1} (\lambda_{\nabla^*})^{\wedge}(n) Y_{n,k}^r(x) y_{n,k}^{(2),\rho_1}(y), \quad y \in \Omega_{\rho_1},$$

with symbol $\{(\lambda_{\nabla^*})^{\wedge}(n)\}_{n=0_2, 0_2+1, \dots}$ defined via

$$(\lambda_{\nabla^*})^{\wedge}(n) = \left(\frac{\rho_1}{r}\right)^n \frac{n+1}{r} \frac{1}{\sqrt{n(n+1)}} = \left(\frac{\rho_1}{r}\right)^n \frac{1}{r} \sqrt{\frac{n+1}{n}}.$$

Let $U \in \text{Pot}(\Omega_{\rho_1}^{ext})$. Let G denote the negative first order radial derivative of U and, furthermore, let g be the surface gradient field of U on Ω_{ρ_1} . Then

$$G(x) = (\lambda_{\nabla^*}g)(x) = \int_{\Omega_{\rho_1}} k_{\lambda_{\nabla^*}}(x, y) \cdot g(y) \, d\omega_{\rho_1}, \quad x \in \Omega_r. \quad (4.6)$$

Integral equation (4.6) links the surface gradient field of the potential U on Ω_{ρ_1} to the values of the negative first order radial derivative on Ω_r .

In fact, the integral equations (4.3), (4.4) and (4.6) define the so-called direct problems or, in other words, they actually show which operator must be applied to the quantities on Ω_{ρ_1} in order to obtain the negative radial derivative of U on some sphere Ω_r . As a matter of fact, when dealing with Lemma 4.2 we have already pointed out that the real problem is just the other way round, i.e. we want to calculate the above mentioned quantities on Ω_{ρ_1} from the radial derivative data on Ω_r . Consequently, we have to solve the integral equations for the sought for quantities on Ω_{ρ_1} (in our case the geomagnetic potential or, which is even more important, the radial as well as the horizontal part of the geomagnetic field vector). These inverse problems and their solution by means of regularization wavelets will be dealt with in Section 4.1.3. As regards this subject, the following theorem will supply some useful information concerning the operators under consideration.

Theorem 4.6 *Let the operators*

$$\begin{aligned}\Lambda_{Pot} &: \mathcal{L}^2(\Omega_{\rho_1}) \rightarrow \mathcal{L}^2(\Omega_r), \\ \Lambda_{AP} &: \mathcal{L}^2(\Omega_{\rho_1}) \rightarrow \mathcal{L}^2(\Omega_r), \\ \lambda_{\nabla^*} &: l_{(2)}^2(\Omega_{\rho_1}) \rightarrow \mathcal{L}^2(\Omega_r)\end{aligned}$$

be defined as in Lemmata 4.3, 4.4 and 4.5, respectively. Then Λ_{Pot} , Λ_{AP} and λ_{∇^*} are compact operators with infinite dimensional range. The corresponding adjoint operators

$$\begin{aligned}\Lambda_{Pot}^* &: \mathcal{L}^2(\Omega_r) \rightarrow \mathcal{L}^2(\Omega_{\rho_1}), \\ \Lambda_{AP}^* &: \mathcal{L}^2(\Omega_r) \rightarrow \mathcal{L}^2(\Omega_{\rho_1}), \\ \lambda_{\nabla^*}^* &: \mathcal{L}^2(\Omega_r) \rightarrow l_{(2)}^2(\Omega_{\rho_1})\end{aligned}$$

are given by

$$\begin{aligned}(\Lambda_{Pot}^* G_r) &= \int_{\Omega_r} K_{\Lambda_{Pot}}(x, \cdot) G_r(x) d\omega_r(x), \quad G_r \in \mathcal{L}^2(\Omega_r), \\ (\Lambda_{AP}^* G_r) &= \int_{\Omega_r} K_{\Lambda_{AP}}(x, \cdot) G_r(x) d\omega_r(x), \quad G_r \in \mathcal{L}^2(\Omega_r), \\ (\lambda_{\nabla^*}^* G_r) &= \int_{\Omega_r} k_{\lambda_{\nabla^*}}(x, \cdot) G_r(x) d\omega_r(x), \quad G_r \in \mathcal{L}^2(\Omega_r).\end{aligned}$$

Furthermore, for the singular systems $\mathcal{S}_{\Lambda_{Pot}}$, $\mathcal{S}_{\Lambda_{AP}}$ and $\mathcal{S}_{\lambda_{\nabla^*}}$ it holds that

$$\begin{aligned}\mathcal{S}_{\Lambda_{Pot}} &= \{(\Lambda_{Pot})^\wedge(n), Y_{n,k}^{\rho_1}, Y_{n,k}^r\}_{(n,k) \in \mathcal{N}}, \\ \mathcal{S}_{\Lambda_{AP}} &= \{(\Lambda_{AP})^\wedge(n), Y_{n,k}^{\rho_1}, Y_{n,k}^r\}_{(n,k) \in \mathcal{N}}, \\ \mathcal{S}_{\lambda_{\nabla^*}} &= \{(\lambda_{\nabla^*})^\wedge(n), y_{n,k}^{(2), \rho_1}, Y_{n,k}^r\}_{(n,k) \in \mathcal{N}^{(2)}}.\end{aligned}$$

Proof. We start with the compactness of the operators. Obviously it is true that $K_{\Lambda_{Pot}}(\cdot, \cdot)$, $K_{\Lambda_{AP}}(\cdot, \cdot) \in \mathcal{C}(\Omega_r) \times \mathcal{C}(\Omega_{\rho_1})$, and $k_{\lambda_{\nabla^*}}(\cdot, \cdot) \in c(\Omega_r) \times \mathcal{C}(\Omega_{\rho_1})$. Consequently, Λ_{Pot} , Λ_{AP} and λ_{∇^*} are compact with infinite dimensional range (cf. [78, 98]).

In order to obtain the representations of the adjoint operators we need to show that, for $F \in \mathcal{L}^2(\Omega_{\rho_1})$, $G \in \mathcal{L}^2(\Omega_r)$ and $f \in l_{(2)}^2(\Omega_{\rho_1})$, it holds that

$$\begin{aligned}(\Lambda_{Pot} F, G)_{\mathcal{L}^2(\Omega_r)} &= (F, \Lambda_{Pot}^* G)_{\mathcal{L}^2(\Omega_{\rho_1})}, \\ (\Lambda_{AP} F, G)_{\mathcal{L}^2(\Omega_r)} &= (F, \Lambda_{AP}^* G)_{\mathcal{L}^2(\Omega_{\rho_1})}, \\ (\lambda_{\nabla^*} f, G)_{\mathcal{L}^2(\Omega_r)} &= (f, \lambda_{\nabla^*}^* G)_{l_{(2)}^2(\Omega_{\rho_1})},\end{aligned}$$

which is a straightforward calculation using Fubini's theorem.

Let us now turn to the singular systems. It suffices to show that

$$\Lambda_{Pot} Y_{n,k}^{\rho_1} = (\Lambda_{Pot})^\wedge (n) Y_{n,k}^r, \quad (4.7)$$

$$\Lambda_{Pot}^* Y_{n,k}^r = (\Lambda_{Pot})^\wedge (n) Y_{n,k}^{\rho_1}, \quad (4.8)$$

in the case of $\mathcal{S}_{\Lambda_{Pot}}$ and

$$\Lambda_{AP} Y_{n,k}^{\rho_1} = (\Lambda_{AP})^\wedge (n) Y_{n,k}^r, \quad (4.9)$$

$$\Lambda_{AP}^* Y_{n,k}^r = (\Lambda_{AP})^\wedge (n) Y_{n,k}^{\rho_1}, \quad (4.10)$$

for $\mathcal{S}_{\Lambda_{AP}}$. As regards $\mathcal{S}_{\lambda_{\nabla^*}}$ we need to show that

$$\lambda_{\nabla^*} y_{n,k}^{(2),\rho_1} = (\lambda_{\nabla^*})^\wedge (n) Y_{n,k}^r, \quad (4.11)$$

$$\lambda_{\nabla^*}^* Y_{n,k}^r = (\lambda_{\nabla^*})^\wedge (n) y_{n,k}^{(2),\rho_1}, \quad (4.12)$$

hold true. Equations (4.7), (4.8), (4.9) (4.10) and (4.12) follow directly from the orthonormality of the spherical harmonics, while Equation (4.11) is a direct consequence of the orthonormality of the vector spherical harmonics. ■

Remark 4.7 *It is clear that from a theoretical point of view it suffices to know Lemma 4.3, since it presents the integral equation the solution of which, i.e. the potential, contains all the necessary information to calculate the gradient field. Nevertheless, this usually involves numerical differentiation which is disadvantageous with respect to errors of any nature. If the potential is subject to any errors, however, numerical differentiation will amplify their effects. By means of Lemmata 4.4 and 4.5 the differentiation has been transferred to the kernel functions which can be handled in a numerically stable framework (see also Remark 4.11). This means that in our approach we have a one-step regularization while, otherwise, differentiation would demand for a second regularization process, too.*

4.1.2 Integral Equations for the Surface Gradient

This section deals with the background for the case of a given surface gradient field. Like in Section 4.1.1 we establish relationships in terms of integral equations which will help us to calculate the geomagnetic field vector on Ω_{ρ_1} from surface gradient data on Ω_r . We begin with the connection of the potential and the surface gradient. From equations (4.1) and (4.5) it can easily be obtained that the following lemma is valid.

Lemma 4.8 *Let the operator $\lambda_{Pot} : \mathcal{L}^2(\Omega_{\rho_1}) \rightarrow l_{(2)}^2(\Omega_r)$ be defined via*

$$(\lambda_{Pot} F)(x) = \int_{\Omega_{\rho_1}} k_{\lambda_{Pot}}(x, y) F(y) d\omega_{\rho_1}(y), \quad F \in \mathcal{L}^2(\Omega_{\rho_1}), \quad x \in \Omega_r,$$

where the vectorial kernel $k_{\lambda_{Pot}}$ is defined by

$$k_{\lambda_{Pot}}(x, y) = \sum_{n=0_2}^{\infty} \sum_{k=1}^{2n+1} (\lambda_{Pot})^\wedge (n) y_{n,k}^{(2),r}(x) Y_{n,k}^{\rho_1}(y), \quad x \in \Omega_r, \quad y \in \Omega_{\rho_1},$$

with symbol $\{(\lambda_{Pot})^\wedge(n)\}_{n=0_2,0_2+1,\dots}$ being given by

$$(\lambda_{Pot})^\wedge(n) = \left(\frac{\rho_1}{r}\right)^n \sqrt{n(n+1)}.$$

Let $U \in Pot(\Omega_{\rho_1}^{ext})$ and let g be the corresponding surface gradient field on Ω_r . Then it holds that

$$g(x) = (\lambda_{Pot}U)(x) = \int_{\Omega_{\rho_1}} k_{\lambda_{Pot}}(x, y)U(y) d\omega_{\rho_1}(y), \quad x \in \Omega_r. \quad (4.13)$$

It is also possible to find an integral operator that connects the surface gradient field on some height r with the negative radial derivative of the corresponding potential on ρ_1 . This is closely related to Lemma 4.5 and can be derived using equations (4.2) and (4.5).

Lemma 4.9 *Let the operator $\lambda_{\partial r} : \mathcal{L}^2(\Omega_{\rho_1}) \rightarrow l_{(2)}^2(\Omega_r)$ be defined via*

$$(\lambda_{\partial r}F)(x) = \int_{\Omega_{\rho_1}} k_{\lambda_{\partial r}}(x, y)F(y) d\omega_{\rho_1}(y), \quad F \in \mathcal{L}^2(\Omega_{\rho_1}) \quad x \in \Omega_r,$$

with the kernel function $k_{\lambda_{\partial r}}$ defined by

$$k_{\lambda_{\partial r}}(x, y) = \sum_{n=0_2}^{\infty} \sum_{k=1}^{2n+1} (\lambda_{\partial r})^\wedge(n) y_{n,k}^{(2),r}(x) Y_{n,k}^{\rho_1}(y), \quad x \in \Omega_r, \quad y \in \Omega_{\rho_1},$$

where the symbol $\{(\lambda_{\partial r})^\wedge(n)\}_{n=0_2,0_2+1,\dots}$ is given via

$$(\lambda_{\partial r})^\wedge(n) = \left(\frac{\rho_1}{r}\right)^n \frac{\rho_1}{n+1} \sqrt{n(n+1)} = \left(\frac{\rho_1}{r}\right)^n \rho_1 \sqrt{\frac{n}{n+1}}.$$

Let $U \in Pot(\Omega_{\rho_1}^{ext})$ and let G be the negative radial derivative on Ω_{ρ_1} . Furthermore, g is supposed to be the corresponding surface gradient field on Ω_r . Then

$$g(x) = (\lambda_{\partial r}G)(x) = \int_{\Omega_{\rho_1}} k_{\lambda_{\partial r}}(x, y)G(y) d\omega_{\rho_1}(y), \quad x \in \Omega_r.$$

What remains is to establish a link between the surface gradient field on Ω_{ρ_1} and on Ω_r . However, this is not in the scope of this thesis since operators in terms of tensor kernels are necessary (see [88] for more details concerning this subject). Nevertheless, it is well known (e.g. [1]) that, for $U \in Pot(\Omega_{\rho_1}^{ext})$, $\nabla^*U \cdot \varepsilon^\vartheta$ and $\nabla^*U \cdot \varepsilon^\varphi$ (i.e. the geomagnetic north and east component) are harmonic functions. Consequently we can use the Abel-Poisson kernel for connecting any of these two quantities on Ω_{ρ_1} with its values on Ω_r .

Lemma 4.10 *Let $U \in Pot(\Omega_{\rho_1}^{ext})$. Let G_{ρ_1} and G_r denote either $\nabla^*U \cdot \varepsilon^\vartheta$ or $\nabla^*U \cdot \varepsilon^\varphi$ on Ω_{ρ_1} and Ω_r , respectively. Then it holds that*

$$rG_r(x) = (\Lambda_{AP\rho_1}G_{\rho_1})(x) = \int_{\Omega_{\rho_1}} K_{\Lambda_{AP}}(x, y)\rho_1 G_{\rho_1}(y) d\omega_{\rho_1}, \quad x \in \Omega_r. \quad (4.14)$$

Remark 4.11 *One might argue that the idea of Lemma 4.10 is unfortunate since one cannot use the information of the whole surface gradient field at once which might lead to a loss of redundancy from a numerical point of view (not from a mathematical point of view, though). In fact, solving integral equation (4.13) of Lemma 4.8, i.e. calculation of the potential, makes use of the whole information available. Numerical differentiation of the potential (i.e. calculating the surface gradient field) would then lead to the desired quantities. Nevertheless, in Remark 4.7 we have already mentioned that this is disadvantageous because differentiation amplifies possible errors, a fact that led us to the introduction of several integral operators that help circumvent this problem by transferring the differentiation to the corresponding integral kernels. Despite the fact that this is not possible here, we can give an alternative using the potential. If we suppose that we have numerically calculated the potential U we can derive an approximation of ∇^*U using*

$$\nabla_{\xi}^*U(r\xi) \simeq \int_{\Omega_{\rho_1}} U(\rho_1\eta) \nabla_{\xi}^*K_j(r\xi, \rho_1\eta) d\omega_{\rho_1}(\eta),$$

where the bandlimited kernel $K_j : \Omega_r \times \Omega_{\rho_1} \rightarrow \mathbb{R}$ is a product kernel of the form

$$K_j(r\xi, \rho_1\eta) = \sum_{n=0}^{N_j} \sum_{k=1}^{2n+1} K^{\wedge}(n) \frac{1}{r} Y_{n,k}(\xi) \frac{1}{\rho_1} Y_{n,k}(\eta),$$

and the symbol can be chosen as in the cases of the bandlimited scaling functions in Section 2.1. On the one hand, our results of Chapter 2 tell us that we can approximate ∇^*U in ε -accuracy (note that U is bandlimited for it has been numerically calculated) by choosing an appropriately high j and by noting that the integral can be calculated precisely using appropriate integration formulas (see e.g. [20]). On the other hand it can be shown that

$$\nabla_{\xi}^*K_j(r\xi, \rho_1\eta) = (\eta - (\xi \cdot \eta)\xi) \frac{1}{r\rho_1} \sum_{n=0}^{N_j} \frac{2n+1}{4\pi} K^{\wedge}(n) P'_n(\xi \cdot \eta),$$

which can be easily calculated by means of the numerically stable Clenshaw algorithm (for more details on this subject see e.g. [81, 51] and the references therein). Actually, we will come back to this subject at the end of Section 4.1.3 where we will be able to incorporate these considerations in the framework of the regularization wavelets.

Last but not least we will now characterize the integral operators of this section in analogy to Theorem 4.6.

Theorem 4.12 *Let the operators*

$$\begin{aligned} \lambda_{Pot} & : \mathcal{L}^2(\Omega_{\rho_1}) \rightarrow l_{(2)}^2(\Omega_r) \\ \lambda_{\partial r} & : \mathcal{L}^2(\Omega_{\rho_1}) \rightarrow l_{(2)}^2(\Omega_r) \end{aligned}$$

be defined as in Lemmata 4.8 and 4.9, respectively. Then λ_{Pot} and $\lambda_{\partial r}$ are compact operators with infinite dimensional range. The corresponding adjoint operators

$$\begin{aligned} \lambda_{Pot}^* & : l_{(2)}^2(\Omega_r) \rightarrow \mathcal{L}^2(\Omega_{\rho_1}) \\ \lambda_{\partial r}^* & : l_{(2)}^2(\Omega_r) \rightarrow \mathcal{L}^2(\Omega_{\rho_1}) \end{aligned}$$

are given by

$$\begin{aligned} (\lambda_{Pot}^* g_r) &= \int_{\Omega_r} k_{\lambda_{Pot}}(x, \cdot) \cdot g_r(x) d\omega_r(x), \quad g_r \in l_{(2)}^2(\Omega_r), \\ (\lambda_{\partial r}^* g_r) &= \int_{\Omega_r} k_{\lambda_{\partial r}}(x, \cdot) \cdot g_r(x) d\omega_r(x), \quad g_r \in l_{(2)}^2(\Omega_r). \end{aligned}$$

Furthermore, for the singular systems $\mathcal{S}_{\lambda_{Pot}}$ and $\mathcal{S}_{\lambda_{\partial r}}$ it holds that

$$\begin{aligned} \mathcal{S}_{\lambda_{Pot}} &= \left\{ (\lambda_{Pot})^\wedge(n), Y_{n,k}^{\rho_1}, y_{n,k}^{(2),r} \right\}_{(n,k) \in \mathcal{N}^{(2)}}, \\ \mathcal{S}_{\lambda_{\partial r}} &= \left\{ (\lambda_{\partial r})^\wedge(n), Y_{n,k}^{\rho_1}, y_{n,k}^{(2),r} \right\}_{(n,k) \in \mathcal{N}^{(2)}}. \end{aligned}$$

Proof. The proof is analogous to the proof of Theorem 4.6. ■

4.1.3 The Inverse Problems and Spherical Regularization Wavelets

In the last sections we have formulated several integral equations connecting functions on Ω_{ρ_1} with functions on Ω_r . In the scope of application of the spherical approximation, the quantities on Ω_r correspond to the actual observables (i.e. the satellite measurements) while those on Ω_{ρ_1} are to be calculated from the former ones (inverse problem). In what follows we want to treat this subject in a unified functionalanalytic framework. Formally, all the integral equations under consideration are of the form

$$AH = K, \quad H \in \mathcal{H}, \quad K \in \mathcal{K},$$

where $A : \mathcal{H} \rightarrow \mathcal{K}$ is a compact operator and \mathcal{H} and \mathcal{K} are separable Hilbert spaces of square-integrable (scalar or vectorial) functions. Table 4.1 summarizes all the information derived in Sections 4.1.1 and 4.1.2: A denotes the operator under consideration, \mathcal{H} and \mathcal{K} are the corresponding Hilbert spaces. $\{\sigma_n, H_{n,k}, K_{n,k}\}$ is the singular system of the operator A . It should be remarked that $\{H_{n,k}\}$ forms a complete orthonormal system in \mathcal{H} , while $\{K_{n,k}\}$ forms a complete orthonormal system in \mathcal{K} (see e.g. ([22, 23, 78]) and the introduction in Chapter 1).

Remembering Hadamard's definition of a well-posed problem, i.e. existence, uniqueness and continuity of the inverse, we realize that the problem of calculating

$$H = A^+ K \tag{4.15}$$

is ill-posed since it violates the first and the third property. The singular system of A indicates the type of ill-posedness, which can be seen from the form of the generalized solution of (4.15), i.e. the Moore-Penrose inverse which in the nomenclature of this chapter reads:

$$A^{-1}K = \sum_{(n,k) \in \mathcal{N}} \sigma_n^{-1}(K, K_{n,k})_{\mathcal{K}} H_{n,k}. \tag{4.16}$$

on Ω_{ρ_1}	on Ω_r	A	\mathcal{H}	\mathcal{K}	$H_{n,k}$	$K_{n,k}$	σ_n
U	$\frac{\partial}{\partial r}U$	Λ_{Pot}	$\mathcal{L}^2(\Omega_{\rho_1})$	$\mathcal{L}^2(\Omega_r)$	$Y_{n,k}^{\rho_1}$	$Y_{n,k}^r$	$\left(\frac{\rho_1}{r}\right)^n \frac{n+1}{r}$
$\frac{\partial}{\partial r}U$	$\frac{\partial}{\partial r}U$	Λ_{AP}	$\mathcal{L}^2(\Omega_{\rho_1})$	$\mathcal{L}^2(\Omega_r)$	$Y_{n,k}^{\rho_1}$	$Y_{n,k}^r$	$\left(\frac{\rho_1}{r}\right)^n$
∇^*U	$\frac{\partial}{\partial r}U$	λ_{∇^*}	$l_{(2)}^2(\Omega_{\rho_1})$	$\mathcal{L}^2(\Omega_r)$	$y_{n,k}^{(2),\rho_1}$	$Y_{n,k}^r$	$\left(\frac{\rho_1}{r}\right)^n \frac{1}{r} \sqrt{\frac{n+1}{n}}$
U	∇^*U	λ_{Pot}	$\mathcal{L}^2(\Omega_{\rho_1})$	$l_{(2)}^2(\Omega_r)$	$Y_{n,k}^{\rho_1}$	$y_{n,k}^{(2),r}$	$\left(\frac{\rho_1}{r}\right)^n \sqrt{n(n+1)}$
$\frac{\partial}{\partial r}U$	∇^*U	$\lambda_{\partial r}$	$\mathcal{L}^2(\Omega_{\rho_1})$	$l_{(2)}^2(\Omega_r)$	$Y_{n,k}^{\rho_1}$	$y_{n,k}^{(2),r}$	$\left(\frac{\rho_1}{r}\right)^n \rho_1 \sqrt{\frac{n}{n+1}}$
$\nabla^*U \cdot \varepsilon^\vartheta$	$\nabla^*U \cdot \varepsilon^\vartheta$	Λ_{AP}	$\mathcal{L}^2(\Omega_{\rho_1})$	$\mathcal{L}^2(\Omega_r)$	$Y_{n,k}^{\rho_1}$	$Y_{n,k}^r$	$\left(\frac{\rho_1}{r}\right)^n$
$\nabla^*U \cdot \varepsilon^\varphi$	$\nabla^*U \cdot \varepsilon^\varphi$	Λ_{AP}	$\mathcal{L}^2(\Omega_{\rho_1})$	$\mathcal{L}^2(\Omega_r)$	$Y_{n,k}^{\rho_1}$	$Y_{n,k}^r$	$\left(\frac{\rho_1}{r}\right)^n$

Table 4.1: Functionalanalytic framework

For arbitrary functions $K \in \mathcal{K}$ (note that we need to assume observational errors or noise in any practical application) the right hand side of (4.16) is not necessarily convergent and in order to force convergence we have to replace the series (4.16) by a filtered version of this singular value expansion. In Chapter 1 we have introduced the necessary definitions and results from a general point of view.

The idea we are going to discuss now is to realize the regularization procedure by a multi-resolution analysis in terms of certain wavelets. This will enable us to obtain a $(j+1)$ -level regularization from a j -level regularization by just adding the corresponding detail information. Since the wavelet coefficients contain (more or less) regional information, our approach realizes a space dependent regularization procedure. It should be noted that any classical regularization technique based on filtering the singular value expansion can be reformulated in terms of our approach. Thus any parameter choice strategy depending on the respective filtering method is also applicable here. Consequently we omit this discussion here (cf. [50] for more details).

Basic tools for our treatment are the decomposition and reconstruction regularization scaling functions and wavelets (cf. [32] and the references therein).

Definition 4.13 *Let $\{\sigma_n, H_{n,k}, K_{n,k}\}$ be the singular system of a compact operator A as given in Table 4.1. Then the corresponding decomposition regularization scaling function at scale $j \in \mathbb{Z}$, $\{\Phi_j^d\}$, is given by*

$$\Phi_j^d(y, \cdot) = \sum_{(n,k) \in \mathcal{N}} (\Phi_j)^\wedge(n) H_{n,k}(y) K_{n,k}(\cdot), \quad y \in \Omega_{\rho_1}.$$

The associated reconstruction regularization scaling function at scale $j \in \mathbb{Z}$, $\{\Phi_j^r\}$, is given

by

$$\Phi_j^r(y, \cdot) = \sum_{(n,k) \in \mathcal{N}} (\Phi_j)^\wedge(n) H_{n,k}(y) H_{n,k}(\cdot), \quad y \in \Omega_{\rho_1}.$$

(Note that the reconstruction regularization scaling function is just a certain realization of the scaling functions in Chapter 2.) In terms of the choices of filters presented in Chapter 1, i.e. truncated singular value decomposition (TSVD), smoothed truncated singular value decomposition (STSVd) and Tikhonov filter (TF), we are led to three possible choices of the generating symbols $\{(\Phi_j)^\wedge(n)\}$:

(i) TSVD

$$(\Phi_j)^\wedge(n) = \begin{cases} \sigma_n^{-1/2} & , \quad n = 0, \dots, N_j \\ 0 & , \quad n \geq N_j + 1 \end{cases},$$

with

$$N_j = \begin{cases} 0 & \text{for } j \in \mathbb{Z}, j < 0 \\ 2^j - 1 & \text{for } j \in \mathbb{Z}, j \geq 0 \end{cases}.$$

(ii) STSVd

$$(\Phi_j)^\wedge(n) = \begin{cases} \sigma_n^{-1/2} & , \quad n = 0, \dots, M_j \\ \sigma_n^{-1/2} (\tau_j(n))^{1/2} & , \quad n = M_j + 1, \dots, N_j \\ 0 & , \quad n \geq N_j + 1 \end{cases},$$

with

$$N_j = \begin{cases} 0 & \text{for } j \in \mathbb{Z}, j < 0 \\ 2^{j+1} - 1 & \text{for } j \in \mathbb{Z}, j \geq 0 \end{cases}$$

and

$$M_j = \begin{cases} 0 & \text{for } j \in \mathbb{Z}, j < 0 \\ 2^j - 1 & \text{for } j \in \mathbb{Z}, j \geq 0 \end{cases}.$$

τ_j is given by $\tau_j(t) = 2 - 2^{-j}(t + 1)$, $t \in [2^j - 1, 2^{j+1} - 1]$, $j \in \mathbb{N}_0$.

(iii) TF

$$\Phi_j^\wedge(n) = \left(\frac{\sigma_n}{\sigma_n^2 + \gamma_j^2} \right)^{1/2}, \quad n \in \mathbb{N}_0, \quad j \in \mathbb{Z},$$

with $\{\gamma_j\}$, $j \in \mathbb{Z}$, being a sequence of real numbers satisfying $\lim_{j \rightarrow \infty} \gamma_j = 0$ and $\lim_{j \rightarrow -\infty} \gamma_j = \infty$.

The reconstruction and decomposition regularization wavelets are again defined via a scaling equation.

Definition 4.14 *Let $\{(\Phi_j)^\wedge(n)\}$ be the generating symbol of a reconstruction and a decomposition regularization scaling function. Then the associated decomposition regularization wavelet at scale $j \in \mathbb{Z}$, $\{\Psi_j^d\}$, is given by*

$$\Psi_j^d(y, \cdot) = \sum_{(n,k) \in \mathcal{N}} (\Psi_j)^\wedge(n) H_{n,k}(y) K_{n,k}(\cdot), \quad y \in \Omega_{\rho_1}.$$

The associated reconstruction regularization wavelet at scale $j \in \mathbb{Z}$, $\{\Psi_j^r\}$, is given by

$$\Psi_j^r(y, \cdot) = \sum_{(n,k) \in \mathcal{N}} (\Psi_j)^\wedge(n) H_{n,k}(y) H_{n,k}(\cdot), \quad y \in \Omega_{\rho_1}.$$

The generating symbol of the regularization wavelets, $\{(\Psi_j)^\wedge(n)\}$, is defined via the refinement equation

$$((\Psi_j)^\wedge(n))^2 = ((\Phi_{j+1})^\wedge(n))^2 - ((\Phi_j)^\wedge(n))^2.$$

Consequently, for the aforementioned filters, we get the following generating symbols for the wavelets:

(i) TSVD

$$(\Psi_j)^\wedge(n) = \begin{cases} 0 & , \quad n = 0, \dots, N_j \\ \sigma_n^{-1/2} & , \quad n = N_j + 1, \dots, N_{j+1} \\ 0 & , \quad n \geq N_{j+1} + 1 \end{cases}$$

(ii) STSVD

$$(\Psi_j)^\wedge(n) = \begin{cases} 0 & , \quad n = 0, \dots, M_j \\ \sigma_n^{-1/2} (1 - \tau_j(n))^{1/2} & , \quad n = M_j + 1, \dots, M_{j+1} \\ \sigma_n^{-1/2} (\tau_{j+1}(n) - \tau_j(n))^{1/2} & , \quad n = M_{j+1} + 1, \dots, N_j \\ \sigma_n^{-1/2} (\tau_{j+1}(n))^{1/2} & , \quad n = N_j + 1, \dots, N_{j+1} \\ 0 & , \quad n \geq N_{j+1} + 1 \end{cases}$$

(iii) TF

$$(\Psi_j)^\wedge(n) = \left(\frac{\sigma_n}{\sigma_n^2 + \gamma_{j+1}^2} - \frac{\sigma_n}{\sigma_n^2 + \gamma_j^2} \right),$$

where N_j , M_j , τ_j and γ_j have been previously defined.

Obviously, the generating symbols $\{(\Phi_j)^\wedge(n)\}$ of the regularization scaling functions are constructed such that $\lim_{j \rightarrow \infty} (\Phi_j)^\wedge(n) = \sigma_n^{-1}$. Due to the refinement equation for the regularization wavelets we can carry over our results from Chapter 2 and formulate the following theorem:

Theorem 4.15 *Let $A : \mathcal{H} \rightarrow \mathcal{K}$ be defined as in Table 4.1. Let $\{\Phi_j^d\}$ and $\{\Phi_j^r\}$ be the corresponding decomposition and reconstruction regularization scaling functions. Suppose $\{\Psi_j^d\}$ and $\{\Psi_j^r\}$ to be the associated decomposition and reconstruction regularization wavelets. Then, for $A \in \{\Lambda_{Pot}, \Lambda_{AP}, \lambda_{Pot}, \lambda_{\partial r}\}$ the sequence $\{S_J\}$ of operators $S_J : \mathcal{K} \rightarrow \mathcal{H}$ given by*

$$S_J(K) = \Phi_J^r * (\Phi_J^d * K) = \Phi_0^r * (\Phi_0^d * K) + \sum_{j=0}^{J-1} \Psi_j^r * (\Psi_j^d * K), \quad K \in \mathcal{K}$$

is a regularization of A^+ , i.e.

$$\lim_{J \rightarrow \infty} S_J(K) = A^+K,$$

where the equality is understood in the \mathcal{H} -sense. For $A = \lambda_{\nabla^*}$ the sequence $\{s_J\}$ of operators $s_J : \mathcal{K} \rightarrow \mathcal{H}$ given by

$$s_J(K) = \Phi_J^r \star (\Phi_J^d * K) = \Phi_0^r \star (\Phi_0^d * K) + \sum_{j=0}^{J-1} \Psi_j^r \star (\Psi_j^d * K), \quad K \in \mathcal{K}$$

is a regularization of A^+ .

Theorem 4.15 forms the theoretical background for the multiscale solution of the aforementioned problems of downward continuation. In a first step, the convolutions of the decomposition kernels against the data function yield sets of scalar coefficients connecting the data at satellite altitude with the sought for quantity at e.g. the mean Earth surface. This can be seen from the construction of the decomposition kernels which are composed of the respective basis functions in \mathcal{H} (consisting of functions on e.g. the mean Earth surface) and \mathcal{K} (consisting of the functions on satellite altitude). From these sets of coefficients one can, in a second step, calculate the solution of the corresponding inverse problem in terms of the reconstruction kernels. It is clear that in practical applications the limit $J \rightarrow \infty$ cannot be performed and one has to choose some suitable J_{max} in order to get a good approximation of the solution. As we have already mentioned, any classical regularization technique for filtering the singular value expansion can be incorporated into our approach and consequently any parameter choice- or stop-strategy depending on the respective filtering method is also applicable here; this is why we omit this discussion here (for a detailed study of how to apply the so-called L-curve method in a multiscale framework the interested reader might consult [50]). In Section 4.1.4 we will show how our results can be used to calculate geomagnetic crustal field contributions at the mean Earth surface from a set of CHAMP FGM-data.

We conclude this section with some considerations useful for practical applications involving surface gradient field data. Up to now, we have presented two ways of calculating the surface gradient field on Ω_{ρ_1} from surface gradient field data on Ω_r , $\rho_1 < r$. The first method is to project the surface gradient field onto certain directions and then downward continue the respective projections using the (inverse) Abel-Poisson kernel (Lemma 4.10 in combination with Theorem 4.15). The second way is to take the detour via the potential (see Lemma 4.8) which can then be used to calculate an approximation of the surface gradient field in an additional step (as shown in Remark 4.11). Having the decomposition and reconstruction regularization scaling functions and wavelets at hand, we can modify the second method such that it is not necessary to determine the potential anymore and an approximation of the surface gradient field on Ω_{ρ_1} is available at once: Let g_r be the surface gradient field on Ω_r corresponding to a potential U . Furthermore, for the time being, let $\{\bar{\Phi}_j^d\}$, $\{\bar{\Phi}_j^r\}$, $\{\bar{\Psi}_j^d\}$ and $\{\bar{\Psi}_j^r\}$ be the regularization kernels corresponding to the operator λ_{Pot} . From our considerations so far we know that, for suitably chosen J_{max} ,

$$U_{J_{max}} = \bar{\Phi}_0^r * (\bar{\Phi}_0^d * g_r) + \sum_{j=0}^{J_{max}-1} \bar{\Psi}_j^r * (\bar{\Psi}_j^d * g_r), \quad (4.17)$$

is a good approximation of U on Ω_{ρ_1} , i.e. $U_{J_{max}} \simeq U$. Presenting (4.17) more explicitly we have, with $\xi \in \Omega, y \in \Omega_{\rho_1}$,

$$U_{J_{max}}(\rho_1\xi) = \int_{\Omega_{\rho_1}} \bar{\Phi}_0^r(\rho_1\xi, y) ST_0(g_r)(y) d\omega_{\rho_1}(y) + \quad (4.18)$$

$$+ \sum_{j=0}^{J_{max}-1} \int_{\Omega_{\rho_1}} \bar{\Psi}_0^r(\rho_1\xi, y) WT_j(g_r)(y) d\omega_{\rho_1}(y), \quad (4.19)$$

where we have used the abbreviations

$$ST_0(g_r)(y) = (\bar{\Phi}_0^d * g_r)(y)$$

and

$$WT_j(g_r)(y) = (\bar{\Psi}_j^d * g_r)(y).$$

Applying the surface gradient to (4.18-4.19) we get

$$\nabla_{\xi}^* U_{J_{max}}(\rho_1\xi) = \int_{\Omega_{\rho_1}} \nabla_{\xi}^* \bar{\Phi}_0^r(\rho_1\xi, y) ST_0(g_r)(y) d\omega_{\rho_1}(y) + \quad (4.20)$$

$$+ \sum_{j=0}^{J_{max}-1} \int_{\Omega_{\rho_1}} \nabla_{\xi}^* \bar{\Psi}_0^r(\rho_1\xi, y) WT_j(g_r)(y) d\omega_{\rho_1}(y), \quad (4.21)$$

i.e. the differentiation is, once again, transferred to the kernel functions. Introducing the abbreviations $\check{\Phi}_0^r(\rho_1\xi, \cdot) = \nabla_{\xi}^* \bar{\Phi}_0^r(\rho_1\xi, \cdot)$ as well as $\check{\Psi}_j^r(\rho_1\xi, \cdot) = \nabla_{\xi}^* \bar{\Psi}_j^r(\rho_1\xi, \cdot)$ for the now vectorial kernels and utilizing the \star -convolution for spherical vectorial kernels (see (2.43)), Equation (4.20-4.21) is equivalent to

$$\nabla^* U_{J_{max}} = \check{\Phi}_0^r \star (\bar{\Phi}_0^d * g_r) + \sum_{j=0}^{J_{max}-1} \check{\Psi}_j^r \star (\bar{\Psi}_j^d * g_r).$$

Summarizing these considerations we end up with the following corollary:

Corollary 4.16 *Let g_r be a surface gradient field on Ω_r . Under the foregoing assumptions, an approximation of the corresponding surface gradient field on Ω_{ρ_1} can be calculated via*

$$\check{\Phi}_0^r \star (\bar{\Phi}_0^d * g_r) + \sum_{j=0}^{J_{max}-1} \check{\Psi}_j^r \star (\bar{\Psi}_j^d * g_r).$$

Finally it should be noted that the kernels $\check{\Phi}_0^r$ and $\check{\Psi}_j^r$ can easily be obtained from $\bar{\Phi}_0^r$ and $\bar{\Psi}_j^r$ by using the information of Table 4.1 and the definition of vector spherical harmonics of type 2 (i.e. $y_{n,k}^{(2)}$, see Chapter 1); more explicitly we arrive at

$$\check{\Phi}_0^r(\cdot, \cdot) = \sum_{(n,k) \in \mathcal{N}^{(2)}} (\Phi_0)^{\wedge}(n) \sqrt{n(n+1)} y_{n,k}^{(2), \rho_1}(\cdot) Y_{n,k}^{\rho_1}(\cdot),$$

and

$$\check{\Psi}_j^r(\cdot, \cdot) = \sum_{(n,k) \in \mathcal{N}^{(2)}} (\Psi_j)^\wedge(n) \sqrt{n(n+1)} y_{n,k}^{(2), \rho_1}(\cdot) Y_{n,k}^{\rho_1}(\cdot).$$

Remark 4.17 *All our considerations of Sections 4.1.1, 4.1.2 as well as 4.1.3 include the evaluation of spherical integrals. It is clear that in every practical application involving discrete satellite measurements these integrals have to be suitably discretized. As we have already mentioned, there are numerous ways to do so and we will not go into detail here.*

4.1.4 Example

In this section we apply the previously presented multiscale approach in spherical approximation to a set of CHAMP vector magnetic FGM data (namely the vertical component) and derive a wavelet representation of the crustal geomagnetic field at mean Earth radius (see also our results in [35]; in [71, 105] details can be found concerning numerical realizations and numerous tests with synthetic data).

CHAMP vector magnetic data spanning September 2001 are used. The data selection follows the common criteria for main and crustal field mapping (see e.g. [58] for a detailed review or [83, 93] for recent studies). From the September 2001 measurements we use night data (local time between 20:00 LT and 04:00 LT) with global index of geomagnetic activity $Kp \leq 2o$. Main field, including secular variations, external field and ring current contributions are subtracted using a model given by the gradient field of a harmonic potential U as presented in Appendix A. In this example we set $\rho_1 = 6371.2$ km to be the mean radius of the Earth. Gauss coefficients (g_n^m, h_n^m) and (q_n^m, s_n^m) as well as secular variation coefficients $(\dot{g}_n^m, \dot{h}_n^m)$ (around $t_0 = 2000$) are taken from the model Ørsted-10b-01 (see [92, 93]) and the one hourly Dst index can be downloaded from the World Data Center for Geomagnetism, Kyoto, (<http://swdcdb.kugi.kyoto-u.ac.jp>). The induced parts are considered to contribute with a factor $Q_1 = 0.27$, a value found by [74].

As experienced before (cf. [83]), there are still contributions of large spatial scale in the residual field which may be due to external as well as internal sources. We extract these parts on the satellite's track by high-pass filtering with an appropriate scaling function model, derived by a Shannon vectorial scaling function of scale 3 (see Section 2.2 and [9, 11]). It should be remarked that this filtering procedure preserves the potential nature of the geomagnetic field, of course.

All the data manipulations mentioned so far are equally applied to polar data and low latitude track segments. However, looking at the residual downward component at low latitudes (dipole latitude less than or equal to 60 degrees) and in polar regions (dipole latitude greater than 60 degrees) one realizes that, in polar regions, the rms varies from 4 nT up to 54 nT. This indicates that there are still magnetic contributions other than those of the crustal field. Most likely these contributions are mainly due to large ionospheric current systems – like the polar electrojet or field aligned currents – which are also present at night local times (cf. e.g. [91] and the references therein as well as our results in Section 5.4).

In order to minimize these effects we choose track segments with minimal residual rms and drop the other data.

In contrast to past satellite missions like POGO or MAGSAT, the orbit of the CHAMP satellite is almost spherical and we assume the spherical approximation to be valid. This assumption is even more justified since, for the present study, we use data acquired within only one month hence covering an altitude range of 442 ± 30 km. Actually, the authors of [14] neglect radial variations in the much more eccentric MAGSAT orbit. Consequently, after subtracting the low frequency contributions, we suppose the altitude variations to be negligible and, in what follows, assume the data to be given on a mean altitude of 442 km (cf. [83]).

In order to apply the method of Section 4.1.3 we need to discretize the appearing integrals by means of an appropriate integration rule. As we have already mentioned in Section 3.3, the method proposed in [20] is advantageous since the resulting regular equiangular longitude-latitude grids mimic the real situation of higher data density in the vicinity of the poles and the corresponding integration weights are given in closed form. Consequently, the next step in our approach is to average the scattered data onto the nodal points of that very integration grid. Figure 4.1 shows the data points chosen from the September 2001 data (blue points) together with grid points onto which the data is averaged. Several techniques

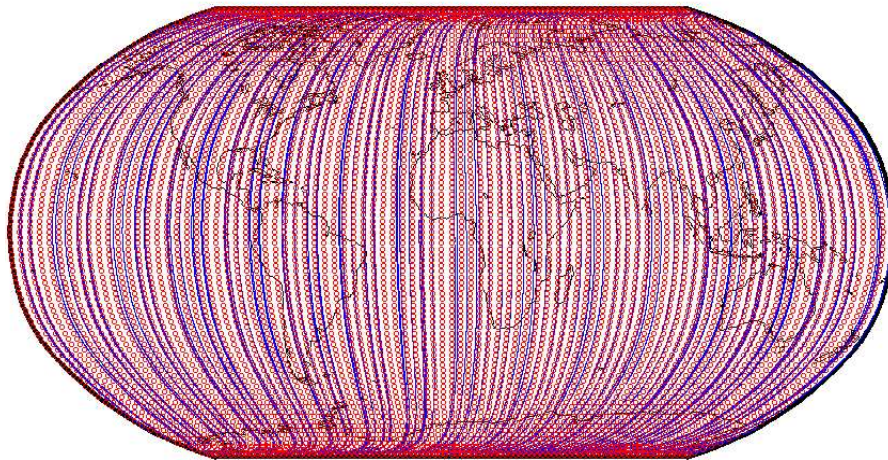


Figure 4.1: Blue dots: Data points from September 2001 used for modelling; Red circles: Nodal points of regular equiangular longitude-latitude grid used for integral discretization.

for averaging given disturbed data to regular grids have been discussed in the literature (see e.g. [3]) and have been used in magnetic field analysis (e.g. [91] and [83] for satellite data and [3] for terrestrial data). Commonly used methods can roughly be divided up into two categories, i.e. distance methods and distribution methods. For the time being we utilize a combination of both methods which is mainly influenced and developed by [84]. For a given point x on the regular grid we search for all data points lying within a spherical distance of 500 km around x . Classical distance methods would weight all data points with respect to their distance thus getting an average value at x . In contrast, the method applied here can be divided up into two steps. First a robust iterative M-estimation to detect outliers in the

distribution of the data in the vicinity of x is performed. The underlying weight function is a manipulated Huber's weight function with zero-weighting for outliers. For more information about robust estimation the reader might consult [59]. Note that there are several different reasons for such outliers, e.g. errors in the performance of the instruments or, especially in the polar regions, magnetic signatures of strong field aligned currents. After detecting and eliminating outliers the remaining data are averaged using a distance weight function given by

$$(0.5 + 0.5 \cos(\pi d/500))^4,$$

where d is the spherical distance between x and the data point at the mean orbital altitude. This weight function is able to bridge the 3° polar gaps and has already been successfully applied by other groups working with CHAMP magnetic data (cf. [83]).

Having averaged the data onto the grid points of the chosen integration rule, we apply the techniques developed in the previous sections to the downward ($-\varepsilon^r$) component of the residual data. To be more precise, we invert the operator equations corresponding to the operators Λ_{AP} and λ_{∇^*} using regularization wavelets constructed from the respective basis systems and singular values (see Table 4.1). For regularizing the inverse problem we select the TSVD filter with a maximum wavelet scale of 3, i.e. the global results obtained in this study correspond to the contributions that could also be derived by a spherical harmonic expansion from degrees 16 up to 32. Observe, however, that the regional results presented can also be interpreted to include contributions of spherical harmonic degrees 16 up to 32, but cannot be derived by standard spherical harmonic techniques since the calculations are confined to certain regions only and are not performed globally. It is clear that deriving higher scale models or using non-bandlimited filtering in terms of the strongly space localizing TF wavelets is only reasonable when the spatial coverage of the data is enhanced by taking into account measurements obtained within longer time intervals. Nevertheless, since the main task of this example is to demonstrate the wavelet approach the application of TSVD seems to be well justified.

Figures 4.2 and 4.3 show global reconstructions of the crustal geomagnetic downward ($-\varepsilon^r$) and north (ε^θ) components. The contrast between continental (strong magnetization) and oceanic (weak magnetization) lithospheric signals is clearly visible. The signals of the north component are weak and comparatively smooth in the Pacific as well as the Atlantic ocean (Figure 4.3). The radial component, however, is weak and smooth in the Pacific region, while in the Atlantic ocean north-south trending signatures can be determined (Figure 4.2). These north-south trending features are also visible in the results obtained from scalar magnetic CHAMP data in [83]. Note that a geophysical interpretation of the results lies beyond the scope of this thesis and the interested reader might consult [58, 83] and the references therein, for example.

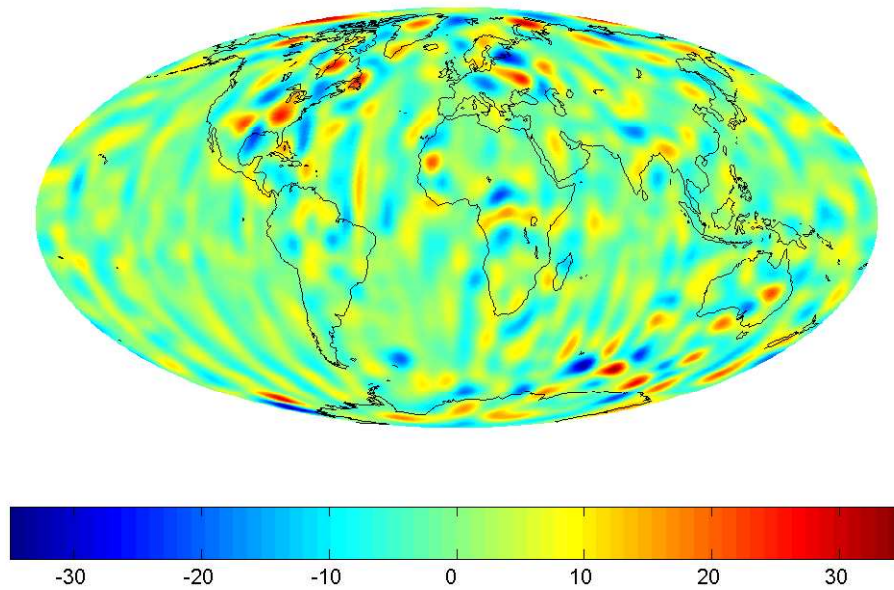


Figure 4.2: Global reconstruction of the lithospheric magnetic contribution, geomagnetic downward ($-\varepsilon^r$) component, continued downward to the Earth's mean spherical surface (6371.2 km) [nT].

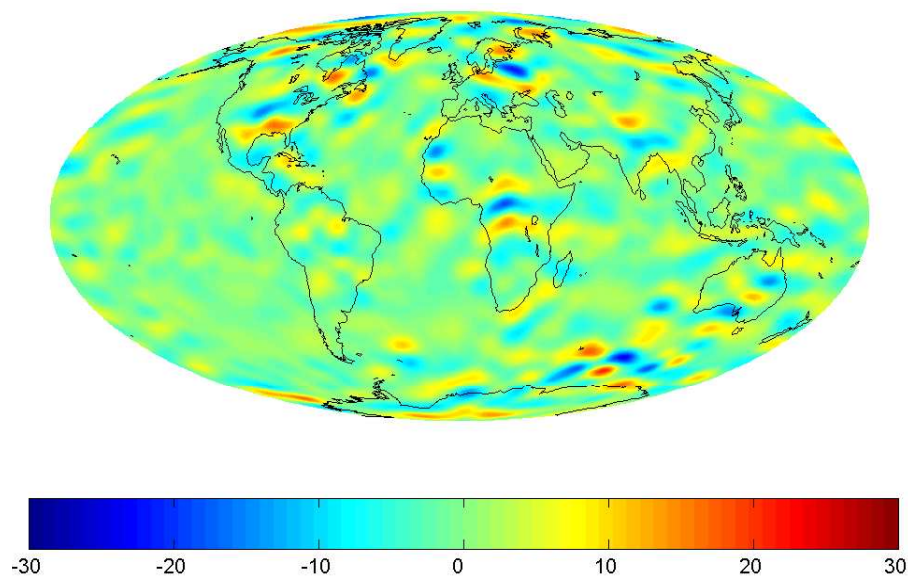


Figure 4.3: Global reconstruction of the lithospheric magnetic contribution, geomagnetic north (ε^θ) component, continued downward to the Earth's mean spherical surface (6371.2 km) [nT].

In order to illustrate the possibility of regional and local calculations Figure 4.4 presents a regional downward continuation over the African continent showing the famous Bangui-Anomaly, while Figure 4.5 illustrates a regional reconstruction over the European continent exhibiting the well known Kiruna and Kursk anomalies. It is well known that, whenever regional data sets are used, there occur oscillatory effects (usually referred to as Gibb's phenomena or geographic truncation errors) at the boundary of that very region. In order to suppress these effects we choose the data window a little larger than the integration window which in turn is somewhat larger than the visualization window. To be specific, the results in Figure 4.4 are derived by restricting the integrations to a spherical cap centered at 20°E , 5°N with a half angle of 50° using a data window with the same center and a half angle of 55° . The reconstruction in Figure 4.5 is calculated on a spherical cap centered at 17°E and 48°N with a half angle of 45° using a data window centered at the same coordinates and having a half angle of 50° .

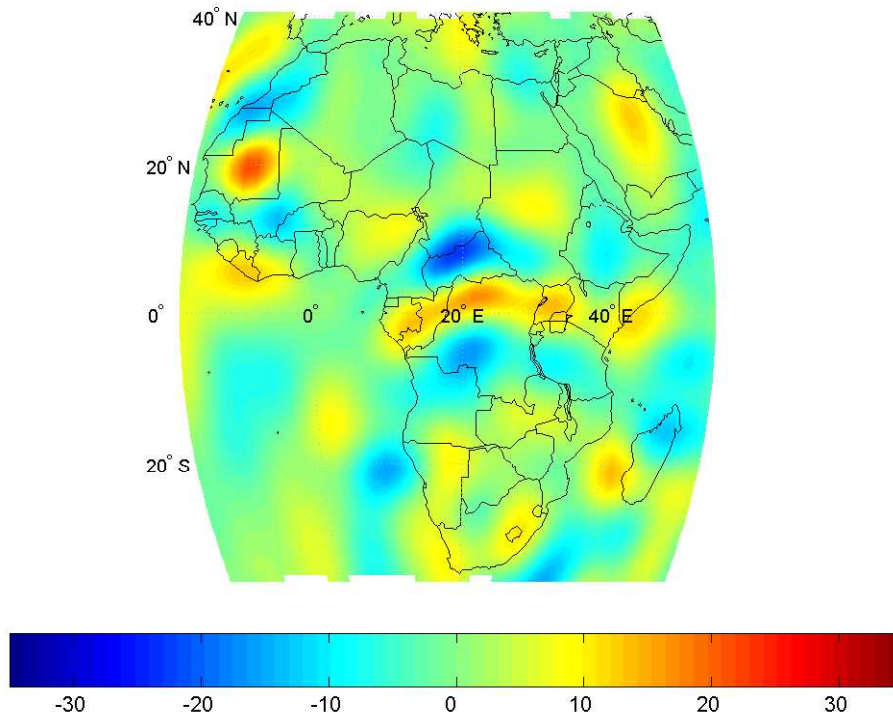


Figure 4.4: Regional reconstruction of the lithospheric magnetic contribution over Africa, geomagnetic down ($-\varepsilon^r$, Z) component, continued downward to the spherical mean Earth's surface (6371.2 km) [nT].

The regional as well as the global reconstructions presented here have been calculated from the same set of data (or subsets thereof) spanning one month. With the growing amount of high quality vector data from modern satellite missions like CHAMP, Ørsted and SAC-C it will be possible to come from regional to very high precision local studies. The method presented here is a suitable technique for dealing with this task. Due to the localization property of the kernel functions it will be possible to choose low data densities over regions of comparatively smooth crustal signals (like the Pacific) and very high density data distributions over areas with significant geomagnetic structures (continents, Bangui area, Kursk

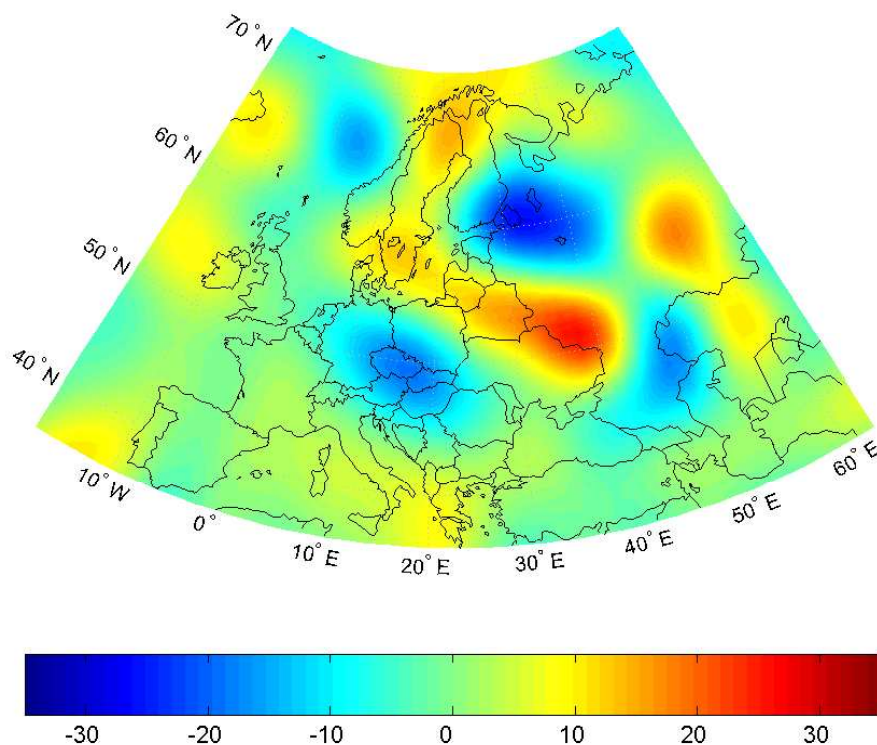


Figure 4.5: Regional reconstruction of the lithospheric magnetic contribution over Europe, geomagnetic down ($-\varepsilon'$, Z) component, continued downward to the spherical mean Earth's surface (6371.2 km) [nT].

area, Arctica etc.). The corresponding wavelet scales (or the regularization parameters) can be selected appropriately in a regionally adaptive manner (see also [50]). In this example we have used a bandlimited approach (TSVD) but it is clear that the higher the data density and, consequently, the higher the achievable resolution, the better the situation for the use of non-bandlimited wavelets (like the ones obtained by Tikhonov filters) which, in the case of crustal field determination, is the next reasonable step.

4.2 Downward Continuation in Non-Spherical Geometries: A Combined Spline and Wavelet Approach

While in the last sections we have been concerned with problems of downward continuation in spherical approximation, this section is intended to approach this subject in non-spherical geometries such that in practical applications it is no longer necessary to consider additional assumptions concerning the geometry of the satellite's orbit. There exist many different multiscale approaches to cope with downward continuation in non-spherical geometries. Most of them are based on the well-known Runge-Walsh Theorem and have been developed for gravitational field determination (see e.g. [29] and the references therein for a very detailed general approach) but can, as far as harmonicity of the geomagnetic field can be assumed, be modified as to be applicable to geomagnetic field determination and downward continuation. One possible way, for example, is to represent the geomagnetic potential in terms of harmonic wavelets (cf. [29] for more details on harmonic wavelets) and then perform a least squares (or other) fit of the corresponding gradient field to the vectorial components of the data; this could be considered to be the multiscale extension of standard spherical harmonic techniques. The approach presented here, however, is especially intended to combine the results from Section 4.1 with a suitable technique accounting for the real orbit geometry and originated from many discussions with the authors of [24] and [50]. Actually, [50] already provides a short introduction of how to use a similar method in gravitational field determination while in [24] a very detailed case study can be found concerning the application of a similar method to the problem of gravitational field modelling from SST and SGG data. While we will introduce the basic theoretical concept as well as the necessary information needed to implement this approach, we direct the interested reader to [24] for an extensive treatment of all the numerical and practical aspects. The basic idea of the approach is the combination of (harmonic) spline approximation (e.g. [26, 25, 27, 44] or, in the case of geomagnetic main field modelling, [99]) and spherical regularization wavelets. While the use of splines provides us with a comparatively easy way to incorporate the orbit geometry, the possibility of employing the spherical regularization wavelets immediately helps us to fall back on our results of Section 4.1, i.e. multiscale regularization can be applied and we still can take advantage of the knowledge of the operators and corresponding singular systems under consideration such that any numerical singular value decomposition can be avoided. The method introduced can roughly be divided into three steps. In the first step a spline is determined that will be used to – in a second step – ‘transport’ the measurements from the actual orbit positions onto a convenient set of nodal points on a sphere with mean orbital radius. In the third step the ‘transported measurements’ are used for downward continuation within the framework of spherical regularization scaling functions and wavelets.

For the sake of brevity we still assume that we are interested in results on a mean (spherical) Earth surface Ω_{ρ_1} . The measurements performed by the satellite give us the possibility to derive, from a specific function G , N discrete samples $G(x_s)$ at positions $\{x_1, \dots, x_N\} \subset \Omega_{\rho_1}^{ext}$ in the exterior $\Omega_{\rho_1}^{ext}$ of the sphere Ω_{ρ_1} with radius $\rho_1 < \inf_{s=1, \dots, N} |x_s|$. In the case of geomagnetic field modelling, G may be any of the horizontal (east, north) components of the presumably internal geomagnetic field, the product of the vertical component of the

internal magnetic field times the radius and, though not really an observable, the geomagnetic potential (see also [1], for example).

In a *first step*, the selected measurements are interpolated by a spline function

$$S = \sum_{s=1}^N a_s \mathcal{L}_x^s K_{\mathcal{H}}(x, \cdot)$$

in a suitable reproducing kernel Hilbert space \mathcal{H} with reproducing kernel $K_{\mathcal{H}}$ (see Chapter 1). For $s = 1, \dots, N$, the spline coefficients a_s of $S \in \mathcal{H}$ are to be determined by solving the linear system of equations

$$\sum_{s=1}^N a_s \mathcal{L}_y^l \mathcal{L}_x^s K_{\mathcal{H}}(x, y) = \sum_{s=1}^N \sum_{n=0}^{\infty} \sum_{k=1}^{2n+1} a_s \frac{1}{A_n} H_{n,k}^{ext}(r; x_s) H_{n,k}^{ext}(r; x_l) = G(x_l), \quad (4.22)$$

where $\{H_{n,k}^{ext}\}$ are the outer harmonics as presented in Chapter 1 and where $\{A_n\}$ is assumed to be a sequence of real numbers satisfying $\sum_{n=0}^{\infty} \frac{2n+1}{4\pi} \frac{1}{A_n^2} < \infty$. The sequence $\{A_n\}$ characterizes the reproducing kernel Hilbert space as well as the corresponding reproducing kernel (different choices of $\{A_n\}$ lead to different kernels like the Abel-Poisson kernel, for example). A detailed discussion of this subject is possible within the theory of Sobolev spaces which is beyond the scope of this thesis. For a detailed description see e.g. [29]. It is noteworthy that, if the data are assumed to be noisy, spline interpolation might not be the most reasonable approach. In this case spline smoothing is usually the favourable technique (for more details see e.g. [26, 44]). However, whether spline interpolation or smoothing is used does not influence the following considerations. The linear system (4.22) usually is highly ill-conditioned (note that, basically, singularity could occur, too; nevertheless, experience shows that singularity is only obtained if the data distribution is very unfavorable; cf. [73] for more details). This is especially the case if the data are not uniformly distributed, i.e. if there are areas where the data density is much higher than anywhere else (since this leads to some almost equal rows in the linear system). In general, this is true for measurements from satellites with an almost polar orbit (like e.g. CHAMP) since one can expect the data density to be much higher in the vicinity of the poles than in equatorial regions (see Figure 4.6 for exemplary CHAMP tracks). Consequently, from the vast amount of observational data $\mathcal{Y} = \{y_1, \dots, y_{N_{max}}\}$, the set $\mathcal{X} = \{x_1, \dots, x_N\} \subset \mathcal{Y}$ used for field determination and downward continuation should be chosen as to ensure a preferably global coverage and uniform distribution in order to reduce the condition of the linear system. A promising technique for data selection is to generate a uniformly distributed set $\tilde{\mathcal{X}} = \{\tilde{x}_1, \dots, \tilde{x}_N\}$ of grid points on the mean orbital sphere $\Omega_{r_{mean}}$ of radius r_{mean} given by

$$\inf_{l=1, \dots, N_{max}} |y_l| \leq r_{mean} = \sum_{l=1}^{N_{max}} \frac{|y_l|}{N_{max}} \leq \sup_{l=1, \dots, N_{max}} |y_l|, \quad y_l \in \mathcal{Y},$$

first. Then, for every grid point $\tilde{x}_s \in \tilde{\mathcal{X}}$, $s = 1, \dots, N$, we choose that very position $y_l \in \mathcal{Y}$, $l = 1, \dots, N_{max}$, that has the shortest minimal Euclidean distance to the grid point \tilde{x}_s , i.e. we set

$$x_s := y_l, \quad \text{if } |\tilde{x}_s - y_l| = \min_{p=1, \dots, N_{max}} |\tilde{x}_s - y_p|.$$

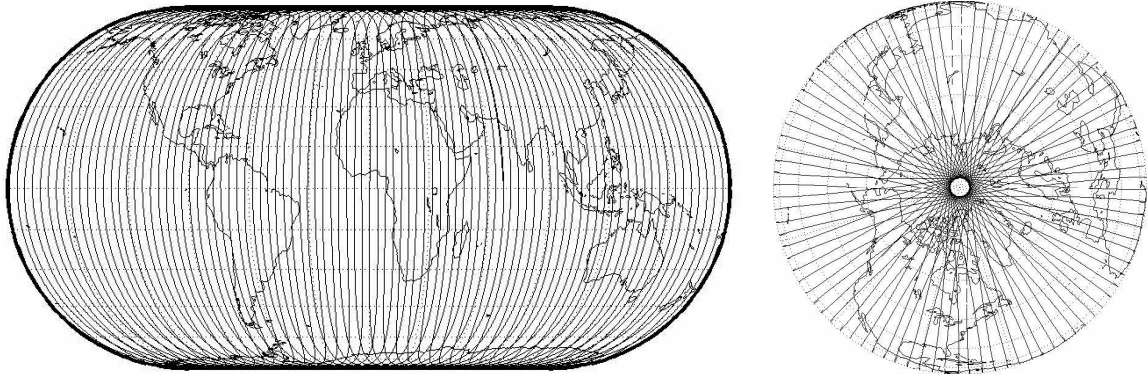


Figure 4.6: Exemplary CHAMP tracks in global view (left) and in polar regions (right) (3 days). The resulting data density in polar regions is higher than in low- or mid-latitude regions.

In [30] algorithms for the construction of various uniformly distributed point systems on the sphere are presented. First numerical tests as well as the results in [24] and [50] indicate that the so-called *Reuter Grid* is well suited for our purposes. For the convenience of the reader we recapitulate the construction principle of that very point set in standard spherical coordinates:

Definition 4.18 *A set $\tilde{\mathcal{X}}_{N(\gamma)}$ of $N(\gamma)$ points on the unit sphere is called Reuter Grid corresponding to the control parameter $\gamma \in \mathbb{N}$, if the points $(\varphi_{ij}, \vartheta_i)$ are given as follows:*

- (i) $\vartheta_0 = 0, \varphi_{0,1} = 0$ (north pole)
- (ii) $\Delta\vartheta = \pi/\gamma$
- (iii) $\vartheta_i = i\Delta\vartheta, 1 \leq i \leq \gamma - 1$
- (iv) $\gamma_i = 2\pi / \arccos((\cos(\Delta\vartheta) - \cos^2(\vartheta_i)) / \sin^2(\vartheta_i))$
- (v) $\varphi_{ij} = (j - 1/2)(2\pi/\gamma_i), 1 \leq j \leq \gamma_i$
- (vi) $\vartheta_\gamma = \pi, \varphi_{\gamma,1} = 0$ (south pole).

The number $N(\gamma)$ of grid points of a Reuter grid can be estimated by the following Lemma (cf. [30]):

Lemma 4.19 *The number $N(\gamma)$ of points of a Reuter grid corresponding to a given control parameter $\gamma \in \mathbb{N}$ can be estimated by*

$$N(\gamma) \leq 2 + \frac{4}{\pi}\gamma^2.$$

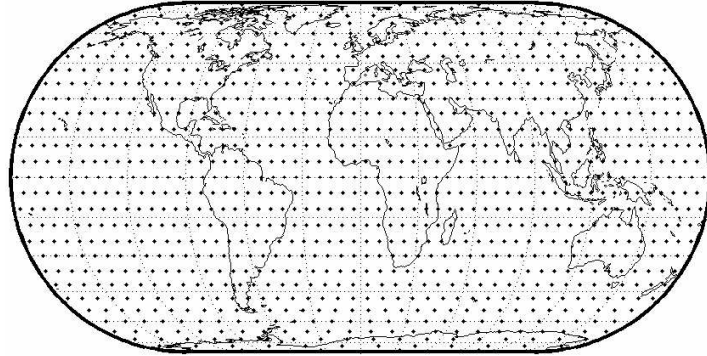


Figure 4.7: Distribution of 1130 grid points of a Reuter Grid ($\gamma = 29$) suggested for data selection.

For the purpose of illustration Figure 4.7 shows a Reuter Grid of 1130 grid points ($\gamma = 29$); note that the point density in low-, mid- and high-latitude areas is approximately equal.

As regards numerical effort it should be noted that directly solving the linear system (4.22) requires $\mathcal{O}(N^3)$ operations and the computational effort of iterative solvers is $\mathcal{O}(N^2)$ in each iteration step. In [50] a special fast multipole method (FMM) is developed which is able to accelerate an iterative solver to $\mathcal{O}(N)$ when certain kernel functions (singularity kernel, Abel-Poisson kernel and logarithmic kernel) are used in the spline approach. The FMM approach is based on the space localization of the kernel functions which allows a far-field near-field approximation of the kernels. For more details on this subject the reader should consult [50, 85] and the references therein. We would also like to mention the works of [37, 51] and [56] which introduce a certain domain decomposition method for such spline systems like (4.22). This so-called Multiplicative Schwartz Alternating Algorithm (MSAA) splits a system of linear equations into several smaller matrices of the same type and solves systems of linear equations with these matrices successively in an iterative algorithm. The smaller subsystems can be solved using direct solvers. Like the Fast Multipole Method mentioned above, MSAA allows a considerable reduction of runtime and memory requirements. It is a task for future work to apply these methods in geomagnetic field modelling.

After having solved the linear system, the *second step* consists of evaluating the resulting spline S at the nodal points of a suitable (approximate) integration formula on the sphere $\Omega_{r_{mean}}$, i.e. the information of the measurements is ‘transported’ to that very sphere by means of the spline (note that this sphere is chosen since it can be expected that the error due to the spline approximation is comparatively small, cf. [24]). This, however, enables us to apply – in a *third step* – the methods that have been developed in Section 4.1, i.e. the downward continuation process is performed by means of the regularization scaling functions and wavelets in a spherical framework.

Remark 4.20 *Though one might argue that the spline is already the solution of the underlying inverse problem, there are two main reasons for us to suggest the combined spline and wavelet approach. First, the linear systems that occur when determining the spline coefficients are almost always ill-conditioned and hence solving the linear systems requires some*

means of regularization. Despite the fact that very sophisticated methods are known, it is clear that regularizing the linear systems includes the regularization of the underlying inverse problem without using (or knowing the effects on) the corresponding singular system. The combined approach, however, gives us complete control over the singular systems since the regularization scaling functions and wavelets are just constructed such that the regularization can be performed within a multiscale framework. Second, the space localization of regularization kernels allows the determination of locally adapted regularization parameters within a global concept, i.e. calculations can be performed using different parameters for different regions thus providing an easy and efficient transition from global to regional modelling.

Finally it should be noted that, at the time being, only first numerical tests have been performed. A thorough application of the combined spline and wavelet approach to geomagnetic data (simulations with synthetic data as well as real vectorial data) is a task for future work. Nevertheless, the previously mentioned results obtained by similar methods in gravitational field determination are promising.

Chapter 5

A Wavelet-Parametrization of the Magnetic Field in Mie Representation

Dealing with satellite measurements of the geomagnetic field b encounters the difficulty that the field is sampled within a source region of b , i.e. there are non-vanishing electric current densities j where the observations are taken. Consequently, data of low-orbiting satellites do usually not meet the prerequisites for the classical Gauss representation of b as the gradient field of a scalar harmonic potential. Assuming the quasi-static approximation of Maxwell's equations, [7, 8, 48, 100] suggest the resolution of the magnetic field by means of the Mie representation as an adequate replacement of the Gauss approach. The Mie representation, i.e. splitting the magnetic field into poloidal and toroidal parts, has the advantage that it can equally be applied in regions of vanishing as well as non-vanishing electric current densities. It is this characteristic that makes the Mie approach a powerful tool for dealing with geomagnetic source problems, i.e. the problems of calculating magnetic effects due to given electric currents (direct source problem) and – vice versa – determining those current distributions that produce a predefined magnetic field (inverse source problem). [21, 91] and [82] thoroughly examine and apply the Mie representation in this context. Most of the considerations in [7, 8] and all the results in [21, 82, 91] are based on a spherical harmonic parametrization, i.e. starting point of the considerations are expansions of the poloidal and toroidal scalars in terms of spherical harmonics. On the one hand, this approach is advantageous since it admits the possibility to incorporate radial dependencies of magnetic fields and electric currents in a natural way. On the other hand, the global support of the spherical harmonics might limit the practicability of this technique since it cannot cope with electric currents (and corresponding magnetic effects) that vary rapidly with latitude or longitude, or that are confined to certain regions. In fact, the author of [7] states that it might be advantageous to find a field parametrization in terms of functions that take efficient account of the specific concentration of the current densities in space. In [81] and [11] we therefore have already presented first methods to deal with the Mie representation in terms of spherical vectorial wavelets thus being able to reflect the various levels of space

localization in form of a vectorial multiresolution analysis. However, these techniques are not able to deal with radial dependencies in a canonical way and hence their application is limited to fixed heights (or neglected radial variations).

In what follows we will introduce a wavelet-parametrization of the magnetic field that is able to deal with both, space localization and radial variations. The approach is inspired by the considerations of [21, 82] and [91] as well as our results in [11] and [81].

5.1 Setup

Since the magnetic field is of zero divergence in \mathbb{R}^3 , the Mie representation can be applied and hence b can be represented as

$$b = \nabla \wedge LP_b + LQ_b, \quad (5.1)$$

where P_b, Q_b are the poloidal and toroidal scalars of b respectively (see also Section 1.4). The sources of the magnetic field are the electric current densities j given by

$$j = \nabla \wedge LP_j + LQ_j, \quad (5.2)$$

where the poloidal and toroidal scalars P_j and Q_j are connected with P_b and Q_b via (e.g. [7, 8])

$$P_j = \frac{1}{\mu_0} Q_b, \quad (5.3)$$

$$Q_j = -\frac{1}{\mu_0} \Delta P_b. \quad (5.4)$$

For each $x = r\xi$ with $r \neq 0$ and $\xi \in \Omega$, (5.1) and (5.2) can be rewritten as

$$b = \xi \frac{\Delta_\xi^* P_b}{r} - \nabla_\xi^* \frac{\partial_r r P_b}{r} + L_\xi^* Q_b \quad (5.5)$$

and

$$j = \xi \frac{\Delta_\xi^* P_j}{r} - \nabla_\xi^* \frac{\partial_r r P_j}{r} + L_\xi^* Q_j, \quad (5.6)$$

where we have omitted the arguments for the sake of clarity and where we have used the abbreviation $\partial_r = \partial/\partial r$ (see also Section 1.4).

Following [7] we assume either the geomagnetic field b or the electric current distributions j to be sampled within a spherical shell $\Omega_{(R_1, R_2)}$, $0 < R_1 < R_2 < \infty$. This assumption takes into account elliptical satellite orbits as well as the decrease in altitude with the lifetime of the satellite. The geomagnetic field within the shell $\Omega_{(R_1, R_2)}$ consists of four different parts (cf. [91]), i.e.

$$b = b_{pol}^{int} + b_{pol}^{ext} + b_{pol}^{sh} + b_{tor}. \quad (5.7)$$

b_{pol}^{int} denotes the poloidal magnetic field due internal toroidal currents in the region with $r < R_1$. b_{pol}^{ext} is the poloidal part caused by external toroidal current densities in the region

with $r > R_2$, and b_{pol}^{sh} is the poloidal magnetic field due to the toroidal electric currents within $\Omega_{(R_1, R_2)}$. Finally, b_{tor} is the toroidal part of b generated by poloidal currents in $\Omega_{(R_1, R_2)}$. If there are no currents in the shell $\Omega_{(R_1, R_2)}$, then $b_{pol}^{sh} = b_{tor} = 0$ and b can be represented as the gradient field of a scalar harmonic potential or by means of the Mie representation equivalently. If only the toroidal currents vanish within the shell, then $b_{pol}^{sh} = 0$, and the magnetic field within the shell can be represented by

$$b = b_{pol}^{int} + b_{pol}^{ext} + b_{tor} \quad (5.8)$$

(see e.g. (5.4), i.e. toroidal currents are the only sources of poloidal magnetic fields).

The situation changes if the toroidal currents within $\Omega_{(R_1, R_2)}$ do not vanish. Let us suppose that the radii of the shell satisfy (cf. [7])

$$R_2 - R_1 \ll \frac{R_2 + R_1}{2}, \quad (5.9)$$

i.e. the thickness of the shell is small compared to the mean radius. Such a shell is called a *thin shell*. As pointed out by [7] and [91], even for non-vanishing (toroidal) current densities in the shell, the magnetic field within a thin shell can (approximately) be represented by (5.8), i.e. the poloidal field b_{pol}^{sh} tends to zero in thin shells while the toroidal part b_{tor} remains finite. Note that (5.8) is as well exactly true in a thick shell provided that the shell contains only radial currents (cf. [91]).

Remark 5.1 *Actually, for thin shells, it holds that $b_{pol}^{sh} \rightarrow 0$ as $(R_2 - R_1)/H \rightarrow 0$, where H is a reference length characterizing the vertical scale of the current density (e.g. [7, 91]). In more detail, if in a thin shell,*

$$R_2 - R_1 \ll H \simeq \frac{R_2 + R_1}{2},$$

i.e. the current density changes significantly on vertical scales that can be compared to the mean radius and that are much larger than the thickness of the shell, then the thin shell approximation (5.8) is surely valid. If, in a thin shell,

$$R_2 - R_1 \simeq H \ll \frac{R_2 + R_1}{2},$$

i.e. the currents change significantly on vertical length scales that are small compared to the mean radius but that can be compared to the thickness of the shell, then the thin shell approximation can as well fail. For more details the interested reader is directed to [7].

In view of the examples presented in Section 5.4, it is noteworthy that the thin shell approximation is surely valid for the MAGSAT mission (see also [91], for example).

5.2 Parametrization of Poloidal Fields

Separating the poloidal magnetic field into internal and external parts in the shell $\Omega_{(R_1, R_2)}$ is obviously possible if there are no toroidal currents in $\Omega_{(R_1, R_2)}$ or, in an approximate sense, if the thin shell approximation is valid.

As can be seen from Equation (5.4), in the case of vanishing toroidal currents, the poloidal scalar can be represented by a harmonic potential due to internal ($r < R_1$) and external ($r > R_2$) sources, i.e. we have (with $x = r\xi, y = r'\eta$)

$$P_b = P_b^{int} + P_b^{ext}, \quad \text{in } \Omega_{(R_1, R_2)}$$

with

$$\begin{aligned} P_b^{int} &= \sum_{(n,k) \in \mathcal{N}} (P_b^{int})^\wedge(R_1; n, k) H_{n,k}^{ext}(R_1, \cdot) \\ &= \sum_{(n,k) \in \mathcal{N}} (P_b^{int})^\wedge(n, k) \left(\frac{R_1}{r}\right)^{n+1} Y_{n,k}(\cdot) \end{aligned} \quad (5.10)$$

and

$$\begin{aligned} P_b^{ext} &= \sum_{(n,k) \in \mathcal{N}} (P_b^{ext})^\wedge(R_2; n, k) H_{n,k}^{int}(R_2, \cdot) \\ &= \sum_{(n,k) \in \mathcal{N}} (P_b^{ext})^\wedge(n, k) \left(\frac{r}{R_2}\right)^n Y_{n,k}(\cdot). \end{aligned} \quad (5.11)$$

$\{H_{n,k}^{ext}(R_1, \cdot)\}, \{H_{n,k}^{int}(R_2, \cdot)\}$ and $\{Y_{n,k}\}$ are systems of outer, inner and spherical harmonics. The corresponding Fourier coefficients are given by

$$\begin{aligned} (P_b^{int})^\wedge(R_1; n, k) &= \int_{\Omega_{R_1}} P_b^{int}(y) H_{n,k}^{ext}(R_1, y) d\omega_{R_1}(y), \\ (P_b^{ext})^\wedge(R_2; n, k) &= \int_{\Omega_{R_2}} P_b^{ext}(y) H_{n,k}^{int}(R_2, y) d\omega_{R_2}(y), \\ (P_b^{int})^\wedge(n, k) &= \int_{\Omega} P_b^{int}(R_1\eta) Y_{n,k}(\eta) d\omega(\eta), \quad R_1\eta = y, \end{aligned} \quad (5.12)$$

$$(P_b^{ext})^\wedge(n, k) = \int_{\Omega} P_b^{ext}(R_2\eta) Y_{n,k}(\eta) d\omega(\eta), \quad R_2\eta = y. \quad (5.13)$$

Note that the integrals in (5.12) and (5.13) are well defined since functions on any sphere Ω_r are isomorphic to functions on Ω .

P_b^{int} and P_b^{ext} can as well be expanded in terms of wavelets, so-called outer and inner harmonic wavelets (see also [29] and the references therein), that can be defined within the framework of Chapter 2.

Definition 5.2 *Let, for $J \in \mathbb{Z}$, $\{(\Phi_J)^\wedge(n)\}_{n=0,1,\dots}$, be the generating symbol of an $\mathcal{L}^2(\Omega)$ -scaling function and let $\{(\Psi_J)^\wedge(n)\}_{n=0,1,\dots}$, be the generating symbol of the associated $\mathcal{L}^2(\Omega)$ -wavelet. Then the outer harmonic scaling functions $\{\Phi_{ext,J}\}$ and wavelets $\{\Psi_{ext,J}\}$ of scale*

J are defined by

$$\begin{aligned}\Phi_{ext,J}(x, y) &= \sum_{(n,k) \in \mathcal{N}} (\Phi_J)^\wedge(n) H_{n,k}^{ext}(R_1, x) H_{n,k}^{ext}(R_1, y) \\ &= \sum_{(n,k) \in \mathcal{N}} (\Phi_J)^\wedge(n) \frac{1}{R_1} \left(\frac{R_1}{r}\right)^{n+1} Y_{n,k}(\xi) \frac{1}{R_1} \left(\frac{R_1}{r'}\right)^{n+1} Y_{n,k}(\eta)\end{aligned}$$

and

$$\begin{aligned}\Psi_{ext,J}(x, y) &= \sum_{(n,k) \in \mathcal{N}} (\Psi_J)^\wedge(n) H_{n,k}^{ext}(R_1, x) H_{n,k}^{ext}(R_1, y) \\ &= \sum_{(n,k) \in \mathcal{N}} (\Psi_J)^\wedge(n) \frac{1}{R_1} \left(\frac{R_1}{r}\right)^{n+1} Y_{n,k}(\xi) \frac{1}{R_1} \left(\frac{R_1}{r'}\right)^{n+1} Y_{n,k}(\eta),\end{aligned}$$

respectively. The inner harmonic scaling functions $\{\Phi_{int,J}\}$ and wavelets $\{\Psi_{int,J}\}$ of scale J are defined by

$$\begin{aligned}\Phi_{int,J}(x, y) &= \sum_{(n,k) \in \mathcal{N}} (\Phi_J)^\wedge(n) H_{n,k}^{int}(R_2, x) H_{n,k}^{int}(R_2, y) \\ &= \sum_{(n,k) \in \mathcal{N}} (\Phi_J)^\wedge(n) \frac{1}{R_2} \left(\frac{r}{R_2}\right)^n Y_{n,k}(\xi) \frac{1}{R_2} \left(\frac{r'}{R_2}\right)^n Y_{n,k}(\eta)\end{aligned}$$

and

$$\begin{aligned}\Psi_{int,J}(x, y) &= \sum_{(n,k) \in \mathcal{N}} (\Psi_J)^\wedge(n) H_{n,k}^{int}(R_2, x) H_{n,k}^{int}(R_2, y) \\ &= \sum_{(n,k) \in \mathcal{N}} (\Psi_J)^\wedge(n) \frac{1}{R_2} \left(\frac{r}{R_2}\right)^n Y_{n,k}(\xi) \frac{1}{R_2} \left(\frac{r'}{R_2}\right)^n Y_{n,k}(\eta),\end{aligned}$$

respectively.

A straightforward calculation leads us to the following result:

Lemma 5.3 *Let $\{\Psi_{ext,J}\}$ as well as $\{\Psi_{int,J}\}$ be given as in Definition 5.2. Then, if no toroidal currents are present in the spherical shell $\Omega_{(R_1, R_2)}$, the poloidal scalar P_b can be represented via*

$$\begin{aligned}P_b &= P_b^{int} + P_b^{ext} \\ &= \underbrace{\sum_{J=0}^{\infty} \Psi_{ext,J} * \mathcal{L}^2(\Omega_{R_1}) \left(\Psi_{ext,J} * \mathcal{L}^2(\Omega_{R_1}) P_b^{int} \right)}_{P_b^{int}} \\ &\quad + \underbrace{\sum_{J=0}^{\infty} \Psi_{int,J} * \mathcal{L}^2(\Omega_{R_2}) \left(\Psi_{int,J} * \mathcal{L}^2(\Omega_{R_2}) P_b^{ext} \right)}_{P_b^{ext}}\end{aligned}$$

$$\begin{aligned}
&= \sum_{J=0}^{\infty} \Psi_{ext,J} *_{\mathcal{L}^2(\Omega_{R_1})} WT_{ext,J}(P_b^{int}) \\
&+ \sum_{J=0}^{\infty} \Psi_{int,J} *_{\mathcal{L}^2(\Omega_{R_1})} WT_{int,J}(P_b^{ext})
\end{aligned}$$

in $\Omega_{(R_1, R_2)}$.

Observe that the last two terms are just introduced as abbreviations. Note that in Lemma 5.3 there occurs no zero order contribution i.e. there is neither a $\Phi_{ext,0} *_{\mathcal{L}^2(\Omega_{R_1})} \Phi_{ext,0}$ -term nor the corresponding inner term. This is due to the fact that the Mie scalars have no zero order moment or, in other words, their mean value over the sphere must be zero.

According to (5.5), we need to calculate $\Delta^* P_b$ as well as $\partial_r r P_b$ in order to derive the corresponding magnetic field:

Lemma 5.4 *Let P_b in $\Omega_{(R_1, R_2)}$ be given as in Lemma 5.3. Then*

$$\begin{aligned}
\Delta^* P_b^{int} &= \sum_{J=0}^{\infty} \tilde{\Psi}_{ext,J} *_{\mathcal{L}^2(\Omega_{R_1})} WT_{ext,J}(P_b^{int}), \\
\Delta^* P_b^{ext} &= \sum_{J=0}^{\infty} \tilde{\Psi}_{int,J} *_{\mathcal{L}^2(\Omega_{R_2})} WT_{int,J}(P_b^{ext}), \\
\partial_r r P_b^{int} &= \sum_{J=0}^{\infty} \hat{\Psi}_{ext,J} *_{\mathcal{L}^2(\Omega_{R_1})} WT_{ext,J}(P_b^{int}), \\
\partial_r r P_b^{ext} &= \sum_{J=0}^{\infty} \hat{\Psi}_{int,J} *_{\mathcal{L}^2(\Omega_{R_2})} WT_{int,J}(P_b^{ext})
\end{aligned}$$

in $\Omega_{(R_1, R_2)}$, where

$$\begin{aligned}
\tilde{\Psi}_{ext,J}(r\xi, r'\eta) &= \sum_{(n,k) \in \mathcal{N}} -n(n+1)(\Psi_J)^\wedge(n) H_{n,k}^{ext}(R_1, x) H_{n,k}^{ext}(R_1, y) \\
\tilde{\Psi}_{int,J}(r\xi, r'\eta) &= \sum_{(n,k) \in \mathcal{N}} -n(n+1)(\Psi_J)^\wedge(n) H_{n,k}^{int}(R_2, x) H_{n,k}^{int}(R_2, y), \\
\hat{\Psi}_{ext,J}(r\xi, r'\eta) &= \sum_{(n,k) \in \mathcal{N}} -n(\Psi_J)^\wedge(n) H_{n,k}^{ext}(R_1, x) H_{n,k}^{ext}(R_1, y), \\
\hat{\Psi}_{int,J}(r\xi, r'\eta) &= \sum_{(n,k) \in \mathcal{N}} (n+1)(\Psi_J)^\wedge(n) H_{n,k}^{int}(R_2, x) H_{n,k}^{int}(R_2, y).
\end{aligned}$$

Proof. From Lemma 5.3 we know that, in $\Omega_{(R_1, R_2)}$,

$$P_b^{int} = \sum_{J=0}^{\infty} \Psi_{ext,J} *_{\mathcal{L}^2(\Omega_{R_1})} WT_{ext,J}(P_b^{int}).$$

This means that

$$\Delta^* P_b^{int} = \sum_{J=0}^{\infty} \int_{\Omega_{R_1}} \Delta^* \Psi_{ext,J}(\cdot, y) WT_{ext,J}(P_b^{int})(y) d\omega_{R_1}(y),$$

i.e. the Beltrami operator is applied to the kernel functions. The expressions for the kernels $\tilde{\Psi}_{ext,J} = \Delta^* \Psi_{ext,J}$ and $\tilde{\Psi}_{int,J} = \Delta^* \Psi_{int,J}$ can be derived directly from the representations in Definition 5.2 and using $\Delta^* Y_{n,k} = -n(n+1)Y_{n,k}$. The representations of the other kernel functions involving radial derivatives can also be calculated in a straightforward way using the series representations of the corresponding kernels in terms of inner and outer harmonics.

■

Summarizing our considerations we can come up with the following theorem:

Theorem 5.5 *If no toroidal currents are present in the spherical shell $\Omega_{(R_1, R_2)}$, then the poloidal magnetic field in that shell is given by $b_{pol} = b_{pol}^{int} + b_{pol}^{ext}$, with*

$$\begin{aligned} b_{pol}^{int} &= \sum_{J=0}^{\infty} \tilde{\psi}_{ext,J}^{(1)} \star_{l^2(\Omega_{R_1})} WT_{ext,J}(P_b^{int}) + \\ &+ \sum_{J=0}^{\infty} \hat{\psi}_{ext,J}^{(2)} \star_{l^2(\Omega_{R_1})} WT_{ext,J}(P_b^{int}), \end{aligned}$$

and

$$\begin{aligned} b_{pol}^{ext} &= \sum_{J=0}^{\infty} \tilde{\psi}_{int,J}^{(1)} \star_{l^2(\Omega_{R_2})} WT_{int,J}(P_b^{ext}) + \\ &+ \sum_{J=0}^{\infty} \hat{\psi}_{int,J}^{(2)} \star_{l^2(\Omega_{R_2})} WT_{int,J}(P_b^{ext}), \end{aligned}$$

where the kernel functions are given by

$$\begin{aligned} \tilde{\psi}_{ext,J}^{(1)}(r\xi, r'\eta) &= \xi \frac{1}{r} \tilde{\Psi}_{ext,J}(r\xi, r'\eta) \\ &= \sum_{(n,k) \in \mathcal{N}} -n(n+1) (\Psi_J)^\wedge(n) \frac{1}{rR_1} \left(\frac{R_1}{r}\right)^{n+1} y_{n,k}^{(1)}(\xi) H_{n,k}^{ext}(R_1, y), \\ \hat{\psi}_{ext,J}^{(2)}(r\xi, r'\eta) &= -\nabla_\xi^* \frac{1}{r} \hat{\Psi}_{ext,J}(r\xi, r'\eta) \\ &= \sum_{(n,k) \in \mathcal{N}^{(i)}} \sqrt{n^3(n+1)} (\Psi_J)^\wedge(n) \frac{1}{rR_1} \left(\frac{R_1}{r}\right)^{n+1} y_{n,k}^{(2)}(\xi) H_{n,k}^{ext}(R_1, y) \end{aligned}$$

as well as

$$\begin{aligned}
\tilde{\psi}_{int,J}^{(1)}(r\xi, r'\eta) &= \xi \frac{1}{r} \tilde{\Psi}_{int,J}(r\xi, r'\eta) \\
&= \sum_{(n,k) \in \mathcal{N}} -n(n+1) (\Psi_J)^\wedge(n) \frac{1}{rR_2} \left(\frac{r}{R_2}\right)^n y_{n,k}^{(1)}(\xi) H_{n,k}^{int}(R_2, y), \\
\hat{\psi}_{int,J}^{(2)}(r\xi, r'\eta) &= -\nabla_\xi^* \frac{1}{r} \hat{\Psi}_{int,J}(r\xi, r'\eta) \\
&= \sum_{(n,k) \in \mathcal{N}^{(2)}} -\sqrt{n(n+1)^3} (\Psi_J)^\wedge(n) \frac{1}{rR_2} \left(\frac{r}{R_2}\right)^n y_{n,k}^{(2)}(\xi) H_{n,k}^{int}(R_2, y).
\end{aligned}$$

Proof. We only need to prove the expressions for the kernel functions. These, however, can be obtained in a straightforward calculation using Definition 5.2 and the definitions of the vector spherical harmonics. ■

Theorem 5.5 presents a wavelet-parametrization for the poloidal magnetic field in a shell $\Omega_{(R_1, R_2)}$ in the absence of toroidal currents within that shell (or in thin shell approximation). This result is consistent with the spherical harmonic parametrizations presented in [82] and [91], but allows for regional modelling within a multiresolution analysis. In order to include the effects of toroidal currents in the shell $\Omega_{(R_1, R_2)}$, additional contributions to P_b except for P_b^{int} and P_b^{ext} need to be incorporated in the approach. For that purpose, let us assume that we need to add a further poloidal scalar P_b^{add} for the poloidal magnetic field, where P_b^{add} is of the form

$$P_b^{add}(r\xi) = P_{b,1}(r) P_{b,2}(\xi), \quad r\xi \in \Omega_{(R_1, R_2)}$$

(i.e. we apply separation of variables). Then, we can express the angular part in terms of $\mathcal{L}^2(\Omega)$ -wavelets $\{\Psi_J\}$ (see the results in Chapter 2):

$$P_b^{add}(r\cdot) = P_{b,1}(r) \left(\sum_{J=0}^{\infty} \Psi_J * \Psi_J * P_{b,2} \right). \quad (5.14)$$

Applying (5.5) to (5.14) helps us to derive the additional contribution to the poloidal magnetic field, that is

$$b_{pol}^{add}(r\cdot) = \frac{1}{r} P_{b,1}(r) \left(\sum_{J=0}^{\infty} \tilde{\psi}_J^{(1)} \star \Psi_J * P_{b,2} \right) + \quad (5.15)$$

$$+ \frac{1}{r} (P_{b,1}(r) + r\partial_r P_{b,1}(r)) \sum_{J=0}^{\infty} \hat{\psi}_J^{(2)} \star \Psi_J * P_{b,2}, \quad (5.16)$$

where the appearing vectorial wavelets are given by $\tilde{\psi}_J^{(1)}(\xi, \eta) = \xi \Delta_\xi^* \Psi_J(\xi, \eta)$ and $\hat{\psi}_J^{(2)}(\xi, \eta) = -\nabla_\xi^* \Psi_J(\xi, \eta)$. The additional poloidal magnetic field (5.15-5.16) is due to the toroidal electric

current density

$$\mu_0 j_{tor}(r\cdot) = -\frac{1}{r^2} \left[(r\partial_r^2 r P_{b,1}(r)) \sum_{J=0}^{\infty} \bar{\psi}_J^{(3)} \star \Psi_J \star P_{b,2} + \right. \quad (5.17)$$

$$\left. + P_{b,1}(r) \sum_{J=0}^{\infty} \tilde{\psi}_J^{(3)} \star \Psi_J \star P_{b,2} \right], \quad (5.18)$$

where the kernel functions $\bar{\psi}_J^{(3)}$ and $\tilde{\psi}_J^{(3)}$ can be derived from the scalar kernels via $\bar{\psi}_J^{(3)}(\xi, \eta) = L_\xi^* \Psi_J(\xi, \eta)$ as well as $\tilde{\psi}_J^{(3)}(\xi, \eta) = L_\xi^* \Delta_\xi^* \Psi_J(\xi, \eta)$. This, however, is straightforward using the definitions of the spherical kernels as well as the definition of vector spherical harmonics.

The radial behaviour of the toroidal currents is, of course, dependent on the underlying physical cause. In the simple case of $P_{b,1} = P_0$, $P_0 \in \mathbb{R} \setminus \{0\}$ constant, the expression (5.17-5.18) for the toroidal current reduces to

$$\mu_0 j_{tor}(r\cdot) = -\frac{1}{r^2} P_0 \sum_{J=0}^{\infty} \tilde{\psi}_J^{(3)} \star \Psi_J \star P_{b,2},$$

i.e. the toroidal current decreases with r^{-2} which is equivalent to the simple assumption that the current decreases solely due to spherical divergence (see also [82]).

5.3 Parametrization of Toroidal Fields

In what follows, we direct our attention to the wavelet-parametrization of toroidal magnetic fields and the corresponding poloidal electric current densities in the spherical shell $\Omega_{(R_1, R_2)}$. Starting point for our considerations is a separation of variables for the toroidal field scalar Q_b , i.e. we assume that

$$Q_b(r\xi) = Q_{b,1}(r)Q_{b,2}(\xi) \text{ in } \Omega_{(R_1, R_2)}. \quad (5.19)$$

Relation (5.3) suggests to proceed likewise in the case of the scalar P_j for the poloidal currents, hence we suppose that

$$P_j(r\xi) = P_{j,1}(r)P_{j,2}(\xi) = \frac{1}{\mu_0} Q_{b,1}(r)Q_{b,2}(\xi) \text{ in } \Omega_{(R_1, R_2)}.$$

Obviously, the angular parts $Q_{b,2}$ and $P_{j,2}$ can be expanded in terms of spherical wavelets $\{\Psi_J\}$, i.e.

$$Q_{b,2} = \sum_{J=0}^{\infty} \Psi_J \star \Psi_J \star Q_{b,2}$$

$$P_{j,2} = \sum_{J=0}^{\infty} \Psi_J \star \Psi_J \star P_{j,2}.$$

Using (5.5) and (5.2) we can come up with the following result:

Theorem 5.6 *Let, for $J \in \mathbb{Z}$, $\{\Psi_J\}$ be an $\mathcal{L}^2(\Omega)$ -wavelet. Under the assumptions above, the toroidal magnetic field in $\Omega_{(R_1, R_2)}$ can be represented via*

$$b_{tor}(r \cdot) = Q_{b,1}(r) \sum_{J=0}^{\infty} \bar{\psi}_J^{(3)} \star \Psi_J \star Q_{b,2}, \quad (5.20)$$

where the kernel $\bar{\psi}_J^{(3)}$ is given via $\bar{\psi}_J^{(3)}(\xi, \eta) = L_\xi^* \Psi_J(\xi, \eta)$.

The corresponding poloidal current density in $\Omega_{(R_1, R_2)}$ is given by

$$\mu_0 j_{pol}(r \cdot) = \frac{1}{r} Q_{b,1}(r) \sum_{J=0}^{\infty} \tilde{\psi}_J^{(1)} \star \Psi_J \star Q_{b,2} + \quad (5.21)$$

$$+ (\partial_r Q_{b,1}(r) + \frac{1}{r} Q_{b,1}(r)) \sum_{J=0}^{\infty} \hat{\psi}_J^{(2)} \star \Psi_J \star Q_{b,2}, \quad (5.22)$$

where the kernel functions $\tilde{\psi}_J^{(1)}$ and $\hat{\psi}_J^{(2)}$ are defined to be $\tilde{\psi}_J^{(1)}(\xi, \eta) = \xi \Delta_\xi^* \Psi_J(\xi, \eta)$ and $\hat{\psi}_J^{(2)}(\xi, \eta) = -\nabla_\xi^* \Psi_J(\xi, \eta)$.

Theorem 5.6 can be seen in correspondence to Theorem 5.5 and presents the wavelet-parametrization of the toroidal magnetic field and the corresponding poloidal electric currents in the spherical shell $\Omega_{(R_1, R_2)}$. Obviously, this representation yields the possibility to derive different models of Q_b in different regions depending on the underlying physical effects and, of course, the data situation. It should be remarked that in [82] an explicit formula for $Q_{b,1}(r)$ is derived assuming that the currents at satellite altitudes are primarily field-aligned and that the magnetic field is, to a good approximation, dipolar. Without going into detail we quote this results in our notation:

Under the previously stated assumptions, the magnitude of the radial current density in the shell $\Omega_{(R_1, R_2)}$ is estimated by (cf. [82])

$$J_{rad}(r\xi) \simeq \xi \left(\frac{r'}{r}\right)^3 \sqrt{\frac{3}{2} - \frac{r}{2r'}} J_{rad}(r'\xi), \quad (5.23)$$

where $r\xi$ and $r'\xi$ are supposed to be two different positions located on the same magnetic field line. This then leads to the following ansatz for the radial part

$$Q_{b,1}(r) = \left(\frac{R_1}{r}\right)^2 \sqrt{\frac{3}{2} - \frac{r}{2R_1}}. \quad (5.24)$$

In order to derive (5.23) the author of [82] assumes that $r - r'$ is small and, consequently, the shift in latitude along a field line is negligible (small angle approximation). None the less, in [82] it is suggested to expand the horizontal part $Q_{b,2}$ in terms of spherical harmonics. Arguably, this is the weak point of that very approach since the spherical harmonic expansion does not really take into account the small angle approximation but connects contributions from all over the sphere. It is an interesting task for future work to numerically test (5.23)

and (5.24) in combination with the wavelet-parametrization (Theorem 5.6), since then it becomes possible to take into account regional contributions only.

It is obvious that the ansatz (5.19) is quite simple and might fail if the radial dependency is very complex (see also the considerations in [82]). Nevertheless, assumption (5.19) is reasonable as long as the data situation is such that the radial behaviour of the field is difficult to extract. This is arguably the case when using data from single satellite missions (see also the comments in [7, 82, 91] concerning time-variations and single satellite missions). Nevertheless, if the data situation allows for determination of higher order radial dependencies (e.g. if data from multi-satellite missions are used, or if measurements from satellites are combined with terrestrial observations) we might expand our ansatz by adding further toroidal scalars with different radial behaviour. In more detail, (5.19) might be replaced by

$$Q_b(r \cdot) = Q_{b,1}(r)Q_{b,2} + Q_{b,3}(r)Q_{b,4} + Q_{b,5}(r)Q_{b,6} + \dots \quad (5.25)$$

such that, following Theorem 5.6,

$$b_{tor}(r \cdot) = Q_{b,1}(r) \sum_{J=0}^{\infty} \bar{\psi}_J^{(3)} \star \Psi_J \star Q_{b,2} + \quad (5.26)$$

$$+ Q_{b,3}(r) \sum_{J=0}^{\infty} \bar{\psi}_J^{(3)} \star \Psi_J \star Q_{b,4} + \quad (5.27)$$

$$+ Q_{b,5}(r) \sum_{J=0}^{\infty} \bar{\psi}_J^{(3)} \star \Psi_J \star Q_{b,6} + \dots \quad (5.28)$$

A similar representation holds true for the current density. [91] approaches this very subject by combining the spherical harmonic parametrization of the toroidal scalar with a Taylor series for the corresponding Fourier coefficients. This is consistent with (5.26-5.28) if the radial dependencies of the radial functions $Q_{b,1}, Q_{b,3}, Q_{b,5}, \dots$ are suitably chosen. As regards practical applications, it should be noted that the wavelet-coefficients in (5.26-5.28) can, by no means, be determined by direct integration anymore but need to be simultaneously estimated using least-squares techniques. Nevertheless, the ansatz as a series representation in terms of space localizing wavelets is arguably suitable in order to determine different radial dependencies in different regions of interest.

The product ansatz for the toroidal field scalar Q_b is reflected in the corresponding toroidal magnetic field (see (5.20)) as well as in the representation of the corresponding poloidal current density. As regards the poloidal current, both its radial (5.21) and its tangential parts (5.22) admit a product representation, too. In more detail, let j_{rad} and j_{∇^*} be the radial and the tangential parts of j_{pol} , respectively. Then it is straightforward that j_{rad} and j_{∇^*} can be represented as

$$j_{rad}(r\xi) = J_{rad,1}(r)j_{rad,2}(\xi)$$

and

$$j_{\nabla^*}(r\xi) = J_{\nabla^*,1}(r)j_{\nabla^*,2}(\xi).$$

In this context, Theorem 5.6 yields that the scalars $J_{rad,1}(r)$ and $J_{\nabla^*,1}(r)$ are given via

$$\begin{aligned}\mu_0 J_{rad,1}(r) &= \frac{1}{r} Q_{b,1}(r), \\ \mu_0 J_{\nabla^*,1}(r) &= (\partial_r Q_{b,1}(r) + \frac{1}{r} Q_{b,1}(r))\end{aligned}$$

and the vectorial parts are

$$\begin{aligned}\mu_0 j_{rad,2} &= \sum_{J=0}^{\infty} \tilde{\psi}_J^{(1)} \star \Psi_J \star Q_{b,2}, \\ \mu_0 j_{\nabla^*,2} &= \sum_{J=0}^{\infty} \hat{\psi}_J^{(2)} \star \Psi_J \star Q_{b,2}.\end{aligned}$$

Using the ansatz (5.19) together with (5.6) immediately leads us to the same results for $J_{rad,1}$ and $J_{\nabla^*,1}$ but, as regards $j_{rad,2}$ and $j_{\nabla^*,2}$, we end up with

$$\begin{aligned}\mu_0 j_{rad,2}(\xi) &= \xi \Delta_\xi^* Q_{b,2}(\xi), \\ \mu_0 j_{\nabla^*,2}(\xi) &= -\nabla_\xi^* Q_{b,2}(\xi),\end{aligned}$$

which is independent from any parametrization of Q_b . From Section 2.2, however, we know that we can expand the radial vector field $\mu_0 j_{rad,2}$ and the tangential vector field $\mu_0 j_{\nabla^*,2}$ using vectorial $l^2(\Omega)$ -wavelets $\{\psi_J^{(i)}\}$ of type $i = 1$ and $i = 2$, respectively. Consequently we are led to the following alternative representation in terms of $l^2(\Omega)$ -wavelets, i.e.

$$\mu_0 j_{rad}(r \cdot) = \mu_0 \sum_{J=0}^{\infty} \psi_J^{(1)} \star \left(\psi_J^{(1)} \star j_{rad} \right) (r) \quad (5.29)$$

$$= \mu_0 \frac{1}{r} Q_{b,1}(r) \sum_{J=0}^{\infty} \psi_J^{(1)} \star \psi_J^{(1)} \star j_{rad,2} \quad (5.30)$$

$$= \mu_0 \sum_{J=0}^{\infty} \psi_J^{(1)} \star \left(\psi_J^{(1)} \star j \right) (r), \quad (5.31)$$

and

$$\mu_0 j_{\nabla^*}(r \cdot) = \mu_0 \sum_{J=0}^{\infty} \psi_J^{(2)} \star \left(\psi_J^{(2)} \star j_{\nabla^*} \right) (r) \quad (5.32)$$

$$= \mu_0 \left(\partial_r Q_{b,1}(r) + \frac{1}{r} Q_{b,1}(r) \right) \sum_{J=0}^{\infty} \psi_J^{(2)} \star \psi_J^{(2)} \star j_{\nabla^*,2} \quad (5.33)$$

$$= \mu_0 \sum_{J=0}^{\infty} \psi_J^{(2)} \star \left(\psi_J^{(2)} \star j \right) (r), \quad (5.34)$$

Note that equations (5.31) and (5.34) are true since only the poloidal current density does contain a radial or ∇^* -contribution (see (5.6)) and therefore we can state that

$$\mu_0 j_{rad}(r \cdot) = \mu_0 \sum_{J=0}^{\infty} \psi_J^{(1)} \star \left(\psi_J^{(1)} \star j_{rad} \right) (r) = \mu_0 \sum_{J=0}^{\infty} \psi_J^{(1)} \star \left(\psi_J^{(1)} \star j \right) (r),$$

and

$$\mu_0 j_{\nabla^*}(r \cdot) = \mu_0 \sum_{J=0}^{\infty} \psi_J^{(2)} \star \left(\psi_J^{(2)} \star j_{\nabla^*} \right) (r) = \mu_0 \sum_{J=0}^{\infty} \psi_J^{(2)} \star \left(\psi_J^{(2)} \star j \right) (r),$$

on each Ω_r with $R_1 < r < R_2$. In other words the radial current density (on each Ω_r with $R_1 < r < R_2$) can be derived from expanding the total current density in terms of spherical vectorial wavelets of type $i = 1$ while the tangential part of the poloidal current density can be calculated via spherical vectorial wavelets of type $i = 2$. Equations (5.29-5.34) can therefore be used to determine the toroidal field scalar (or, of course, the corresponding toroidal magnetic field) in a comparatively easy way. If we suppose the current density j to be given on a dense grid covering the whole spherical shell $\Omega_{(R_1, R_2)}$, then an – to some degree – easy method to obtain $Q_{b,1}(r)$ and $Q_{b,2}(\xi)$ is the following:

- (1) For a sequence of spheres Ω_{r_l} of radii r_l , $l = 0, 1, \dots, l_{max}$, with $R_1 < r_0 < r_1 < \dots < r_{l_{max}} < R_2$, a wavelet expansion of the current density j is performed in terms of spherical vectorial wavelets of type $i = 1$ up to an appropriate maximum scale J_{max} (i.e. (5.31) is computed). From the wavelet expansions on the spheres with radii r_l the values of $Q_{b,1}(r_l)$ are determined via (5.30) and then interpolated to obtain $Q_{b,1}(r)$.
- (2) In a second step the wavelet coefficients $\psi_J^{(1)} \star j_{rad,2}$ are calculated from the wavelet coefficients $\left(\psi_J^{(1)} \star j \right) (r_l)$ of the current density on one sphere Ω_{r_l} via

$$\frac{1}{r_l} Q_{b,1}(r_l) \left(\psi_J^{(1)} \star j_{rad,2} \right) = \left(\psi_J^{(1)} \star j \right) (r_l)$$

(see (5.30-5.31)).

- (3) From (5.6) and (5.30) it is clear that

$$\xi(\Delta_\xi^* Q_{b,2}(\xi)) \simeq \left(\sum_{J=0}^{J_{max}} \psi_J^{(1)} \star \psi_J^{(1)} \star j_{rad,2} \right) (\xi)$$

and therefore

$$\Delta_\xi^* Q_{b,2}(\xi) \simeq \left(\sum_{J=0}^{J_{max}} \Psi_J \star \psi_J^{(1)} \star j_{rad,2} \right) (\xi), \quad (5.35)$$

where $\Psi_J(\xi, \eta) = \xi \cdot \psi_J^{(1)}(\eta, \xi)$ is given by

$$\Psi_J(\xi, \eta) = \sum_{(n,k) \in \mathcal{N}^{(1)}} \left(\psi_J^{(1)} \right)^\wedge (n) Y_{n,k}(\xi) Y_{n,k}(\eta).$$

Equation (5.35) is the well known Beltrami differential equation and can be solved by means of the corresponding Green's function which is explicitly known (cf. [30]).

A similar approach can be applied in order to determine the poloidal current density j_{pol} in $\Omega_{(R_1, R_2)}$ from the corresponding toroidal field b_{tor} . Assuming the product ansatz for Q_b and applying (5.5) we see that the toroidal magnetic field admits a product representation as well (see also Theorem 5.6), i.e.

$$b_{tor}(r\xi) = B_{tor,1}(r)b_{tor,2}(\xi)$$

where $b_{tor,2} = L^*Q_{b,2}$ can be expressed in terms of spherical vectorial $l^2(\Omega)$ -wavelets $\{\psi_J^{(3)}\}$ of type $i = 3$ as follows

$$b_{tor,2} = \sum_{J=0}^{\infty} \psi_J^{(3)} \star \psi_J^{(3)} * b_{tor,2}. \quad (5.36)$$

We know from Theorem 5.6 that the scalar $B_{tor,1}$ is just given by

$$B_{tor,1}(r) = Q_{b,1}(r).$$

Since the toroidal magnetic field b_{tor} is the only part of b that contributes a L^* -portion it is clear that

$$b_{tor}(r\cdot) = \sum_{J=0}^{\infty} \psi_J^{(3)} \star \left(\psi_J^{(3)} * b_{tor} \right) (r) = \sum_{J=0}^{\infty} \psi_J^{(3)} \star \left(\psi_J^{(3)} * b \right) (r),$$

on any sphere Ω_r with $R_1 < r < R_2$. Summarizing the above considerations we are led to

$$b_{tor}(r\cdot) = Q_{b,1}(r) \sum_{J=0}^{\infty} \psi_J^{(3)} \star \psi_J^{(3)} * b_{tor,2} = \sum_{J=0}^{\infty} \psi_J^{(3)} \star \left(\psi_J^{(3)} * b \right) (r) \quad (5.37)$$

on any sphere Ω_r with $R_1 < r < R_2$. This yields one possible way of determining the poloidal field scalar (and consequently the corresponding poloidal electric current density) from magnetic measurements in $\Omega_{(R_1, R_2)}$. In what follows, we assume the geomagnetic field to be sampled on a dense grid throughout the whole spherical shell $\Omega_{(R_1, R_2)}$.

- (1) For a sequence of spheres Ω_{r_l} of radii r_l , $l = 0, 1, \dots, l_{max}$, with $R_1 < r_0 < r_1 < \dots < r_{l_{max}} < R_2$, a wavelet expansion of the magnetic field b is performed in terms of spherical vectorial wavelets of type $i = 3$ up to an appropriate maximum scale J_{max} (i.e. the right hand side of (5.37) is computed). From the wavelet expansions on the spheres with radii r_l the values of $Q_{b,1}(r_l)$ are determined and then interpolated to obtain $Q_{b,1}(r)$.

- (2) The second step consists of calculating the coefficients $\psi_J^{(3)} * b_{tor,2}$ from the coefficients $\left(\psi_J^{(3)} * b \right) (r_l)$ on one fixed sphere Ω_{r_l} via

$$Q_{b,1}(r_l) \psi_J^{(3)} * b_{tor,2} = \left(\psi_J^{(3)} * b \right) (r_l)$$

(see (5.37)).

(3) Finally, since $b_{tor,2} = L^*Q_{b,2} = \sum_{J=0}^{\infty} \psi_J^{(3)} \star \psi_J^{(3)} * b_{tor,2}$, we can state that

$$Q_{b,2}(\xi) \simeq \sum_{J=0}^{J_{max}} \Psi_J * \psi_J^{(3)} * b_{tor,2},$$

where the kernels $\Psi_J(\xi, \eta)$ are constructed such that $\psi_J^{(3)}(\eta, \xi) = L_\xi^* \Psi_J(\eta, \xi)$, i.e.

$$\Psi_J(\eta, \xi) = \sum_{(n,k) \in \mathcal{N}^{(3)}} \frac{1}{\sqrt{n(n+1)}} \left(\psi_J^{(3)} \right)^\wedge (n) Y_{n,k}(\eta) Y_{n,k}(\xi). \quad (5.38)$$

Finally, neglecting radial dependencies, the previous approach can be simplified and easily applied to calculate radial current densities on a sphere Ω_r , with $R_1 < r < R_2$, from measurements of the magnetic field on that very sphere. We assume that the magnetic field b is sampled on a dense grid on the sphere Ω_r . We have already made use of the fact that, with a suitably chosen maximum scale J_{max} , we can approximate the toroidal part b_{tor} on Ω_r via a series expansion in terms of $l^2(\Omega)$ -wavelets

$$b_{tor}(r\xi) \simeq \left(\sum_{J=0}^{J_{max}} \psi_J^{(3)} \star \left(\psi_J^{(3)} * b \right) (r) \right) (\xi).$$

Using the fact that $b_{tor}(r, \cdot) = L^*Q_b$ we immediately get an approximation for the toroidal scalar, i.e.

$$Q_b(r\xi) \simeq \left(\sum_{J=0}^{J_{max}} \Psi_J * \left(\psi_J^{(3)} * b \right) (r) \right) (\xi) \quad (5.39)$$

where, as before, the kernel is given by (5.38), i.e. it holds that $\psi_J^{(3)}(\eta, \xi) = L_\xi^* \Psi_J(\eta, \xi)$. Using (5.39) together with (5.6) we arrive at an approximation of the radial current density on Ω_r corresponding to the toroidal magnetic field there:

$$\begin{aligned} \mu_0 j_{rad}(r\xi) &= \frac{1}{r} \xi \Delta_\xi^* Q_b(r\xi) \\ &\simeq \frac{1}{r} \left(\sum_{J=0}^{J_{max}} \tilde{\psi}_J^{(1)} * \left(\psi_J^{(3)} * b \right) (r) \right) (\xi), \end{aligned} \quad (5.40)$$

with $\tilde{\psi}_J^{(1)}(\eta, \xi) = \xi \Delta_\xi^* \Psi_J(\eta, \xi)$, i.e.

$$\tilde{\psi}_J^{(1)}(\eta, \xi) = \sum_{(n,k) \in \mathcal{N}^{(3)}} -\sqrt{n(n+1)} \left(\psi_J^{(3)} \right)^\wedge (n) Y_{n,k}(\eta) y_{n,k}^{(1)}(\xi).$$

Note that this equation is just a different expression of a well known fact, i.e. the toroidal magnetic field at a certain altitude is solely due to the radial current distributions at that very height. It is Equation (5.40) that serves as the starting point for the numerical example in the next section.

5.4 Example

As an example of the wavelet parametrization of the magnetic field, electric current distributions at satellite altitudes are determined from data sets of vectorial MAGSAT data. The method is based on our considerations in Section 5.3, especially Equation (5.40). In [91] a similar technique, in terms of spherical harmonics however, is applied to MAGSAT data, too. The current distributions under consideration are due to ionospheric F region currents which are extensively treated in the literature (see [91] and the references therein).

The data sets used in this example are similar to those used in [91]. They have kindly been made available to us by the author of [91] who has also carried out the preprocessing and averaging processes. MAGSAT was orbiting the Earth in a Sun synchronous orbit thus acquiring only data at dawn and dusk local times. Neglecting the variations in altitude of the MAGSAT satellite, one month of MAGSAT data (centered at March 21, 1980) is transformed to geomagnetic components and is then averaged onto the equiangular longitude-latitude grid (90×90 grid points) proposed in [20], which has already been used in Sections 3.3 and 4.1.4. Averaging the data onto the nodal points of the integral formula is performed using a robust Tuckey's biweight method (cf. [59]). The dusk and dawn data are treated separately such that two separate data sets are obtained. Prior to the averaging process a geomagnetic field model (GSFC(12/83) up to degree and order 12) due to [75] is subtracted from the measurements in order to avoid spurious effects due to the neglected altitude variations (cf. [91]).

According to Equation (5.40) the radial current distribution at a fixed height can be calculated from the wavelet coefficients of the toroidal field at that altitude, i.e. $(\psi_J^{(3)} * b)(r)$. As regards the present example, we calculate these coefficients by means of spherical vectorial cubic polynomial (CP) wavelets up to scale 5 from the evening data set. Then, in a second step, these coefficients are utilized to calculate the corresponding radial current distribution in accordance with Equation (5.40). Figures 5.1 and 5.2 show the reconstruction of the radial current density $J_{rad} = (\xi \cdot j_{rad}(\xi))$ using two different color-scales in order to enhance the visibility of the appearing features. The largest radial current densities ($|J_{rad}| \lesssim 150$ nA/m²) are present in the polar regions. In agreement with the results in [91] the main current flow in the polar cap is directed into the ionosphere ($J_{rad} < 0$) during evening. At the poleward boundary of the polar oval the currents flow out of the ionosphere ($J_{rad} > 0$) while the main current direction is into the ionosphere at the equatorward boundary. At the magnetic dip equator one realizes comparatively weak upward currents ($|J_{rad}| \lesssim 25$ nA/m²) accompanied by even weaker downward currents at low latitudes. These current distributions are the radial components of the so-called meridional current system of the equatorial electrojet. Following the discussion in [91] Figure 5.3 presents the same results as Figures 5.1 and 5.2 but in a different projection, thus enabling a better view of the meridional currents. As can be expected from theoretical considerations, the corresponding signatures follow the geomagnetic dip equator.

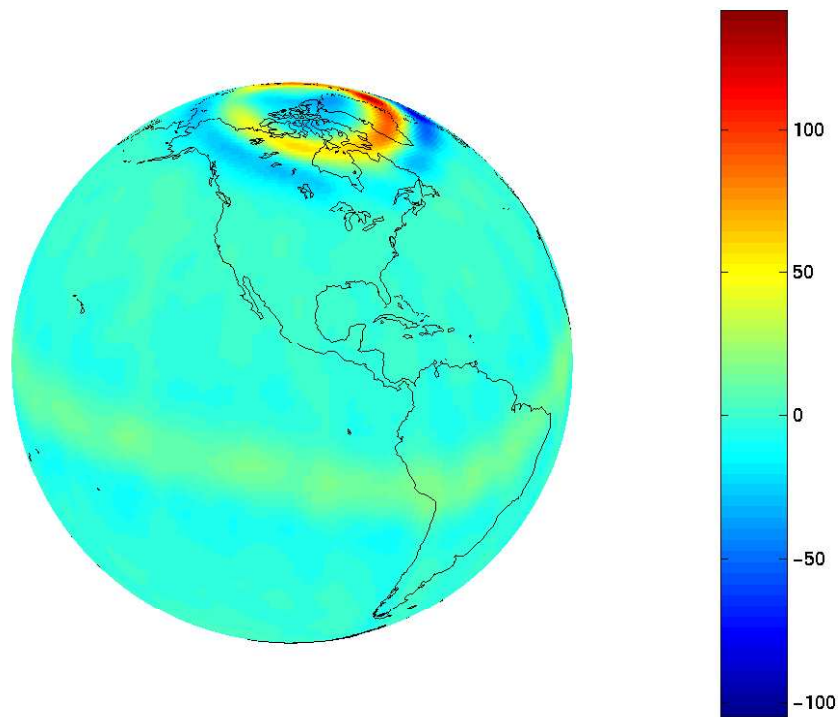


Figure 5.1: Radial current density during evening local time obtained from a vectorial cubic polynomial wavelet expansion of MAGSAT data up to scale 5 [nA/m^2].

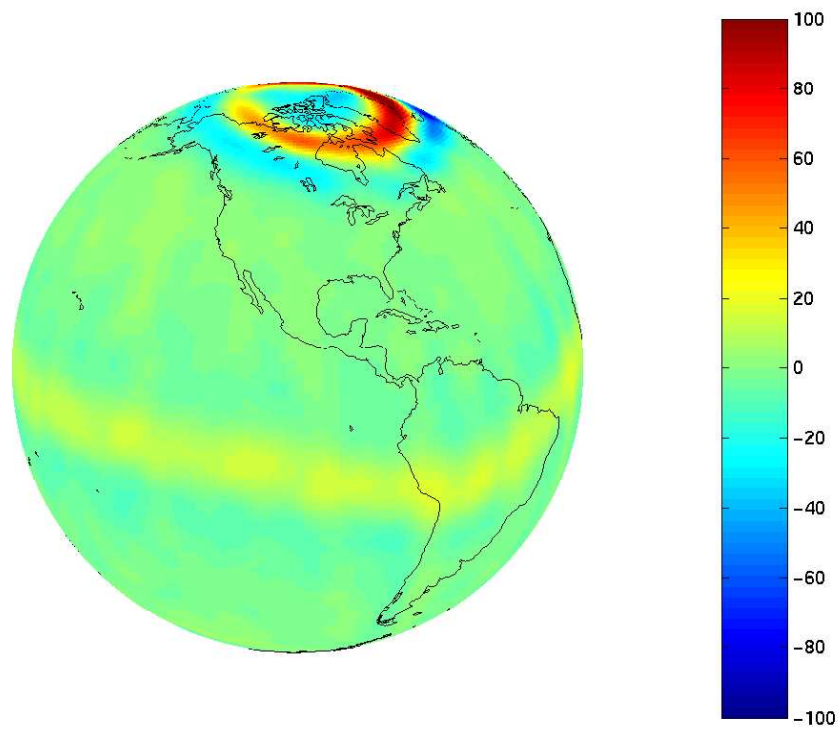


Figure 5.2: Radial current density during evening local time obtained from a vectorial cubic polynomial wavelet expansion of MAGSAT data up to scale 5. [nA/m^2]

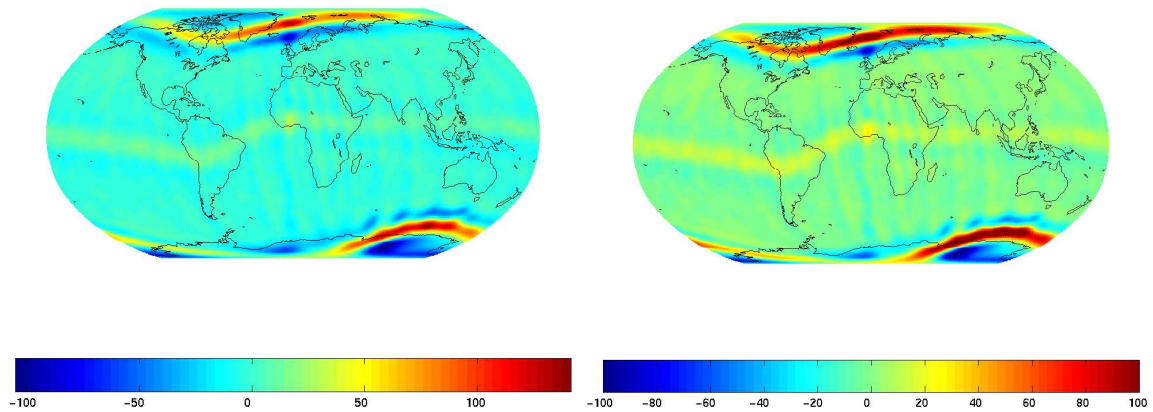


Figure 5.3: Radial current density during evening local time obtained from a vectorial cubic polynomial wavelet expansion of MAGSAT data up to scale 5; left and right differ in the color-scales used. [nA/m^2]

In order to demonstrate the possibility of regional calculations again, Figure 5.4 presents a reconstruction of the radial current systems during dusk local times over the polar region. These results are obtained using vectorial cubic polynomial wavelets of scales 4 and 5 and a data window centered at the geographic north pole with a half angle of 60° as well as an integration window with the same center but a half angle of 55° (the white border approximately illustrates the extend of the calculation region). As we have indicated in Section 4.1.4, the visualization window is smaller than the calculation window in order to suppress Gibbs phenomena.

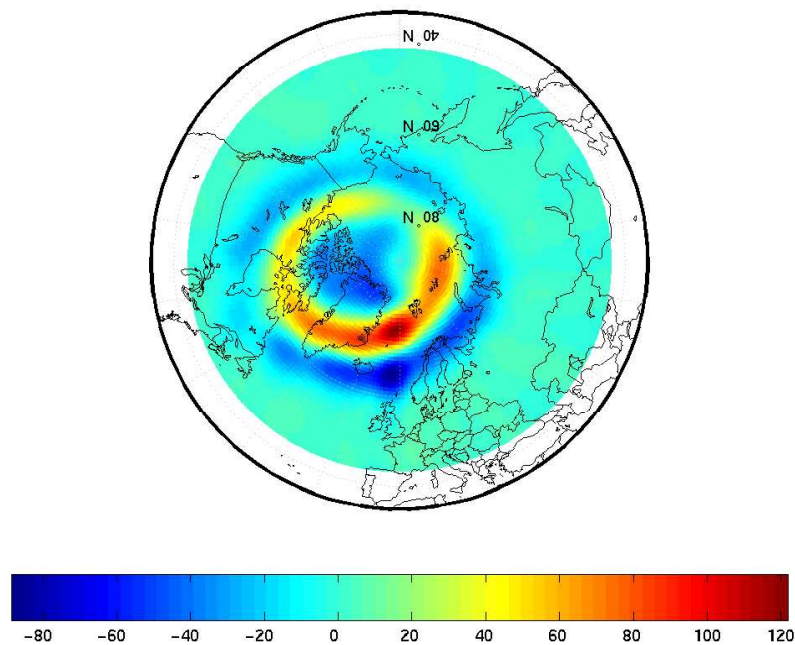


Figure 5.4: Local reconstruction of radial current density during evening local time obtained from a vectorial cubic polynomial wavelet expansion of MAGSAT data at scales 4 and 5. The white area corresponds to the calculation region. [nA/m^2]

Comparing Figure 5.4 with Figures 5.1 or 5.2 shows that the structures of the radial currents are clearly visible though slightly weaker in magnitude. This slight difference is due to the fact that we have omitted the contributions of wavelet scales up to 3. Consequently, the signatures seen in our results are clearly effects of higher wavelet scales (4 and 5) and the contributions of lower scales can be neglected. This, however, demonstrates the regional character of the radial current distributions and suggests the use of regional methods like the one presented here.

Finally, for the sake of completeness, we present a global reconstruction of the radial current densities during morning local time (Figure 5.5). This result is obtained from the dawn data

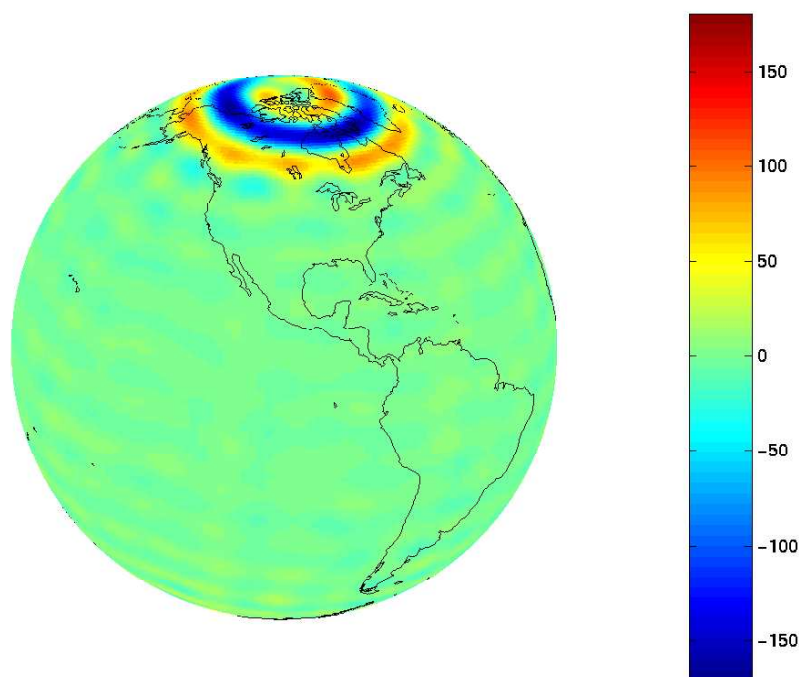


Figure 5.5: Radial current density during morning local time obtained from a vectorial Shannon wavelet expansion of MAGSAT data up to scale 4. [nA/m^2]

set by means of vectorial Shannon wavelets up to scales 4. As expected, in the polar regions the current direction during morning local time is reversed with respect to the dusk data. The meridional current system of the equatorial electrojet is not present in the dawn data set.

As regards future studies, the next reasonable step is to incorporate the variations in altitude of the satellite – at least to some extent – in the analysis of electric current distributions. This would allow for the determination of horizontal current distributions, as well. Furthermore, it is an interesting task to derive – either in studies using synthetic data, or based on satellite data sampled over large time intervals, or using data from multi satellite missions – a wavelet parametrization of the poloidal and toroidal magnetic fields from the corresponding electric currents or vice versa. This, however, is beyond the scope of this thesis.

It should be noted that within the Graduiertenkolleg "Mathematik und Praxis" (Graduate

Research Training Programme "Mathematics and Practice"), Dipl.-Math. C. Mayer, Geomathematics Group, University of Kaiserslautern, prepares his PhD thesis in the project "Modelling of Ionospheric Current Systems". He is especially concerned with the determination and modelling of electric current densities from geomagnetic satellite measurements. In this context techniques similar to those presented here are derived and applied to various data sets. It is surely an interesting task for future studies to compare his approaches to the methods of this chapter and to eventually combine both techniques.

Chapter 6

Multiscale Methods for the Analysis of Time-Dependent Spherical Vector Fields

Besides its spatial variations, the geomagnetic field is subject to a variety of fluctuations on a wide range of time scales, as manifold as the responsible physical processes. Due to its dynamo action the Earth's core, for example, contributes geomagnetic variations on time scales of years up to more than several centuries – the secular-variation is one of the most prominent examples thereof. The Earth's electromagnetic environment is also a source of a diversity of geomagnetic fluctuations spanning the whole range from milliseconds to days – well known examples of the latter are the Sq- and Dst-variations. The reader interested in the many geophysical processes and the resulting temporal fluctuations might, for instance, consult [66, 67, 68, 69, 70] and the references therein.

The standard method for approaching the time-dependency of the geomagnetic field is to assume the existence of a corresponding scalar potential which then is expressed in terms of spherical harmonics with time-dependent Fourier coefficients. The temporal variation of the field is therefore fully carried over to the temporal behaviour of the expansion coefficients. Depending on the processes under consideration there exist several sophisticated techniques of modelling the evolution of the Fourier coefficients in time; [66] presents a general introduction, for up-to-date overviews and applications the reader is directed to e.g. [77, 93, 96] and the references therein.

What we introduce here are two variants of a technique combining a wavelet approach for the temporal as well as the spatial domain. We therefore assume that the (spherical) vector field under consideration can be expanded in terms of vector spherical harmonics with time-dependent Fourier coefficients or, in other words, we also assume that the time-dependency of the vector field is fully represented by its expansion coefficients with respect to vector spherical harmonics. Though we will not need to calculate the expansion explicitly, this assumption helps us to find the appropriate multiscale technique for the temporal domain – Legendre kernels – and the spatial domain – spherical vectorial kernels. This combination

of different wavelet techniques will enable us to approximate all different combinations of temporal and spatial variations, e.g. small or large scale temporal variations combined with global or regional spatial effects. It is clear that this (especially the combination of regional spatial effects with different temporal variations) can only be achieved if the data situation is appropriate, a prerequisite that can, most probably, not be met by measurements of single satellite missions. Nevertheless, our approach can be seen as a first step into the direction of the newly planned multi-satellite mission SWARM. The scientific aims of the SWARM mission are the sophisticated separation of the various field sources and, what is more important in the context of this chapter, the accurate determination of the spatial and temporal structure of the geomagnetic field achieved by a constellation of four to six satellites with high-precision magnetometers. This multi-point principle will lead to measurements of relatively high temporal resolution complementary to those of single-satellite missions (for more information on the SWARM mission see e.g. <http://www.dsri.dk/swarm>).

Variant 1, presented in Section 6.1 is inspired by the time-space approach for scalar fields given in [86] and finally leads to similar results as variant 2 of Section 6.2, a technique based on the principle of tensor-product wavelets (see e.g. [79, 80] and, closely related to our approach, [101]).

6.1 Time-Space-Multiscale Approach: Variant 1

Without loss of generality we suppose the time interval under consideration to be transformed to the unit interval $[-1, 1]$. Consequently, we consider elements of the space $l^2(\Omega \times [-1, 1])$ when we refer to time-dependent vector fields. The corresponding norm is given by

$$\|f\|_{l^2(\Omega \times [-1, 1])} = \left(\int_{-1}^1 \int_{\Omega} (f(\xi, t) \cdot f(\xi, t)) \, d\omega(\xi) dt \right)^{1/2}, \quad f \in l^2(\Omega \times [-1, 1]).$$

As usual, for fixed $t \in [-1, 1]$, any $f \in l^2(\Omega \times [-1, 1])$ can be represented by its Fourier series with respect to $\|\cdot\|_{l^2(\Omega)}$, i.e.

$$f(\cdot, t) = \sum_{i=1}^3 \sum_{n=0_i}^{\infty} \sum_{k=1}^{2n+1} (f^{(i)})^{\wedge}(n, k)(t) y_{n,k}^{(i)}(\cdot). \quad (6.1)$$

It is clear that the same holds true for every time dependent vector field of type $i \in \{1, 2, 3\}$ and therefore we introduce the spaces $l_{(i)}^2(\Omega \times [-1, 1])$, for $i \in \{1, 2, 3\}$, such that

$$l^2(\Omega \times [-1, 1]) = \bigoplus_{i=1}^3 l_{(i)}^2(\Omega \times [-1, 1]).$$

Note that Equation (6.1) shows that, in the spectral domain, the time-dependency of the vector field under consideration is transferred to its Fourier coefficients. As regards this subject the following lemma will help us find the appropriate multiscale technique for dealing with the time-dependency:

Lemma 6.1 *Let $f \in l^2(\Omega \times [-1, 1])$. Then the corresponding Fourier coefficients fulfill*

$$(f^{(i)})^\wedge(n, k)(\cdot) \in \mathcal{L}^2([-1, 1]), \quad i \in \{1, 2, 3\}, \quad (n, k) \in \mathcal{N}^{(i)}.$$

Proof. Since $f \in l^2(\Omega \times [-1, 1])$ we now that

$$\int_{-1}^1 \int_{\Omega} (f(\xi, t) \cdot f(\xi, t)) \, d\omega(\xi) dt < \infty.$$

This is equivalent to

$$\begin{aligned} & \int_{-1}^1 \|f(\cdot, t)\|_{l^2(\Omega)}^2 \, dt < \infty \\ \Leftrightarrow & \int_{-1}^1 \sum_{i=1}^3 \sum_{n=0_i}^{\infty} \sum_{k=1}^{2n+1} ((f^{(i)})^\wedge(n, k)(t))^2 < \infty. \end{aligned}$$

But then it is clear that

$$\int_{-1}^1 ((f^{(i)})^\wedge(n, k)(t))^2 \, dt < \infty.$$

■

In Section 2.1.6 we have already introduced the use of Legendre scaling functions and wavelets as a multiscale technique appropriate for dealing with functions in $\mathcal{L}^2([-1, 1])$. Therefore, we may define temporal scaling functions and wavelets as follows:

Definition 6.2 *Assume, for $J \in \mathbb{Z}$, $\{(\Phi_J)^\wedge(n)\}_{n=0,1,\dots}$ to be the generating symbol of an $\mathcal{L}^2([-1, 1])$ -scaling function and let $\{(\Psi_J)^\wedge(n)\}_{n=0,1,\dots}$ be the generating symbol of the associated $\mathcal{L}^2([-1, 1])$ -wavelet. Then the temporal scaling functions $\{\Phi_{temp,J}\}$ and wavelets $\{\Psi_{temp,J}\}$ of scale J are defined by*

$$\begin{aligned} \Phi_{temp,J}(s, t) &= \sum_{n=0}^{\infty} \Phi_J^\wedge(n) P_n^*(s) P_n^*(t), \quad s, t \in [-1, 1], \\ \Psi_{temp,J}(s, t) &= \sum_{n=0}^{\infty} \Psi_J^\wedge(n) P_n^*(s) P_n^*(t), \quad s, t \in [-1, 1], \end{aligned}$$

respectively.

The corresponding temporal convolutions are given by the $\mathcal{L}^2([-1, 1])$ -convolutions as presented in Section 2.1.6.

As regards the spatial domain, Chapter 2 – especially Section 2.2.4 – provides us with the necessary kernel functions, i.e. the spherical vector scaling functions and wavelets will serve as the spatial kernels. In this context, the following lemma will be helpful.

Lemma 6.3 *Let the families $\{\varphi_J^{(i)}\}$, $\{\psi_J^{(i)}\}$, $i \in \{1, 2, 3\}$, $J \in \mathbb{Z}$, be a spherical vector scaling function and the associated spherical vector wavelet, respectively. Then*

$$\int_{-1}^1 \left(\varphi_J^{(i)} \star \varphi_J^{(i)} * f(\cdot, t) \right)^2 dt < \infty$$

as well as

$$\int_{-1}^1 \left(\psi_J^{(i)} \star \psi_J^{(i)} * f(\cdot, t) \right)^2 dt < \infty$$

hold true.

Proof. We start with the scaling function. From our treatment so far we know

$$\begin{aligned} & \int_{-1}^1 \left(\varphi_J^{(i)} \star \varphi_J^{(i)} * f(\cdot, t) \right)^2 dt \\ &= \int_{-1}^1 \left(\sum_{(n,k) \in \mathcal{N}^{(i)}} \left((\varphi_J^{(i)})^\wedge(n) \right)^2 \underbrace{(f^{(i)})^\wedge(n,k)(t) y_{n,k}^{(i)}(\xi)}_{\in \mathcal{L}^2([-1,1])} \right)^2 dt \\ &= \sum_{(n,k) \in \mathcal{N}^{(i)}} \sum_{(l,m) \in \mathcal{N}^{(i)}} \left((\varphi_J^{(i)})^\wedge(n) \right)^2 \left((\varphi_J^{(i)})^\wedge(l) \right)^2 y_{n,k}^{(i)}(\xi) y_{l,m}^{(i)}(\xi) \\ & \quad \cdot \int_{-1}^1 (f^{(i)})^\wedge(n,k)(t) (f^{(i)})^\wedge(l,m)(t) dt. \end{aligned}$$

But

$$\begin{aligned} & \int_{-1}^1 (f^{(i)})^\wedge(n,k)(t) (f^{(i)})^\wedge(l,m)(t) dt \\ &= \int_{-1}^1 \int_{\Omega} f(\xi, t) \cdot y_{n,k}^{(i)}(\xi) d\omega(\xi) \int_{\Omega} f(\xi, t) \cdot y_{l,m}^{(i)}(\xi) d\omega(\xi) dt \\ &\leq \left(\int_{-1}^1 \left(\int_{\Omega} f(\xi, t) \cdot y_{n,k}^{(i)}(\xi) d\omega(\xi) \right)^2 dt \right)^{1/2} \left(\int_{-1}^1 \left(\int_{\Omega} f(\xi, t) \cdot y_{l,m}^{(i)}(\xi) d\omega(\xi) \right)^2 dt \right)^{1/2} \end{aligned}$$

$$\begin{aligned}
&\leq \left(\int_{-1}^1 \int_{\Omega} (f(\xi, t))^2 d\omega(\xi) \underbrace{\int_{\Omega} (y_{n,k}^{(i)}(\xi))^2 d\omega(\xi)}_{=1} dt \right)^{1/2} \\
&\quad \cdot \left(\int_{-1}^1 \int_{\Omega} (f(\xi, t))^2 d\omega(\xi) \underbrace{\int_{\Omega} (y_{l,m}^{(i)}(\xi))^2 d\omega(\xi)}_{=1} dt \right)^{1/2} \\
&= \|f\|_{l^2(\Omega \times [-1,1])}^2.
\end{aligned}$$

Therefore,

$$\begin{aligned}
&\int_{-1}^1 \left(\varphi_J^{(i)} \star \varphi_J^{(i)} \star f(\cdot, t) \right)^2 dt \\
&\leq \|f\|_{l^2(\Omega \times [-1,1])}^2 \sum_{(n,k) \in \mathcal{N}^{(i)}} \sum_{(l,m) \in \mathcal{N}^{(i)}} \left| \left((\varphi_J^{(i)})^{\wedge(n)} \right)^2 \left((\varphi_J^{(i)})^{\wedge(l)} \right)^2 \right| |y_{n,k}^{(i)}(\xi) \cdot y_{l,m}^{(i)}(\xi)| \\
&= \|f\|_{l^2(\Omega \times [-1,1])}^2 \cdot \left(\sum_{(n,k) \in \mathcal{N}^{(i)}} \left((\varphi_J^{(i)})^{\wedge(n)} \right)^2 |y_{n,k}^{(i)}(\xi)| \right)^2.
\end{aligned}$$

From [30] we know that

$$|y_{n,k}^{(i)}(\xi)|^2 \leq \frac{2n+1}{4\pi}.$$

Together with the admissibility of the generating symbol $\left\{ (\varphi_J^{(i)})^{\wedge(n)} \right\}$ this guarantees that the last sum is finite such that the proof is complete. The proof for the wavelet part can be done analogously. ■

Hence, we are now in a position to combine the spatial ($l^2(\Omega)$ -product kernels) and the temporal ($\mathcal{L}^2([-1,1])$ -product kernels) approach. In order to keep the following treatment clear, we introduce an auxiliary convolution:

Definition 6.4 *Let K be a $\mathcal{L}^2([-1,1])$ -product kernel and let $k^{(i)}$ be a $l^2(\Omega)$ -product kernel of type $i \in \{1, 2, 3\}$. Then, for $f \in l^2(\Omega \times [-1,1])$, the convolution*

$$K * K * (k^{(i)} \star k^{(i)} \star f) \tag{6.2}$$

is understood in the following sense:

$$\begin{aligned}
& K * K * (k^{(i)} \star k^{(i)} * f) \\
&= K^{(2)} * (k^{(i)} \star k^{(i)} * f) \\
&= \int_{-1}^1 K(\cdot, s) \sum_{(n,k) \in \mathcal{N}^{(i)}} ((k^{(i)})^\wedge(n))^2 ((f^{(i)})^\wedge(n, k))(s) y_{n,k}^{(i)} ds \\
&= \sum_{(n,k) \in \mathcal{N}^{(i)}} ((k^{(i)})^\wedge(n))^2 y_{n,k}^{(i)} \int_{-1}^1 K^{(2)}(\cdot, s) ((f^{(i)})^\wedge(n, k))(s) ds \\
&= \sum_{(n,k) \in \mathcal{N}^{(i)}} \sum_{m=0}^{\infty} ((k^{(i)})^\wedge(n)(K)^\wedge(m))^2 ((f^{(i)})^\wedge(n, k))^\wedge(m) y_{n,k}^{(i)} P_m^*.
\end{aligned}$$

That is, the convolution of the temporal kernels is not meant to be acting on the vector field (which is not defined in the sense of the convolutions presented in Chapter 2), but on its time-dependent Fourier coefficients w.r.t. vector spherical harmonics (note that interchanging sum and integral is guaranteed by the Beppo-Levi theorem). However, concerning Definition 6.4 a remark is indicated since we do not suppose the Fourier coefficients of the vector field under consideration to be known.

Remark 6.5 *From a purely mathematical point of view Definition 6.4 is justified and satisfactory. From a practical point of view, however, (6.2) cannot be computed from a given function f since the series expansion in terms of vector spherical harmonics is not known and – what is yet more important – is not even wanted for we intend to use expansions in terms of scaling functions and wavelets. Nevertheless, Definition 6.4 will be used in the following treatment since it helps us keeping the upcoming proofs clear and straightforward. For practical applications, however, the right way to perform the convolutions is given by*

$$k^{(i)} \star (K * K * (k^{(i)} * f)),$$

which can be calculated directly from any given function $f \in l^2(\Omega \times [-1, 1])$ in terms of the convolutions defined in Chapter 2. It is easy to show that

$$K * K * (k^{(i)} \star k^{(i)} * f) = k^{(i)} \star (K * K * (k^{(i)} * f))$$

holds true.

Having the necessary tools at hand, we can now turn to the definitions of scale and detail spaces in the combined temporal and spatial multiscale approach:

Definition 6.6 Let the families $\{\Phi_{temp,j_1}\}$ and $\{\Psi_{temp,j_1}\}$, $j_1 \in \mathbb{Z}$, of $\mathcal{L}^2([-1,1])$ -product kernels be temporal scaling functions and wavelets, respectively. Furthermore, the families of $l^2(\Omega)$ -product kernels $\{\varphi_{j_2}^{(i)}\}$ and $\{\psi_{j_2}^{(i)}\}$, $i \in \{1, 2, 3\}$, $j_2 \in \mathbb{Z}$, are supposed to be spherical vector scaling functions and wavelets, respectively. Then the time-space scale spaces (6.3) and the time-space detail spaces (6.4),(6.5) and (6.6) of type i are defined by

$$\mathcal{V}\mathcal{V}_{j_1,j_2}^{(i)} = \left\{ \Phi_{temp,j_1} * \Phi_{temp,j_1} * \left(\varphi_{j_2}^{(i)} * \varphi_{j_2}^{(i)} * f \right) \mid f \in l^2(\Omega \times [-1,1]) \right\}, \quad (6.3)$$

$$\mathcal{V}\mathcal{W}_{j_1,j_2}^{(i)} = \left\{ \Phi_{temp,j_1} * \Phi_{temp,j_1} * \left(\psi_{j_2}^{(i)} * \psi_{j_2}^{(i)} * f \right) \mid f \in l^2(\Omega \times [-1,1]) \right\}, \quad (6.4)$$

$$\mathcal{W}\mathcal{V}_{j_1,j_2}^{(i)} = \left\{ \Psi_{temp,j_1} * \Psi_{temp,j_1} * \left(\varphi_{j_2}^{(i)} * \varphi_{j_2}^{(i)} * f \right) \mid f \in l^2(\Omega \times [-1,1]) \right\}, \quad (6.5)$$

$$\mathcal{W}\mathcal{W}_{j_1,j_2}^{(i)} = \left\{ \Psi_{temp,j_1} * \Psi_{temp,j_1} * \left(\psi_{j_2}^{(i)} * \psi_{j_2}^{(i)} * f \right) \mid f \in l^2(\Omega \times [-1,1]) \right\}. \quad (6.6)$$

The corresponding time-space scale and detail spaces are given by

$$\mathcal{V}\mathcal{V}_{j_1,j_2} = \bigoplus_{i=1}^3 \mathcal{V}\mathcal{V}_{j_1,j_2}^{(i)}, \quad (6.7)$$

$$\mathcal{V}\mathcal{W}_{j_1,j_2} = \bigoplus_{i=1}^3 \mathcal{V}\mathcal{W}_{j_1,j_2}^{(i)}, \quad (6.8)$$

$$\mathcal{W}\mathcal{V}_{j_1,j_2} = \bigoplus_{i=1}^3 \mathcal{W}\mathcal{V}_{j_1,j_2}^{(i)}, \quad (6.9)$$

$$\mathcal{W}\mathcal{W}_{j_1,j_2} = \bigoplus_{i=1}^3 \mathcal{W}\mathcal{W}_{j_1,j_2}^{(i)}. \quad (6.10)$$

Note that the first index always represents the scale for the temporal kernels while the second index represents the scale for the spatial kernel functions.

While the spaces in (6.3), (6.6), (6.7) and (6.10) are what one would expect from the theory of \mathcal{H} - and \mathfrak{h} -wavelets, the occurrence of the hybrid spaces (6.4), (6.5), (6.8) and (6.9) is – on first sight – somewhat surprising (note that in the following ‘hybrid’ denotes the combination of temporal scaling functions and spatial wavelets and the other way round; the expression ‘pure’ will indicate the combination of temporal and spatial scaling functions or wavelets only). Our further investigations concerning the interrelationships of the spaces will clarify this subject and justify Definition 6.6 ex post. In the second variant of the time-space multiscale approach, as given in Section 6.2, the hybrid spaces come into play more naturally.

We now turn to the relationships of the spaces in Definition 6.6. We restrict our considerations to the time-space scale and detail spaces of type $i \in \{1, 2, 3\}$, since the results are, by definition, valid for the time-space scale and detail spaces as well. Let $f \in l^2(\Omega \times [-1,1])$ and, furthermore, let $j_1, j_2, j_3, j_4 \in \mathbb{N}$, with $j_1 \leq j_3$ and $j_2 \leq j_4$. It is clear that, for $i \in \{1, 2, 3\}$,

$$\Phi_{temp,j_3}^{(2)} * \left(\varphi_{j_4}^{(i)} * \varphi_{j_4}^{(i)} * f \right) = \Phi_{temp,j_3} * \Phi_{temp,j_3} * \left(\varphi_{j_4}^{(i)} * \varphi_{j_4}^{(i)} * f \right) \in \mathcal{V}\mathcal{V}_{j_3,j_4}^{(i)}$$

is valid. Due to our considerations in Chapter 2 we get

$$\begin{aligned}
& \Phi_{temp,j_3}^{(2)} * \left(\varphi_{j_4}^{(i)} \star \varphi_{j_4}^{(i)} * f \right) \\
&= \Phi_{temp,j_1}^{(2)} * \left(\varphi_{j_4}^{(i)} \star \varphi_{j_4}^{(i)} * f \right) + \sum_{j=j_1}^{j_3-1} \Psi_{temp,j}^{(2)} * \left(\varphi_{j_4}^{(i)} \star \varphi_{j_4}^{(i)} * f \right) \\
&= \Phi_{temp,j_1}^{(2)} * \left(\varphi_{j_2}^{(i)} \star \varphi_{j_2}^{(i)} * f + \sum_{j=j_2}^{j_4-1} \psi_j^{(i)} \star \psi_j^{(i)} * f \right) + \\
&\quad + \sum_{j=j_1}^{j_3-1} \Psi_{temp,j}^{(2)} * \left(\varphi_{j_2}^{(i)} \star \varphi_{j_2}^{(i)} * f + \sum_{j=j_2}^{j_4-1} \psi_j^{(i)} \star \psi_j^{(i)} * f \right) \\
&= \Phi_{temp,j_1}^{(2)} * \left(\varphi_{j_2}^{(i)} \star \varphi_{j_2}^{(i)} * f \right) + \sum_{j=j_2}^{j_4-1} \Phi_{temp,j_1}^{(2)} * \left(\psi_j^{(i)} \star \psi_j^{(i)} * f \right) + \\
&\quad + \sum_{j=j_1}^{j_3-1} \Psi_{temp,j}^{(2)} * \left(\varphi_{j_2}^{(i)} \star \varphi_{j_2}^{(i)} * f \right) + \sum_{j=j_1}^{j_3-1} \sum_{j'=j_2}^{j_4-1} \Psi_{temp,j}^{(2)} * \left(\psi_{j'}^{(i)} \star \psi_{j'}^{(i)} * f \right).
\end{aligned}$$

This, however, is equivalent to the following relation

$$\mathcal{V}\mathcal{V}_{j_1,j_2}^{(i)} + \sum_{j=j_2}^{j_4-1} \mathcal{V}\mathcal{W}_{j_1,j}^{(i)} + \sum_{j=j_1}^{j_3-1} \mathcal{W}\mathcal{V}_{j,j_2}^{(i)} + \sum_{j=j_1}^{j_3-1} \sum_{j'=j_2}^{j_4-1} \mathcal{W}\mathcal{W}_{j,j'}^{(i)} \subset \mathcal{V}\mathcal{V}_{j_3,j_4}^{(i)}, \quad (6.11)$$

for all $i \in \{1, 2, 3\}$. Hence,

$$\mathcal{V}\mathcal{V}_{j_1,j_2} + \sum_{j=j_2}^{j_4-1} \mathcal{V}\mathcal{W}_{j_1,j} + \sum_{j=j_1}^{j_3-1} \mathcal{W}\mathcal{V}_{j,j_2} + \sum_{j=j_1}^{j_3-1} \sum_{j'=j_2}^{j_4-1} \mathcal{W}\mathcal{W}_{j,j'} \subset \mathcal{V}\mathcal{V}_{j_3,j_4}.$$

Similar considerations lead us to the following lemma:

Lemma 6.7 *Let the time-space scale and detail spaces (of type $i \in \{1, 2, 3\}$) be defined as in Definition 6.6. Then, for all $i \in \{1, 2, 3\}$, the following relations hold true:*

- (i) $\mathcal{V}\mathcal{V}_{j_1,j_2}^{(i)} + \mathcal{V}\mathcal{W}_{j_1,j_2}^{(i)} \subset \mathcal{V}\mathcal{V}_{j_1,j_2+1}^{(i)}$,
- (ii) $\mathcal{V}\mathcal{V}_{j_1,j_2}^{(i)} + \mathcal{W}\mathcal{V}_{j_1,j_2}^{(i)} \subset \mathcal{V}\mathcal{V}_{j_1+1,j_2}^{(i)}$,
- (iii) $\mathcal{W}\mathcal{V}_{j_1,j_2}^{(i)} + \mathcal{W}\mathcal{W}_{j_1,j_2}^{(i)} \subset \mathcal{W}\mathcal{V}_{j_1,j_2+1}^{(i)}$,
- (iv) $\mathcal{V}\mathcal{W}_{j_1,j_2}^{(i)} + \mathcal{W}\mathcal{W}_{j_1,j_2}^{(i)} \subset \mathcal{V}\mathcal{W}_{j_1+1,j_2}^{(i)}$,
- (v) $\mathcal{V}\mathcal{V}_{j_1,j_2}^{(i)} + \mathcal{V}\mathcal{W}_{j_1,j_2}^{(i)} + \mathcal{W}\mathcal{V}_{j_1,j_2}^{(i)} \subset \mathcal{V}\mathcal{V}_{j_1+1,j_2+1}^{(i)}$
- (v) $\mathcal{V}\mathcal{V}_{j_1,j_2}^{(i)} + \mathcal{V}\mathcal{W}_{j_1,j_2}^{(i)} + \mathcal{W}\mathcal{V}_{j_1,j_2}^{(i)} + \mathcal{W}\mathcal{W}_{j_1,j_2}^{(i)} \subset \mathcal{V}\mathcal{V}_{j_1+1,j_2+1}^{(i)}$

Equivalent relations hold for the time-space scale and detail spaces.

Proof. Let $f \in l^2(\Omega \times [-1, 1])$. Obviously,

$$\begin{aligned} & \Phi_{temp,j_1}^{(2)} * \left(\varphi_{j_2}^{(i)} \star \varphi_{j_2}^{(i)} * f \right) + \Phi_{temp,j_1}^{(2)} * \left(\psi_{j_2}^{(i)} \star \psi_{j_2}^{(i)} * f \right) \\ &= \Phi_{temp,j_1}^{(2)} * \left(\varphi_{j_2}^{(i)} \star \varphi_{j_2}^{(i)} * f + \psi_{j_2}^{(i)} \star \psi_{j_2}^{(i)} * f \right) \\ &= \Phi_{temp,j_1}^{(2)} * \left(\varphi_{j_2+1}^{(i)} \star \varphi_{j_2+1}^{(i)} * f \right). \end{aligned}$$

But this is just (i). Relations (ii) to (iv) can be derived similarly.

Furthermore, from (i) we know that

$$\mathcal{V}\mathcal{W}_{j_1,j_2}^{(i)} + \mathcal{W}\mathcal{W}_{j_1,j_2}^{(i)} \subset \mathcal{V}\mathcal{W}_{j_1,j_2+1}^{(i)}. \quad (6.12)$$

In combination with (ii) we can deduce that

$$\mathcal{V}\mathcal{W}_{j_1,j_2+1}^{(i)} + \mathcal{W}\mathcal{W}_{j_1,j_2}^{(i)} \subset \mathcal{V}\mathcal{W}_{j_1+1,j_2+1}^{(i)}. \quad (6.13)$$

Combining (6.12) and (6.13) completes the proof of (v). Relation (vi) can be derived by connecting (6.12) and (iii).

Last but not least, by forming the orthogonal sums of the time-space scale and detail spaces of type $i \in \{1, 2, 3\}$ we end up with the corresponding results for the time-space scale and detail spaces. ■

From Lemma 6.7 it is easy to see that, for all $i \in \{1, 2, 3\}$ and $j_1, j_2, j_3, j_4 \in \mathbb{N}$, with $j_1 \leq j_3$ and $j_2 \leq j_4$, we get

$$\mathcal{V}\mathcal{W}_{j_3-1,j_4}^{(i)} \supset \mathcal{V}\mathcal{W}_{j_3-2,j_4}^{(i)} + \mathcal{W}\mathcal{W}_{j_3-2,j_4}^{(i)} \supset \cdots \supset \mathcal{V}\mathcal{W}_{j_1,j_4}^{(i)} + \sum_{j=j_1}^{j_3-1} \mathcal{W}\mathcal{W}_{j,j_4}^{(i)}$$

as well as

$$\mathcal{W}\mathcal{W}_{j_3,j_4-1}^{(i)} \supset \mathcal{W}\mathcal{W}_{j_3,j_4-2}^{(i)} + \mathcal{W}\mathcal{W}_{j_3,j_4-2}^{(i)} \supset \cdots \supset \mathcal{W}\mathcal{W}_{j_3,j_2}^{(i)} + \sum_{j=j_2}^{j_4-1} \mathcal{W}\mathcal{W}_{j_3,j}^{(i)}.$$

Consequently,

$$\sum_{j=j_1}^{j_3-1} \mathcal{W}\mathcal{W}_{j,j_2}^{(i)} + \sum_{j=j_1}^{j_3-1} \sum_{j'=j_2}^{j_4-1} \mathcal{W}\mathcal{W}_{j,j'}^{(i)} \subset \sum_{j=j_1}^{j_3-1} \mathcal{W}\mathcal{W}_{j,j_4}^{(i)}.$$

By adding $\mathcal{V}\mathcal{W}_{j_1,j_4}$ this leads to

$$\mathcal{V}\mathcal{W}_{j_1,j_4} + \sum_{j=j_1}^{j_3-1} \mathcal{W}\mathcal{W}_{j,j_2}^{(i)} + \sum_{j=j_1}^{j_3-1} \sum_{j'=j_2}^{j_4-1} \mathcal{W}\mathcal{W}_{j,j'}^{(i)} \subset \mathcal{V}\mathcal{W}_{j_3,j_4}. \quad (6.14)$$

Linking relations (i) and (ii) from Lemma 6.7 with equations (6.11) and (6.14) we can come up with the following result:

Theorem 6.8 *Let the time-space scale and detail spaces of type $i \in \{1, 2, 3\}$, as well as the corresponding time-space scale and detail spaces be defined as in Definition 6.6. Additionally, let $j_1, j_2, j_3, j_4 \in \mathbb{N}$, with $j_1 \leq j_3$ and $j_2 \leq j_4$. Then*

$$\mathcal{V}\mathcal{V}_{j_1, j_2}^{(i)} + \sum_{j=j_1}^{j_3-1} \mathcal{W}\mathcal{V}_{j, j_2}^{(i)} + \sum_{j=j_2}^{j_4-1} \mathcal{V}\mathcal{W}_{j_1, j}^{(i)} + \sum_{j=j_1}^{j_3-1} \sum_{j'=j_2}^{j_4-1} \mathcal{W}\mathcal{W}_{j, j'}^{(i)} = \mathcal{V}\mathcal{V}_{j_3, j_4}^{(i)}, \quad i \in \{1, 2, 3\},$$

and,

$$\mathcal{V}\mathcal{V}_{j_1, j_2} + \sum_{j=j_1}^{j_3-1} \mathcal{W}\mathcal{V}_{j, j_2} + \sum_{j=j_2}^{j_4-1} \mathcal{V}\mathcal{W}_{j_1, j} + \sum_{j=j_1}^{j_3-1} \sum_{j'=j_2}^{j_4-1} \mathcal{W}\mathcal{W}_{j, j'} = \mathcal{V}\mathcal{V}_{j_3, j_4}$$

are valid.

This immediately shows the following corollary to be true, i.e.

Corollary 6.9 *Under the assumptions of Theorem 6.8 the time-space scale spaces of type $i \in \{1, 2, 3\}$, as well as the time-space scale spaces fulfill*

$$\mathcal{V}\mathcal{V}_{j_1, j_2}^{(i)} \subset \mathcal{V}\mathcal{V}_{j_3, j_4}^{(i)}, \quad i \in \{1, 2, 3\},$$

and

$$\mathcal{V}\mathcal{V}_{j_1, j_2} \subset \mathcal{V}\mathcal{V}_{j_3, j_4},$$

respectively.

What remains is to show the approximation properties of the time-space approach. We let $f \in l^2(\Omega \times [-1, 1])$ and look at the following expression:

$$\begin{aligned} f_{j_1, j_2}^{(i)} &= \Phi_{temp, j_1} * \Phi_{temp, j_1} * \left(\varphi_{j_2}^{(i)} \star \varphi_{j_2}^{(i)} \star f \right) \\ &= \Phi_{temp, j_1}^{(2)} * \left(\varphi_{j_2}^{(i)} \star \varphi_{j_2}^{(i)} \star f \right) \\ &= \int_{-1}^1 \Phi_{temp, j_1}^{(2)}(\cdot, s) \sum_{(n, k) \in \mathcal{N}^{(i)}} \left((\varphi_{j_2}^{(i)})^\wedge(n) \right)^2 ((f^{(i)})^\wedge(n, k))(s) y_{n, k}^{(i)} ds \\ &= \sum_{(n, k) \in \mathcal{N}^{(i)}} \left((\varphi_{j_2}^{(i)})^\wedge(n) \right)^2 y_{n, k}^{(i)} \int_{-1}^1 \Phi_{temp, j_1}^{(2)}(\cdot, s) ((f^{(i)})^\wedge(n, k))(s) ds \\ &= \sum_{(n, k) \in \mathcal{N}^{(i)}} \sum_{m=0}^{\infty} \left((\varphi_{j_2}^{(i)})^\wedge(n) (\Phi_{j_1})^\wedge(n) \right)^2 \\ &\quad \cdot ((f^{(i)})^\wedge(n, k))^\wedge(m) y_{n, k}^{(i)} P_m^*. \end{aligned} \tag{6.15}$$

(Note that interchanging summation and integration is justified by the theorem of Beppo-Levi.) This result will help us proof the next theorem:

Theorem 6.10 *Let the families $\{\Phi_{temp,j_1}\}$ and $\{\varphi_{j_2}^{(i)}\}$, $j_1, j_2 \in \mathbb{Z}, i \in \{1, 2, 3\}$, be temporal scaling functions and spherical vector scaling functions of type i , respectively. Let $f \in l^2(\Omega \times [-1, 1])$ with $f = \sum_{i=1}^3 f^{(i)}$ and*

$$f_{j_1, j_2}^{(i)} = \Phi_{temp, j_1} * \Phi_{temp, j_1} * \left(\varphi_{j_2}^{(i)} \star \varphi_{j_2}^{(i)} * f \right).$$

Then

$$\lim_{\substack{j_1 \rightarrow \infty \\ j_2 \rightarrow \infty}} \|f^{(i)} - f_{j_1, j_2}^{(i)}\|_{l^2(\Omega \times [-1, 1])} = 0 \quad (6.16)$$

as well as

$$\lim_{\substack{j_1 \rightarrow \infty \\ j_2 \rightarrow \infty}} \left\| f - \sum_{i=1}^3 f_{j_1, j_2}^{(i)} \right\|_{l^2(\Omega \times [-1, 1])} = 0. \quad (6.17)$$

Proof. Using Equation (6.15) we can deduce that

$$\begin{aligned} & \|f^{(i)} - f_{j_1, j_2}^{(i)}\|_{l^2(\Omega \times [-1, 1])}^2 \\ &= \sum_{(n, k) \in \mathcal{N}^{(i)}} \sum_{m=0}^{\infty} \left(1 - \left((\varphi_{j_2}^{(i)})^{\wedge(n)} (\Phi_{j_1})^{\wedge(n)} \right)^2 \right)^2 \left(((f^{(i)})^{\wedge(n, k)})^{\wedge(m)} \right)^2 \\ &\leq \|f^{(i)}\|_{l^2(\Omega \times [-1, 1])}^2, \end{aligned}$$

where in the last step we have made use of the characteristics of the generating symbols of the scaling functions. Due to this uniform convergence we end up with (6.16). The proof for (6.17) can be derived analogously. ■

Finally, combining Theorems 6.8 and 6.10 we get the following result:

Corollary 6.11 *Let $f \in l^2(\Omega \times [-1, 1])$ with $f = \sum_{i=1}^3 f^{(i)}$. Under the terms of Theorems 6.8 and 6.10 the equalities*

$$\begin{aligned} f^{(i)} &= \lim_{\substack{j_1 \rightarrow \infty \\ j_2 \rightarrow \infty}} \left(\Phi_{temp, 0}^{(2)} * \left(\varphi_0^{(i)} \star \varphi_0^{(i)} * f \right) + \sum_{j=0}^{j_2-1} \Phi_{temp, 0}^{(2)} * \left(\psi_j^{(i)} \star \psi_j^{(i)} * f \right) + \right. \\ &\quad \left. + \sum_{j=0}^{j_1-1} \Psi_{temp, j}^{(2)} * \left(\varphi_0^{(i)} \star \varphi_0^{(i)} * f \right) + \sum_{j=0}^{j_1-1} \sum_{j'=0}^{j_2-1} \Psi_{temp, j}^{(2)} * \left(\psi_{j'}^{(i)} \star \psi_{j'}^{(i)} * f \right) \right), \end{aligned}$$

$i \in \{1, 2, 3\}$, as well as

$$\begin{aligned} f &= \lim_{\substack{j_1 \rightarrow \infty \\ j_2 \rightarrow \infty}} \left(\Phi_{temp, 0}^{(2)} * (\varphi_0 \star \varphi_0 * f) + \sum_{j=0}^{j_2-1} \Phi_{temp, 0}^{(2)} * (\psi_j \star \psi_j * f) + \right. \\ &\quad \left. + \sum_{j=0}^{j_1-1} \Psi_{temp, j}^{(2)} * (\varphi_0 \star \varphi_0 * f) + \sum_{j=0}^{j_1-1} \sum_{j'=0}^{j_2-1} \Psi_{temp, j}^{(2)} * (\psi_{j'} \star \psi_{j'} * f) \right) \end{aligned}$$

hold true in the sense of $\|\cdot\|_{l^2(\Omega \times [-1, 1])}$.

What we have established with Theorems 6.8 and 6.10 in combination with Corollaries 6.9 and 6.11 is basically a multiresolution analysis of the space $l^2(\Omega \times [-1, 1])$ that is, in the terms of this chapter, a combined temporal and spatial multiresolution analysis. There remains the question of how to interpret the time-space scale and detail spaces.

We start with the scale spaces $\mathcal{V}\mathcal{V}_{j_1, j_2}^{(i)}$. As previously mentioned, double convolutions with scaling functions can, in the spectral domain, be interpreted as low-pass filtering of the function under consideration. Therefore, if $f \in l^2(\Omega \times [-1, 1])$ denotes a time-dependent vector field and $P_{\mathcal{V}\mathcal{V}_{j_1, j_2}^{(i)}}(f)$ denotes the projection of f onto the space $\mathcal{V}\mathcal{V}_{j_1, j_2}^{(i)}$, then

$$\sum_{i=1}^3 P_{\mathcal{V}\mathcal{V}_{j_1, j_2}^{(i)}}(f) \in \mathcal{V}\mathcal{V}_{j_1, j_2}$$

can be understood as that part of f that shows coarse spatial structures varying comparatively slowly with time. $P_{\mathcal{V}\mathcal{V}_{j_1, j_2}^{(1)}}(f)$, $P_{\mathcal{V}\mathcal{V}_{j_1, j_2}^{(2)}}(f)$ and $P_{\mathcal{V}\mathcal{V}_{j_1, j_2}^{(3)}}(f)$ are the corresponding radial part, the part of zero surface curl and of zero surface divergence, respectively.

Looking at the definition of the detail spaces $\mathcal{V}\mathcal{W}_{j_1, j_2}^{(i)}$, one realizes that these spaces contain information obtained by applying temporal scaling functions as well as spatial (spherical vector) wavelets to functions $f \in l^2(\Omega \times [-1, 1])$. Consequently, if $P_{\mathcal{V}\mathcal{W}_{j_1, j_2}^{(i)}}(f)$ denotes the projection of f onto the spaces $\mathcal{V}\mathcal{W}_{j_1, j_2}^{(i)}$, then

$$\sum_{i=1}^3 P_{\mathcal{V}\mathcal{W}_{j_1, j_2}^{(i)}}(f) \in \mathcal{V}\mathcal{W}_{j_1, j_2}$$

can be interpreted as the temporally slowly varying spatial detail information of f or, in other words, regional spatial structures of lower temporal variation. $P_{\mathcal{V}\mathcal{W}_{j_1, j_2}^{(1)}}(f)$, $P_{\mathcal{V}\mathcal{W}_{j_1, j_2}^{(2)}}(f)$ and $P_{\mathcal{V}\mathcal{W}_{j_1, j_2}^{(3)}}(f)$ may be understood accordingly.

As regards the spaces $\mathcal{W}\mathcal{V}_{j_1, j_2}^{(i)}$, similar reasoning leads us to the conclusion that

$$\sum_{i=1}^3 P_{\mathcal{W}\mathcal{V}_{j_1, j_2}^{(i)}}(f) \in \mathcal{W}\mathcal{V}_{j_1, j_2},$$

represents coarse spatial structures of $f \in l^2(\Omega \times [-1, 1])$ of higher temporal variation.

Finally,

$$\sum_{i=1}^3 P_{\mathcal{W}\mathcal{W}_{j_1, j_2}^{(i)}}(f) \in \mathcal{W}\mathcal{W}_{j_1, j_2},$$

may be interpreted as that part of $f \in l^2(\Omega \times [-1, 1])$ that consists of regional details in space which show – more or less – short-term temporal fluctuations. With respect to what we have said before, the interpretation of $P_{\mathcal{W}\mathcal{W}_{j_1, j_2}^{(i)}}(f)$ and $P_{\mathcal{V}\mathcal{W}_{j_1, j_2}^{(i)}}(f)$, $i \in \{1, 2, 3\}$, is straightforward.

6.2 Time-Space-Multiscale Approach: Variant 2

We now turn to the second variant of the time-space multiscale approach. In order to formulate variant 1 we started with the a priori definition of the time-space scale and detail spaces which then was justified ex post during the course of our considerations. Though variant 2 will, in the end, lead to results similar to the treatment in Section 6.1, the modus operandi will be just the other way round and will resemble the considerations in Chapter 2. The advantage of this second approach lies surely in the fact that the spaces of Definition 6.6 come into play more naturally. Based on the temporal scaling functions and wavelets defined in Definition 6.2 and the spherical vectorial (i.e. spatial) kernels, we will define certain tensor-product kernels which will then serve as the time-space scaling functions and wavelets (for more details on tensor-product wavelets see e.g. [79, 80, 101]).

Starting point is the definition of the generating symbol of a time-space scaling function:

Definition 6.12 *Suppose, for $j_1 \in \mathbb{Z}$, $\{(\Phi_{j_1})^\wedge(n_1)\}_{n_1=0,1,\dots}$ to be the generating symbol of a temporal scaling function. Furthermore, for $i \in \{1, 2, 3\}$ and $j_2 \in \mathbb{Z}$, we assume $\{(\varphi_{j_2}^{(i)})^\wedge(n_2)\}_{n_2=0_i, 0_i+1, \dots}$ to be the generating symbols of spherical vectorial scaling functions of type i . Then the generating symbols of time-space (tensor-product) scaling functions of type i are given by the sequence*

$$\left\{ (\hat{\varphi}_{j_1, j_2}^{(i)})^\wedge(n_1; n_2) \right\}_{\substack{n_1=0,1,\dots \\ n_2=0_i, 0_i+1, \dots}},$$

with

$$(\hat{\varphi}_{j_1, j_2}^{(i)})^\wedge(n_1; n_2) = (\Phi_{j_1})^\wedge(n_1) (\varphi_{j_2}^{(i)})^\wedge(n_2).$$

The sequence of vectors

$$\left\{ (\hat{\varphi}_{j_1, j_2}^{(i)})^\wedge(n_1; n_2) \right\}_{\substack{n_1=0,1,\dots \\ n_2=0_i, 0_i+1, \dots}},$$

with

$$(\hat{\varphi}_{j_1, j_2}^{(i)})^\wedge(n_1; n_2) = \left((\hat{\varphi}_{j_1, j_2}^{(1)})^\wedge(n_1; n_2), (\hat{\varphi}_{j_1, j_2}^{(2)})^\wedge(n_1; n_2), (\hat{\varphi}_{j_1, j_2}^{(3)})^\wedge(n_1; n_2) \right)^T,$$

is called the generating symbol of a time-space (tensor-product) scaling function.

The time-space scaling functions are defined as follows:

Definition 6.13 *Let $\left\{ (\hat{\varphi}_{j_1, j_2}^{(i)})^\wedge(n_1; n_2) \right\}_{\substack{n_1=0,1,\dots \\ n_2=0_i, 0_i+1, \dots}}$, $i \in \{1, 2, 3\}$, $j_1, j_2 \in \mathbb{Z}$ be the generating symbols of time-space scaling functions of type i . Then the families of kernels $\left\{ \hat{\varphi}_{j_1, j_2}^{(i)} \right\}$ denote the time-space (tensor-product) scaling functions of type $i \in \{1, 2, 3\}$ and are defined by*

$$\hat{\varphi}_{j_1, j_2}^{(i)}(\xi, \eta; s, t) = \sum_{n_1=0}^{\infty} \sum_{(n_2, k) \in \mathcal{N}^{(i)}} (\hat{\varphi}_{j_1, j_2}^{(i)})^\wedge(n_1; n_2) Y_{n_2, k}(\xi) P_{n_1}^*(s) y_{n_2, k}^{(i)}(\xi) P_{n_1}^*(t),$$

where $\xi, \eta \in \Omega$ and $s, t \in [-1, 1]$. The corresponding time-space scaling functions are given by the families of kernels $\{\hat{\varphi}_{j_1, j_2}\}$ defined via

$$\hat{\varphi}_{j_1, j_2} = \sum_{i=1}^3 \hat{\varphi}_{j_1, j_2}^{(i)}.$$

As in variant 1, the first index always denotes the scale of the temporal part, while the second index represents the scale of the spatial part. It is noteworthy that the characteristics of the generating symbols, like admissibility for example, carry over to the time-space case as well.

In Chapter 2 we have derived the wavelets from the associated scaling functions by means of so-called refinement equations for the generating symbols (see Definitions 2.10 and 2.21). We will now proceed likewise and define the symbols of the time-space wavelets by means of a refinement equation.

Definition 6.14 Let $\left\{ (\hat{\varphi}_{j_1, j_2}^{(i)})^\wedge(n_1; n_2) \right\}_{\substack{n_1=0, 1, \dots \\ n_2=0_i, 0_i+1, \dots}}$, $i \in \{1, 2, 3\}$, $j_1, j_2 \in \mathbb{Z}$ be the generating symbols of time-space scaling functions of type i . The generating symbols of the associated pure time-space wavelets of type i are given by the sequences $\left\{ (\hat{\psi}_{j_1, j_2}^{(i)})^\wedge(n_1; n_2) \right\}_{\substack{n_1=0, 1, \dots \\ n_2=0_i, 0_i+1, \dots}}$, with

$$(\hat{\psi}_{j_1, j_2}^{(i)})^\wedge(n_1; n_2) = (\Psi_{j_1})^\wedge(n_1) (\psi_{j_2}^{(i)})^\wedge(n_2),$$

fulfilling the refinement equation

$$\begin{aligned} \left((\hat{\psi}_{j_1, j_2}^{(i)})^\wedge(n_1; n_2) \right)^2 &= \left(((\Phi_{j_1+1})^\wedge(n_1))^2 - ((\Phi_{j_1})^\wedge(n_1))^2 \right) \cdot \\ &\cdot \left(\left((\varphi_{j_2+1}^{(i)})^\wedge(n_2) \right)^2 - \left((\varphi_{j_2}^{(i)})^\wedge(n_2) \right)^2 \right). \end{aligned} \quad (6.18)$$

The sequence of vectors

$$\left\{ (\hat{\psi}_{j_1, j_2}^{(i)})^\wedge(n_1; n_2) \right\}_{\substack{n_1=0, 1, \dots \\ n_2=0_i, 0_i+1, \dots}},$$

with

$$(\hat{\psi}_{j_1, j_2}^{(i)})^\wedge(n_1; n_2) = \left((\hat{\psi}_{j_1, j_2}^{(1)})^\wedge(n_1; n_2), (\hat{\psi}_{j_1, j_2}^{(2)})^\wedge(n_1; n_2), (\hat{\psi}_{j_1, j_2}^{(3)})^\wedge(n_1; n_2) \right)^T,$$

is called the generating symbol of the associated pure time-space (tensor-product) wavelets

Before we use the previous definition in order to construct time-space wavelets, we should have a closer look at the refinement equation (6.18) in order to see what effects arise from the 'simultaneous' refinement in time and space.

Expanding the product we arrive at

$$\begin{aligned}
& ((\Psi_{j_1})^\wedge(n_1))^2 \left((\psi_{j_2}^{(i)})^\wedge(n_2) \right)^2 \\
&= ((\Phi_{j_1+1})^\wedge(n_1))^2 \left((\varphi_{j_2+1}^{(i)})^\wedge(n_2) \right)^2 - ((\Phi_{j_1+1})^\wedge(n_1))^2 \left((\varphi_{j_2}^{(i)})^\wedge(n_2) \right)^2 + \\
&\quad + ((\Phi_{j_1})^\wedge(n_1))^2 \left((\varphi_{j_2}^{(i)})^\wedge(n_2) \right)^2 - ((\Phi_{j_1})^\wedge(n_1))^2 \left((\varphi_{j_2+1}^{(i)})^\wedge(n_2) \right)^2 \\
&= ((\Phi_{j_1+1})^\wedge(n_1))^2 \left((\varphi_{j_2+1}^{(i)})^\wedge(n_2) \right)^2 + ((\Phi_{j_1})^\wedge(n_1))^2 \left((\varphi_{j_2}^{(i)})^\wedge(n_2) \right)^2 + \\
&\quad - ((\Phi_{j_1})^\wedge(n_1))^2 \left[\left((\varphi_{j_2}^{(i)})^\wedge(n_2) \right)^2 + \left((\psi_{j_2}^{(i)})^\wedge(n_2) \right)^2 \right] + \\
&\quad - \left((\psi_{j_2}^{(i)})^\wedge(n_2) \right)^2 \left[\left((\Phi_{j_1})^\wedge(n_1) \right)^2 + \left((\Psi_{j_1})^\wedge(n_1) \right)^2 \right],
\end{aligned}$$

where in the last step we have made use of the refinement equations for the Legendre as well as the spherical vector wavelets. Expanding the products again, cancelling out the equal terms and rearranging slightly we end up with

$$(\Phi_{j_1+1})^\wedge(n_1)(\varphi_{j_2+1}^{(i)})^\wedge(n_2) = (\Phi_{j_1})^\wedge(n_1)(\varphi_{j_2}^{(i)})^\wedge(n_2) + \quad (6.19)$$

$$+ (\Phi_{j_1})^\wedge(n_1)(\psi_{j_2}^{(i)})^\wedge(n_2) + \quad (6.20)$$

$$+ (\Psi_{j_1})^\wedge(n_1)(\varphi_{j_2}^{(i)})^\wedge(n_2) + \quad (6.21)$$

$$+ (\Psi_{j_1})^\wedge(n_1)(\psi_{j_2}^{(i)})^\wedge(n_2). \quad (6.22)$$

It is this results that enlightens the definitions of the time-space scale and detail spaces of variant 1. The right-hand side of Equation (6.19), i.e. an expression related to scaling functions for the temporal and the spatial part, corresponds to the spaces $\mathcal{V}\mathcal{W}_{j_1, j_2}^{(i)}$. The term (6.20) is related to $\mathcal{W}\mathcal{W}_{j_1, j_2}^{(i)}$, while (6.21) corresponds to the spaces $\mathcal{W}\mathcal{V}_{j_1, j_2}^{(i)}$. Finally, expression (6.22) relates to $\mathcal{W}\mathcal{W}_{j_1, j_2}^{(i)}$. Therefore, the necessity for the hybrid spaces $\mathcal{V}\mathcal{W}_{j_1, j_2}^{(i)}$ and $\mathcal{W}\mathcal{V}_{j_1, j_2}^{(i)}$ to occur arises naturally from the fact that two refinement equations, namely for the temporal as well as the spatial wavelets, need to be fulfilled simultaneously (see refinement equation (6.18)). Consequently, from (6.19) to (6.22) there appear four different expressions in order to go from an approximation of scales j_1 and j_2 to scales $j_1 + 1$ and $j_2 + 1$, respectively. Basically this is just another way of expressing the results of Corollary 6.11.

Equations (6.19) to (6.22) now show us what kinds of time-space kernels are necessary. While the kernel functions corresponding to (6.19) are just the previously defined time-space scaling functions of Definition 6.13, we need to construct three different types of wavelets, i.e. two kinds of hybrid time-space wavelets which are really a combination of scaling functions and wavelets, and one kind of pure time-space wavelets.

Definition 6.15 Let $\left\{(\hat{\varphi}_{j_1, j_2}^{(i)})^\wedge(n_1; n_2)\right\}_{\substack{n_1=0,1,\dots \\ n_2=0_i, 0_i+1, \dots}}$, $i \in \{1, 2, 3\}$, $j_1, j_2 \in \mathbb{Z}$ be the generating symbols of time-space scaling functions of type $i \in \{1, 2, 3\}$. Additionally, suppose $\left\{(\hat{\psi}_{j_1, j_2}^{(i)})^\wedge(n_1; n_2)\right\}_{\substack{n_1=0,1,\dots \\ n_2=0_i, 0_i+1, \dots}}$ to be the generating symbol of the associated pure time-space wavelets of type i . Let $\xi, \eta \in \Omega$ and $s, t \in [-1, 1]$. The pure time-space (tensor-product) wavelets of type i , i.e. the families $\left\{\hat{\psi}_{j_1, j_2}^{(i)}\right\}$, are defined by

$$\hat{\psi}_{j_1, j_2}^{(i)}(\xi, \eta; s, t) = \sum_{n_1=0}^{\infty} \sum_{(n_2, k) \in \mathcal{N}^{(i)}} (\hat{\psi}_{j_1, j_2}^{(i)})^\wedge(n_1; n_2) Y_{n_2, k}(\xi) P_{n_1}^*(s) y_{n_2, k}^{(i)}(\xi) P_{n_1}^*(t).$$

The hybrid time-space (tensor-product) wavelets of type i , i.e. $\left\{\hat{\sigma}_{j_1, j_2}^{(i)}\right\}$ and $\left\{\hat{\tau}_{j_1, j_2}^{(i)}\right\}$ are given by

$$\hat{\sigma}_{j_1, j_2}^{(i)}(\xi, \eta; s, t) = \sum_{n_1=0}^{\infty} \sum_{(n_2, k) \in \mathcal{N}^{(i)}} (\Phi_{j_1})^\wedge(n_1) (\psi_{j_2}^{(i)})^\wedge(n_2) Y_{n_2, k}(\xi) P_{n_1}^*(s) y_{n_2, k}^{(i)}(\xi) P_{n_1}^*(t)$$

and

$$\hat{\tau}_{j_1, j_2}^{(i)}(\xi, \eta; s, t) = \sum_{n_1=0}^{\infty} \sum_{(n_2, k) \in \mathcal{N}^{(i)}} (\Psi_{j_1})^\wedge(n_1) (\varphi_{j_2}^{(i)})^\wedge(n_2) Y_{n_2, k}(\xi) P_{n_1}^*(s) y_{n_2, k}^{(i)}(\xi) P_{n_1}^*(t),$$

respectively. The corresponding pure and hybrid time-space wavelets or, in more detail, the families $\left\{\hat{\psi}_{j_1, j_2}^{(i)}\right\}$, $\left\{\hat{\sigma}_{j_1, j_2}^{(i)}\right\}$ and $\left\{\hat{\tau}_{j_1, j_2}^{(i)}\right\}$ are defined by

$$\begin{aligned} \hat{\psi}_{j_1, j_2} &= \sum_{i=1}^3 \hat{\psi}_{j_1, j_2}^{(i)}, \\ \hat{\sigma}_{j_1, j_2} &= \sum_{i=1}^3 \hat{\sigma}_{j_1, j_2}^{(i)}, \\ \hat{\tau}_{j_1, j_2} &= \sum_{i=1}^3 \hat{\tau}_{j_1, j_2}^{(i)}. \end{aligned}$$

The next step in formulating this variant of time-space approximation is the introduction of convolutions of the time-space kernels with time-dependent vector fields.

Definition 6.16 Let $\left\{\hat{k}_{j_1, j_2}^{(i)}\right\}$ be a time-space scaling function or wavelet of type $i \in \{1, 2, 3\}$, $j_1, j_2 \in \mathbb{Z}$. For $f \in l^2(\Omega \times [-1, 1])$ the time-space decomposition convolution of f is given by

$$\left(\hat{k}_{j_1, j_2}^{(i)} * f\right)(\eta; s) = \int_{-1}^1 \left(\int_{\Omega} \hat{k}_{j_1, j_2}^{(i)}(\eta, \xi; \cdot, s, t) \cdot f(\eta; s) d\omega(\eta) \right) ds, \quad s, t \in [-1, 1], \quad \eta, \xi \in \Omega. \quad (6.23)$$

If we let $F_{j_1, j_2}^{(i)} = \hat{k}_{j_1, j_2}^{(i)} * f$, then the time-space reconstruction convolution of f is defined to be

$$\left(\hat{k}_{j_1, j_2}^{(i)} \star F_{j_1, j_2}^{(i)} \right) (\xi; t) = \int_{\Omega} \left(\int_{-1}^1 F_{j_1, j_2}^{(i)}(\eta; s) \hat{k}_{j_1, j_2}^{(i)}(\xi, \eta; s, t) ds \right) d\omega(\eta). \quad (6.24)$$

Note that Definition 6.16 is just the canonical extension of Definition 2.15 to the case of time-dependent spherical vector fields. In other words, the decomposition convolution assigns a scalar function, the so-called 'coefficients', to the vector field under consideration. The reconstruction convolution is used to approximate the vector field from these scalar coefficients.

Finally, having introduced the kernel functions and convolutions, the last ingredient for the variant 2 multiscale approach are the corresponding scale- and detail spaces. While in the first variant there are four spaces defined via four different combinations of temporal and spatial kernels, the spaces of the second variant are given in correspondence to the four different time-space kernels. In other words, what is a mere definition in the first approach is directly related to the existence of four types of time-space kernels and therefore an immediate consequence of the combined time and space refinement.

Definition 6.17 Suppose $\{\hat{\varphi}_{j_1, j_2}^{(i)}\}$ to be time-space scaling functions of type $i \in \{1, 2, 3\}$ and let $\{\hat{\psi}_{j_1, j_2}^{(i)}\}$, $\{\hat{\sigma}_{j_1, j_2}^{(i)}\}$ and $\{\hat{\tau}_{j_1, j_2}^{(i)}\}$ be the associated pure and hybrid time-space wavelets of scales $j_1, j_2 \in \mathbb{Z}$. The pure time-space scale spaces of type i are defined by

$$\widehat{\mathcal{V}}_{j_1, j_2}^{(i)} = \left\{ \hat{\varphi}_{j_1, j_2}^{(i)} \star (\hat{\varphi}_{j_1, j_2}^{(i)} * f) \mid f \in l^2(\Omega \times [-1, 1]) \right\}.$$

The hybrid time-space detail spaces of type i are given by

$$\widehat{\mathcal{V}}\widehat{\mathcal{W}}_{j_1, j_2}^{(i)} = \left\{ \hat{\sigma}_{j_1, j_2}^{(i)} \star (\hat{\sigma}_{j_1, j_2}^{(i)} * f) \mid f \in l^2(\Omega \times [-1, 1]) \right\},$$

$$\widehat{\mathcal{W}}\widehat{\mathcal{V}}_{j_1, j_2}^{(i)} = \left\{ \hat{\tau}_{j_1, j_2}^{(i)} \star (\hat{\tau}_{j_1, j_2}^{(i)} * f) \mid f \in l^2(\Omega \times [-1, 1]) \right\},$$

while the pure time-space detail spaces of type i are defined via

$$\widehat{\mathcal{W}}\widehat{\mathcal{W}}_{j_1, j_2}^{(i)} = \left\{ \hat{\psi}_{j_1, j_2}^{(i)} \star (\hat{\psi}_{j_1, j_2}^{(i)} * f) \mid f \in l^2(\Omega \times [-1, 1]) \right\}.$$

Correspondingly we define

$$\begin{aligned} \widehat{\mathcal{V}}_{j_1, j_2} &= \bigoplus_{i=1}^3 \widehat{\mathcal{V}}_{j_1, j_2}^{(i)}, \\ \widehat{\mathcal{V}}\widehat{\mathcal{W}}_{j_1, j_2} &= \bigoplus_{i=1}^3 \widehat{\mathcal{V}}\widehat{\mathcal{W}}_{j_1, j_2}^{(i)}, \end{aligned}$$

$$\widehat{\mathcal{W}\mathcal{V}}_{j_1, j_2} = \bigoplus_{i=1}^3 \widehat{\mathcal{W}\mathcal{V}}_{j_1, j_2}^{(i)},$$

$$\widehat{\mathcal{W}\mathcal{W}}_{j_1, j_2} = \bigoplus_{i=1}^3 \widehat{\mathcal{W}\mathcal{W}}_{j_1, j_2}^{(i)}$$

to be the pure time-space scale space as well as the hybrid and pure time-space detail spaces.

What remains is to show that the definitions so far suffice to get a multiresolution analysis of a time-dependent vector field $f \in l^2(\Omega \times [-1, 1])$, i.e. that variant 2 bears results that correspond to Theorems 6.8 and 6.10, as well as Corollaries 6.9 and 6.11. By means of direct calculations it is not hard to verify the following lemma which will help us to carry over the results of variant 1 to variant 2.

Lemma 6.18 *Suppose the families $\{\Phi_{temp, j_1}\}$ and $\{\varphi_{j_2}^{(i)}\}$, $j_1, j_2 \in \mathbb{Z}, i \in \{1, 2, 3\}$, to be temporal scaling functions and spherical vector scaling functions of type i , respectively. Furthermore, let $\{\hat{\varphi}_{j_1, j_2}^{(i)}\}$ be time-space scaling functions of type i and let $\{\hat{\psi}_{j_1, j_2}^{(i)}\}$, $\{\hat{\sigma}_{j_1, j_2}^{(i)}\}$ and $\{\hat{\tau}_{j_1, j_2}^{(i)}\}$ be the associated pure and hybrid time-space wavelets. For $f \in l^2(\Omega \times [-1, 1])$ it holds that*

$$\begin{aligned} \Phi_{temp, j_1} * \Phi_{temp, j_1} * \left(\varphi_{j_2}^{(i)} \star \varphi_{j_2}^{(i)} * f \right) &= \hat{\varphi}_{j_1, j_2}^{(i)} \star (\hat{\varphi}_{j_1, j_2}^{(i)} * f), \\ \Phi_{temp, j_1} * \Phi_{temp, j_1} * \left(\psi_{j_2}^{(i)} \star \psi_{j_2}^{(i)} * f \right) &= \hat{\sigma}_{j_1, j_2}^{(i)} \star (\hat{\sigma}_{j_1, j_2}^{(i)} * f), \\ \Psi_{temp, j_1} * \Psi_{temp, j_1} * \left(\varphi_{j_2}^{(i)} \star \varphi_{j_2}^{(i)} * f \right) &= \hat{\tau}_{j_1, j_2}^{(i)} \star (\hat{\tau}_{j_1, j_2}^{(i)} * f), \end{aligned}$$

as well as

$$\Psi_{temp, j_1} * \Psi_{temp, j_1} * \left(\psi_{j_2}^{(i)} \star \psi_{j_2}^{(i)} * f \right) = \hat{\psi}_{j_1, j_2}^{(i)} \star (\hat{\psi}_{j_1, j_2}^{(i)} * f),$$

where the convolutions on the left hand side are understood in the sense of Definition 6.4, while the convolutions on the right hand side are in accordance with Definition 6.16.

This means that the insights of variant 1 can immediately be translated into the language of variant 2, thus enabling us to formulate the final result:

Theorem 6.19 *Let, for $j_1, j_2 \in \mathbb{Z}$, $\{\hat{\varphi}_{j_1, j_2}^{(i)}\}$ be time-space scaling functions of type $i \in \{1, 2, 3\}$ and let $\{\hat{\psi}_{j_1, j_2}^{(i)}\}$, $\{\hat{\sigma}_{j_1, j_2}^{(i)}\}$ and $\{\hat{\tau}_{j_1, j_2}^{(i)}\}$ be the associated pure and hybrid time-space wavelets of type i . $\{\hat{\varphi}_{j_1, j_2}\}$, $\{\hat{\psi}_{j_1, j_2}\}$, $\{\hat{\sigma}_{j_1, j_2}\}$ and $\{\hat{\tau}_{j_1, j_2}\}$ are assumed to be the corresponding time-space scaling functions, the hybrid and the pure time-space wavelets, respectively.*

Suppose $f \in l^2(\Omega \times [-1, 1])$ with $f = \sum_{i=1}^3 f^{(i)}$. Then,

$$\begin{aligned} f^{(i)} &= \lim_{\substack{j_1 \rightarrow \infty \\ j_2 \rightarrow \infty}} \left(\hat{\varphi}_{j_1, j_2}^{(i)} \star (\hat{\varphi}_{j_1, j_2}^{(i)} \star f) \right) \\ &= \lim_{\substack{j_1 \rightarrow \infty \\ j_2 \rightarrow \infty}} \left(\hat{\varphi}_{0,0}^{(i)} \star (\hat{\varphi}_{0,0}^{(i)} \star f) + \sum_{j=0}^{j_2-1} \hat{\sigma}_{0,j}^{(i)} \star (\hat{\sigma}_{0,j}^{(i)} \star f) + \right. \\ &\quad \left. + \sum_{j=0}^{j_1-1} \hat{\tau}_{j,0}^{(i)} \star (\hat{\tau}_{j,0}^{(i)} \star f) + \sum_{j=0}^{j_1-1} \sum_{j'=0}^{j_2-1} \hat{\psi}_{j,j'}^{(i)} \star (\hat{\psi}_{j,j'}^{(i)} \star f) \right), \end{aligned}$$

as well as

$$\begin{aligned} f &= \lim_{\substack{j_1 \rightarrow \infty \\ j_2 \rightarrow \infty}} \left(\hat{\varphi}_{j_1, j_2} \star (\hat{\varphi}_{j_1, j_2} \star f) \right) \\ &= \lim_{\substack{j_1 \rightarrow \infty \\ j_2 \rightarrow \infty}} \left(\hat{\varphi}_{0,0} \star (\hat{\varphi}_{0,0} \star f) + \sum_{j=0}^{j_2-1} \hat{\sigma}_{0,j} \star (\hat{\sigma}_{0,j} \star f) + \right. \\ &\quad \left. + \sum_{j=0}^{j_1-1} \hat{\tau}_{j,0} \star (\hat{\tau}_{j,0} \star f) + \sum_{j=0}^{j_1-1} \sum_{j'=0}^{j_2-1} \hat{\psi}_{j,j'} \star (\hat{\psi}_{j,j'} \star f) \right) \end{aligned}$$

hold true in the sense of the $l^2(\Omega \times [-1, 1])$ -metric. Accordingly, for the time-space scale and detail spaces of Definition 6.17 we have

$$\widehat{\mathcal{V}}_{j_1, j_2}^{(i)} + \sum_{j=j_1}^{j_3-1} \widehat{\mathcal{W}}_{j, j_2}^{(i)} + \sum_{j=j_2}^{j_4-1} \widehat{\mathcal{V}}_{j_1, j}^{(i)} + \sum_{j=j_1}^{j_3-1} \sum_{j'=j_2}^{j_4-1} \widehat{\mathcal{W}}_{j, j'}^{(i)} = \widehat{\mathcal{V}}_{j_3, j_4}^{(i)}, \quad i \in \{1, 2, 3\},$$

and,

$$\widehat{\mathcal{V}}_{j_1, j_2} + \sum_{j=j_1}^{j_3-1} \widehat{\mathcal{W}}_{j, j_2} + \sum_{j=j_2}^{j_4-1} \widehat{\mathcal{V}}_{j_1, j} + \sum_{j=j_1}^{j_3-1} \sum_{j'=j_2}^{j_4-1} \widehat{\mathcal{W}}_{j, j'} = \widehat{\mathcal{V}}_{j_3, j_4},$$

with $j_3, j_4 \in \mathbb{Z}$ and $j_1 \leq j_3$, $j_2 \leq j_4$.

No matter which variant is used it is obvious that, as far as numerical applications are concerned, one main task is to visualize the huge amount of information obtained, i.e. the content of the three scale spaces and the nine detail spaces. Concerning numerical realization, visualization and first numerical examples utilizing synthetic vector data, the interested reader is redirected to [64]. Together with the author of [64] we have developed and implemented a multiscale analysis and visualization tool for time-dependent spherical vector fields which is introduced circumstantially in the aforementioned work. We do not go into detail here, since this would be way beyond the scope of this thesis. Nevertheless, for illustrational purposes we present some impressions of the analysis and visualization tool in action. Figures 6.1 and 6.2 show screen shots of the tool during a time-space analysis process of synthetic test vector fields. In Figure 6.1 a global vector field is analyzed that varies slowly in time but shows sudden short local disturbances. In Figure 6.2 a similar vector field is analyzed but this time the local disturbances appear and decay a bit more slowly (cf. [64]).

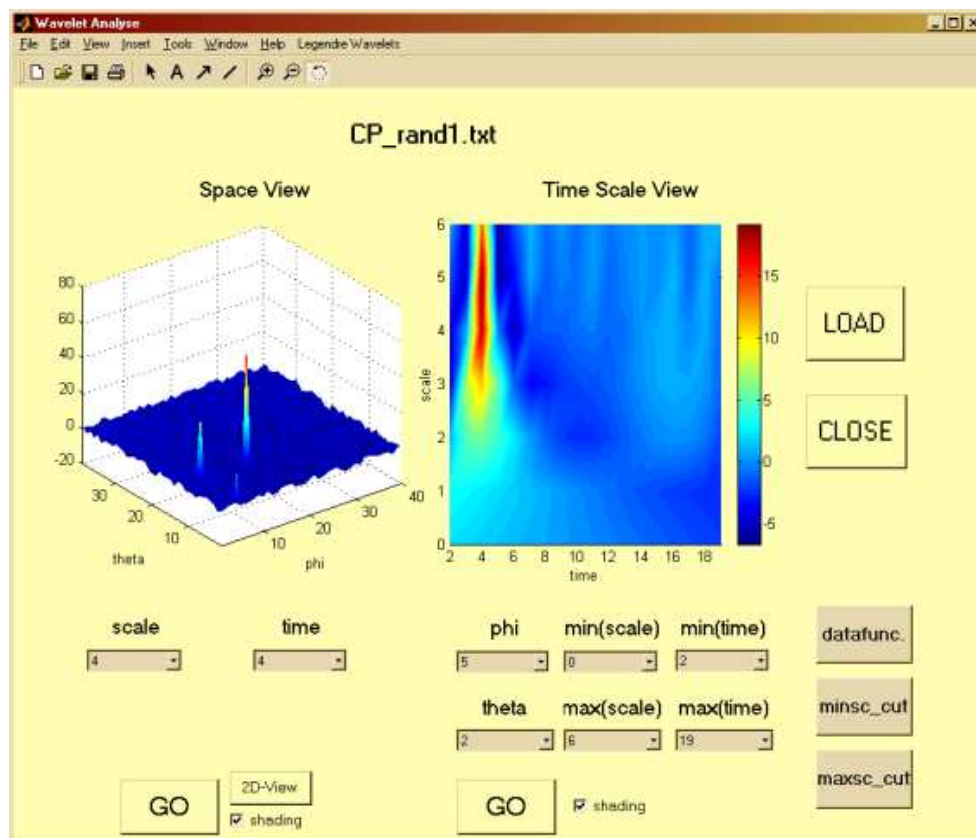


Figure 6.1: Multiscale analysis and visualization tool for time-dependent spherical vector fields. Left window: At a high spatial wavelet scale local effects are detected in a global vector field. Right window: The corresponding wavelet coefficients in the temporal domain indicate the very moment of their appearance and the comparatively short duration of the effects.

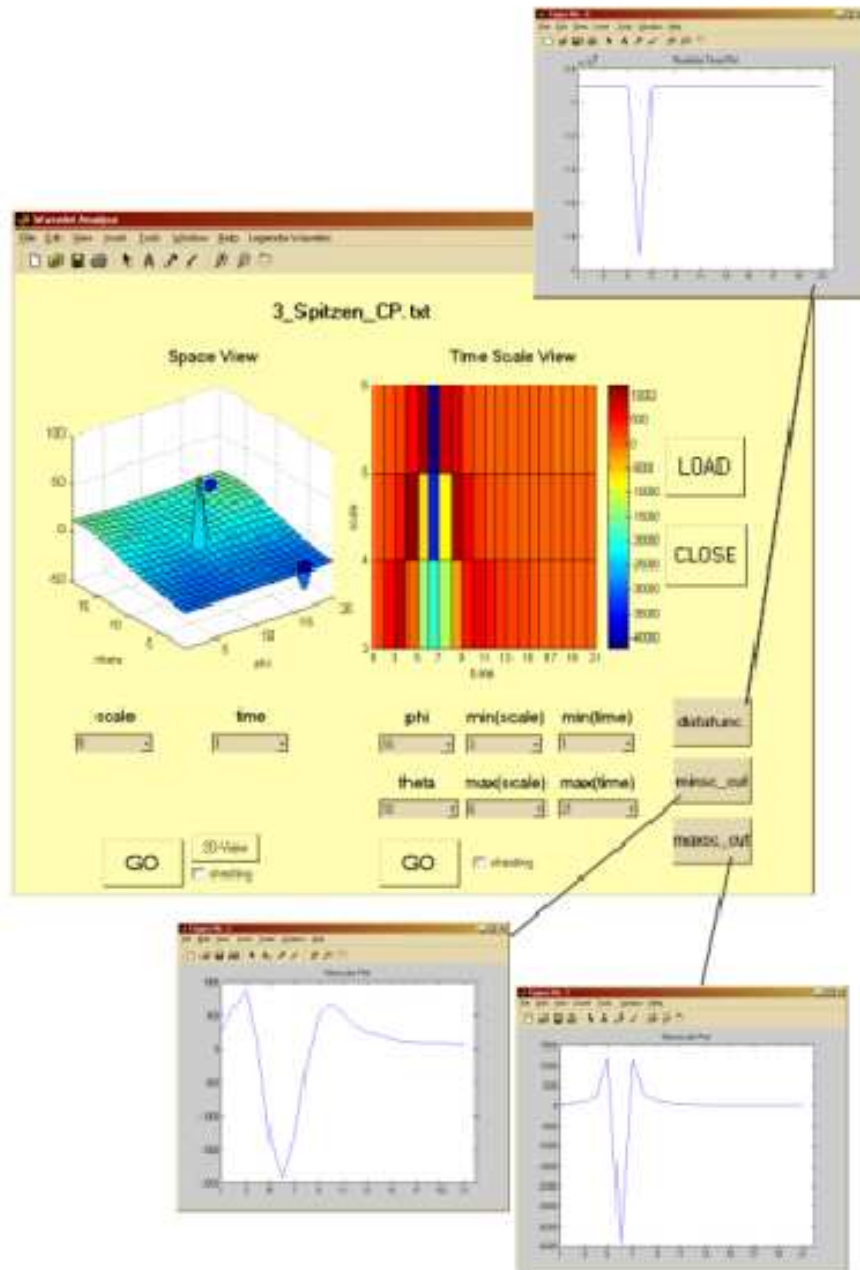


Figure 6.2: Multiscale analysis and visualization tool for time-dependent spherical vector fields. Left window: At a high spatial wavelet scale local effects are detected in a global vector field. Right window: The corresponding wavelet coefficients in the temporal domain indicate the very moment of their appearance and the comparatively long duration of the effects. The pop-ups show additional auxiliary information.

Summary and Outlook

During the course of this thesis a comprehensive theoretical framework for the application of multiscale methods in spaceborne magnetometry is introduced and examined from a mathematical point of view. A general approach to scalar as well as vectorial wavelet techniques is established in Chapter 2 and several concrete examples, i.e. Legendre wavelets, scalar spherical wavelets and vectorial spherical wavelets, are shown to be deducible from these general principles.

Based on the knowledge of a priori known covariance kernels, basic concepts of spectral and multiscale selective reconstruction from error-affected data are outlined for spherical scalar as well as vector fields in Chapter 3. The resulting techniques, i.e. multiscale signal-to-noise thresholding for scalar and vector fields are able to deal with noise that spatially changes its frequency behaviour, i.e. the multiscale character of our modelling approaches from Chapter 2 is maintained. In the case of denoising of vector fields, two different approaches, i.e. tensor based and vector based, are derived. The tensor based approach is the canonical extension of the scalar case but might lead to numerical obstacles in applications. The vector based technique is shown to lead to results equivalent to the tensor approach, but seems to be numerically easier to handle. A numerical example, utilizing synthetic geomagnetic vector data, is presented which provides an insight into the principles of multiscale signal-to-noise thresholding and demonstrates its efficiency. As regards the future application to real satellite data, it is necessary to develop appropriate covariance kernels that are especially well suited for current satellite missions. Having those kernels at hand, multiscale signal-to-noise thresholding can be reasonably combined with multiscale regularization techniques, for example, and then be applied for the determination and downward continuation of geomagnetic crustal field signatures from satellite data.

Chapter 4 is concerned with the determination and downward continuation of crustal field signals from vectorial satellite measurements within a multiscale framework. Since, on the one hand, one cannot expect the measurements to be free of noise, the problem of downward continuation is ill-posed and requires sophisticated means of regularization. On the other hand, crustal signatures are of comparatively small spatial extent such that a suitable approximation demands appropriate, space localizing trial functions. We combine both aspects, i.e. regularization and localizing ansatz functions, in our approach. The basic idea is to formulate the problem in terms of integral equations relating the radial or tangential field at satellite altitudes with the magnetic field at the Earth's surface. The integral equations are then solved in terms of scalar as well as vectorial regularization wavelets. The prob-

lem is tackled in two steps. First, the formalism is derived in spherical approximation, i.e. assuming that the satellite's orbit as well as the Earth's surface can be approximated by spheres of fixed radii. In a second step a combined spline and wavelet approach is considered that enables us to incorporate the real orbit geometries as well as the real Earth's surface if necessary. In a numerical example (in spherical approximation) we derive, from one month of CHAMP vector data, global as well as regional wavelet models of the crustal field signatures at Earth's mean spherical surface. The application of the combined spline and wavelet approach is an interesting task for future studies. Additionally, as we have already mentioned, it is interesting to study the combination of multiscale signal-to-noise thresholding and multiscale downward continuation in detail. Another task for future investigations is the simultaneous use of geomagnetic satellite as well as observatory data in a multiscale framework.

The Mie representation for the geomagnetic field has the advantage that it can equally be applied in regions of vanishing as well as non-vanishing electric current densities. The standard method of deriving the Mie representation is given by a spherical harmonic parametrization, i.e. by expanding the corresponding Mie scalars in terms of spherical harmonics. Considering the measurements (magnetic field or currents) to be given in a spherical shell we present, in Chapter 5, a wavelet parametrization of the magnetic field and the corresponding electric current densities in Mie representation. On the one hand, the use of wavelets as trial functions for field parametrization enables us to cope with electric currents (and corresponding magnetic effects) that vary rapidly with latitude or longitude, or that are confined to certain regions. Consequently, we are able to reflect the various levels of space localization in form of a vectorial multiresolution analysis and can thus take efficient account of the specific concentration of the current densities in space. On the other hand, radial dependencies can suitably be modelled within this approach by means of a product ansatz for the toroidal magnetic Mie scalar and by series expansions of the poloidal magnetic Mie scalar in terms of harmonic wavelets. Using our approach, the direct as well as the inverse geomagnetic source problem admit a treatment within a multiscale framework. In more detail, we present explicit multiscale algorithms for the approximation of the toroidal field from given (poloidal) current densities (in a spherical shell) and, vice versa, for the determination of the poloidal current densities from a given corresponding (toroidal) field. Neglecting variations in altitude, we present a numerical example that illustrates the multiscale approximation of radial current distributions from two sets of vectorial MAGSAT magnetic field data (dawn and dusk local time). Global as well as regional reconstructions of the radial current densities are calculated and demonstrate the efficiency of the multiscale approach. As regards future studies, the next reasonable step is to incorporate the variations in altitude of the satellite – at least to some extent – since this would allow for the determination of horizontal current distributions, also. Additionally, – either in studies using synthetic data, or based on satellite data sampled over large time intervals, or using data from multi satellite missions and including observatory data – a wavelet parametrization of the poloidal and toroidal magnetic fields from the corresponding electric currents (or vice versa) should be derived in future works.

Future multi-satellite missions are believed to be able to resolve not only the spatial but also the temporal structures of the geomagnetic field. In view of such missions we introduce, in Chapter 6, two variants of multiscale time- and space-dependent modelling. While

the first variant uses suitable combinations of separate wavelet techniques for the spatial as well as the temporal domain, the second technique tackles the subject by means of certain tensor-product wavelets combining temporal and spatial multiresolution techniques. This combination of different wavelet techniques enables us to approximate all different combinations of temporal and spatial variations, e.g. small or large scale temporal variations combined with global or regional spatial effects are accessible within a multiresolution framework. Future studies should include the time-space multiscale analysis of data obtained from realistic multi-satellite simulations.

Appendix A

Standard Geomagnetic Nomenclature

In this Appendix we present, for the convenience of the reader, some brief information concerning the geophysical nomenclature. We start with the denomination of geomagnetic coordinates and then present a special realization of spherical harmonics. A representation of a geomagnetic potential in terms of this very system of spherical harmonics is also given.

In Chapter 1 spherical polar coordinates have been introduced. If the parametrization is chosen such that $-180^\circ \leq \varphi < 180^\circ$, $-90^\circ \leq \vartheta \leq 90^\circ$ and if the equator is identified with $\vartheta = 0^\circ$ while $\varphi = 0^\circ$ is identified with Greenwich, then the corresponding unit vectors $-\hat{\varepsilon}^r$, $\hat{\varepsilon}^\varphi$ and $\hat{\varepsilon}^\vartheta$ can be identified with the components of the geomagnetic coordinates, i.e. the assignment of Table A.1 holds true.

Local Coordinates	Geomagnetic Coordinates	Name
$\hat{\varepsilon}^\vartheta$	X	north component
$\hat{\varepsilon}^\varphi$	Y	east component
$-\hat{\varepsilon}^r$	Z	downward or vertical component

Table A.1: Relation of spherical and geomagnetic coordinates

It should be noted that the tangential components, i.e. the geomagnetic north and east component, are frequently referred to as the horizontal components.

Spherical harmonics have been introduced in Chapter 1 in coordinate free form, thus leaving open the numerical realization. As there exist infinitely many $\mathcal{L}^2(\Omega)$ -orthonormal systems of spherical harmonics one special example frequently used in geomagnetic applications is presented for the convenience of the reader. It is the system of Schmidt semi-normalized spherical harmonics in terms of Legendre functions (cf., e.g. [55]). Consider the $2n + 1$

functions, expressed in polar coordinates

$$\tilde{Y}_{n,k}(\xi) = c_{n,k} P_n^{|k|}(t) \cos(k\varphi), \quad k = -n, \dots, 0, \quad (\text{A.1})$$

$$\tilde{Y}_{n,k}(\xi) = c_{n,k} P_n^{|k|}(t) \sin(k\varphi), \quad k = 1, \dots, n, \quad (\text{A.2})$$

where the normalization coefficients $c_{n,k}$ are given by

$$c_{n,k} = \sqrt{\frac{2(n-|k|)!}{(n+|k|)!}},$$

and P_n^k denotes the associated Legendre functions of degree n and order k :

$$P_n^k(t) = (1-t^2)^{k/2} \left(\frac{d}{dt}\right)^k P_n(t),$$

$k = 1, \dots, n$, $t \in [-1, +1]$. Note that the tilde is supposed to point at the fact that in this very example the second index of the function $\tilde{Y}_{n,k}$ runs from $k = -n \dots n$, which is a special realization of the $2n + 1$ linearly independent spherical harmonics of degree n . Graphical impressions of the system (A.1-A.2) can be found in Figure A.1.

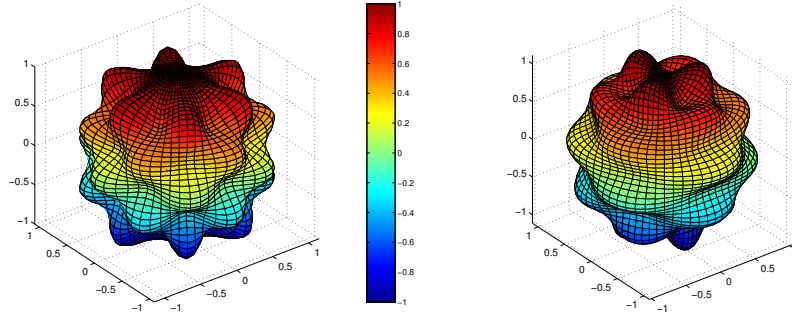


Figure A.1: Spherical harmonics of degree 10 and orders 6 (left) and -3 (right).

Next we present a realization of a geomagnetic potential U in terms of the special previously mentioned system of spherical harmonics:

$$\begin{aligned} U = & \rho_1 \left\{ \sum_{n=1}^{13} \sum_{k=0}^n (g_n^k \cos(k\varphi) + h_n^k \sin(k\varphi)) \left(\frac{\rho_1}{r}\right)^{n+1} \bar{P}_n^k(\cos(\vartheta)) \right. \\ & + \sum_{n=1}^{13} \sum_{k=0}^n (\dot{g}_n^k \cos(m\varphi) + \dot{h}_n^k \sin(k\varphi)) \left(\frac{\rho_1}{r}\right)^{n+1} (t - t_0) \bar{P}_n^k(\cos(\vartheta)) \\ & + \sum_{n=1}^2 \sum_{k=0}^n (\dot{q}_n^k \cos(k\varphi) + s_n^k \sin(k\varphi)) \left(\frac{r}{\rho_1}\right)^n \bar{P}_n^k(\cos(\vartheta)) \\ & \left. + Dst \left[\frac{r}{\rho_1} + Q_1 \left(\frac{\rho_1}{r}\right)^2 \right] [\tilde{q}_1^0 \bar{P}_1^0(\cos(\vartheta)) + (\tilde{q}_1^1 \cos(\varphi) + \tilde{s}_1^1 \sin(\varphi)) \bar{P}_1^1(\cos(\vartheta))] \right\}, \end{aligned}$$

where $\bar{P}_n^k = c_{n,k}P_n^k$. The quantities (g_n^k, h_n^k) and (q_n^k, s_n^k) are the so-called Gauss coefficients (special realizations of the Fourier coefficients) describing internal and external sources, respectively. The pair $(\dot{g}_n^k, \dot{h}_n^k)$ gives the linear secular variation around a certain reference time t_0 . The last term of the equation above accounts for the variability of the contributions from the magnetospheric ring current (as measured by Dst index) and the corresponding internal, induced counterpart. For more details concerning this or similar geomagnetic potentials as well as the individual contributions the reader might consult [74, 92, 93], for example.

Bibliography

- [1] J. Achache, A. Abtout, and J.L. Le Mouél. The downward continuation of Magsat crustal anomaly field over southeast asia. *J. Geophys. Res., B*, 92(11):11,584–11,596, 1987. [96](#), [103](#), [118](#)
- [2] O. Amm. Ionospheric elementary current systems in spherical coordinates and their application. *J. Geomag. Geoelectr.*, 49:947–955, 1997. [2](#)
- [3] O. Amm. *Direkte Bestimmung flächenhafter Verteilungen ionosphärischer elektrodynamischer Parameter aus Bodenmessungen: Theorie und Anwendungen in sphärischen Koordinaten*. PhD thesis, Naturwissenschaftliche Fakultät, Technische Universität Braunschweig, 1998. [112](#)
- [4] O. Amm. The elementary current method for calculating ionospheric current systems from multi-satellite and ground magnetometer data. *J. Geophys. Res.*, 106(A11), 2000. [2](#)
- [5] O. Amm and A. Viljanen. Ionospheric disturbance magnetic field continuation from the ground to the ionosphere using spherical elementary current systems. *Earth Planets Space*, 51:431–440, 1999. [2](#)
- [6] N. Aronszajn. Theory of reproducing kernels. *Trans. Am. Math. Soc.*, 68:337–404, 1950. [13](#)
- [7] G.E. Backus. Poloidal and toroidal fields in geomagnetic field modeling. *Rev. Geophys.*, 24:75–109, 1986. [2](#), [23](#), [24](#), [122](#), [123](#), [124](#), [132](#)
- [8] G.E. Backus, R. Parker, and C. Constable. *Foundations of Geomagnetism*. Cambridge University Press, Cambridge, 1996. [1](#), [2](#), [20](#), [23](#), [24](#), [122](#), [123](#)
- [9] M. Bayer. *Geomagnetic Field Modelling from Satellite Data by First and Second Generation Vector Wavelets*. PhD thesis, Geomathematics Group, Department of Mathematics, University of Kaiserslautern. Shaker, Aachen, 2000. [5](#), [55](#), [94](#), [111](#)
- [10] M. Bayer, S. Beth, and W. Freedon. Geophysical field modelling by multiresolution analysis. *Acta Geod. Geoph. Hung.*, 33(2-4):289–319, 1998. [55](#), [56](#), [58](#), [61](#)
- [11] M. Bayer, W. Freedon, and T. Maier. A vector wavelet approach to iono- and magnetospheric geomagnetic satellite data. *J. Atmos. Sol.-Terr. Phys.*, 63:581–597, 2001. [2](#), [5](#), [94](#), [111](#), [122](#), [123](#)

- [12] S. Beth. *Multiscale Approximation by Vector Radial Basis Functions on the Sphere*. PhD thesis, Geomathematics Group, Department of Mathematics, University of Kaiserslautern. Shaker, Aachen, 2000. 3, 58
- [13] J. Cain, D.R. Schmitz, and L. Muth. Small-scale features in the earth's magnetic field observed by Magsat. *J. Geophys. Res.*, 89:1070–1076, 1984. 91, 95
- [14] J. Cain, Z. Wang, C. Kluth, and D.R. Schmitz. Derivation of a geomagnetic model to $n=63$. *Geophys. J. Int.*, 97:432–441, 1989. 95, 112
- [15] Y. Cohen and J. Achache. New global vector magnetic anomaly maps derived from magsat data. *J. Geophys. Res.*, B, 95(7):10,783–10,800, 1990. 95
- [16] P.J. Davis. *Interpolation and Approximation*. Dover Publications Inc., New York, 1975. 13, 28
- [17] D.L. Donoho and I.M. Johnstone. Ideal spatial adaptation by wavelet shrinkage. *Biometrika*, 81:425–455, 1994. 62, 74
- [18] D.L. Donoho and I.M. Johnstone. Adapting to unknown smoothness via wavelet shrinkage. *J. Amer. Statistical Association*, 90:1200–1224, 1995. 62, 74
- [19] E.F. Donovan. Modeling the magnetic effects of field-aligned currents. *J. Geophys. Res.*, 98:529–543, 1993. 2
- [20] J.R. Driscoll and D.M. Healy. Computing Fourier transforms and convolutions on the 2-sphere. *Adv. Appl. Math.*, 15:202–250, 1994. 91, 104, 112, 137
- [21] U. Engels and N. Olsen. Computation of magnetic fields within source regions of ionospheric and magnetospheric currents. *J. Atmos. Sol.-Terr. Phy.*, 60:1585–1592, 1998. 2, 3, 122, 123
- [22] H.W. Engl. *Integralgleichungen*. Springer, Wien, New York, 1997. 25, 96, 105
- [23] H.W. Engl, M. Hanke, and A. Neubauer. *Regularization of Inverse Problems*. Kluwer, Dordrecht, Boston, London, 1996. 25, 96, 105
- [24] M. Fengler. *Multiscale Modelling of the Earth's Gravitational Potential from Discrete Noisy CHAMP-Ephemerides*. Diploma Thesis, Geomathematics Group, Department of Mathematics, University of Kaiserslautern, 2001. 117, 119, 120
- [25] W. Freeden. On approximation by harmonic splines. *Manuscr. Geod.*, 6:193–244, 1981. 4, 12, 13, 117
- [26] W. Freeden. On spherical spline interpolation and approximation. *Math. Meth. in the Appl. Sci.*, 3:551–575, 1981. 4, 12, 117, 118
- [27] W. Freeden. A spline interpolation method for solving boundary value problems of potential theory from discretely given data. *Numer. Meth. of Partial Diff. Equations*, 3:375–398, 1987. 13, 117

- [28] W. Freeden. The uncertainty principle and its role in physical geodesy. In W. Freeden, editor, *Progress in Geodetic Science*, pages 225–236, Aachen, 1998. Shaker. 3, 45
- [29] W. Freeden. *Multiscale Modelling of Spaceborne Geodata*. B.G. Teubner, Stuttgart, Leipzig, 1999. 3, 5, 13, 28, 96, 117, 118, 125
- [30] W. Freeden, T. Gervens, and M. Schreiner. *Constructive Approximation on the Sphere (With Applications to Geomathematics)*. Oxford Science Publications, Clarendon, 1998. 3, 5, 11, 12, 13, 15, 18, 20, 22, 23, 37, 38, 41, 42, 58, 72, 119, 134, 146
- [31] W. Freeden, O. Glockner, and R. Litzenberger. A general Hilbert space approach to wavelets and its application in geopotential determination. *Numer. Func. Anal. and Optimiz.*, 20:853–879, 1999. 28
- [32] W. Freeden, O. Glockner, and M. Thalhammer. Multiscale gravitational field recovery from GPS-satellite-to-satellite tracking. *Studia Geoph. Geod.*, 43:229–264, 1999. 96, 97, 98, 106
- [33] W. Freeden and T. Maier. On multiscale denoising of spherical functions: Basic theory and numerical aspects. *Electron. Trans. Numer. Anal.*, 14:40–62, 2001. 28, 38, 62, 67, 75
- [34] W. Freeden and T. Maier. Spectral and multiscale signal-to-noise thresholding of spherical vector fields and their application to earth’s magnetic field determination. *SIAM*, 2002 (submitted). 58, 62, 77
- [35] W. Freeden, T. Maier, and C. Mayer. Multiscale crustal field determination from CHAMP vector magnetic data. *Geophys. Res. Lett.*, 2002 (submitted). 111
- [36] W. Freeden, T. Maier, and S. Zimmermann. A survey on wavelet methods for (geo) applications. *Rev. Mat. Complut. (accepted)*, 2002. 28
- [37] W. Freeden and C. Mayer. Multiresolution data analysis – numerical realization by use of domain decomposition methods and fast multipole techniques. In *Proceedings of the V Hotine–Marussi Symposium on Mathematical Geodesy, Matera, Italy (submitted)*, 2002. 4, 120
- [38] W. Freeden and V. Michel. Basic aspects of geopotential field approximation from satellite-to-satellite tracking data. *Math. Meth. Appl. Sci.*, 24:827–846, 2001. 96
- [39] W. Freeden, V. Michel, and H. Nutz. Satellite-to-satellite tracking and satellite gravity gradiometry (advanced techniques for high-resolution geopotential field determination). *J. Engrg. Math. (accepted)*, 2002. 96
- [40] W. Freeden, V. Michel, and M. Stenger. Multiscale signal-to-noise thresholding. *Acta Geod. Geoph. Hung.*, 36:55–86, 2001. 62, 67
- [41] W. Freeden and F. Schneider. An integrated wavelet concept of physical geodesy. *Journal of Geodesy*, 72:259–281, 1998. 41

- [42] W. Freeden and F. Schneider. Regularization wavelets and multiresolution. *Inverse Problems*, 14:225–243, 1998. 96
- [43] W. Freeden and M. Schreiner. New wavelet methods for approximating harmonic functions. In F. Sansò, editor, *Geodetic Theory Today*, volume 114, pages 112–121. International Association of Geodesy Symposia, Springer, 1995. 12
- [44] W. Freeden, M. Schreiner, and R. Franke. A survey on spherical spline approximation. *Surv. Math. Ind.*, 7:29–85, 1997. 13, 117, 118
- [45] W. Freeden and U. Windheuser. Spherical wavelet transform and its discretization. *Adv. Comput. Math.*, 5:51–94, 1996. 12, 18
- [46] W. Freeden and U. Windheuser. Combined spherical harmonic and wavelet expansion - a future concept in Earths gravitational potential determination. *Appl. Comput. Harm. Anal.*, 4:1–37, 1997. 3, 12
- [47] C. F. Gauss. Allgemeine Theorie des Erdmagnetismus. Resultate aus den Beobachtungen des magnetischen Vereins im Jahre 1838 (english translation: General theory of terrestrial magnetism). In R. Taylor, editor, *Scientific Memoirs Selected from the Transactions of Foreign Academies of Science and Learned Societies and from Foreign Journals*, volume 2, pages 184–251, 1841. 2
- [48] G. Gerlich. Magnetfeldbeschreibung mit verallgemeinerten poloidalen und toroidalen Skalaren. *Z. Naturforsch.*, 8:1167–1172, 1972. 2, 23, 122
- [49] W. Gilbert. *De Magnete, Magneticisque Corporibus, et de Magno Magnete Tellure: Physiologia nova, plurimis et argumentis, et experimentis demonstrata*. Peter Short, London, 1600. 1
- [50] O. Glockner. *On Numerical Aspects of Gravitational Field Modelling from SST and SGG by Harmonic Splines and Wavelets (with Application to CHAMP data)*. PhD thesis, Geomatics Group, Department of Mathematics, University of Kaiserslautern. Shaker, Aachen, 2002. 4, 106, 109, 116, 117, 119, 120
- [51] M. Gutting. *Multiscale Gravitational Field Modeling from Oblique Derivatives*. Diploma Thesis, Geomatics Group, Department of Mathematics, University of Kaiserslautern, 2002. 4, 104, 120
- [52] J. Hadamard. *Lectures on the Cauchy Problem in Linear Partial Differential Equations*. Yale University Press, New Haven, 1923. 25
- [53] G.V. Haines. MAGSAT vertical field anomalies above 40°N from spherical cap harmonic analysis. *J. Geophys. Res.*, B, 90(3):2593–2598, 1985. 95
- [54] G.V. Haines. Spherical cap harmonic analysis. *J. Geophys. Res.*, B, 90(3):2583–2591, 1985. 95
- [55] W.A. Heiskanen and H. Moritz. *Physical Geodesy*. W.H. Freeman and Company, 1967. 18, 62, 166

- [56] K. Hesse. *Domain Decomposition Methods for Multiscale Geopotential Determination from SST and SGG*. PhD thesis, Geomathematics Group, Department of Mathematics, University of Kaiserslautern, 2002. 4, 120
- [57] H. Heuser. *Funktionalanalysis: Theorie und Anwendungen, 3rd Edition*. Teubner, Stuttgart, 1992. 26
- [58] W.J. Hinze and R.A. Langel. *The Magnetic Field of the Earth's Lithosphere; The Satellite Perspective*. Cambridge University Press, Stanford, 1998. 1, 95, 96, 97, 111, 113
- [59] R.V. Hogg. An introduction to robust estimation. In G.N. Launer and R.L. Wilkinson, editors, *Robustness in Statistics*, pages 1–17, San Diego, California, 1979. Academic. 113, 137
- [60] R. Holme. Modelling of attitude error in vector magnetic data: Application to ørsted data. *Earth Planets Space*, 52:1187–1197, 2000. 62
- [61] R. Holme and J. Bloxham. Alleviation of the Backus effect in geomagnetic field modelling. *Geophys. Res. Lett.*, 22:1641–1644, 1995. 62
- [62] R. Holme and J. Bloxham. The treatment of attitude errors in satellite geomagnetic data. *Phys. Earth Planet. Int.*, 98:221–233, 1996. 62
- [63] R. Holme and A. Jackson. The cause and treatment of anisotropic errors in near-Earth geomagnetic data. *Phys. Earth Planet. Int.*, 103:375–388, 1997. 62
- [64] A. Horn. *Multiscale Analysis of Geomagnetic Vector Data*. Diploma Thesis, Geomathematics Group, Department of Mathematics, University of Kaiserslautern, 2001. 160
- [65] T. Iijima and A. Potemra. Large-scale characteristics of field-aligned currents associated with substorms. *J. Geophys. Res.*, 90:2593–2598, 1978. 2
- [66] J.A. Jacobs. *Geomagnetism, Volume 1*. Academic Press, 1987. 1, 2, 142
- [67] J.A. Jacobs. *Geomagnetism, Volume 2*. Academic Press, 1987. 1, 142
- [68] J.A. Jacobs. *Geomagnetism, Volume 3*. Academic Press, 1987. 1, 142
- [69] W. Kertz. *Einführung in die Geophysik 1*. B.I. Hochschultaschenbücher, Mannheim, Wien, Zürich, 1969. 142
- [70] W. Kertz. *Einführung in die Geophysik 2*. B.I. Hochschultaschenbücher, Mannheim, Wien, Zürich, 1969. 142
- [71] K. Kohrt. *Crustal Field Modelling of the Geomagnetic Field from Spaceborne Data*. Diploma Thesis, Geomathematics Group, Department of Mathematics, University of Kaiserslautern, 2001. 111
- [72] R. Kress. *Linear Integral Equations*. Springer, Berlin, Heidelberg, New York, 1989. 26

- [73] J. Kusche. *Inverse Probleme bei der Gravitationsfeldbestimmung mittels SST- und SGG-Satellitenmissionen*. Habilitationsschrift. Institute of Theoretical Geodesy, University of Bonn, 2000. 118
- [74] R.A. Langel and R.H. Estes. Large-scale, near-Earth magnetic fields from external sources and the corresponding induced internal field. *J. Geophys. Res.*, 90:2487–2494, 1985. 2, 111, 168
- [75] R.A. Langel and R.H. Estes. The near-Earth magnetic field at 1980 determined from magsat data. *J. Geophys. Res.*, 90:2495–2510, 1985. 137
- [76] R.A. Langel, N. Olsen, and T.J. Sabaka. A comprehensive model of the near-earth magnetic field: Phase 3. Technical Report TM-2000-209894, NASA, 2000. 2
- [77] R.A. Langel, T.J. Sabaka, R.T. Baldwin, and J.A. Conrad. The near-Earth magnetic field from magnetospheric and quiet-day ionospheric sources and how it is modeled. *Phys. Earth Planet. Inter.*, 98:235–267, 1996. 2, 142
- [78] A.K. Louis. *Inverse und schlecht gestellte Probleme*. Teubner, Stuttgart, 1989. 25, 96, 101, 105
- [79] A.K. Louis, P. Maaß, and A. Rieder. *Wavelets*. Teubner, Stuttgart, 1994. 143, 154
- [80] P. Maaß and H.-G. Rieder. Wavelets and digital image processing. *Surv. Math. Ind.*, 4:195–235, 1994. 143, 154
- [81] T. Maier. *Multiscale Analysis of the Geomagnetic Field*. Diploma Thesis, Geomatics Group, Department of Mathematics, and Computational Material Science Group, Department of Physics, University of Kaiserslautern, 1999. 5, 55, 94, 104, 122, 123
- [82] S. Maus. *New Statistical Methods in Gravity and Magnetism*. Habilitation, Gemeinsame Naturwissenschaftliche Fakultät der Technischen Universität Carolo-Wilhelmina zu Braunschweig, 2001. 3, 24, 122, 123, 129, 130, 131, 132
- [83] S. Maus, M. Rother, R. Holme, H. Lühr, N. Olsen, and V. Haak. First champ satellite magnetic data resolve uncertainty about strength of the lithospheric magnetic field. *Geophys. Res. Lett.* (submitted), 2002. 95, 96, 97, 111, 112, 113
- [84] C. Mayer. *personal communication*. Geomatics Group, Department of Mathematics, University of Kaiserslautern, 2002. 112
- [85] D. Michel. *On the Combination of Harmonic Splines and Fast Multipole Methods for CHAMP Data Modelling*. Diploma Thesis, Geomatics Group, Department of Mathematics, University of Kaiserslautern, 2001. 120
- [86] V. Michel. *A Multiscale Method for the Gravimetry Problem. Theoretical and Numerical Aspects of Harmonic and Anharmonic Modelling*. Dissertation, Geomatics Group, Department of Mathematics, University of Kaiserslautern. Shaker, Aachen, 1999. 143

- [87] V. Michel. *A Multiscale Approximation for Operator Equations in Separable Hilbert Spaces – Case Study: Reconstruction and Description of the Earth’s Interior*. Habilitation, Geomatics Group, Department of Mathematics, University of Kaiserslautern. Shaker, Aachen, 2002. 58
- [88] H. Nutz. *A Unified Setup of Gravitational Field Observables*. PhD thesis, Geomatics Group, Department of Mathematics, University of Kaiserslautern. Shaker, Aachen, 2001. 103
- [89] R.T. Ogdon. *Essential Wavelets for Statistical Applications and Data Analysis*. Birkhäuser, Boston, Basel, Berlin, 1997. 62, 63
- [90] N. Olsen. A new tool for determining ionospheric currents from magnetic satellite data. *Geophys. Res. Lett.*, 24:3635–3638, 1996. 2
- [91] N. Olsen. Ionospheric F region currents at middle and low latitudes estimated from MAGSAT data. *J. Geophys. Res., A*, 3:4563–4576, 1997. 2, 3, 24, 111, 112, 122, 123, 124, 129, 132, 137
- [92] N. Olsen. Ørsted initial field model. *Geophys. Res. Lett.*, 27:3607–3610, 2000. 111, 168
- [93] N. Olsen. A model of the geomagnetic field and its secular variation for epoch 2000 estimated from Ørsted data. *Geophys. J. Int.*, 4:453–462, 2002. 2, 95, 97, 111, 142, 168
- [94] A.D. Richmond. The computation of magnetic effects of field-aligned magnetospheric currents. *J. Atmosph. and Terrestrial Physics*, 36:245–252, 1974. 2
- [95] R. Rummel. Spherical spectral properties of the Earth’s gravitational potential and its first and second derivatives. In *Lecture Notes in Earth Science*, volume 54, pages 359–404, 1997. 62, 63, 77
- [96] T.J. Sabaka, N. Olsen, and R.A. Langel. A Comprehensive Model of the Near-Earth Magnetic Field: Phase 3. *NASA/TM-2000-209894*, 2000. 142
- [97] B.J. Schmitt. The poloidal-toroidal representation of solenoidal fields in spherical domains. *Analysis*, 15:257–277, 1995. 2, 23
- [98] F. Schneider. *Inverse Problems in Satellite Geodesy and Their Approximate Solution*. PhD thesis, Geomatics Group, Department of Mathematics, University of Kaiserslautern. Shaker, Aachen, 1997. 96, 101
- [99] L. Shure, R.L. Parker, and G.E. Backus. Harmonic splines for geomagnetic modelling. *Phys. Earth Planet. Inter.*, 28:215–229, 1982. 4, 117
- [100] D.P. Stern. Representation of magnetic fields in space. *Rev. Geophys.*, (14):199–214, 1976. 122
- [101] M. Viell. *Die Theorie der uni- und multivariaten Legendre-Wavelets und ihre Anwendungen in der Refraktionsanalyse*. Diploma Thesis, Geomatics Group, Department of Mathematics, University of Kaiserslautern, 1998. 41, 143, 154

-
- [102] J.B. Weaver, X. Yansun, D.M. Healy jr., and L.D. Cromwell. Filtering noise from images with wavelet transforms. *Magnet. Reson. Med.*, 24:288–295, 1991. 62
- [103] K.A. Whaler. Downward continuation of magsat lithospheric anomalies to the Earth's surface. *Geophys. J. Int.*, 116:267–278, 1994. 95
- [104] A.M. Yaglom. *An Introduction to Stationary Random Functions*. Dover, New York, 1962. 64
- [105] S. Zimmermann. *Multiskalenanalyse des Krustenfeldes aus Satellitendaten*. Diploma Thesis, Geomathematics Group, Department of Mathematics, and Computational Material Science Group, Department of Physics, University of Kaiserslautern, 2001. 94, 111

Wissenschaftlicher Werdegang

19. Feb. 1973 Geboren in Pirmasens
- 1979 - 1983 Grundschule in Münchweiler
- 1983 - 1992 Hugo-Ball Gymnasium in Pirmasens
- 1992 Abitur
- 1992 - 2000 Studium der Physik
mit Nebenfächern Physikalische Chemie (Grundstudium),
Mathematik, Medizinische Physik und Technik (Hauptstudium)
an der Universität Kaiserslautern
- 1996 5 monatiger Studienaufenthalt an der
University of California, Los Angeles, USA
- 2000 Diplom in Physik
- 2000 - Wissenschaftlicher Mitarbeiter der
AG Geomathematik, Universität Kaiserslautern,
im Drittmittelprojekt
"Time-Space Dependent Multiscale Modelling of the Magnetic Field
Using Satellite Data (DFG FR 761/10-1)"
des DFG Schwerpunktprogramms "Erdmagnetische Variationen:
Raum-Zeit Struktur, Ursachen und Wirkungen auf das System Erde".

Scientific Career

- Feb. 19. 1973 Born in Pirmasens
- 1979 - 1983 Elementary School in Münchweiler
- 1983 - 1992 Hugo-Ball Gymnasium in Pirmasens
- 1992 Abitur
- 1992 - 2000 Majoring in Physics
with minors Physical Chemistry (stage studies),
Mathematics, Medical Physics and Engineering (advanced studies)
at the University of Kaiserslautern
- 1996 5 months of Physics and Mathematics at the
University of California, Los Angeles, USA
- 2000 German Diplom in Physics
- 2000 - Research associate at the
Geomathematics Group, University of Kaiserslautern,
in the research project
"Time-Space Dependent Multiscale Modelling of the Magnetic Field
Using Satellite Data (DFG FR 761/10-1)"
of the DFG priority programme "Geomagnetic variations:
spatio-temporal structure, processes, and effects on system Earth".

Eidesstattliche Erklärung

Hiermit erkläre ich an Eides statt, dass ich die vorliegende Arbeit selbst und nur unter Verwendung der in der Arbeit genannten Hilfen und Literatur angefertigt habe.

Kaiserslautern, 20. September 2002